3

SAINT PETERSBURG STATE UNIVERSITY STUDIES IN EARTH SCIENCES

Vadim M. Kovrugin

Crystal Chemistry of Novel Oxide Compounds of Se^{4+} and Se^{6+}

Saint Petersburg | 2015

The series *Saint Petersburg State University Studies in Earth Sciences* presents final results of research carried out in postgraduate geological programs at St. Petersburg State University. Most of this research is here presented after publication in leading scientific journals.

The supervisors of these works are well-known scholars of St. Petersburg State University and invited foreign researchers. The material of each book has been considered by a permanent editorial board as well as a special international commission comprised of well-known Russian and international experts in their respective fields of study.

Printed in Russia by St. Petersburg State University Press
11/21 6th Line, St. Petersburg, 199004
ISSN 2308-6602
ISBN 978-5-288-05619-2

ABSTRACT

This work deals with the synthesis and characterization of novel oxide materials containing selenium in the oxidation states of +4 or +6. The structural types occurring in 33 known oxoselenite minerals have an amazing variety, and cover the whole field from *0D* isolated complexes to *3D* frameworks, which offer unexploited potentialities in terms of physical properties. This thesis aims to synthetize and investigate new Se based compounds, using methods inspired by mineralogical processes.

Information based on original building units assembled into original architectures have been deduced and compared to related inorganic phases of the literature. In the present study, our innovative so-called "geo-inspired" approach is applied in order to obtain complex novel crystalline compounds. This approach assumes emulation and modelling of natural crystal growth processes.

Herein, we used either a traditional descriptive procedure based on consideration of the crystal structures in terms of coordinations of cations, or the modern theory of anion-centered tetrahedra developed by the St. Petersburg school of crystallography and the UCCS group of solid-state chemistry in Lille, in cases when the traditional structural interpretation does not reflect basic principles of crystal architecture. Thus, several metal-oxide chemical systems with $Se^{4+/6+}$ and various metals ($Cu^{+/2+}$, Ni^{2+}, Co^{2+}, $V^{4+/5+}$, Mn^{2+}, Fe^{3+}, Pb^{2+}, Bi^{3+}, U^{6+}) were studied in the context of the present work.

The thesis contains results of synthetic procedures, and crystal chemical characterization of 39 new metal selenites, selenates, and selenite-selenates. The analogy of selenite groups with phosphites was also investigated. Main results are described with references to more detailed publications given in the appendices.

Keywords: selenite, selenate, uranyl, vanadate, phosphite, copper, nickel, cobalt, manganese, lead, bismuth, iron, synthesis, crystal structure, single crystal X-ray analysis, oxocentered tetrahedra

RÉSUMÉ

Ce manuscrit est consacré à la synthèse et la caractérisation de nouveaux matériaux d'oxyde à base de sélénium dans les états d'oxydation +4 ou +6. Les types structuraux rencontrés parmi les 33 oxy sélénites minéraux montrent une diversité structurale étonnante, et couvrent le champ des dimensionnalités *0D* à *3D*, offrant ainsi des potentialités inexploitées en termes des propriétés physiques. Cette thèse a visé la synthèse de l'étude de nouveaux composés du Se, en utilisant des méthodes de synthèse essentiellement inspirées des conditions de croissance des minéraux.

Les informations basées sur l'assemblage de briques élémentaires originales dans des architectures structurales ont été déduites et comparées aux données de la littérature sur des phases proches.

Lors de ce travail, notre approche « géo-inspirée » innovante été appliquée afin d'obtenir de nouveaux polytypes complexes. Nous avons donc utilisé des procédés simulant les conditions de croissance des minéraux. En termes de description, nous avons également utilisé soit le modèle « standard » basé sur l'examen des structures cristallines en termes de coordinations de cations, soit des outils plus modernes basés sur l'assemblage de tétraèdres anions-centrés développée par l'école de la cristallographie de Saint-Pétersbourg et par le groupe de chimie du solide de l'UCCS, à Lille, et ce dans les cas où l'interprétation structurale traditionnelle ne reflète pas les principes de base de la cristallochimie. Finalement, plusieurs systèmes chimiques métal-oxyde avec du $Se^{4+/6+}$ et divers métaux ($Cu^{+/2+}$, Ni^{2+}, Co^{2+}, $V^{4+/5+}$, Mn^{2+}, Fe^{3+}, Pb^{2+}, Bi^{3+}, U^{6+}) ont été étudiés dans le cadre de ce manuscrit.

La thèse contient les résultats des procédures synthétiques et de la caractérisation cristallochimique des 39 nouveaux sélénites, sélénates et sélénite-sélénates des métaux. Les principaux résultats sont donnés et font référence aux publications plus détaillées données en annexe.

Mots-clés: sélénite, sélénate, uranyle, vanadate, phosphite, cuivre, nickel, cobalt, manganèse, fer, plomb, bismuth, synthèse, structure cristalline, analyse sur monocristal par diffraction des Rayons-X, tétraèdres oxocentrés

Supervisors

Prof. Dr. Sergey V. Krivovichev
Department of Crystallography
Institute of Earth Sciences
Saint-Petersburg State University, Russia

Prof. Dr. Olivier Mentré
Unité de Catalyse et de Chimie du Solide
UMR 8181 CNRS
Université Lille 1, France

Co-Encadrant

Ass. Prof. Dr. Marie Colmont
Unité de Catalyse et de Chimie du Solide
UMR 8181 CNRS
Université Lille 1, France

Opponents

Prof. Dr. Anatoly N. Zaitsev (Chairman)
Department of Mineralogy
Institute of Earth Sciences
Saint-Petersburg State University, Russia

Prof. Dr. Vladimir G. Krivovichev
Department of Mineralogy
Institute of Earth Sciences
Saint-Petersburg State University, Russia

Prof. Dr. Igor V. Pekov
Department of Mineralogy
Faculty of Geology
Moscow State University, Russia

Prof. Dr. Olivier Mentré
Unité de Catalyse et de Chimie du Solide
UMR 8181 CNRS
Université Lille 1, France

Ass. Prof. Dr. Olivier Hernandez
Institut des Sciences Chimiques de Rennes
UMR 6226 CNRS
Université Rennes 1, France

Ass. Prof. Dr. Dmitri O. Charkin
Department of Inorganic Chemistry
Faculty of Chemistry
Moscow State University, Russia

Ass. Prof. Dr. Sergey N. Britvin
Department of Crystallography
Institute of Earth Sciences
Saint-Petersburg State University, Russia

ACKNOWLEDGEMENTS

First, I would like to express my sincere gratitude to my supervisors, Prof. Dr. Sergey V. Krivovichev and Prof. Dr. Oliver Mentré. I am extremely thankful and indebted to them for sharing valuable expertise, encouragement extended to me. They gave me an incredible opportunity to work and write this thesis under their High-level guidance.

A heartfelt, special word of my thanks goes to Ass. Prof. Dr. Marie Colmont, my French co-encadrant, for insightful discussions, her genuine caring and concern, and devoting so much time to me during this international co-tutorial project.

Besides my mentors, I would also like to thank the members of the defence committee: Ass. Prof. Dr. Olivier Hernandez, Ass. Prof. Dr. Dmitri O. Charkin, Prof. Dr. Igor V. Pekov, Prof. Dr. Anatoly N. Zaitsev, Prof. Dr. Vladimir G. Krivovichev, and Ass. Prof. Dr. Sergey N. Britvin, for their acceptance to be in the jury, and for having critically reviewed my work.

I wish to express my sincere thanks to Ass. Prof. Dr. Vladislav V. Gurzhiy, who was always willing to help and to give his helpful advices. I started with him my undergraduate research work dealing with the uranyl compounds, which has been evolved into this Ph.D. thesis.

I am also very thankful to Ass. Prof. Dr. Oleg I. Siidra for his excellent scientific suggestions, knowledge, professionalism, and our common publications. He visited annually the UCCS laboratory to work on joint projects with French colleagues, when I was staying in France, and helped me in practice with my research in the lab.

My gratitude is also extended to the personnel of the UCCS laboratory in Lille, Frédéric Capet, Maxence Vandewalle, Nora Djelal, Laurence Burylo, Prof. Sylvie Daviero-Minaud, Prof. Marrielle Huvé, and Prof. Pascal Roussel. Their work was of high quality and efficient. I would like to emphasize my comrades, Almaz and Jacob, with whom I was collaborating in Lille at the beginning of my work. I am also thankful to all my international friends, PhD students, who are (or have been) working in the lab for creating a jovial atmosphere in the workplace: Anne-Lise, Annie, Blaise, Clément, Denys, Esperanza, Florence, Florent, Frédérique, Guillaume, Guiliano, Manon, Margot, Marine, Nacho, Nathalie, Nicolas, Raynald, Rénald, Tanguy, Xavier.

The present co-tutorial research work would not have been possible without the scholarship doctoral program of the Embassy of France in Russia: *la bourse de doctorat en cotutelle de thèse en Fédération de Russie* (*la bourse doctorale Vernadski*). This co-tutorial research project allows students to be enrolled simultaneously at each involved institution and be awarded a double doctoral degree by the two institutions in the case of a successful defence of the thesis. I am very grateful to the French Government for creating this outstanding doctoral program allowing students to gain invaluable international experience.

I would like also to thank my parents for supporting and helping me throughout my life. I should especially thank my mom, Svetlana, for being so caring, responsible, loving and having great faith in my abilities.

Last, but certainly not least, I would like to give my thanks to my cat, Belka, who inspired me from the beginning of my education started in school and still to this day.

The present work was carried out under the framework of the international co-tutorial thesis project between St. Petersburg State University (Russia) and University of Lille 1 (France) supported by the Embassy of France in Russia, the French Government, and managed by the Agency Campus France.

Financial support was also provided through the Multi-InMaDe project (grant ANR 2011-JS-0800301), the Federal Target Program "Scientific and Scientific-Pedagogical Personnel of the Innovative Russia" (grant 02.740.11.0326), Russian Science Foundation (grant 14-17-00071), Russian Foundation for Basic Research (grant 12-05-33097), and the St. Petersburg State University (internal grants 3.37.84.2011, 3.38.136.2014).

The experimental work including X-ray diffraction studies were performed in the Unité de catalyse et de chimie du solide of the University of Lille 1, and in the X-ray Diffraction Resource Centre of the St. Petersburg State University. The Fonds Européen de Développement Régional (FEDER), CNRS, Région Nord Pas-de-Calais, and Ministère de l'Education Nationale de l'Enseignement Supérieur et de la Recherche are acknowledged for funding the X-ray diffractometers in the University of Lille 1.

LIST OF FIGURES

FIGURE 2.1 General scheme of the CVT method – (a), the source zone of the tube – (b), the crystals of $K[Cu_5O_2](SeO_3)_2Cl_3$ (**c2.1**) picked out from the source zone – (c), and a common view of the sealed silica tube after the CVT synthesis – (d) 31

FIGURE 2.2 The crystal structures of $A[Cu_5O_2](SeO_3)_2Cl_3$ ($A^+ = K^+$ (**c2.1**), Na^+ (**c2.2**)) in two different projections featuring side and top view of the $[O_2Cu_5]^{6+}$ sheet of oxocentered $(OCu_4)^{6+}$ tetrahedra highlighted by red colour 33

FIGURE 2.3 The crystal structures of $K[Cu_3O](SeO_3)_2Cl$ (**c2.3**) and $Na_2[Cu_7O_2](SeO_3)_4Cl_4$ (**c2.4**). The $(OCu_4)^{6+}$ tetrahedra are highlighted by red colour 34

FIGURE 2.4 Projections of the $[Cu(HSeO_3)_2]^0$ sheet (a) and the crystal structure of $[NaCl][Cu(HSeO_3)_2]$ (**c2.5**) featuring two-dimensional $[Cu(HSeO_3)_2]$ sheets with intercalated –Na–Cl–Na– chains 35

FIGURE 2.5 Projections of the structures of $[Cu^+Cl_2][Pb_2Cu_9O_4](SeO_3)_4Cl_5$ (**c2.6**) – (a) and (b), $[Cu^+Cl_2][PbCu_5O_2](SeO_3)_2Cl_3$ (**c2.7**) – (c), and $K_{(1-x)}[Cu^+Cl_2][Pb_xCu^{2+}_{(6-x)}O_2](SeO_3)_2Cl_{(4-x)}$, $x = 0.20$ (**c2.8**) – (d) ... 37

FIGURE 2.6 Coordination environment of the dimers composed of oxocentered tetrahedra in the crystal structures of different minerals and synthetic compounds listed in Table 2.3 39

FIGURE 3.1 Experimental crystallization diagram of the PbO–NiO–SeO_2–H_2O system at 200 °C with the pH zones shown in background by grey colors – (a); series of the experiments with a PbO / NiO / SeO_2 molar ratio of 5 : 3 : 10 corresponding to the $\boldsymbol{P_1}$ point with various pH values – (b) 42

FIGURE 3.2 General projection of the crystal structures of α–Pb$M(SeO_3)_2$ ($M = Ni^{2+}$ (**c3.1**), Co^{2+} (**c3.4**)) along the *b*-axis – (a), and the

corresponding black-and-white graph – (b), M^{2+} Se^{4+} are black and white circles, respectively.....44

FIGURE 3.3 The crystal structure of β–$PbNi(SeO_3)_2$ (**c3.2**) in two different projections – (a) and (b), and the black-and-white graph corresponding to the Ni–Se sheet in the structure– (c).....45

FIGURE 3.4 General projection of the crystal structure of $PbNi_2(SeO_2OH)_2(SeO_3)_2$ (**c3.3**) along the *b* and *c*-axis – (a) and (b), respectively; its black-and-white graph – (c); and more detailed fragment of the structure – (d) 46

FIGURE 4.1 Experimental crystallization diagram of the $PbCl_2$–V_2O_5–SeO_2–H_2O (a) and PbO–V_2O_5–SeO_2–H_2O (b) systems at 200 °C with the pH zones shown in the background by grey colours.....49

FIGURE 4.2 Projections of the structures and optical microscope images of the crystals of **c4.1**, **c4.2**, **c4.3**, and α–$Pb_4(V_3O_8)_2(SeO_3)_3(H_2O)$. VO_6 octahedra, VO_5 square pyramids, SeO_3 triangular pyramids, and Pb^{2+} cations are blue, green, orange, and grey, respectively.....51

FIGURE 4.3 Vanadate tetrameric structural units in the structures of α-$(V_2O_3)(SeO_3)_2$ and β–$(V_2O_3)(SeO_3)_2$ (**c4.1**) – (a) and (b), respectively 52

FIGURE 4.4 Structural units in the crystal structure of β-$Pb_4(V^{5+}{}_3O_8)_2(SeO_3)_3(H_2O)$ (**c4.3**).....54

FIGURE 4.5 Mode of packing of the vanadate selenite ribbons in the crystal structures of α–$Pb_4(V_3O_8)_2(SeO_3)_3(H_2O)$ – (a) and β-$Pb_4(V_3O_8)_2(SeO_3)_3(H_2O)$ (**c4.3**) – (b).....55

FIGURE 5.1 View of the crystal structure of $Mn(SeO_4)(H_2O)_2$ (**c5.1**) projected along the *a*-axis – (a); heteropolyhedral sheet parallel to the (001) plane – (b) and its black-and-white graph with symbols designating the direction of bonds to adjacent sheets – (c) 59

FIGURE 5.2 Projection of the crystal structure of $Mn_2[Bi_2O](SeO_3)_4$ (**c5.2**) (b) composed of $[MnO_4]^{6-}$ (a) and $[Bi_2O]^{4+}$ chains (c) 60

FIGURE 5.3 General projections of the crystal structure of $MnBi(SeO_3)_2Cl$ (**c5.3**) along [010] – (a) and [001] – (b) (disordered O sites are omitted for clarity); anionic arrangement of metal cations in the structure – (c) 61

FIGURE 5.4 Projection of the crystal structure of $Mn_4(Mn_5,Bi)(SeO_3)_8Cl_5$ (**c5.4**) along [100] – (c), the sheet of square antiprisms – (a), the tetrameric unit – (d), and their arrangement in the structure – (b)..... 63

FIGURE 5.5 Projection of the crystal structure of $Bi_6(SeO_3)_4Cl_{10}$ (**c5.5**) on the (010) plane, showing BiO_xCl_y polyhedra (yellow) and SeO_3 groups (orange) sharing their edges and corners 64

FIGURE 5.6 Projection of the crystal structure of β–$Bi(SeO_3)Cl$ (**c5.6**) along [100] – (a). An alternation of three different parallel layers: $[Bi_{14}(SeO_3)_{24}]^{6-}$ – (b), $[Bi_{12}Cl_{32}]^{4+}$ – (c), and $[Bi_8Cl_{16}]^{8+}$ – (d)..... 65

FIGURE 5.7 Projection of the crystal structure of $PbBi_{10}(SeO_3)_{12}Cl_8$ (**c5.7**) along the *a*-axis – (b), two parallel cationic and anionic layers: $[(Pb,Bi)_{14}(SeO_3)_{24}]^{n-}$ – (a) and $[(Pb,Bi_8)Cl_{16}]^{n+}$ – (c)..... 66

FIGURE 6.1 Topological diversity of inorganic structural units in the crystal structures of novel compounds. Uranyl pentagonal bipyramids and selenate/selenite groups are shown by yellow and orange in polyhedral representation and by black and white vertices in graphs 71

FIGURE 6.2 Dimensional fields on the compositional diagram of the $UO_2TO_4 – A_2TO_4 – H_2O$ (*A* = monovalent cation, *T* = S, Se, Cr, Mo) system. 75

FIGURE 7.1 Lewis structures and simplified artistic representation of orbital models of $(ESeO_3)^{2-}$ (a) and $(HPO_3)^{2-}$ (b) anions, which highlights the similar geometrical role of H_{HPO3} and E_{SeO3}. 76

FIGURE 7.2 View of the crystal structures of $Fe_2(SeO_3)_3$ (**c7.1**) and $Fe_2(HPO_3)_3$ (**c7.2**) along the *c*-axis – (a) and (c), respectively; mode of linkage of iron (brown) and selenite (orange) polyhedra in **c7.1** – (b)..... 78

LIST OF TABLES

TABLE 2.1 Crystallographic data and refinement parameters for **c2.1**, **c2.2**, **c2.3**, **c2.4**, **c2.5**, **c2.6**, **c2.7**, and **c2.8** 30

TABLE 2.2 Experimental details of the CVT syntheses of **c2.1**, **c2.2**, **c2.3**, **c2.4**, **c2.5**, **c2.6**, **c2.7**, and **c2.8** 31

TABLE 2.3 Crystallographic data for minerals and inorganic copper compounds based upon dimers composed of oxocentered tetrahedra 39

TABLE 3.1 Crystallographic data and refinement parameters for α–$PbNi(SeO_3)_2$ (**c3.1**), β–$PbNi(SeO_3)_2$ (**c3.2**), $PbNi_2(SeO_2OH)_2(SeO_3)_2$ (**c3.3**), and α–$PbCo(SeO_3)_2$ (**c3.4**) 40

TABLE 4.1 Crystallographic data and refinement parameters for β-$(V_2O_3)(SeO_3)_2$ (**c4.1**), $Pb_2(VO)(SeO_3)_3$ (**c4.2**), and β-$Pb_4(V_3O_8)_2(SeO_3)_3(H_2O)$ (**c4.3**) 48

TABLE 5.1 Crystallographic data and refinement parameters for **c5.1**, **c5.2**, **c5.3**, **c5.4**, **c5.5**, **c5.6**, and **c5.7** 57

TABLE 6.1 Crystallographic data and refinement parameters for **c6.1**, **c6.2**, **c6.3**, **c6.4**, **c6.5**, **c6.6**, **c6.7**, and **c6.8** 67

TABLE 6.2 Crystallographic data and refinement parameters for **c6.9**, **c6.10**, **c6.11**, **c6.12**, **c6.13**, **c6.14**, **c6.15**, and **c6.16** 68

TABLE 6.3 Experimental details of the isothermal evaporation syntheses of novel uranyl selenates and selenite-selenates (temperature: 23°C; time of crystal growth: 72 hours) 69

TABLE 7.1 Crystallographic data and refinement parameters for $Fe_2(SeO_3)_3$ (**c7.1**) and $Fe_2(HPO_3)_3$ (**c7.2**) 77

TABLE 7.2 Calculated partial charges for featured selected compounds 79

TABLE OF CONTENTS

ABSTRACT 3
ACKNOWLEDGEMENTS 7
LIST OF FIGURES 9
LIST OF TABLES 12
TABLE OF CONTENTS 13
LIST OF INCLUDED ARTICLES 15
OTHER PUBLICATIONS 17
LIST OF NEW COMPOUNDS 20
1 INTRODUCTION 22
2 BRIEF DESCRIPTION OF RESULTS 27
2.1 Objects and methods 27
2.2 Crystal chemical studies of copper selenites 30
2.2.1 Synthetic procedures 31
2.2.2 Structural description of eight novel phases 32
2.2.3 Linkage of selenite groups with $[OCu_4]^{6+}$ dimers 38
2.3 Crystal chemical studies of nickel and cobalt selenites 40
2.3.1 Crystal growth in the $PbO–NiO–SeO_2–H_2O$ system 41
2.3.2 Structural description of four novel phases 43
2.4 Crystal chemical studies of vanadate selenites 48
2.4.1 Pathways for synthesis of lead vanadate selenites 48
2.4.2 Structural description of three novel phases 50
2.5 Crystal chemical studies of selenium compounds with manganese and bismuth 57
2.5.1 Synthetic procedures 58
2.5.2 Structural description of seven novel phases 59
2.6 Crystal chemical studies of uranyl selenates and selenite-selenates 67

2.6.1 Synthetic procedures 69
2.6.2 Structural description of sixteen novel phases 69
2.6.3 Dimensional reduction 74
2.7 Analogy between electron lone pairs of selenites and H–P bonds phosphites 76
2.7.1 Synthesis and structural characterization of iron selenite and phosphite 77
2.7.2 Calculation of partial charges 78
3 CONCLUSION AND PERSPECTIVES 80
REFERENCES 83
APPENDIX 91
INCLUDED ARTICLES 93
A-I Unprecedented layer topology in the crystal structure of a new organically templated uranyl selenite-selenate 93
A-II Structural topology and dimensional reduction in uranyl oxysalts: eight novel phases in the methylamine–$(UO_2)(NO_3)_2$–H_2SeO_4–H_2O system 97
A-III Revised bismuth chloroselenite system: evidence of a noncentrosymmmetric structure with a giant unit cell 115
A-IV pH-Controlled pathway and systematic hydrothermal phase diagram for elaboration of synthetic lead nickel selenites 125
A-V Oxocentered Cu(II) lead selenite honeycomb lattices hosting $Cu(I)Cl_2$ groups obtained by chemical vapor transport reactions 137
A-VI Topologically and geometrically flexible structural units in seven new organically templated uranyl selenates and selenite-selenates 143
A-VII Emulating exhalative chemistry: synthesis and structural characterization of ilinskite, $Na[Cu_5O_2](SeO_3)_2Cl_3$, and its K-analogue 155
A-VIII $[NaCl][Cu(HSeO_3)_2]$, NaCl-intercalated $Cu(HSeO_3)_2$: synthesis, crystal structure and comparison with related compounds 167
Кристаллохимия новых кислородных соединений четырех- и шестивалентного селена (Russian translation) 175

LIST OF INCLUDED ARTICLES

A-I Kovrugin V.M., Gurzhiy V.V., Krivovichev S.V., Tananaev I.G., Myasoedov B.F. Unprecedented layer topology in the crystal structure of a new organically templated uranyl selenite-selenate. Mendeleev Communications. 2012, 22 (1), 11–12.

A-II Kovrugin V.M., Gurzhiy V.V., Krivovichev S.V. Structural topology and dimensional reduction in uranyl oxysalts: eight novel phases in the methylamine–$(UO_2)(NO_3)_2$–H_2SeO_4–H_2O system. Structural Chemistry. 2012, 23 (6), 2003–2017.

A-III Aliev A., Kovrugin V.M., Colmont M., Terryn C., Huvé M., Siidra O.I., Krivovichev S.V., Mentré O. Revised bismuth chloroselenite system: evidence of a noncentrosymmmetric structure with a giant unit cell. Crystal Growth & Design. 2014, 14 (6), 3026–3034.

A-IV Kovrugin V.M., Colmont M., Colis S., Terryn C., Siidra O.I., Krivovichev S.V., Mentré O. pH controlled pathway and systematic hydrothermal phase diagram for elaboration of synthetic lead nickel selenites. Inorganic Chemistry. 2015, 54 (5), 2425–2434.

A-V Kovrugin V.M., Colmont M., Siidra O.I., Mentré O., Al-Shuray A., Gurzhiy V.V., Krivovichev S.V. Oxocentered Cu(II) lead selenite honeycomb lattices hosting $Cu(I)Cl_2$ groups obtained by chemical vapor transport reactions. Chemical Communications. 2015, 51 (46), 9563–9566.

A-VI Gurzhiy V.V., Kovrugin V.M., Tyumentseva O.S., Mikhaylenko P.A., Krivovichev S.V. Tananaev I.G. Topologically and geometrically flexible structural units in seven new organically templated uranyl selenates and selenite-selenates. Journal of Solid State Chemistry. 2015, 229, 32–40.

A-VII Kovrugin V.M., Siidra O.I., Colmont M., Mentré O., Krivovichev S.V. Emulating exhalative chemistry: synthesis and structural characterization of ilinskite, $Na[Cu_5O_2](SeO_3)_2Cl_3$, and its K-analogue. Mineralogy and Petrology. 2015, 109, 421–430.

A-VIII Kovrugin V.M., Krivovichev S.V., Mentré O., Colmont M. $[NaCl][Cu(HSeO_3)_2]$, NaCl-intercalated $Cu(HSeO_3)_2$: synthesis, crystal structure and comparison with related compounds. Zeitschrift für Kristallographie. 2015, in press, doi: 10.1515/zkri-2015-1849.

OTHER PUBLICATIONS

P-I Kovrugin V.M., Gurzhiy V.V., Krivovichev S.V. Synthesis and crystal structure of new uranyl selenate. Volume of Abstracts of the Young Scientific Conference of St Petersburg State University "Geology is our Future". Russia, St. Petersburg, 29–30 Apr. 2009, p. 27–28. [in Russian]

P-II Gurzhiy V.V., Kovrugin V.M., Krivovichev S.V., Tananaev I.G., Myasoedov B.F. Synthesis and crystal structure of $(CH_3NH_3)_4(H_3O)_2[(UO_2)_5(SeO_4)_8(H_2O)](H_2O)_4$. Volume of Abstracts of the XXIV International Chugaev Conference on Coordination Chemistry. Russia, Repino, 15–19 Jun. 2009, p. 256–257. [in Russian]

P-III Kovrugin V.M., Gurzhiy V.V., Krivovichev S.V. Geometrical isomerism in layered uranyl selenates: synthesis and crystal structure of $(CH_3NH_3)_4(H_3O)_2[(UO_2)_5(SeO_4)_8(H_2O)](H_2O)_4$. . Volume of Abstracts of the International Scientific Conference "Clays, clay minerals, and layered materials 2009". Russia, Zvenigorod, 21–25 Sept. 2009, p. 89.

P-IV Gurzhiy V.V., Kovrugin V.M., Krivovichev S.V., Tananaev I.G., Myasoedov B.F. Inorganic uranyl selenates: synthesis and structure of new compounds in the $(UO_2)(NO_3)_2$–H_2SeO_4–H_2O–CH_3NH_2 (methylamine) system. Volume of Abstracts of the III Russian Meeting on Organic Mineralogy with International Participation "Organic Mineralogy 2009". Russia, Syktyvkar, 10–12 Nov. 2009. p. 21–24. [in Russian]

P-V Kovrugin V.M., Gurzhiy V.V., Krivovichev S.V. Synthesis, structural studies and topological analysis of new uranyl selenates with methylamine. Volume of Abstracts of the IV Russian School on Radiochemistry and Nuclear Technologies. Russia, Ozersk, 6–10 Sept. 2010, p. 57–58. [in Russian]

P-VI Kovrugin V.M., Gurzhiy V.V., Krivovichev S.V. Geometrical isomerism in new uranyl selenates. Volume of Abstracts of the International Scientific

Conference “Fedorov Session 2010”. Russia, St-Petersburg, 12–15 Oct. 2010, p. 36–37. [in Russian]

P-VII Kovrugin V.M., Gurzhiy V.V., Krivovichev S.V., Tananaev I.G. Synthesis and crystal structures of new uranyl selenite-selenate $[C_2H_8N][(H_5O_2)(H_2O)][(UO_2)_2(SeO_4)_3(H_2SeO_3)](H_2O)$ with novel type of inorganic layer. Volume of Abstracts of the 6th National Crystal Chemical Conference. Russia, Suzdal, 1–4 Jun. 2011, p. 114–116. [in Russian]

P-VIII Kovrugin V.M., Gurzhiy V.V., Krivovichev S.V., Tananaev I.G. Geometrical isomerism in layered uranyl selenite-selenates: synthesis and crystal structure of $(C_2H_8N)_3(C_2H_7N)[(UO_2)_3(SeO_4)_4(HSeO_3)(H_2O)]$. Volume of Abstracts of the XVII International Conference on Crystal Chemistry, X-ray Diffraction and Spectroscopic Studies of Minerals. Russia, St-Petersburg, 20–24 Jun. 2011, p. 96–97.

P-IX Kovrugin V.M., Gurzhiy V.V., Krivovichev S.V., Tananaev I.G. Dimensional reduction in uranyl oxysalts with general formula $A_n(UO_2)_p(TO_4)_q(H_2O)_r$ (A = monovalent cation, T = S, Se, Cr, Mo). Volume of Abstracts of the Joint meeting DGK, DMG, ÖMG. Austria, Salzburg, 20–24 Sept. 2011, p. 96.

P-X Kovrugin V.M., Gurzhiy V.V., Krivovichev S.V. Geometrical features of two novel layered uranium selenite-selenates. Volume of Abstracts of the European Mineralogical Conference. Germany, Frankfurt-am-Main, 6–8 Sept 2012, p. 564.

P-XI Kovrugin V.M., Gurzhiy V.V., Krivovichev S.V. Dimensional reduction in uranyl oxysalts with monovalent cations. Volume of Abstracts of the International Scientific Conference “Fedorov Session 2012”. Russia, Saint-Petersburg, 9–11 Oct. 2012, p. 423–424. [in Russian]

P-XII Kovrugin V., Gurzhiy V., Krivovichev S. Application of the principle of dimensional reduction to uranyl oxysalts with monovalent cations. Volume of Abstracts of the GACMAC 2013 Joint Annual Meeting. Canada, MB, Winnipeg, 22–24 May 2013, p. 123.

P-XIII Kovrugin V., Colmont M., Mentré O., Krivovichev S. Crystal structures of two novel compounds in the PbO–NiO–SeO_2 system. Volume of Abstracts of the GACMAC 2013 Joint Annual Meeting. Canada, MB, Winnipeg, 22–24 May 2013, p. 123–124.

P-XIV Kovrugin V.M., Colmont M., Mentré O., Siidra O.I., Krivovichev S.V. Crystal structures of two novel polymorphic modifications of $PbNi(SeO_3)_2$ Volume of Abstracts of the 7th National Crystal Chemical Conference. Russia, Suzdal, 17–21 Jun. 2013, p. 115. [in Russian]

P-XV Kovrugin V.M., Siidra O.I., Mentré O., Krivovichev S.V. Structural variety of novel Pb and Bi selenites. Abstract book of the 28th European Crystallographic Meeting. UK, Warwick. 25–29 Aug 2013. Acta Crystallographica, 2013, A69, p. s136.

P-XVI Kovrugin V.M., Colmont M., Mentré O., Siidra O.I., Krivovichev S.V. Synthesis and Crystal Structure of $Pb_4(V_3O_8)_2(SeO_3)_3$. Abstract book of the 28th European Crystallographic Meeting. UK, Warwick. 25–29 Aug 2013. Acta Crystallographica, 2013, A69, p. s465.

P-XVII Kovrugin V.M., Colmont M., Mentré O., Siidra O.I., Krivovichev S.V. Synthesis and Crystal Structure of $Pb_2(VO_2)(SeO_3)_2Cl$. Volume of Abstracts of the International Scientific Conference "Crystallogenesis and Mineralogy – III". Russia, Novosibirsk, 27 Sept–01 Oct 2013, p. 91.

P-XVIII Kovrugin V.M., Colmont M., Siidra O.I., Krivovichev S.V., Mentré O. Chemical vapor transport method as a pathway to novel copper selenites. Volume of Abstracts of the National Scientific Conference "CRISTECH 2014". France, Autrans, 6–8 Oct 2014, p. 27.

LIST OF NEW COMPOUNDS

c2.1 – $K[Cu_5O_2](SeO_3)_2Cl_3$
c2.2 – $Na[Cu_5O_2](SeO_3)_2Cl_3$
c2.3 – $K[Cu_3O](SeO_3)_2Cl$
c2.4 – $Na_2[Cu_7O_2](SeO_3)_4Cl_4$
c2.5 – $[NaCl][Cu(HSeO_3)_2]$
c2.6 – $[Cu^+Cl_2][Pb_2Cu^{2+}{}_9O_4](SeO_3)_4Cl_5$
c2.7 – $[Cu^+Cl_2][PbCu^{2+}{}_5O_2](SeO_3)_2Cl_3$
c2.8 – $K_{(1-x)}[Cu^+Cl_2][Pb_xCu^{2+}{}_{(6-x)}O_2](SeO_3)_2Cl_{(4-x)}$, $x = 0.20$
c3.1 – α–$PbNi(SeO_3)_2$
c3.2 – β–$PbNi(SeO_3)_2$
c3.3 – $PbNi_2(SeO_2OH)_2(SeO_3)_2$
c3.4 – α–$PbCo(SeO_3)_2$
c4.1 – β–$(V^{5+}{}_2O_3)(SeO_3)_2$
c4.2 – $Pb_2(V^{4+}O)(SeO_3)_3$
c4.3 – β–$Pb_4(V^{5+}{}_3O_8)_2(SeO_3)_3(H_2O)$
c5.1 – $Mn(SeO_4)(H_2O)_2$
c5.2 – $Mn_2[Bi_2O](SeO_3)_4$
c5.3 – $MnBi(SeO_3)_2Cl$
c5.4 – $Mn_4(Mn_5,Bi)(SeO_3)_8Cl_5$
c5.5 – $Bi_6(SeO_3)_4Cl_{10}$
c5.6 – β–$Bi(SeO_3)Cl$
c5.7 – $PbBi_{10}(SeO_3)_{12}Cl_8$
c6.1 – $[CH_6N]_2[(UO_2)(SeO_4)_2(H_2O)](H_2O)$
c6.2 – $[CH_6N]_2[(UO_2)(SeO_4)_2(H_2O)]$
c6.3 – $[CH_6N]_2[(UO_2)_2(SeO_4)_3]$
c6.4 – $[CH_6N](H_3O)[(UO_2)_2(SeO_4)_3(H_2O)](H_2O)$
c6.5 – $[CH_6N]_4[(UO_2)_3(SeO_4)_5](H_2O)_4$
c6.6 – $[CH_6N](H_5O_2)(H_3O)_2[(UO_2)_3(SeO_4)_5](H_2O)_4$
c6.7 – $[CH_6N]_4(H_3O)_2[(UO_2)_5(SeO_4)_8(H_2O)](H_2O)_4$
c6.8 – $[CH_6N]_{1.5}(H_5O_2)_{1.5}(H_3O)_3[(UO_2)_5(SeO_4)_8(H_2O)](H_2SeO_4)_{2.6}(H_2O)_3$
c6.9 – $[C_2H_8N]_2[(UO_2)(SeO_4)_2(H_2O)]$
c6.10 – $[C_2H_8N]_2[(UO_2)_2(SeO_4)_3(H_2O)]$
c6.11 – $[C_4H_{15}N_3][H_3O]_{0.5}[(UO_2)_2(SeO_4)_{2.93}(SeO_3)_{0.07}(H_2O)](NO_3)_{0.5}$

c6.12 – $[C_2H_8N]_3[H_5O_2][(UO_2)_2(SeO_4)_3(H_2O)_2]_2(H_2O)_5$

c6.13 – $[C_2H_8N]_2[H_3O][(UO_2)_3(SeO_4)_4(HSeO_3)(H_2O)](H_2SeO_3)_{0.2}$

c6.14 – $[C_4H_{12}N]_3[H_3O][(UO_2)_3(SeO_4)_5(H_2O)]$

c6.15 – $[C_2H_8N]_3(C_2H_7N)[(UO_2)_3(SeO_4)_4(HSeO_3)(H_2O)]$

c6.16 – $[C_2H_8N][(H_5O_2)(H_2O)][(UO_2)_2(SeO_4)_3(H_2SeO_3)](H_2O)$

c7.1 – $Fe_2(SeO_3)_3$

1 INTRODUCTION

Nowadays, in the domain of the fundamental studies and elaboration of novel crystalline materials investigations have been slowed down. Actual researchers' activity focuses on more lucrative projects dedicated to specific materials suitable for particular applications in electronics, nuclear, energy, space industries *etc*… In most of the cases, the following research scenario is based on the modifications and re-investigations of already well-known compounds in order to optimize their physical and chemical properties by doping, coating, shaping *etc*… the so-called "material science". The current situation leads to deficiencies of new atomic-scale architectures for the needs of a whole range of various material sciences with their increasing demands for novel materials based on specific crystal structures determining different innovating properties.

On the other hand, nature has not yet revealed all its own secrets concerning the origin and physical conditions of the crystal growth of all mineral species on the Earth. The structural architectures found in known crystalline compounds designed by nature's hand cover a whole range from *0D* to *3D* frameworks, and offer unexploited potentialities in terms of study of their innovating physical properties. The ways of natural formation of many mineral groups remains undiscovered. At the same time, researchers use a wide variety of synthetic methods in attempts to perceive the nature and to emulate the natural techniques in laboratory. For example, the *chemical vapour transport reactions method* provides a unique opportunity to model physical and chemical conditions existing in fumarolic environments and may be used not only to model exhalative processes, but also to predict possible mineral phases that may form

in fumaroles. In particular, the K-analogue of ilinskite, a rare mineral sublimate from the fumaroles of the Tolbachik volcano (Kamchatka peninsula, Russia), synthesized under the framework of the present study, is not known in Nature, whereas it may well form from volcanic gases in a K-rich local geochemical environment. This is just an isolated example among so many others.

This thesis is at the interface between solid-state chemistry and mineralogy. It is one of the first dedicated to the synthesis of various series of novel metal-oxide compounds using innovative so-called "geo-inspired" approach. Here we assume the emulation and modelling of natural crystal growth processes in order to obtain complex functional materials with a potential in terms of specific physical properties.

Over the past two decades, the chemistry of selenium-containing compounds has been developed intensively by many researchers, generating a large amount of experimental knowledge in various fundamental and applied research areas: in medicine [Rayman 2000], biochemistry [Tapiero et al. 2003], organic chemistry [Pyrzynska 1996], physical chemistry [Qu and Peng 2002; Hsu et al. 2008], nuclear technology [Puranen et al. 2010], Earth sciences [Mandarino 1994; Séby et al. 2001], and structural chemistry [Choudhury et al. 2002; Krivovichev et al. 2005a].

Selenium has been shown to be a versatile chemical element in terms of crystal chemistry. Depending on the growth conditions, selenium occurs in several oxidation states and is, therefore, redox sensitive, at the interface between anionic (Se^{2-}) and cationic (Se^{4+}, Se^{6+}) functions. The present work focuses on the Se oxide compounds in the oxidation states of +4 (selenites) and +6 (selenates) with broad structural diversifications. The field of selenides (Se^{2-}) essentially insoluble in water is out of the scope of this work. However, it should to be note that they are more prevalent in Nature (85 approved minerals by the International Mineralogical Association) than Se oxysalts.

In geochemical environments, selenites and selenates are relatively rare oxo-anion groups. By the end of the XX^{th} century, only 16 selenium oxysalts were known to occur naturally. Last twenty years have witnessed an impressive progress in the chemistry of natural selenium-based phases resulted in discovery of another 17 new minerals. It gives a total of 33 different mineral species approved by the International Mineralogical Association (IMA) to date. Natural selenites notably dominate selenates among known minerals, as probable result of the easy reduction processes of selenates to selenites and elemental selenium in aqueous environments.

The study of selenites and selenates has occupied scientists for over a century and a half. The first Se compound, so-called mineral "kerstenite" (discredited in 2006 by the IMA and referred to molybdenite or olsacherite), was sketchily described by *C. Kersten* in [Kersten 1839]. Nevertheless, although much chemical information about Se compounds has been reported in details so far, only a few reviews have been published. In 1994 *J. Mandarino* summarized geochemical characteristics of natural and synthetic selenites [Mandarino 1994]. Five years later *V. Verma* presented a complete review of synthetic, thermoanalytical, IR, Raman and X-ray studies on metal selenites [Verma 1999]. The absence of actual reviews on selenites and selenates prompted the present work as well. Here, we also tried to rationalize structural features and principles of crystal growth, an important task for the implementation and design of novel functional oxide materials.

Selenium atom has the electron configuration [Ar] $3d^{10}\ 4s^2\ 4p^4$, and, therefore, six valence electrons in the outermost shell. In the crystal structures of selenates, Se^{6+} are tetrahedrally coordinated by four O^{2-} resulted in $(Se^{6+}O_4)^{2-}$ anionic groups commonly described with two Se–O single and two Se=O double bonds. In selenites, Se^{4+} cation form a $(Se^{4+}O_3)^{2-}$ triangular pyramid with Se located at its apical corner, given as two Se–O single and one Se=O double bond. A lone electron pair is stereochemically active and acts as a complementary external ligand forming $(ESe^{4+}O_3)^{2-}$ tetrahedra (*E* – lone electron pair). Note curious exceptions in which lone electron pair directly bonds to metals observed *e.g.* in $BaCoAs_2O_5$ [David et al. 2014].The co-presence of such lone pairs combined with the electronic properties of other metals (transition, heavy, and actinide) in the structures of compounds leads to engaging inorganic chemistry. Furthermore, the interest to selenium oxide compounds has also been stimulated by the attempts to understand purely fundamental reasons for such structural diversity and its underlying crystal chemical mechanisms.

Inorganic copper oxoselenites attract considerable attention due to their fascinating structural and physical properties as well as mineralogical and geochemical importance. Of special interest are mixed-valence Cu^{+}–Cu^{2+} systems with separate symmetrically independent monovalent and divalent copper sites due to their contrasted coordinations combined in one crystal structure. The specific feature of many copper oxoselenites is the presence in their crystal structures of oxocentered (μ_4–O)Cu_4 tetrahedral units that polymerize to form extended structural complexes

[Krivovichev et al. 2013b]. In Section 2.2, we report on the structural characterization of eight novel copper oxoselenites inspired by mineralogical discoveries in such unusual geological conditions as volcanic fumaroles.

The research on ternary oxoselenite systems with lead and nickel/cobalt as transition metals constituents was not yet carried out. In Section 2.3, we present a scrupulous investigation of the crystal growth in the $PbO–NiO–SeO_2$ system in hydrothermal conditions. It led to the synthesis of four novel lead nickel/cobalt selenites.

The crystal chemistry of selenium-containing vanadates possesses specific structural properties due to the peculiar features of VO_4, VO_5 and VO_6 groups. In addition, this richness of coordination number is increased by the various valence states offered in the crystal structures [Evans and Hughes 1990; Schindler et al. 2000; Boudin et al. 2000]. The incorporation of asymmetric selenite groups and heavy cations, such as Pb^{2+}, with stereochemically active lone electron pairs into the structures of vanadates could result in a formation of structural cavities leading to materials with open architectures. In Section 2.4, we describe the pathways for synthesis of lead vanadate selenites, report on crystal structures of three novel phases, and discuss the phenomenon of polymorphism in vanadate selenites.

Section 2.5 contains a structural characterization of seven new compounds: one manganese selenate, three bismuth selenites, and three manganese bismuth selenites. The last three phases are the first examples of oxide compounds containing both bismuth and manganese cations.

Sixteen novel uranyl selenates and mixed valence selenite-selenates discussed in Section 2.6 demonstrate an exceptional structural diversity, which is studied using a graph theory. The diversity of polyhedral units found in uranyl selenates and selenite-selenates formed by polymerization of U and Se coordination polyhedra is unique: starting from isolated complexes to nanotubules [Krivovichev et al. 2005b; Krivovichev et al. 2005a; Alekseev et al. 2008]. The topology and geometry of these units is controlled by a number of factors governing interactions between organic and inorganic substructures, *i.e.* hydrophillic-hydrophobic interactions, charge-density matching and weak hydrogen bonding. Composition–structure relationships in uranyl selenates and selenite-selenates is rationalized using the principle of dimensional reduction previously

proposed by *J. Long et al.* [Long et al. 1996; Tulsky and Long 2001; Alekseev et al. 2007; Krivovichev 2009].

In Section 2.7, the analogy between lone electron pairs of selenite groups and H–P bonds of the phosphite anions is discussed through two isotypic compounds, $Fe_2(SeO_3)_3$ and $Fe_2(HPO_3)_3$. It demonstrates that in solids containing $(HPO_3)^{2-}$ and $(ESeO_3)^{2-}$ anions, the H atom is negatively charged and possesses a partial hydridic character in the phosphites.

The present work was carried out under the framework of the international co-tutorial thesis project between St. Petersburg State University (Russia) and University of Lille 1 (France). It contains the results of syntheses, and crystal chemical characterization of 39 novel oxide compounds containing selenium in the oxidation states of +4 and +6.

Brief overview is provided in Part 2 of the thesis. It is subdivided into seven parts:

1. Objects and methods
2. Crystal chemical studies of copper selenites
3. Crystal chemical studies of nickel and cobalt selenites
4. Crystal chemical studies of vanadium selenites
5. Crystal chemical studies of selenium compounds with manganese and bismuth
6. Crystal chemical studies of uranyl selenates and selenite-selenates
7. Analogy between electron lone pairs of selenites and H–P bonds in phosphites

Detailed description of the theoretical and experimental results can be found in 8 original papers appended at the end of the present thesis.

2 BRIEF DESCRIPTION OF RESULTS

This work presents the results of synthetic, and crystal chemical characterization of a large variety of novel oxide crystalline compounds containing selenium in the oxidation states of +4 and +6. These two states are characterized by different oxo-anions, namely $(SeO_3)^{2-}$ and $(SeO_4)^{2-}$. Within the framework of this thesis, an innovative so-called "geo-inspired" approach assumed emulation and modelling of natural crystal growth processes was applied. For the crystal chemical studies we used either a traditional descriptive procedure based on consideration of the crystal structures in terms of coordinations of cations, or the modern theory of anion-centered tetrahedra [Krivovichev et al. 2013b] developed by the St. Petersburg school of crystallography and the UCCS group of solid-state chemistry in Lille, in cases when the traditional structural interpretation does not reflect basic principles of structural architecture. Experimental details for all studied phases are discussed in relevant chapters.

2.1 Objects and methods

Crystalline samples studied in the present work were synthesized and characterized in the University of Lille 1, Unité de catalyse et chimie du solide (France), and the St. Petersburg State University, Department of crystallography (Russia).

In the present work, we used several methods to synthesize the crystalline products, which were selected due to their analogy with crystallogenetic chemical processes occurring in nature. In particular, the *chemical vapour transport reactions*

(CVT reactions) [Binnewies et al. 2013] were used for synthesis of a series of copper oxoselenites, bismuth selenite oxochlorides, and one vanadate selenite. This method can be considered as modelling of the natural environments, *e.g.* where copper oxoselenites are formed from the condensation of volcanic gases emanating from cooling magmatic chambers deep under the Earth's surface long after the period of eruptive activities. Likely, during these volcanic CVT reactions the selenites and metal halides play the role of transport agents as it was originally suggested by *Filatov et al.* [Filatov et al. 1992].

The crystalline samples of lead nickel/cobalt selenites, lead vanadate selenites, and one manganese bismuth selenite were prepared by using the *hydrothermal techniques*. The aqueous reactions were performed in 23 ml Teflon-lined autoclaves that were heated in mechanical convection ovens. Although the thermal treatment varied from one phase to another, in general, the autoclaves were held static for several days, followed by controlled slow cooling to room temperature. This kind of process is regarded as similar to that known from the oxidation zones of mineral deposits at small depths or subsurface zones, where most of known natural selenium oxysalts are formed.

For synthesis of a large series of uranyl selenates and selenite-selenates the *isothermal evaporation* from aqueous solutions under ambient conditions was applied. Analogous process of oxidation of high-level radioactive liquid waste (created by the reprocessing of spent nuclear fuel) accompanying the decay of unstable uranium isotopes results in their release into the environment and formation of various crystalline uranyl compounds containing different elements formed in thermal fission. Although ^{79}Se isotope exists in spent nuclear fuel as a fission product in small amount (<0.05% [Choppin 2001]), its long half-life of $3.27 \cdot 10^5$ years [Jörg et al. 2010] combined with its high mobility leads to wide geochemical and mineralogical abundance of selenium-containing uranyl complexes in the oxidation zones of uranium deposits and the areas of deep geological repositories for disposal of radioactive wastes.

Single-crystal X-ray diffraction data for novel phases were collected using a Stoe IPDS II Image-Plate X-ray diffractometer (University of St. Petersburg, Russia), a Bruker DUO APEX II CCD four-circle diffractometer with a Mo-IμS micro-focus tube (University of St. Petersburg, Russia; University of Lille 1, France), and a Bruker X8 APEX II CCD diffractometer with a fine-focus X-ray tube (University of Lille 1, France). More than a hemisphere of *3D* data were collected for each crystal using monochromatic MoK_α X-radiation, λ = 0.71073 Å.

The crystal structures were solved by direct methods and refined by means of the SHELX program package [Sheldrick 2008]. The final structural models were checked for missing symmetry operations using the PLATON program [Spek 2009]. For convenience, sometimes JANA 2006 [Petříček et al. 2014] and the charge filling method implemented in SUPERFLIP [Palatinus and Chapuis 2007] was also used. The final models included all atomic positional parameters and anisotropic-displacement parameters for atoms in all studied crystal structures.

Powder X-ray diffraction analyses of the powder samples were performed at room temperature using a D8 Advance Bruker AXS diffractometer, CuK_α X-radiation, λ = 1.5418 Å (University of Lille 1, France).

Infra-red absorption spectra were measured between 4000 and 400 cm^{-1} with a Perkin–Elmer Spectrum Two spectrometer equipped with a diamond attenuated total reflectance (ATR) accessory (University of Lille 1, France).

Scanning electron microscope and energy-dispersive X-ray (SEM/EDS) analyses were performed on a HITACHI S4700 microscope at 20 kV acceleration voltage and a current of 15 μA at different magnifications (University of Lille 1, France). The ratios were determined using a semi-quantitative routine deconvolution.

The magnetic properties of the samples were analysed in collaboration with Dr. Silviu Colis at the Institut de Physique et Chimie des Matériaux de Strasbourg (IPCMS, France) using a MPMS SQUID-VSM (Quantum Design) magnetometer in a temperature and field range of 1.8–300 K and 0–7 T. The susceptibility versus temperature was measured under 0.02 T after the sample was cooled in a field of 0.1 T (FC) or in zero field (ZFC). In some cases, the powders were previously magnetically "aligned" at 7 T in a polymeric gel that freezes the particle orientation below ~303 K.

Multiphoton SHG microscopy measurements on single crystals have been carried out in collaboration with Dr. Christine Terryn at Plateforme Imagerie Cellulaire et Tissulaire, Université de Reims (France). A laser-scanning microscope LSM 710 NLO Zeiss was used for the measurements with the excitation provided by a CHAMELEON femtosecond Titanium-Sapphire laser set at 860 nm, tuning the power until SHG was detected on selected single crystal samples deposited on a glass plate. Samples were imaged with a 20x, 0.8 NA objective lens. Emitted signal of SHG was collected with a band-pass filter (420 to 440 nm).

2.2 Crystal chemical studies of copper selenites

Crystallographic data and experimental parameters for the crystal structures of eight novel compounds listed below are summarized in Table 2.1.

c2.1 – $K[Cu_5O_2](SeO_3)_2Cl_3$
c2.2 – $Na[Cu_5O_2](SeO_3)_2Cl_3$
c2.3 – $K[Cu_3O](SeO_3)_2Cl$
c2.4 – $Na_2[Cu_7O_2](SeO_3)_4Cl_4$
c2.5 – $[NaCl][Cu(SeO_2OH)_2]$
c2.6 – $[Cu^+Cl_2][Pb_2Cu^{2+}{}_9O_4](SeO_3)_4Cl_5$
c2.7 – $[Cu^+Cl_2][PbCu^{2+}{}_5O_2](SeO_3)_2Cl_3$
c2.8 – $K_{(1-x)}[Cu^+Cl_2][Pb_xCu^{2+}{}_{(6-x)}O_2](SeO_3)_2Cl_{(4-x)}$, $x = 0.20$

TABLE 2.1 Crystallographic data and refinement parameters for **c2.1**, **c2.2**, **c2.3**, **c2.4**, **c2.5**, **c2.6**, **c2.7**, and **c2.8**

	c2.1	**c2.2**	**c2.3**	**c2.4**	**c2.5**	**c2.6**	**c2.7**	**c2.8**
M_r (g mol^{-1})	749.07	732.96	535.09	1172.40	755.83	1869.77	2103.20	1992.64
sp. gr.	*Pnma*	*Pnma*	*P*–1	*P*–1	*C*2/*c*	*C*2/*m*	*C*2/*m*	*C*2/*m*
a (Å)	18.1691(6)	17.749(2)	7.6821(5)	7.4362(6)	13.9874(7)	18.605(17)	18.4956(4)	15.116(1)
b (Å)	6.4483(2)	6.4412(6)	8.1179(5)	8.3361(7)	7.2594(4)	6.204(6)	6.1454(1)	6.1853(4)
c (Å)	10.5684(4)	10.488(1)	8.7836(6)	9.134(1)	9.0421(5)	12.673(11)	15.2985(4)	9.2672(9)
α (°)	90	90	113.19(1)	110.28(1)	90	90	90	90
β (°)	90	90	108.73(1)	106.21(1)	127.04(1)	109.87(2)	119.31(1)	95.965(5)
γ (°)	90	90	98.245(4)	105.16(1)	90	90	90	90
V (Å^3)	1238.19(7)	1199.0(2)	453.32(5)	467.94(8)	732.81(7)	1376(2)	1516.3(1)	861.7(1)
Z	4	4	2	1	2	2	2	1
ρ (g/cm^3)	4.018	4.060	3.920	4.160	3.425	4.514	4.607	3.840
μ (mm^{-1})	15.333	15.523	15.757	16.263	13.313	25.78	25.02	15.52
λ (MoKα) (Å)	0.71073	0.71073	0.71073	0.71073	0.71073	0.71073	0.71073	0.71073
total rflns	9584	7946	5607	11190	3926	12055	8423	5430
indep rflns	2233	2042	1749	2842	1170	3370	2841	1479
R_{int}	0.027	0.098	0.050	0.047	0.026	0.093	0.025	0.030
R_1 [I > 2σ(I)]	0.018	0.049	0.048	0.027	0.021	0.035	0.028	0.045
wR_2 [I > 2σ(I)]	0.040	0.065	0.117	0.060	0.051	0.040	0.077	0.116
R_1 [all data]	0.023	0.099	0.080	0.032	0.030	0.095	0.029	0.061
wR_2 [all data]	0.041	0.077	0.133	0.062	0.053	0.048	0.078	0.125
GOF	1.035	0.991	1.014	1.070	1.081	0.716	1.126	1.070
$\Delta\rho_{max}$, $\Delta\rho_{min}$, (e Å^{-3})	0.74, −0.77	1.62, −1.67	1.62, −1.62	0.85, −0.95	0.70, −0.65	1.75, −1.86	4.19, −3.39	4.25, −1.99

2.2.1 Synthetic procedures

Single crystals of all novel copper selenites were prepared by the chemical vapour transport (CVT) reactions. In the course of the CVT reactions, a precursor is partially transported by a gaseous agent from a source zone to a deposition zone under the action of a temperature gradient. The general scheme of the CVT method is shown in Figure 2.1a.

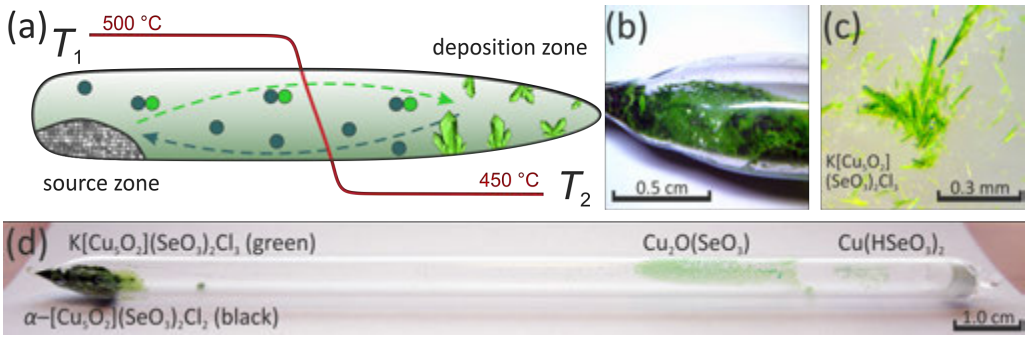

FIGURE 2.1 General scheme of the CVT method – (a), the source zone of the tube – (b), the crystals of $K[Cu_5O_2](SeO_3)_2Cl_3$ (**c2.1**) picked out from the source zone – (c), and a common view of the sealed silica tube after the CVT synthesis – (d)

Mixtures of initial reagents in a various molar ratios (Table 2.2) were ground and loaded into silica tubes (*ca.* 15 cm), which were further evacuated to 10^{-2} mbar and sealed. The tubes were placed horizontally into a tubular two-zone furnace, heated to 500–550 °C for 3–4 days and subsequently slowly cooled to room temperature. The temperature gradient between the source (hot) and deposition (cold) zones of the tube in the furnace was about 50 °C.

Crystals of novel phases were observed in the different zones of the tubes in association with already known compounds are shown in Figure 2.1d.

TABLE 2.2 Experimental details of the CVT syntheses of **c2.1**, **c2.2**, **c2.3**, **c2.4**, **c2.5**, **c2.6**, **c2.7**, and **c2.8**

molar ratios:	**c2.1**	**c2.2**	**c2.3**	**c2.4**	**c2.5**	**c2.6**	**c2.7**	**c2.8**
SeO_2	2	2	2	2	2	1	1	1
CuO	4	4	4	4	4	0	2	2
$CuCl_2$	1	1	1	1	1	2.25	1.50	1.50
CuCl	0	0	0	0	0	1.25	0	0
KCl	1	0	3	0	0	0	0	1

TABLE 2.2 *Continued*

molar ratios:	**c2.1**	**c2.2**	**c2.3**	**c2.4**	**c2.5**	**c2.6**	**c2.7**	**c2.8**
NaCl	0	1	0	3	3	0.50	1	0
PbO	0	0	0	0	0	0.75	0.50	0.50
conditions:	**c2.1**	**c2.2**	**c2.3**	**c2.4**	**c2.5**	**c2.6**	**c2.7**	**c2.8**
temperature (°C)	500	500	500	500	500	500	550	550
time (h)	72	72	72	72	72	96	72	72
cooling (h)	24	24	24	24	24	12	6	6

2.2.2 Structural description of eight novel phases

$A[Cu_5O_2](SeO_3)_2Cl_3$ ($A = K^+, Na^+$)

$K[Cu_5O_2](SeO_3)_2Cl_3$ (**c2.1**) and $Na[Cu_5O_2](SeO_3)_2Cl_3$ (**c2.2**), are isotypic and represent synthetic analogues of natural Na-ilinskite [Vergasova et al. 1997; Krivovichev et al. 2013a]. The crystal structures of **c2.1** (K) and **c2.2** (Na) contain four symmetrically independent copper sites with different mixed-ligand coordination environments. The Cu(1) site is coordinated by five ligands to form {Cu[(4O)+Cl]} square pyramids. The Cu(3) site has a distorted [3O+Cl] square coordination. The coordinations of the Cu(2) and Cu(4) sites in **c2.1** (K) and **c2.2** (Na) are different as due to the shift of the Cl(3) site induced by the greater size of the K^+ cations compared to Na^+. Thus, the Cu(2) site has a distorted square pyramidal [(3O+Cl)+Cl] coordination in **c2.2** (Na), and a distorted [(3O+Cl)+2Cl] octahedral environment in the crystal structure of **c2.1** (K). The Cu(4) atom possesses an octahedral [(4O)+2Cl] coordination in **c2.2** (Na), whereas the shift of the Cl(3) atoms is influenced by larger size of K^+ cations in **c2.1** (K) results in the change of a coordination polyhedron of Cu(4) to a five-fold square {Cu[(4O+Cl)]} pyramid with one axial Cu(4)–Cl(3) bond, analogous to the environment of the Cu(1) sites in both structures. There are two symmetrically independent selenium sites in the crystal structures of **c2.1** (K) and **c2.2** (Na), which have typical oxygen coordination of triangular pyramid with a stereochemically active lone pair of electrons as a complementary ligand. The arrangement of coordinating ligands of Na^+ in **c2.2** (Na) consists of one oxygen and four chlorine atoms, forming a distorted {Na[(O+2Cl)+2Cl]} trigonal bipyramid. K^+ cations in **c2.1** (K) are surrounded by five oxygen and four chlorine atoms each.

Interestingly, the crystal structures of **c2.1** (K) and **c2.2** (Na) contain "additional" oxygen atoms, which are coordinated solely by Cu^{2+} cations, resulting in the formation of oxocentered $(OCu_4)^{6+}$ tetrahedra. The $(OCu_4)^{6+}$ tetrahedra share common corners to form the $[Cu_5O_2]^{6+}$ sheets parallel to (100) (Figure 2.2). The $[Cu_5O_2]^{6+}$ sheets in the crystal structures of **c2.1** (K) and **c2.2** (Na) are surrounded by selenite triangular pyramids and chlorine anions to produce a microporous framework. The pores are filled by alkali metal cations and lone pairs of electrons of the selenite groups. Detailed description of the crystal structures of **c2.1** (K) and **c2.2** (Na) can be found in the article **A-VII** (*see* Included Articles).

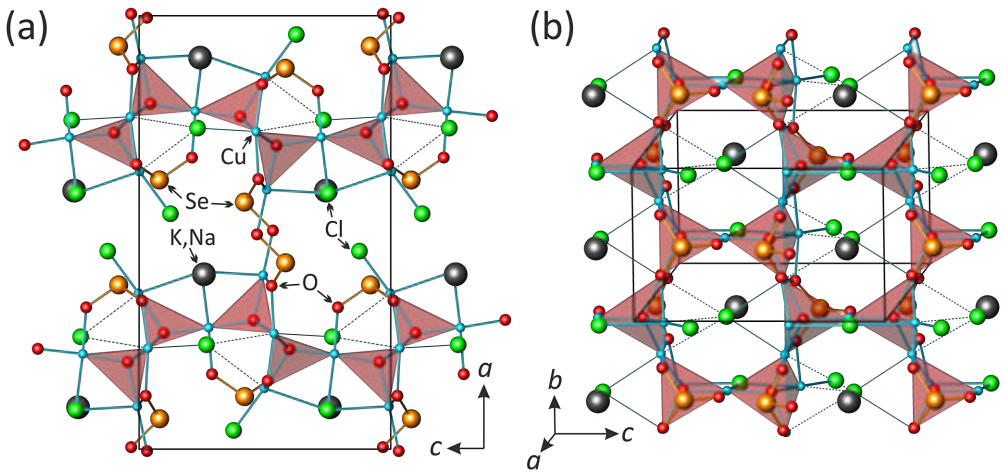

FIGURE 2.2 The crystal structures of $A[Cu_5O_2](SeO_3)_2Cl_3$ ($A^+ = K^+$ (**c2.1**), Na^+ (**c2.2**)) in two different projections featuring side and top view of the $[O_2Cu_5]^{6+}$ sheet of oxocentered $(OCu_4)^{6+}$ tetrahedra highlighted by red colour

$K[Cu_3O](SeO_3)_2Cl$ and $Na_2[Cu_7O_2](SeO_3)_4Cl_4$

The structure of $K[Cu_3O](SeO_3)_2Cl$ (**c2.3**) contains three symmetrically independent Cu^{2+} sites. The Cu(1) site is surrounded by four O and one Cl atoms to form an unusual distorted trigonal bipyramid in a {Cu[(2O+Cl)+2O]} coordination. The Cu(2) atom has a typical planar-square [(4O)] coordination. The coordination polyhedron of Cu(3) can be described as a distorted {Cu[(4O)+(O+Cl)]} octahedron. All these various Cu coordination polyhedra are combined into sheets parallel to (001). The structure of **c2.3** contains two symmetrically independent Se^{4+} cations that form typical $(SeO_3)^{2-}$

triangular pyramids. The K^+ cation is coordinated by seven O^{2-} and two Cl^- anions in a distorted arrangement.

In the crystal structure of $Na_2[Cu_7O_2](SeO_3)_4Cl_4$ (**c2.4**), there are four symmetrically independent Cu sites. The Cu(1) site forms a {Cu[(4O)]} square, similar to the Cu(2) site in the structure of **c2.3**. The Cu(2) and Cu(4) sites are coordinated by three O and one Cl to form {Cu[(3O+Cl)]} planar squares. The same [(3O+Cl)] coordination has been also observed in the crystal structures of **c2.1** and **c2.2**. The Cu(3) site in the crystal structure of **c2.4** has a triangular bipyramidal [(2O+Cl)+2O] coordination Two symmetrically independent Se sites form typical $(SeO_3)^{2-}$ trigonal pyramids. The symmetrically unique Na^+ cation is surrounded by six O^{2-} and one Cl^- anion to form an approximately triangular prismatic oxygen environment.

In the crystal structure of **c2.3**, two $(OCu_4)^{6+}$ tetrahedra share a common Cu···Cu edge to form the $[O_2Cu_6]^{8+}$ dimer, while in **c2.4** $[O_2Cu_7]^{10+}$ dimeric units and formed by two $(OCu_4)^{6+}$ tetrahedra sharing a common Cu atom. The selenite groups and Cl atoms surround these dimers to form the $\{[O_2Cu_6](SeO_3)_4Cl_2]\}^{2-}$ and $\{[O_2Cu_7](SeO_3)_4Cl_4]\}^{2-}$ structural units in **c2.3** and **c2.4**, respectively, which are further interconnected into sheets (Figure 2.3).

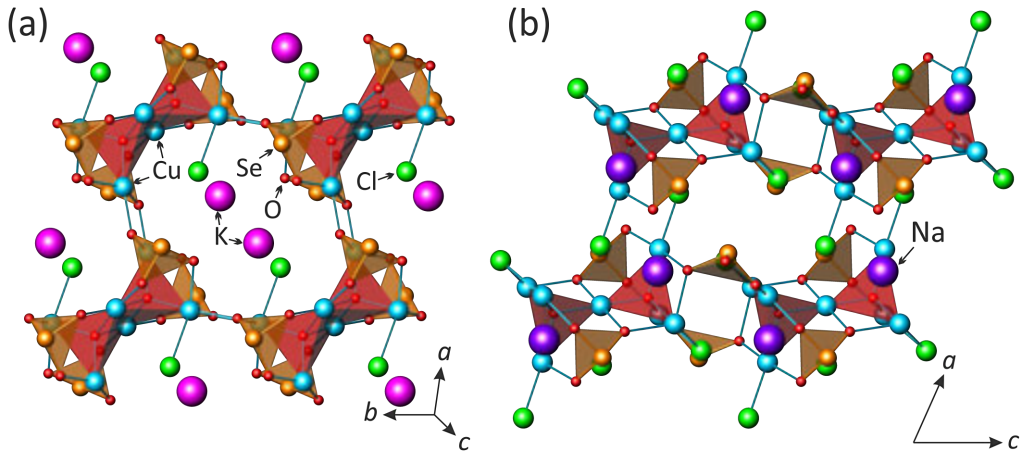

FIGURE 2.3 The crystal structures of $K[Cu_3O](SeO_3)_2Cl$ (**c2.3**) and $Na_2[Cu_7O_2](SeO_3)_4Cl_4$ (**c2.4**). The $(OCu_4)^{6+}$ tetrahedra are highlighted by red colour

The interlayer space is occupied by the alkali cations. A comparison of the mode of linkage of $(SeO_3)^{2-}$ with the oxocentered dimers in known copper oxoselenites is given in the Chapter 2.2.3.

[NaCl][Cu(SeO₂OH)₂]

The crystal structure of [NaCl][Cu(SeO₂OH)₂] (**c2.5**) contains one symmetrically independent Cu site octahedrally coordinated by four O and two Cl atoms. The Cu site forms a CuO_4 square complemented by two long Cu–Cl bonds resulting in a [(4O)+(2Cl)] coordination observed for Cu(4) in the structure of **c2.2**. There is one Se site coordinated by three O atoms to form a trigonal SeO_3 pyramid typical for selenites. One of the three Se–O bonds is elongated compared to two other bonds owing to the protonation of the $O_h(1)$ site. The CuO_4 squares and SeO_2OH groups share common oxygen atoms to form electroneutral $[Cu(SeO_2OH)_2]^0$ sheets parallel to the (100) plane (Figure 2.4). Between two $(SeO_2OH)^-$ group the $O_h(1)\cdots O(2)$ hydrogen bond creates a $[(SeO_2OH)_2]^{2-}$ dimer that provides additional stabilization of the copper diselenite sheet.

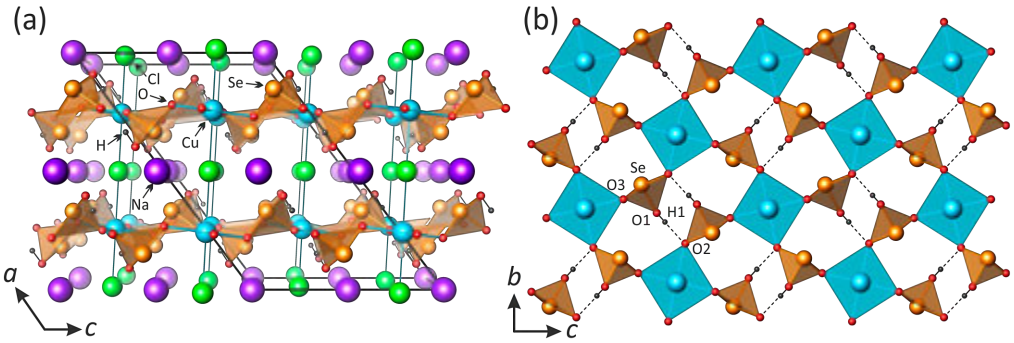

FIGURE 2.4 Projections of the $[Cu(HSeO_3)_2]^0$ sheet (a) and the crystal structure of [NaCl][Cu(HSeO₃)₂] (**c2.5**) featuring two-dimensional $[Cu(HSeO_3)_2]$ sheets with intercalated –Na–Cl–Na– chains

In the crystal structure of **c2.5**, the $[Cu(HSeO_3)_2]^0$ sheets alternate with the sheets consisting of zigzag –Na–Cl–Na–Cl– chains formed by Cl atoms and disordered Na sites. The chains are parallel to the *c*-axis. The linkage between the alternating electroneutral $[Cu(HSeO_3)_2]^0$ and $[NaCl]^0$ sheets is provided by the Cu–Cl and Na–O bonds. The coordination of Na is fivefold and consists of three O and two Cl atoms.

The **c2.5** compound can be considered as a member of the series of compounds based upon the $M(SeO_2OH)_2$ sheets (M = Cu^{2+}, Co^{2+}, Cd^{2+}). The prototype structure for this group is $[Cu(SeO_2OH)_2]$ [Effenberger 1985] that does not have any chemical species separating the copper hydroselenite sheets. In other compounds, the interlayer space between the $[Cu(SeO_2OH)_2]^0$ sheets is occupied by structural units of different complexity. In all the compounds, the $[Cu(SeO_2OH)_2]^0$ sheets have approximately the same planar dimensions (measured as distances between a couple of atoms related by symmetry operations), except for $[Cu(SeO_2OH)_2](H_2O)_2$ [Lafront and Trombe 1995], where the sheets are strongly corrugated. Detailed description of **c2.5** can be found in the article **A-VIII** (*see* Included Articles).

$[Cu^+Cl_2][Pb_2Cu^{2+}{}_9O_4](SeO_3)_4Cl_5$, $[Cu^+Cl_2][PbCu^{2+}{}_5O_2](SeO_3)_2Cl_3$, and $K_{(1-x)}[Cu^+Cl_2][Pb_xCu_{(6-x)}O_2](SeO_3)_2Cl_{(4-x)}$, x = 0.20

The crystal structures of these three compounds are very unusual owing to the incorporation of linear $(Cu^+Cl_2)^-$ units in the voids of a pseudo honeycomb sheets made of oxo-centetred $(O(Cu/Pb)_4)^{6+}$ tetrahedra and $(SeO_3)^{2-}$ groups. In $[Cu^+Cl_2][Pb_2Cu_9O_4](SeO_3)_4Cl_5$ (**c2.6**), $[Cu^+Cl_2][PbCu_5O_2](SeO_3)_2Cl_3$ (**c2.7**), and $K_{(1-x)}[Cu^+Cl_2][Pb_xCu^{2+}{}_{(6-x)}O_2](SeO_3)_2Cl_{(4-x)}$, x = 0.20 (**c2.8**), Cu^+ cations form two relatively short Cu^+–Cl bonds, which result in the formation of tightly bonded $(Cu^+Cl_2)^-$ anionic groups that can be considered as separate structural entities. The Cu^{2+} cations have mixed oxochloride coordinations with typical trends of Jahn-Teller d^9 ions. The Cu(1) and Cu(2) sites in **c2.6**, the Cu(4) site in **c2.7**, and Cu(3) site in **c2.8** form distorted {Cu[(4O)+(2Cl)]} octahedra similar to those found for Cu(4) and Cu(1) in the structures of **c2.2** and **c2.5**, respectively. The Cu(3) site in **c2.6**, the Cu(2) and Cu(3) sites in **c2.7**, and the Cu(1) site in **c2.8** are octahedrally [(3O+Cl)+2Cl] coordinated with CuO_3Cl squares complemented by two long Cu–Cl bonds. The same coordination was observed for Cu(2) in the structure of **c2.1**. The Cu(4) site in **c2.6** forms a trigonal {Cu[(3O)+(O+Cl)]} bipyramids, whereas the Cu(1) site in **c2.7** and the Cu(4) site in **c2.8** are [(2O+Cl)+(O+Cl)] coordinated. The Pb atoms have asymmetrical coordinations consisting of three strong Pb–O bonds located in one coordination hemisphere and four long Pb–Cl in another. This coordination of Pb^{2+} cations is consistent with the presence of stereoactive lone electron pairs. Se^{4+} cations form standard $(SeO_3)^{2-}$ selenite triangular pyramidal oxoanions. The structure of **c2.8** has one

symmetrically independent K site with the site-occupation factor (s.o.f.) equal to 0.8. Its coordination polyhedron can be described as a distorted hexagonal bipyramid.

In the crystal structure of **c2.6** there are two additional O atoms, that form (OCu^{2+}_3Pb) and (OCu^{2+}_4) tetrahedra, respectively. The oxocentered tetrahedra share common corners to form $[O_4Pb_2Cu^{2+}_9]^{14+}$ double chains. These chains are growing parallel to the *b*-axis, and its common value for the three compounds ($b \approx 6.2$ A) denotes similar arrangement between the oxocentered building units in the full series. These types of chains of anion-centered tetrahedra are original and have not been observed in inorganic compounds previously. The SeO_3 groups are attached to the triangular bases of oxocentered tetrahedra that results in formation of *1D* $\{[O_4Pb_2Cu^{2+}_9](SeO_3)_4\}^{6+}$ complex interconnected *via* Pb–O bonds into *2D* metal-oxide double sheets (Figure 2.5a). The projection of the sheets in the (*b*,*c*) plane leads to a honeycomb-like lattice of tetrahedra (Figure 2.5b). In contrast, monometallic $[O_2Cu_5]$ honeycomb-sheets are reported in several compounds based upon anion-centered tetrahedra [Krivovichev et al. 2013b].

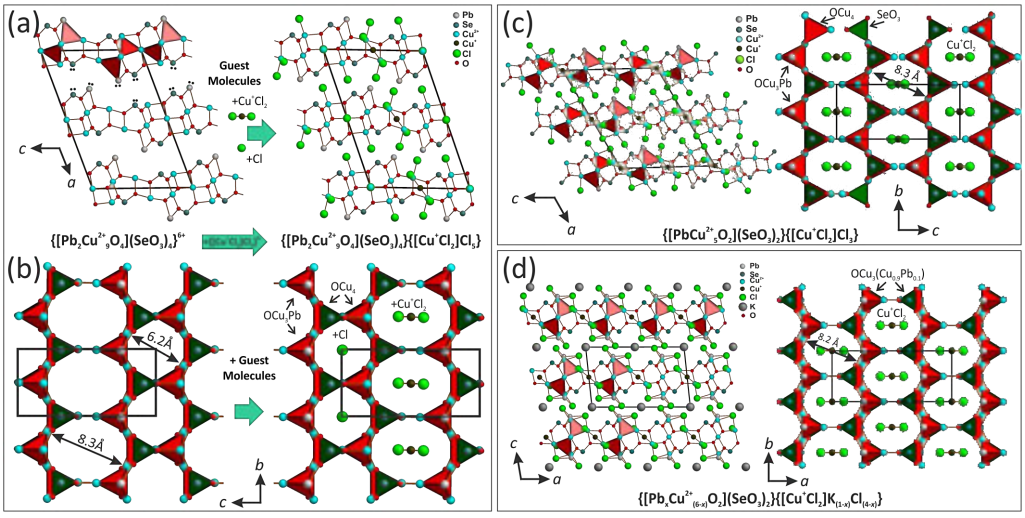

FIGURE 2.5 Projections of the structures of $[Cu^+Cl_2][Pb_2Cu_9O_4](SeO_3)_4Cl_5$ (**c2.6**) – (a) and (b), $[Cu^+Cl_2][PbCu_5O_2](SeO_3)_2Cl_3$ (**c2.7**) – (c), and $K_{(1-x)}[Cu^+Cl_2][Pb_xCu^{2+}_{(6-x)}O_2](SeO_3)_2Cl_{(4-x)}$, $x = 0.20$ (**c2.8**) – (d)

The sheets are surrounded by Cl^- anions in the interleaves and accommodate both linear $[Cu^+Cl_2]^-$ anions and Cl^- ions in the larger and smaller honeycomb windows,

respectively. Taking into account the relative strength of the Cu^{+}–Cl bonds and weak interactions between them and the rest of the structure, these units may be considered as guest anions embedded in the complex metal oxochloride matrix based upon anion-centered tetrahedra.

A very similar 'host-guest' principle is at work in the structures of **c2.7** and **c2.8** as well. Here, the (OCu^{2+}_3Pb) and (OCu^{2+}_4) tetrahedra share corners to produce single chains extending along the common *b* parameter that have the $[O_2PbCu_5]^{8+}$ and $[O_2Pb_xCu^{2+}_{(6-x)}]^{8+}$ compositions, respectively. The experimental partial Pb^{2+} for Cu^{2+} substitution is allowed by the oxocentered framework in this particular topology. Together with SeO_3 groups, these chains form *1D* $\{[O_2M_6](SeO_3)_2\}^{4+}$ metal-oxide (M = Cu^{2+}, Pb^{2+}) backbones of the structures that are arranged to form pseudo honeycomb sheets (Figure 2.5c, d). Due to the elementary single-chains, only large honeycomb windows are created that accommodate the $(Cu^{+}Cl_2)^{-}$ guest anions as observed in **c2.6**. The structure of **c2.8** contains additional K^{+} cations located in the interlayer space between the metal oxoselenite chloride sheets. In all three structures, lone electron pairs on the Pb^{2+} and Se^{4+} cations are oriented toward the interlayer space, thus conforming the 'chemical scissor' principle of structural organization in compounds with lone electron pair cations. Detailed description of the crystal structures of **c2.6**, **c2.7**, and **c2.8** can be found in the article **A-V** (*see* Included Articles).

2.2.3 Linkage of selenite groups with $[OCu_4]^{6+}$ dimers

The novel compounds **c2.3** and **c2.4** are the new members of a structural family of minerals and synthetic compounds (Table 2.3) characterized by dimers composed of edge-sharing $(O(Cu/Pb)_4)^{6+}$ tetrahedra polymerized into $[O_2(Cu/Pb)_6]^{8+}$ units or corner-sharing $(OCu_4)^{6+}$ tetrahedra into $[O_2Cu_7]^{10+}$ units. Figure 2.6 provides an overview of the observed coordination environments of the dimers of oxocentered tetrahedra in the crystal structures of related copper minerals and synthetic compounds. Existence and frequent occurrence of such oxocentered units in different structures provides an indirect evidence for the importance of such units as pre-nucleation building blocks existing in gaseous media as it occurs in volcanic fumaroles or evacuated silica ampoules used in the CVT method.

TABLE 2.3 Crystallographic data for minerals and inorganic copper compounds based upon dimers composed of oxocentered tetrahedra

Cu:O	Fig.	Chemical formula	Mineral	Space group	*a* (Å); *α* (°)	*b* (Å); *β* (°)	*c* (Å); *γ* (°)	*V* (Å^3)	Ref.
6:2	2.6a	$K[Cu_3O](SeO_3)_2Cl$		*P*–1	7.682; 113.2	8.118; 108.7	8.784; 98.2	453	**c2.3**
6:2	2.6a	$Cu[Cu_3O](SeO_3)_3$–I		$P2_1/a$	15.990	13.518; 90.5	17.745	3836	[1]
6:2	2.6b	$Cu[Cu_3O](SeO_3)_3$–II		*P*–1	7.992; 77.3	8.141; 66.6	8.391; 81.4	484	[1]
6:2	2.6c	$KPb_{0.5}Cu[PbCu_5O_2]$ $Zn(SeO_3)_2Cl_{10}$	prewittite	*Pnnm*	9.132	19.415	13.213	2343	[2]
6:2	2.6d	$NaK[Cu_3O](SO_4)_3$	euchlorine	*C*2/*c*	18.41	9.43; 113.7	14.21	2259	[3]
6:2	2.6d	$K_2[Cu_3O](SO_4)_3$	fedotovite	*C*2/*c*	19.037	9.479; 111.0	14.231	2397	[4]
6:2	2.6e	$(NMe_2H_2)_4[Cu_6O_2]$ $(SO_4)_6(DMF)_4$		$P2_1/n$	13.105	10.514; 103.2	18.753	2516	[5]
6:2	2.6f	$(NMe_2H_2)_4[Cu_6O_2]$ $(SO_4)_6(DMF)_2$		*P*–1	8.588; 106.5	10.684; 104.6	12.817; 105.9	1012	[5]
7:2	2.6h	$KCd[Cu_7O_2](SeO_3)_2Cl_9$	burnsite	$P6_3/mmc$	8.781	8.781	15.521	1036	[6]
7:2	2.6g	$Na_2[Cu_7O_2](SeO_3)_4Cl_4$		*P*–1	7.436; 110.3	8.336; 106.2	9.134; 105.2	468	**c2.4**

References: 1 – [Effenberger and Pertlik 1986]; 2 – [Shuvalov et al. 2013]; 3 – [Scordari and Stasi 1990]; 4 – [Starova et al. 1991]; 5 – [Burrows et al. 2012]; 6 – [Krivovichev et al. 2002; Burns et al. 2002].

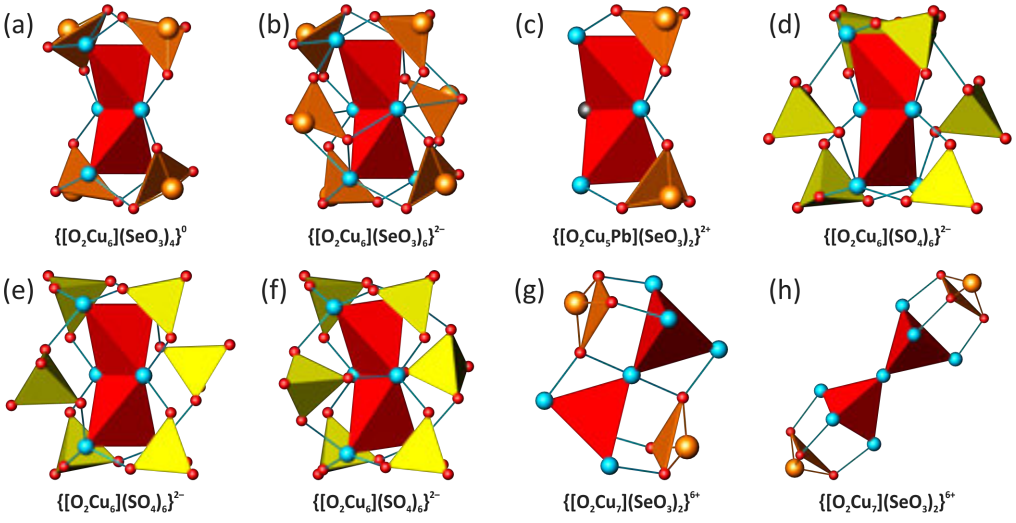

FIGURE 2.6 Coordination environment of the dimers composed of oxocentered tetrahedra in the crystal structures of different minerals and synthetic compounds listed in Table 2.3

2.3 Crystal chemical studies of nickel and cobalt selenites

Here we continue to consider divalent transition metals in which the Jahn-Teller effect characteristic for metallic cation is more or less pronounced depending on its coordination. One of the goals was to explore topologies of selenite compounds in which the transition metal adopts an octahedral coordination. Crystallographic data and experimental parameters for the crystal structures of the compounds studied in this chapter are summarized in Table 3.1. Detailed description of the solid phases produced in the studied system and analysis of the magnetic properties can be found in the article **A-IV** (*see* Included Articles).

TABLE 3.1 Crystallographic data and refinement parameters for α–$PbNi(SeO_3)_2$ (**c3.1**), β–$PbNi(SeO_3)_2$ (**c3.2**), $PbNi_2(SeO_2OH)_2(SeO_3)_2$ (**c3.3**), and α–$PbCo(SeO_3)_2$ (**c3.4**)

	c3.1	**c3.2**	**c3.3**	**c3.4**
M_r (g mol^{-1})	519.82	519.82	834.47	520.04
space group	*Pnma*	$Cmc2_1$	$P2/c$	*Pnma*
a (Å)	12.7476(4)	5.4715(4)	13.6824(10)	12.8208(4)
b (Å)	5.4562(2)	9.1963(6)	5.2692(5)	5.4902(2)
c (Å)	7.8332(2)	11.4436(9)	19.3476(13)	7.9085(2)
β (°)	90	90	129.524(4)	90
V (Å^3)	544.83(3)	575.81(7)	1075.94(16)	556.67(3)
Z	4	4	4	4
ρ (g/cm^3)	6.337	5.996	5.151	6.205
μ (mm^{-1})	47.637	45.074	32.668	46.221
λ (MoK_α) (Å)	0.71073	0.71073	0.71073	0.71073
total rflns	10212	2345	5454	3226
indep rflns	823	686	2083	742
R_{int}	0.0336	0.0260	0.0459	0.0260
R_1 [$I > 2\sigma(I)$]	0.0139	0.0141	0.0496	0.0186
wR_2 [$I > 2\sigma(I)$]	0.0360	0.0346	0.0992	0.0429
R_1 [all data]	0.0165	0.0142	0.0783	0.0203
wR_2 [all data]	0.0387	0.0346	0.1104	0.0439
GOF	1.090	1.109	1.187	1.142
$\Delta\rho_{max}$,$\Delta\rho_{min}$ (e Å^{-3})	1.573, –1.110	1.310, –1.073	2.916, –2.912	0.971, –1.887
ICSD	428905	428906	428907	428904

2.3.1 Crystal growth in the PbO–NiO–SeO_2–H_2O system

Synthetic procedures

In this system, we present a systematic exploration of the phase diagram by a hydrothermal technique, a rare methodology belonging to the group of the solvothermal methods, where most of the reported phases are obtained fortuitously. The exploration of the crystal growth in the PbO–NiO–SeO_2–H_2O system consisted of examination of 36 possible combinations of molar ratios of the solid precursors within the Gibbs triangle (Figure 3.1). In all syntheses the mPbO + nNiO + (k/5)SeO_2 (m, n, k = 1, 2,… 8) molar sum was fixed as constant equaled to 10 mmol, and the mixture was completed with 6 ml of distilled water. It has been experimentally established that only acidic conditions favor the crystallization of structural varieties. Thus, a large stoichiometric excess of SeO_2 was necessary to achieve successful reactions, and the amount of selenium dioxide was multiplied by five. The pH values increase from ~1 to ~5.5–6.0 on decreasing the SeO_2 content in studied experimental range. The solid products were systematically analyzed by powder XRD analysis, while representative crystals of each of the present phases were also selected by morphology and colors and tested by single-crystal XRD analysis. It led to the single crystal phase distribution given in Figure 3.1a, where the crystallization domains of phases are illustrated by different colors.

The hydrothermal chemical reactions were performed during 36 hours in 23 mL Teflon-lined vessels heated in an oven at 200 °C. At the end of the experiment time, the vessels were cooled during 48 hours. The precipitate was filtered through filter paper. Single crystals of three novel lead nickel selenites, α–$PbNi(SeO_3)_2$ (**c3.1**), β–$PbNi(SeO_3)_2$ (**c3.2**), and $PbNi_2(SeO_2OH)_2(SeO_3)_2$ (**c3.3**), have been observed in the mixtures with already reported compounds: $Ni(SeO_3)(H_2O)$ [Engelen et al. 1996], $Ni_3(SeO_3)_3(H_2O)$ [Wildner 1991; Mcmanus et al. 1991], $Ni_{12}(OH)_6(SeO_3)_8(OH)_2$ [Amorós et al. 1996], and $Pb(SeO_3)$ [Popovkin et al. 1963; Fischer 1972; Koskenlinna and Valkonen 1977]. Single crystals of the cobalt selenite, α–$PbCo(SeO_3)_2$ (**c3.4**), were obtained by the reaction analogous to that used to obtain compound **c3.1**. Attempts to synthesize the Co-analogue of compounds **c3.2** and **c3.3** using similar techniques proved unsuccessful. The novel lead selenites crystals occur as yellow needles (**c3.1**), yellow prisms (**c3.2**), green plates (**c3.3**), and purple needles (**c3.4**) up to 300 μm in maximal dimension.

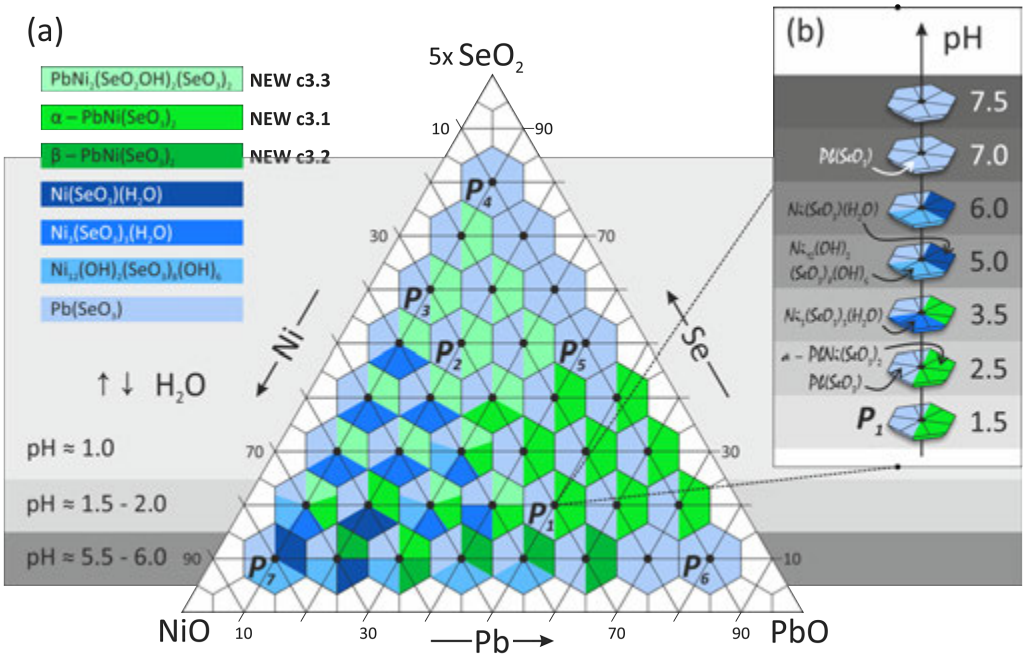

FIGURE 3.1 Experimental crystallization diagram of the PbO–NiO–SeO_2–H_2O system at 200 °C with the pH zones shown in background by grey colors – (a); series of the experiments with a PbO / NiO / SeO_2 molar ratio of 5 : 3 : 10 corresponding to the ***P*$_1$** point with various pH values – (b)

Brief analysis of the synthesized phases

The analysis of the different produced solid phases allows a rough rationalization based on the starting stoichiometry and pH value. The $Pb(SeO_3)$ compound is the most frequent phase in the system, and it has been observed as a solid product with variable degree of crystallinity in each hydrothermal experiment, sometimes found as a predominant white powder. This proves a preferred complexation of Pb^{2+} by $(SeO_3)^{2-}$ and enhanced precipitation independently of the pH.

In addition, we note that rich lead compounds appear in the right zone of the diagram while lead-free nickel selenites have been obtained at the left side with low Pb concentrations. This result, even though expected, demonstrates formation mechanisms controlled by the solution concentrations of each species. Finally, occulting the systematic presence of $Pb(SeO_3)$, low pH values favor reactivity of $(SeO_2OH)^-$

groups (*e.g.* in **c3.3**), while selenite groups dominate at higher pH values (*e.g.* in **c3.1** and **c3.2** polymorphs).

Role of pH

To gain more information about the reaction processes in the PbO–NiO–SeO_2–H_2O phase diagram, an in-depth investigation was carried out for the particular ***P1*** (PbO / NiO / SeO_2 molar ratio of 5 : 3 : 10) stoichiometric mixture at various pH values up to 7.5 (in order to prevent the reduction of SeO_2 to γ – Se metal [Pourbaix 1974; Takeno 2005]). The reagents were mixed with 1.75 M aqueous NaOH solution until the required pH values. Then, the hydrothermal treatment was applied. The resulted products of these series as a function of the pH values are shown in Figure 3.1b.

The results obtained in the course of the hydrothermal experiments demonstrate an essential role of the pH values, especially dealing with the influence of the degree of condensation of the ionic species. Once more at all pH the $Pb(SeO_3)$ is revealed as very stable. For the other products, we observe that water molecules and, subsequently, hydroxide anions are progressively incorporated into the compound structures on increasing the pH. In particular, at low pH of 1.5–2.5 only condensed compounds, α–$PbNi(SeO_3)_2$ (**c3.1**) and $Pb(SeO_3)$ are formed. The reaction occurring with pH value of 3.5 leads to reported compound $Ni_3(SeO_3)_3(H_2O)$ with one-third of Ni^{2+} coordinated by water molecules. Increasing the pH to 5.0–6.0 markedly increases the incorporation of water molecules and/or hydroxyl groups leading to $Ni_{12}(OH)_6(SeO_3)_8(OH)_2$ and $Ni(SeO_3)(H_2O)$. The crystal structure of the latter is only composed of $NiO_5(H_2O)$ polyhedra, while the tubular crystal structure of $Ni_{12}(OH)_2(SeO_3)_8(OH)_6$ contains half of the protonated $(NiO_5(OH))^{9-}$ octahedra. With pH values greater than 7.0, only the very stable solid products $Pb(SeO_3)$ phase is observed.

2.3.2 Structural description of four novel phases

α–PbM(SeO₃)₂ (M = Ni²⁺, Co²⁺)

The isotypic compounds **c3.1** and **c3.4** are built up from a *3D* framework composed of anionic $(SeO_3)^{2-}$ and $(MO_6)^{10-}$ building units sharing common corners (Figure 3.2). We find one symmetrically independent M^{2+} position with rather regular $(MO_6)^{10-}$ octahedral coordination. There are two independent Se atoms per formula unit, where

Se^{4+} cations form typical $(SeO_3)^{2-}$ triangular pyramids. The unique Pb^{2+} site is surrounded by O anions shared by $(SeO_3)^{2-}$ and $(MO_6)^{10-}$ groups. It forms asymmetric Pb^{2+} coordination with a stereochemically active lone pair directed toward the empty space.

In Figure 3.2b, a *3D* metal cationic framework of the crystal structures of **c3.1** and **c3.4** is represented as a black-and-white graph with black and white nodes symbolizing coordination polyhedra of M^{2+} and Se^{4+}, respectively. It highlights the topological connectivity of the SeO_3 and MO_6 polyhedra in complex *3D* framework with stretched rectangular channels extending along [010] direction occupied by the lead cations and the Se^{4+} lone pairs. In the (010) plane, their sections are arranged in a crossed manner with alternate of the two orientations [201] and the [20-1] with respect to the *Pnma* symmetry. The channels are bordered by six MO_6 and six SeO_3 polyhedra (Figure 3.2a).

Divalent lead cations reside in the cavities and balance the charge of the framework of the compounds **c3.1** and **c3.4**. Detailed description of the crystal structures of **c3.1** and **c3.4** can be found in article **A-IV** (*see* Included Articles).

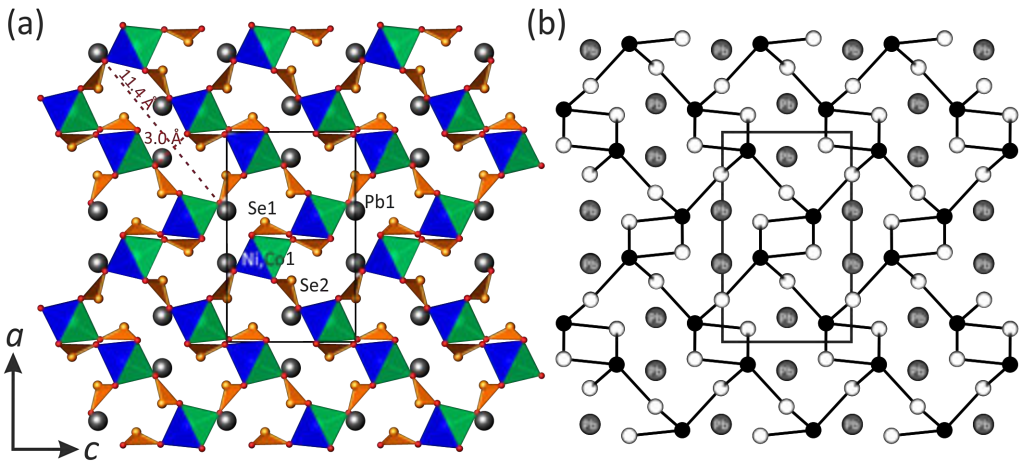

FIGURE 3.2 General projection of the crystal structures of α–Pb$M(SeO_3)_2$ (M = Ni^{2+} (**c3.1**), Co^{2+} (**c3.4**)) along the *b*-axis – (a), and the corresponding black-and-white graph – (b), M^{2+} Se^{4+} are black and white circles, respectively

β–PbNi(SeO₃)₂

The crystal structure of **c3.2** contains one symmetrically independent Ni^{2+} cation that forms a slightly distorted NiO_6 octahedron. Two independent Se^{4+} sites have a trigonal

pyramidal coordination. In the crystal structure of **c3.2** a coordination polyhedron of a unique Pb^{2+} ion is asymmetric and obviously indicates that the $6s^2$ lone pair is stereochemically active.

Similarly to what found in the α–$PbNi(SeO_3)_2$ form (**c3.1**), the β–form is built up from isolated NiO_6 octahedra interlinked by SeO_3 groups via common oxygen corners. However, the linkage modes differ in both structures. The crystal structure of **c3.2** (Figure 3.3) is essentially two dimensional (*2D*) and is based upon $[Ni(SeO_3)_2]^{2-}$ sheets, which lay parallel to (001). The lone pairs of electrons of Se^{4+} cations are oriented in the [001] direction toward the vacant part of the interlayer space. Cavities are filled by the Pb^{2+} cations, which serve to balance charge and achieve the cohesion between the sheets.

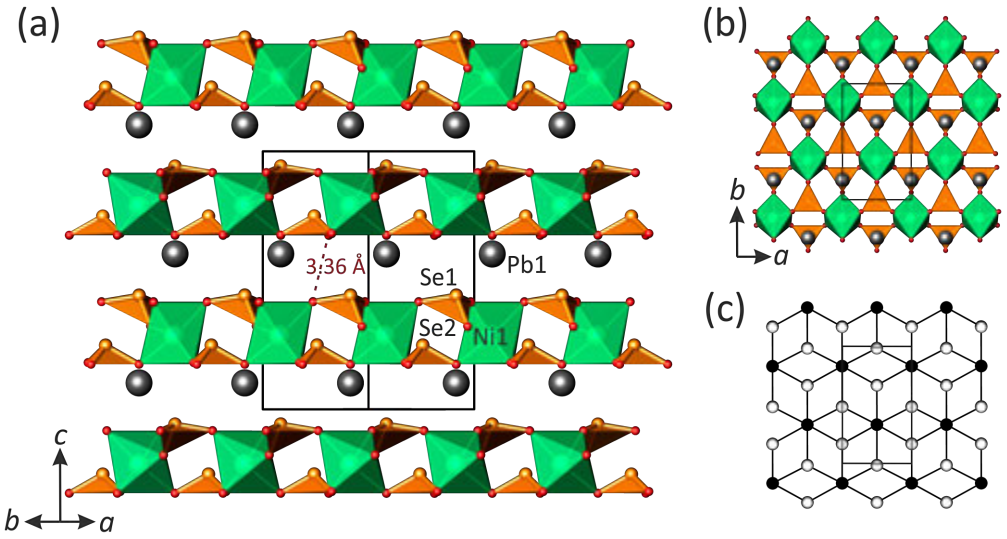

FIGURE 3.3 The crystal structure of β–$PbNi(SeO_3)_2$ (**c3.2**) in two different projections – (a) and (b), and the black-and-white graph corresponding to the Ni–Se sheet in the structure– (c)

The shortest interlayer O···O contacts across the interlayer is about 3.36 Å, much greater than the sum of van der Waals radii and involves a true *2D*-character. The black-and-white graph corresponding to the layered nickel selenite structural units is shown in Figure 3.3c. This kind of layered topology is one of the most common in inorganic oxysalts [Krivovichev 2004; Krivovichev 2009]. The noncentrosymmetric character of **c3.2** is well evidenced on Figure 3.3a where only "up" SeO_3 orientations are found in the

crystal structure. Detailed description of the crystal structure of **c3.2** can be found in the article **A-IV** (*see* Included Articles).

$PbNi_2(SeO_2OH)_2(SeO_3)_2$

In the crystal structure of **c3.3** there are two symmetrically independent Ni^{2+} sites with rather regular octahedral coordination. The four crystallographically inequivalent Se^{4+} atoms are asymmetrically coordinated by three oxygen atoms in a trigonal pyramidal geometry. However, two of them are protonated leading to strongly distorted $(Se(3)O_2OH)^-$ and $(Se(4)O_2OH)^-$ trigonal pyramids with one long Se–O bond, and two shorter Se–O bonds. The two independent Pb^{2+} cations are eight-fold oxygen coordinated. They both show a distorted square antiprismatic arrangement with lone pairs of electrons oriented toward the longest oxygen neighbors.

In the crystal structure of **c3.3**, the NiO_6 octahedra are sharing their vertices with SeO_3 groups, forming a *3D* framework encapsulating channels propagating along the [010] direction (Figure 3.4a). Four independent channels are occupied alternately by divalent lead cations and lone pairs of electrons of the Se^{4+} cations.

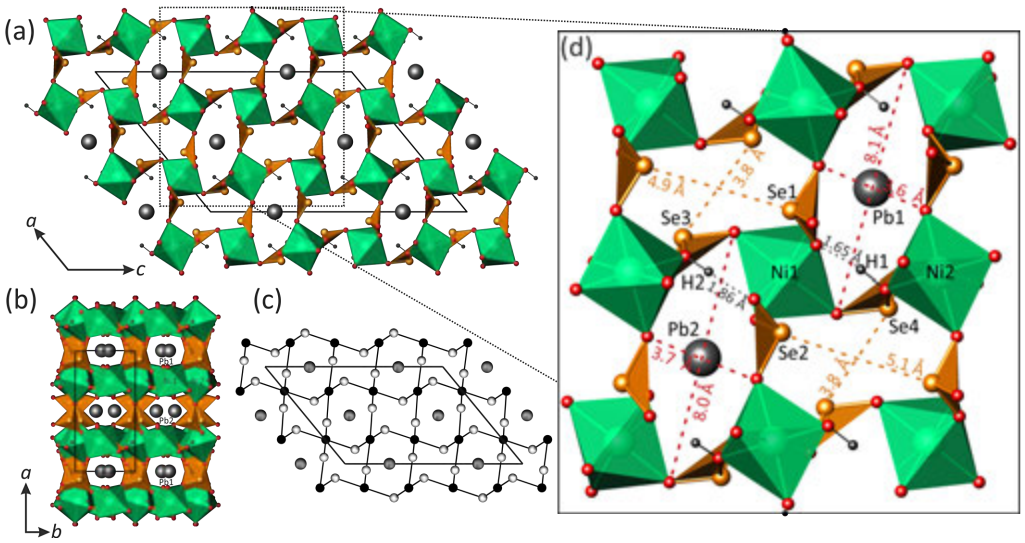

FIGURE 3.4 General projection of the crystal structure of $PbNi_2(SeO_2OH)_2(SeO_3)_2$ (**c3.3**) along the *b* and *c*-axis – (a) and (b), respectively; its black-and-white graph – (c); and more detailed fragment of the structure – (d)

It is striking that in the (*a*,*b*) projection the similitude between Pb(1) and Pb(2) channels suggests a *V*/2 sub-cell. In fact the projection in the (*a*,*b*) plane evidences channels growing along the *c*-axis with a clear distinction between Pb(1) and Pb(2) sites (Figure 3.4b).

Figure 3.4c shows the black-and-white graph corresponding to a *3D* metal cationic framework of **c3.3**. Its structural architecture is closely related to that observed in the crystal structure of $PbFe_2(SeO_3)_4$ [Johnston and Harrison 2004] and represents an interesting topological variation of the primitive cubic (**pcu**) network [Krivovichev 2014]. Detailed description of the crystal structure of **c3.3** can be found in the article **A-IV** (*see* Included Articles).

2.4 Crystal chemical studies of vanadate selenites

Crystallographic data and experimental parameters for the crystal structures of the compounds studied in this chapter are summarized in Table 4.1.

TABLE 4.1 Crystallographic data and refinement parameters for β–$(V_2O_3)(SeO_3)_2$ (**c4.1**), $Pb_2(VO)(SeO_3)_3$ (**c4.2**), and β–$Pb_4(V_3O_8)_2(SeO_3)_3(H_2O)$ (**c4.3**)

	c4.1	**c4.2**	**c4.3**
M_r (g mol^{-1})	403.80	862.20	1789.30
space group	$P2_1/c$	$P2_1/n$	P–1
a (Å)	7.1812(3)	5.1938(3)	7.1425(2)
b (Å)	7.0753(2)	16.1141(9)	7.1933(2)
c (Å)	14.0486(5)	11.2533(6)	21.5261(7)
α (°)	90	90	90.0190(10)
β (°)	101.5462(15)	90.527(2)	98.1800(10)
γ (°)	90	90	94.5980(10)
V (Å^3)	699.35(4)	941.79(9)	1091.12(6)
Z	4	4	2
ρ (g/cm^3)	3.835	6.081	5.446
μ (mm^{-1})	13.105	48.272	38.305
λ (MoK_α) (Å)	0.71073	0.71073	0.71073
total rflns	7488	9381	21653
indep rflns	2126	3062	6579
R_{int}	0.0252	0.0305	0.0272
R_1 [$I > 2\sigma(I)$]	0.0232	0.0236	0.0260
wR_2 [$I > 2\sigma(I)$]	0.0503	0.0411	0.0535
R_1 [all data]	0.0298	0.0322	0.0302
wR_2 [all data]	0.0527	0.0429	0.0549
GOF	1.065	1.059	1.042
$\Delta\rho_{max}$,$\Delta\rho_{min}$ (e Å^{-3})	1.03, –0.49	1.40, –1.34	5.06, –2.96

2.4.1 Pathways for synthesis of lead vanadate selenites

The PbO–VO_x–SeO_2 ternary system has not been widely explored so far, and it counts only six known phases, namely, $Pb_2(V^{5+}{}_2O_5)(SeO_3)_2$ [Li et al. 2010], $Pb_2(V^{4+}O)_3(SeO_3)_5$ [Li et al. 2010], $Pb_4(V^{5+}O_2)_2(SeO_3)_4(Se_2O_5)$ [Yeon et al. 2012], α–$Pb_4(V^{5+}{}_3O_8)_2(SeO_3)_3(H_2O)$ [Cao et al. 2014], $Pb_2(V^{5+}O_2)(SeO_3)_2Cl$ [Cao et al. 2014], and $Pb(V^{5+}O_2)(SeO_3)F$ [Cao et al. 2014]. Further investigation was motivation for us in this part of the present study. Most of the reported compounds have been prepared by the hydrothermal techniques at 200–230 °C, which is expected owing to good solubility and

reactivity of $(Se^{4+}O_3)^{2-}$ anions in solution, while Pb^{2+} oxysalts are prone to the phase formation in aqueous solutions as demonstrated by our previous results. Only two of the compounds, $Pb_4(V^{5+}O_2)_2(SeO_3)_4(Se_2O_5)$ [Yeon et al. 2012] and $Pb_2(V^{5+}O_2)(SeO_3)_2Cl$ [Cao et al. 2014], were synthesized using the CVT method. Interestingly, the latter can be also obtained by the hydrothermal method [Cao et al. 2014].

In the context of the present work, single crystals of the new β–$(V^{5+}{}_2O_3)(SeO_3)_2$ (**c4.1**) have been grown by the chemical vapor transport (CVT) method described in general form in the Section 2.1, while new Pb-containing phases, $Pb_2(V^{4+}O)(SeO_3)_3$ (**c4.2**) β–$Pb_4(V^{5+}{}_3O_8)_2(SeO_3)_3(H_2O)$ (**c4.3**), were obtained by using the hydrothermal techniques in the course of the phase diagram exploration. Due to time restrictions, "hydrothermal" phase diagrams using both PbO and $PbCl_2$ precursor have not been studied systematically, in contrast with the Ni-containing system developed in the Section 2.3. Our investigation of the systems included an examination of several combinations of molar ratios of the solid precursors within the Gibbs' triangle (Figure 4.1) in a similar way as described in the Chapter 2.3.1.

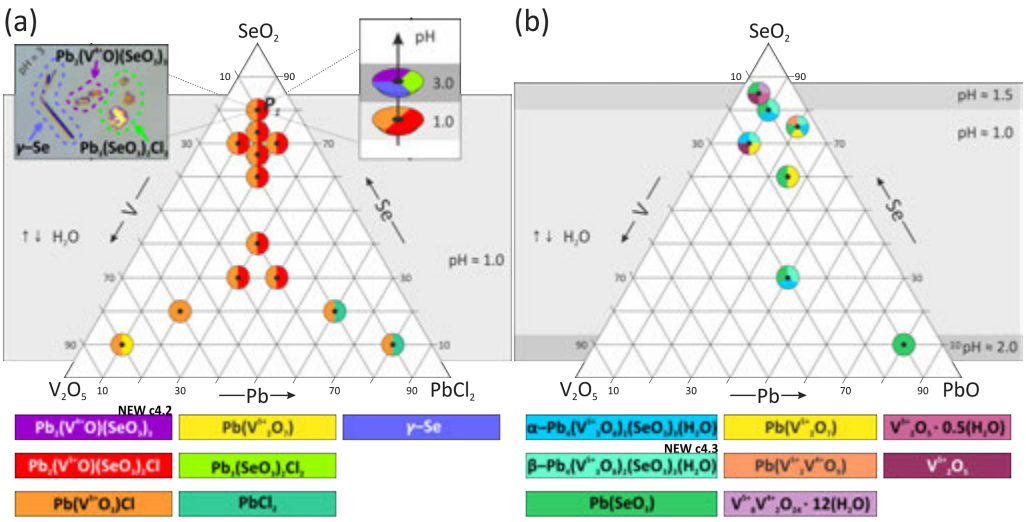

FIGURE 4.1 Experimental crystallization diagram of the $PbCl_2$–V_2O_5–SeO_2–H_2O (a) and PbO–V_2O_5–SeO_2–H_2O (b) systems at 200 °C with the pH zones shown in the background by grey colours

The reaction products have been identified by means of single crystal (for both systems) and powder (for the PbO–V_2O_5–SeO_2–H_2O system) X-ray diffraction

methods. As in the case of the Ni-system, self-acidification was achieved owing to the SeO_2 reaction with water according to the following reactions:

$$SeO_2 + H_2O \leftrightarrow H_2SeO_3 \quad (1)$$

$$H_2SeO_3 \leftrightarrow H^+ + (HSeO_3)^- \ (pK_a = 2.62) \quad (2)$$

$$(HSeO_3)^- \leftrightarrow H^+ + (SeO_3)^{2-} \ (pK_a = 8.32) \quad (3)$$

In the $PbCl_2$–V_2O_5–SeO_2–H_2O system, the $Pb_2(VO_2)(SeO_3)_2Cl$ [Cao et al. 2014] and $Pb(VO_3)Cl$ [Jo et al. 2009] phases dominate, while $PbCl_2$ and $Pb(V_2O_7)$ occur in the $PbCl_2$-rich and V_2O_5-rich regions of the diagram, respectively. Using the PbO precursor, more contrasted phases have been identified depending on the zone of the crystallization diagram. Our study allowed to identify one new phase in each system, namely, $Pb_2(V^{4+}O)(SeO_3)_3$ (**c4.2**), and β–$Pb_4(V^{5+}{}_3O_8)_2(SeO_3)_3(H_2O)$ (**c4.3**), described below.

2.4.2 Structural description of three novel phases

β–$(V_2O_3)(SeO_3)_2$

The crystal structure of the new β–polymorph of $(V_2O_3)(SeO_3)_2$ (**c4.1**) contains two V^{5+} atoms and two Se^{4+} atoms. The V(1) site is coordinated by six oxygen atoms to form an irregular $[1_s+4+1_t]$-octahedron with one short (V(1)–O(4) = 1.586 Å) and one elongated bond (V(1)–O(3) = 2.385 Å). The V(2) site forms a square $[1_s+4]$-pyramid with one short V(2)–O(9) = 1.570 Å bond. This kind of five-fold coordination has been observed, *e.g.* in the crystal structures of $A_4Cd(VO)(V_2O_7)_2Cl$ (*A* = Rb, Tl) [Mertens and Müller-Buschbaum 1997]. Se^{4+} cations form the typical $(SeO_3)^{2-}$ triangular pyramids with a stereoactive lone pair acting as a complementary ligand.

In the structure of **c4.1**, a pair of edge-sharing vanadate octahedra shares their common oxygen corners with two vanadate square pyramids to from a $(V_4O_{18})^{16-}$ tetramer. The selenite anions play different structural roles. The $Se(2)O_3$ triangular pyramids are attached to the tetramer in such a way that selenite triangular O–O–O bases are relatively parallel to the V–V–V–V plane of the tetramer. The $Se(1)O_3$ groups are located in between the vanadate tetramers and provide their linkage into the metal-oxide sheets through the formation of the Se–O–V bridges (Figure 4.2a). The *2D* vanadate selenite complexes with an interlayer spacing of about 3.3 Å are oriented parallel to (-201) plane. The structural feature of this type of sheets in addition to their

electroneutrality is the presence of large lengthy channels of size 3 × 10 Å running along [100].

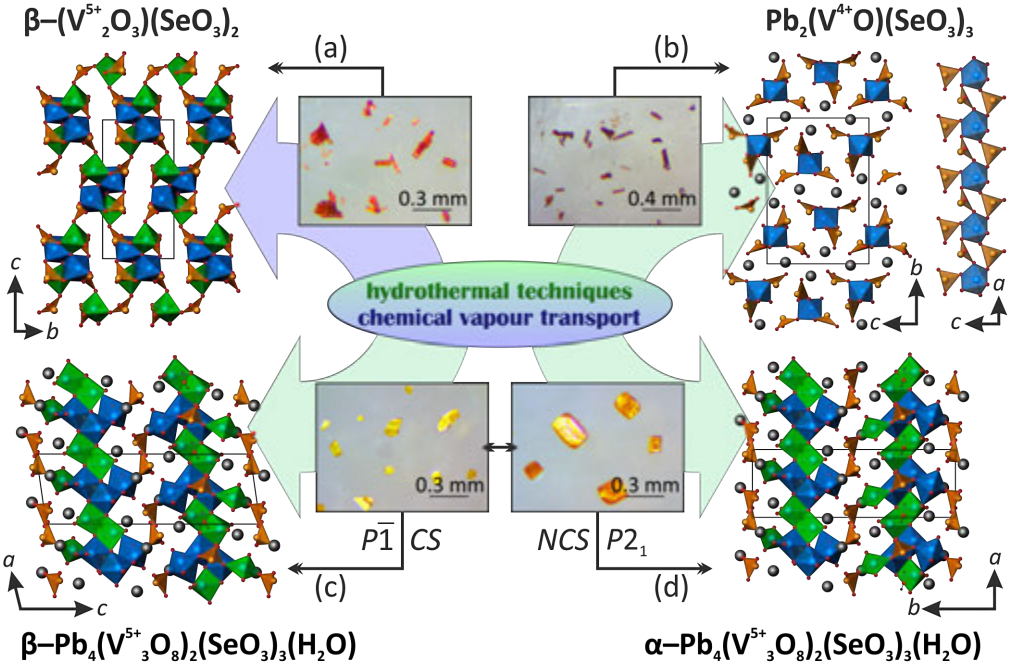

FIGURE 4.2 Projections of the structures and optical microscope images of the crystals of **c4.1**, **c4.2**, **c4.3**, and α–$Pb_4(V_3O_8)_2(SeO_3)_3(H_2O)$. VO_6 octahedra, VO_5 square pyramids, SeO_3 triangular pyramids, and Pb^{2+} cations are blue, green, orange, and grey, respectively

Polymorphism of $(V_2O_3)(SeO_3)_2$

The crystal structures of the two polymorphs, α–$(V_2O_3)(SeO_3)_2$ [Lee and Kwon 1996] and β–$(V_2O_3)(SeO_3)_2$ (**c4.1**), both consist of vanadate tetrameric structural units with different geometry. The crystal structure of α–modification is based upon chains extended along the *a*-axis, and composed of $(SeO_3)^{2-}$ pyramids and square-like octahedral $(V_4O_{18})^{16-}$ tetramers shown in Figure 4.3a. The tetramer is built up from two pairs of edge-shared V^{5+} octahedra linked through common oxygen equatorial corners. Its V^{5+} centres have rather regular square planar geometry with the two V(1)···V(2) distances equal to 3.41 Å and 3.53 Å, and the V–V–V angles between 88.7° and 91.3°. In contrast, in the structure of β–form (**c4.1**), the tetramer is cruciform (Figure 4.3b). The two mutually perpendicular V(1)···V(1)' and V(2)···V(2)' distances across the tetramer

are 3.20 Å and 6.28 Å, respectively. The distribution of short and long V–O distances is highlighted in the Figure 4.3b.

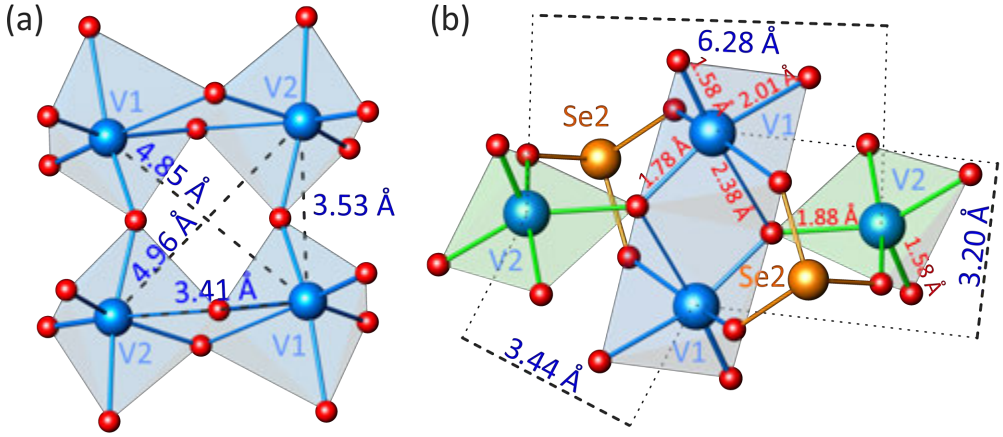

FIGURE 4.3 Vanadate tetrameric structural units in the structures of α–$(V_2O_3)(SeO_3)_2$ and β–$(V_2O_3)(SeO_3)_2$ (**c4.1**) – (a) and (b), respectively

It is noteworthy that the crystal structures of both polymorphic compounds are related with those of chemically similar $(V_2O_3)(TeO_3)_2$ [Darriet and Galy 1973; Millet et al. 1999] and $(V_2O_3)(XO_4)_2$ (X = S, Se) [Tudo et al. 1969; Richter and Mattes 1992; Tyutyunnik et al. 2010]. Such a wide variety of the crystal structures of similar chemical compositions can be caused by the presence of chemically differ strong short, equatorial and weak long bonds in VO_n polyhedra, which give rise to a large diversity of different geometries of structural units. Also contributing is the fact that the asymmetric selenite groups with stereochemically active lone electron pair could form structural cavities leading to materials with open architectures.

$Pb_2(V^{4+}O)(SeO_3)_3$

This phase is fundamentally different from the other ones since it contains so-called *vanadyl* $(V{=}O)^{2+}$ ions. In the crystal structure of $Pb_2(V^{4+}O)(SeO_3)_3$ (**c4.2**), there is a unique V^{4+} position octahedrally coordinated by six O atoms and isolated in the cell. The $(VO_6)^{8-}$ octahedron contains one short *vanadyl* bond (V(1)–O(7) = 1.615 Å), four equatorial bonds with the average bond length of 2.035 Å, and one shortened *trans*-bond (V(1)–O(5) = 2.096 Å). Occurrence of such short *trans*-bond length is rather rare

for the compounds with octahedrally coordinated V^{4+} sites [Schindler et al. 2000], and is commonly more closed to 2.2 Å. Nevertheless, it has been observed, *e.g.* in the crystal structures of $A_2(VO)_3(P_2O_7)_2$ (A = Rb, K) [Leclaire et al. 1988; Lii et al. 1990]. In both cases, the valence bond of this "*long*" oxygen corner is completed by bonding to an oxo-anion (SeO_3 or P_2O_7), while the V=O oxygen atom it is not further bonded. Three symmetrically independent Se sites form typical $(SeO_3)^{2-}$ triangular pyramids. The structure of **c4.2** contains two symmetrically independent Pb^{2+} sites. Both lead cations are surrounded by ten common O atoms with vanadate and selenite groups. Generally, all Pb^{2+} cations demonstrate short and strong Pb–O bonds in one coordination hemisphere and long weaker Pb–O bonds in another.

The structure of **c4.2** can be considered as formed from *1D* vanadate selenite chains with divalent lead cations located in between providing *3D* cohesion of the structure (Figure 4.2b). Single vanadate octahedra share five their oxygen corners with adjacent selenite triangular pyramids to form $[(VO_2)(SeO_3)_3]^{4-}$ chains running along the *a*-axis. Both bidentate $Se(2)O_3$ and $Se(3)O_3$ groups bridge between two adjacent $V(1)O_6$ octahedra, whereas $Se(1)O_3$ triangular pyramid is monodentate and shares only one corner with the *trans*-one of the vanadate octahedron. Orientation of the *1D* structural units can be considered as planar and parallel to (010) with divalent lead cations providing their linkage (Figure 4.2b).

β–$Pb_4(V_3O_8)_2(SeO_3)_3(H_2O)$

New β–polymorphic modification of $Pb_4(V_3O_8)_2(SeO_3)_3(H_2O)$ (**c4.3**) contains six V^{5+}, three Se^{4+}, and four Pb^{2+} cations per one unit cell. Pentavalent vanadium cations occupy six-fold and five-fold sites. V(1), V(2), and V(4) sites are octahedrally [1_s+4+1_t] coordinated by six O atoms with each one short bond. V(3), V(5), and V(6) have a distorted square [1_s+(1_s+3)]-pyramidal environment with two short bonds (<V–O_s> equals 1.643 Å, 1.651 Å, and 1.652 Å for V(3), V(5), and V(6), respectively) and three equatorial bonds. In the structure of **c4.3**, there are three symmetrically independent Se^{4+} cations that have typical oxygen coordination of triangular pyramid. The coordination polyhedra of four unique Pb^{2+} cations are strongly distorted because of the stereoactivity of their $6s^2$ lone electron pairs. Pb(1) and Pb(2) cations are surrounded by eight O atoms with six and seven relatively short strong Pb–O bonds. The O(26) atom located at a distance of 2.616 Å from Pb(1) belongs to a water molecule. It links via

hydrogen bonding with non-bonded oxygen vertex of the Se(3)O group (O(26)–O(20) = 2.644 Å), and it forms a long hydrogen contact (O(26)–O(17) = 3.269 Å) with the oxygen atom bridged between Se(3)O and V(3)O_5 groups. Pb(3) and Pb(4) sites are coordinated by nine O atoms. Six of them are located at relatively short distances.

The crystal structure of **c4.3** is built up from vanadate selenite *1D* structural units (Figure 4.4) further bridged by divalent lead cations into a *3D* framework (Figure 4.5). It will be discussed in the next chapter by analogy to the α–form.

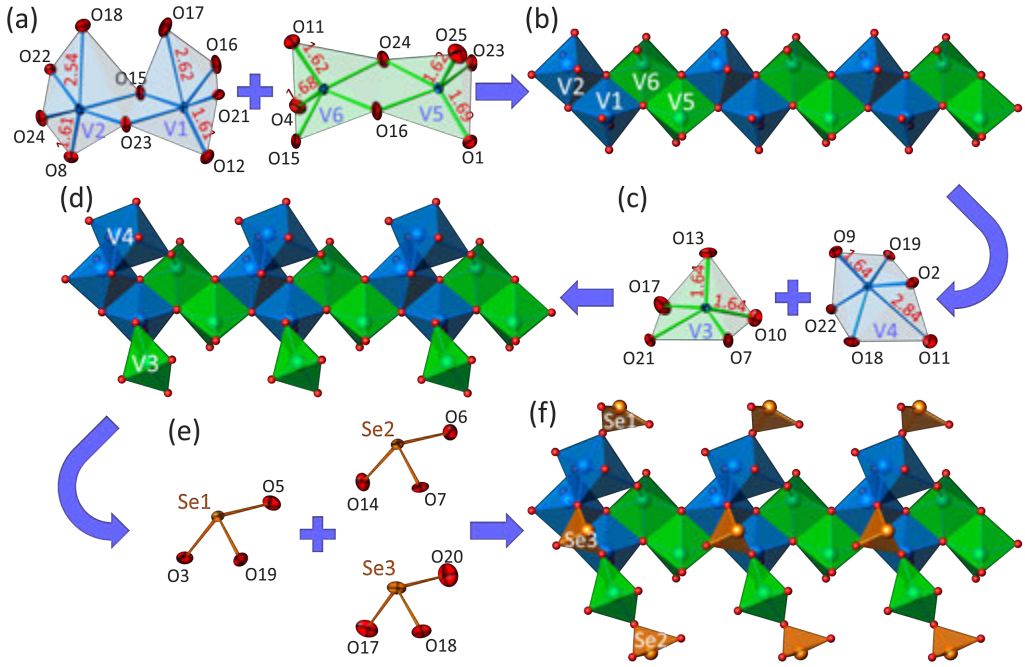

FIGURE 4.4 Structural units in the crystal structure of β–$Pb_4(V^{5+}{}_3O_8)_2(SeO_3)_3(H_2O)$ (**c4.3**)

An interesting feature of the crystal structure of **c4.3** is a presence of two chiral vanadate selenite arch-like ribbons related to each other by the inversion centre (Figure 4.2c). Adjacent chiral ribbons bridged via strong metal oxide linkages form *2D* structural units parallel to (010) (Figure 4.5b). Pb(1) and Pb(2) cations provide additional interconnection of the layers into a *3D* framework. Water molecules filled the remaining void space in the structure and hydrogen bonding does not participate in the connection of adjacent structural units.

Polymorphism of $Pb_4(V_3O_8)_2(SeO_3)_3(H_2O)$

Both α– and β–polymorphic compounds have been synthesized within the framework of the present study. The α–form of $Pb_4(V_3O_8)_2(SeO_3)_3(H_2O)$ has been very recently described in [Cao et al. 2014]. It crystallizes in the monoclinic noncentrosymmetric $P2_1$ space group, while the β–modification (**c4.3**) has triclinic symmetry, space group $P\bar{1}$. Crystal structures of both polymorphs based upon the same *1D* vanadate selenite units are very similar and have very close unit-cell parameters with approximately equal volumes (Figure 4.5).

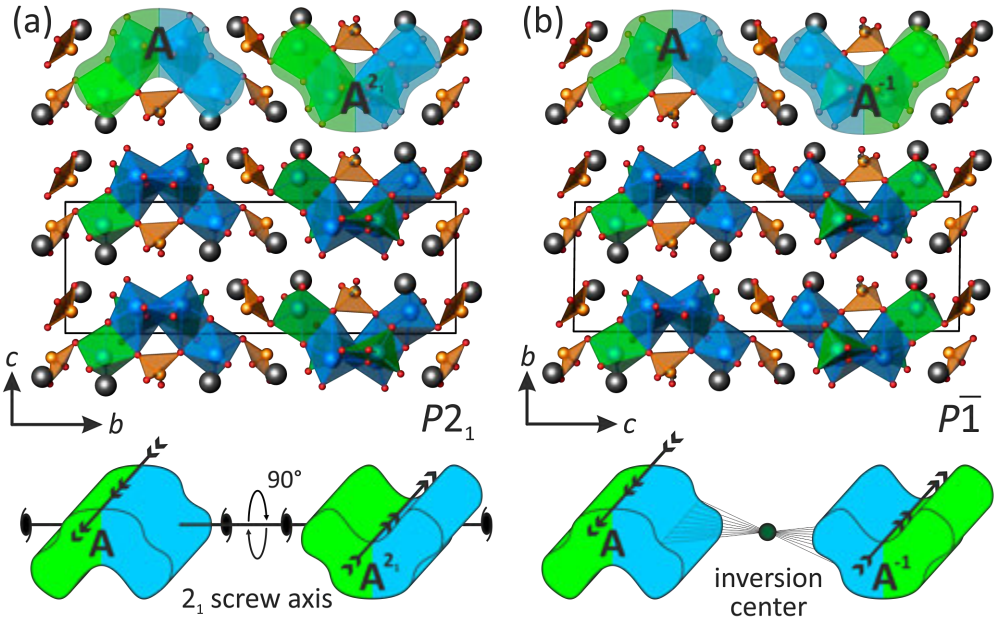

FIGURE 4.5 Mode of packing of the vanadate selenite ribbons in the crystal structures of α–$Pb_4(V_3O_8)_2(SeO_3)_3(H_2O)$ – (a) and β–$Pb_4(V_3O_8)_2(SeO_3)_3(H_2O)$ (**c4.3**) – (b)

Significant differences between them are that the structure of α–$Pb_4(V_3O_8)_2(SeO_3)_3(H_2O)$ consists of two vanadate selenite ribbons (designated as **A** and $\mathbf{A}^{21}$) rotated as a result of operation of the 2_1 screw axis, whereas the structure of β–modification (**c4.3**) contains two chiral inverted vanadate selenite ribbons (designated as **A** and $\mathbf{A}^{-1}$) related to each other by the inversion centre (Figure 4.2c, d).

The mode of packing of the vanadate selenite ribbons along the *b*- and *c*-axis respectively for the two forms remains the same in both polymorphic modifications.

This is achieved by the same position of lead cations and SeO_3 groups in the two structures, which is very rare to the best of our knowledge.

In the structure of the α–polymorph, the ribbon **A** is connected to adjacent rotated ribbon $\mathbf{A^{21}}$ forming a layer composed of alternating ribbons in a …**A** – $\mathbf{A^{21}}$ – **A** – $\mathbf{A^{21}}$ – **A**… sequence (Figure 4.5a). The structure of β–phase (**c4.3**) has a …**A** – $\mathbf{A^{-1}}$ – **A** – $\mathbf{A^{-1}}$ – **A**… packing sequence of the vanadate selenite ribbons (Figure 4.5b). Adjacent layers of the same sequences in both structures are placed directly under each other.

2.5 Crystal chemical studies of selenium compounds with manganese and bismuth

Bi^{3+} ion has strong affinity to oxocentered topologies [Huvé et al. 2006; Colmont et al. 2008; Aliev et al. 2012; Kozin et al. 2013; Colmont et al. 2013; Aliev et al. 2013; Lü et al. 2014], and, therefore, its combination with SeO_3 groups promises to appear very unusual phases. In addition, the substitution of Bi^{3+} for Mn^{2+} ion in several oxocentered phases [Abraham et al. 2002; Aliev et al. 2014] encouraged us to work with manganese phases as well. Although our results showed only one oxocentered new phase (**c5.2**), seven novel compounds have been identified. Crystallographic data and experimental parameters for the crystal structures of the compounds studied in this chapter and listed below are summarized in Table 5.1.

c5.1 – $Mn(SeO_4)(H_2O)_2$
c5.2 – $Mn_2[Bi_2O](SeO_3)_4$
c5.3 – $MnBi(SeO_3)_2Cl$
c5.4 – $Mn_4(Mn_5,Bi)(SeO_3)_8Cl_5$
c5.5 – $Bi_6(SeO_3)_4Cl_{10}$
c5.6 – β–$Bi(SeO_3)Cl$
c5.7 – $PbBi_{10}(SeO_3)_{12}Cl_8$

TABLE 5.1 Crystallographic data and refinement parameters for **c5.1**, **c5.2**, **c5.3**, **c5.4**, **c5.5**, **c5.6**, and **c5.7**

	c5.1	**c5.2**	**c5.3**	**c5.4**	**c5.5**	**c5.6**	**c5.7**
M_r (g mol^{-1})	233.93	1051.68	553.29	1896.37	2116.22	371.4	4104.1
space group	*Pbca*	*Pccn*	*P*–1	*Pbcm*	$P2_1/c$	*Cc*	*Ccca*
a (Å)	10.4353(5)	10.8771(3)	7.0926(8)	10.7914(2)	21.460(2)	22.7052(3)	15.819(6)
b (Å)	9.2420(5)	19.9770(5)	7.2695(6)	15.9782(3)	8.4012(9)	76.785(4)	17.871(7)
c (Å)	10.5349(6)	5.5058(1)	8.0160(8)	17.5682(3)	15.3370(18)	16.0550(3)	15.857(6)
α (°)	90	90	88.226(4)	90	90	90	90
β (°)	90	90	72.005(3)	90	110.639(5)	135.000(2)	90
γ (°)	90	90	64.560(4)	90	90	90	90
V (Å^3)	1016.02(9)	1196.37(5)	352.47(6)	3029.23(10)	2587.7(5)	19792.4(12)	4483(3)
Z	8	4	2	4	4	192	4
ρ (g/cm^3)	3.059	5.839	5.213	4.158	5.432	5.981	6.079
μ (mm^{-1})	9.71	43.63	37.40	19.55	47.37	52.08	53.17
λ (Mo$K_α$) (Å)	0.71073	0.71073	0.71073	0.71073	0.71073	0.71073	0.71073
total rflns	6089	8112	7238	32242	25390	242854	10469
indep rflns	1808	1895	2194	4767	4534	35097	2253
R_{int}	0.0295	0.0247	0.0198	0.0310	0.0421	0.0962	0.0496
R_1 [$I > 2σ(I)$]	0.0227	0.0285	0.0208	0.0220	0.0291	0.0612	0.0667
wR_2 [$I > 2σ(I)$]	0.0467	0.0620	0.0436	0.0529	0.0711	0.0645	0.0639

TABLE 5.1 *Continued*

	c5.1	**c5.2**	**c5.3**	**c5.4**	**c5.5**	**c5.6**	**c5.7**
R_1 [all data]	0.0302	0.0325	0.0219	0.0317	0.0333	0.1124	0.1057
wR_2 [all data]	0.0489	0.0637	0.0441	0.0565	0.0767	0.0694	0.0859
GOF	1.030	1.143	1.056	1.021	1.088	1.32	0.92
$\Delta\rho_{max}$,$\Delta\rho_{min}$ (e Å^{-3})	0.70, −0.93	2.54, −1.47	1.90, −1.67	0.73, −1.16	3.42, −2.95	5.39, −4.51	5.38, −7.01

2.5.1 Synthetic procedures

Novel compounds studied in this chapter have been synthesized by different techniques.

Evaporation method from aqueous solution of hydrated manganese(II) chloride (2.4 mmol), 40% selenic acid H_2SeO_4 (4.7 mmol) and distilled water (10 ml) was used for synthesis of $Mn(SeO_4)(H_2O)_2$ (**c5.1**). The solution was stirred with a magnetic stirrer at 80 °C for 3 hours until it became fully homogeneous, then was poured onto a watch glass and left in a fume hood at room temperature. It should to be noted that on heating above 160 °C the selenic acid $H_2Se^{6+}O_4$ can be easily decomposed with the formation of selenious acid $H_2Se^{4+}O_3$ and oxygen [De 2003]. Single crystals of **c5.1** suitable for X-ray analysis were grown after two days.

Single crystals of $Mn_2[Bi_2O](SeO_3)_4$ (**c5.2**), have been obtained from the hydrothermal reaction of SeO_2 (2.5 mmol), MnO_2 (2.0 mmol), Mn_2O_3 (0.25 mmol), and BiOCl (3.0 mmol) performed in 6 mL of distilled water. The reaction was run in the 23 mL autoclave for two days at 200 °C and then cooled at a rate of 3.7 °C/h to 22 °C.

The other compounds have been prepared using the CVT method. The $MnBi(SeO_3)_2Cl$ (**c5.3**) and $Bi_6(SeO_3)_4Cl_{10}$ (**c5.5**) compounds were grown together as a result of the same chemical vapour transport reaction of SeO_2 (4 mmol), Mn_2O_3 (1.0 mmol), Bi_2O_3 (1.0 mmol) and $BiCl_3$ (2.0 mmol) performed in a sealed evacuated silica tube over a temperature gradient of 400 °C to 350 °C during 100 hours. The $Mn_4(Mn_5,Bi)(SeO_3)_8Cl_5$ (**c5.4**) phase was synthesized by the CVT reaction of the same stoichiometric mixture that used for two previous compounds. The temperature gradient was 450 °C to 400 °C for 240 hours of thermal treatment.

Concurrently, in the UCCS research group, other two new compounds, β−$Bi(SeO_3)Cl$ (**c5.6**) and $PbBi_{10}(SeO_3)_{12}Cl_8$ (**c5.7**), have been synthesized by Dr. Almaz Aliev. The crystals of **c5.6** were grown by the CVT reaction of the mixture of SeO_2 (1.0 mmol), MnO_2 (1.0 mmol), BiOCl (1.0 mmol), and a drop of concentrated solution of

HCl, while the mixture of SeO_2 (1.0 mmol), PbO (1.0 mmol), BiOCl (1.0 mmol), and a drop of concentrated solution of HCl was used for preparation of the compound **c5.7**. The drops of hydrochloric acid were considered and used as a transport agent in these cases.

2.5.2 Structural description of seven novel phases

$Mn(SeO_4)(H_2O)_2$

The crystal structure of $Mn(SeO_4)(H_2O)_2$ (**c5.1**) contains one symmetrically inequivalent octahedrally coordinated Mn^{2+} cation. Four of six of its oxygen ligands are interacting with adjacent Se^{6+} cations, while two others belong to water molecules arranged in *cis*-position relative to each other. A unique crystallographically independent Se^{6+} site has tetrahedral coordination and linked by sharing of all its four vertices with adjacent $MnO_4(H_2O)_2$ octahedra into a *3D* framework (Figure 5.1a).

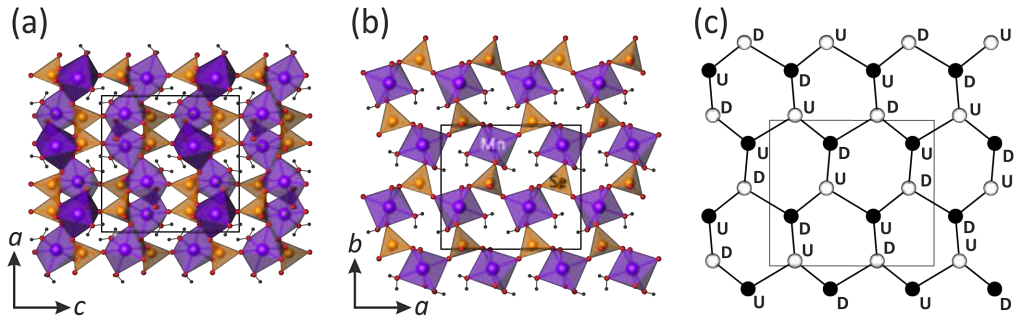

FIGURE 5.1 View of the crystal structure of $Mn(SeO_4)(H_2O)_2$ (**c5.1**) projected along the *a*-axis – (a); heteropolyhedral sheet parallel to the (001) plane – (b) and its black-and-white graph with symbols designating the direction of bonds to adjacent sheets – (c)

The framework of the crystal structure of **c5.1** can be regarded as composed of interlinked heteropolyhedral sheets (Figure 5.1b). The structural topology of analogous framework was described by *S.V. Krivovichev* at the example of $Zn(SeO_4)(H_2O)_2$ using a graphical approach [Krivovichev 2007]. The representation of the sheet as a black-and-white graph is shown in Figure 5.1c. It is based upon hexagonal non-planar rings. The orientations of black (Mn^{2+}) and white (Se^{6+}) vertices relative to the graph plane are

depicted by symbols U (up) and D (down). The symbols also designate the direction of links between adjacent sheets within the *3D* framework of the crystal structure.

The structure of **c5.1** belongs to the variscite structural type $M(TO_4)(H_2O)_2$, where $M = Fe^{3+}$, Al^{3+}, Ga^{3+}, In^{3+} or Zn^{2+}, and $T = P^{5+}$, As^{5+} or Se^{6+}. This type includes such minerals as mansfieldite $Al(AsO_4)(H_2O)_2$, scorodite $Fe(AsO_4)(H_2O)_2$, yanomamite $In(AsO_4)(H_2O)_2$, strengite $Fe(PO_4)(H_2O)_2$, and variscite $Al(PO_4)(H_2O)_2$ itself. It should to be noted, that $Mn(SeO_4)(H_2O)_2$ is the second example of the variscite-type compound containing metal cations in the oxidation state of +2.

$Mn_2[Bi_2O](SeO_3)_4$

The structure of $Mn_2[Bi_2O](SeO_3)_4$ (**c5.2**) contains only a single crystallographic Bi site coordinated by 8 oxygen atoms. The coordination polyhedron of Bi^{3+} can be described as a distorted square antiprism. The unique Mn^{2+} cation site has a distorted octahedral coordination. Each MnO_6 octahedron shares two edges with adjacent octahedra to form $[MnO_4]^{6-}$ zigzag chains running along the *c*-axis (Figure 5.2a). Two crystallographically independent Se^{4+} sites form typical selenite pyramids.

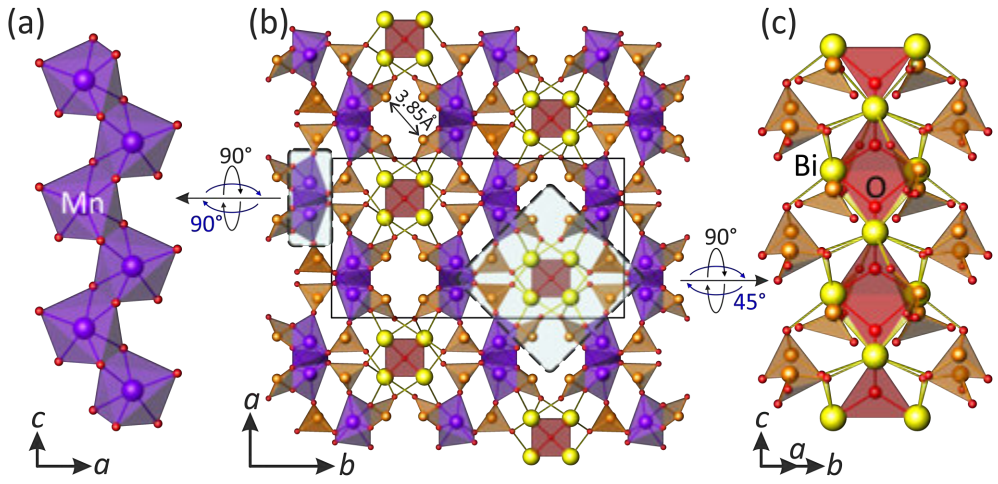

FIGURE 5.2 Projection of the crystal structure of $Mn_2[Bi_2O](SeO_3)_4$ (**c5.2**) (b) composed of $[MnO_4]^{6-}$ (a) and $[Bi_2O]^{4+}$ chains (c)

The crystal structure of **c5.2** contains an "additional" oxygen atom, which is coordinated solely by four Bi^{3+} cations forming oxocentered $(OBi_4)^{10+}$ tetrahedra. They share *trans*-oriented edges to form infinite $[Bi_2O]^{4+}$ chains along the *c*-axis (Figure 5.2c).

These chains are rather common in the crystal chemistry of oxocentered bismuth phases, *e.g.* in $[Bi_2O]AuO_4$ [Krivovichev et al. 2013b]. The chains are further linked through SeO_3 groups and $[MnO_4]^{6-}$ structural units into a *3D* framework with pseudo-tetragonal empty channels occupied by lone electron pairs of Se^{4+} cations (Figure 5.2b).

The structural architecture of **c5.2** is closely related to that observed in the crystal structures of $Tb_2O[SeO_3]_2$ [Wontcheu and Schleid 2002] and $M_3O_2Cl[SeO_3]_2$ (M^{3+} = Tb [Wontcheu and Schleid 2005] and Y [Zitzer et al. 2011]). In their structures the lone electron pairs of Se^{4+} cations form similar channels running between cationic $[Tb_2O]^{4+}$ chains in $Tb_2O[SeO_3]_2$ and $[M_3O_2]^{5+}$ double chains in $M_3O_2Cl[SeO_3]_2$ (M^{3+} = Tb and Y).

MnBi(SeO₃)₂Cl

In the crystal structure of $MnBi(SeO_3)_2Cl$ (**c5.3**), there is one symmetrically inequivalent Mn site. The Mn^{2+} cations form $(MnO_4Cl_2)^{8-}$ octahedra, which are interconnected *via* common Cl–Cl and O–O edges to infinite zigzag chains running along the *a*-axis (Figure 5.3). The chains are further linked by typical selenite SeO_3 groups into sheets parallel to (001).

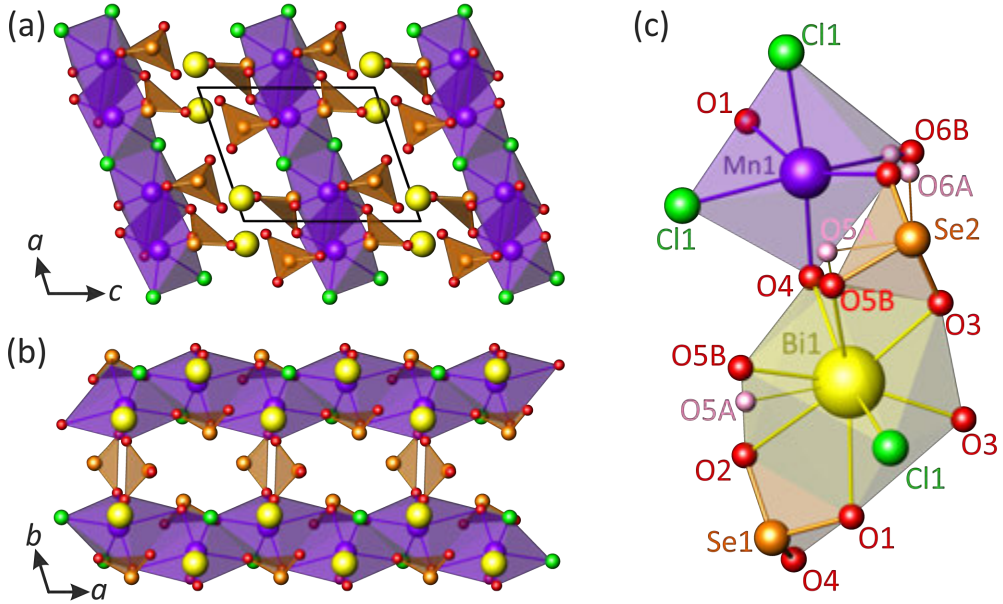

FIGURE 5.3 General projections of the crystal structure of $MnBi(SeO_3)_2Cl$ (**c5.3**) along [010] – (a) and [001] – (b) (disordered O sites are omitted for clarity); anionic arrangement of metal cations in the structure – (c)

During the structure solution and refinement process, two possible conformations of one of two symmetrically inequivalent selenite anions were observed due to disorder of two O sites. A refinement of the occupancies of the disordered O atoms gave ratios of 0.50/0.50 and 0.67/0.33 for O(5)a/O(5)b and O(6)a/O(6)b, respectively. A refinement of the anisotropic thermal parameters of the O(3) site located at the third corner of the $Se(2)O_3$ group resulted in normal thermal values, while the Se(2) showed the high thermal parameters. In the structure of **c5.3**, a symmetrically unique Bi^{3+} cation is in nine-fold distorted coordination of eight oxygen and single chlorine atoms (Figure 5.3c). The Bi^{3+} cations separate the sheets composed of selenite and manganese polyhedra from one another and serve to balance charge.

The structure of **c5.3** is isotypic with previously studied $MnSm(SeO_3)_2Cl$, $CoSm(SeO_3)_2Cl$, and $CuGd(SeO_3)_2Cl$ [Wickleder and Hamida 2003].

$Mn^{2+}_4(Mn^{2+}_5,Bi^{3+})(SeO_3)_8Cl_5$

The compound $Mn_4(Mn_5,Bi)(SeO_3)_8Cl_5$ (**c5.4**) is an example of a partially Bi/Mn disordered structure, in the sense that several subunits assembled in the crystal structure show statistic cationic distribution over mixed sites. The crystal structure of **c5.4** is based upon *2D* structural units composed of distorted square antiprisms of four crystallographically inequivalent mixed sites statistically occupied by Mn^{2+} and Bi^{3+} cations. The edge-sharing antiprisms are arranged in check-wise fashion (Figure 5.4a). A refinement of the mixed sites gave the following cationic distributions: $0.97Mn^{2+}/0.03Bi^{3+}$, $0.92Mn^{2+}/0.08Bi^{3+}$, $0.87Mn^{2+}/0.13Bi^{3+}$, and $0.37Mn^{2+}/0.63Bi^{3+}$ for Mn(3), Mn(4), Mn(5), and Bi(6), respectively, under restraints of neutral charge.

In the structure of **c5.4**, there are two fully ordered Mn^{2+} sites, which are octahedrally surrounded by three oxygen and three chlorine atoms each. A couple of the octahedra share their common Cl_3 face to form a dimer, which is further linked through one of the Cl corners with adjacent dimer into a square-like tetrameric unit. Four symmetrically inequivalent Se^{4+} triangular pyramids are connected to the O corners of the tetrameric unit as shown in Figure 5.4d. An inspection of a Fourier difference electron-density map showed that two of five crystallographically independent Cl^- sites are disordered. A refinement of their occupancies indicated the same 0.58/0.42 ratio for both Cl(1)a/Cl(1)b and Cl(2)a/Cl(2)b sites. The arrangement of the tetrameric units in the structure of **c5.4** is shown in Figure 5.4b.

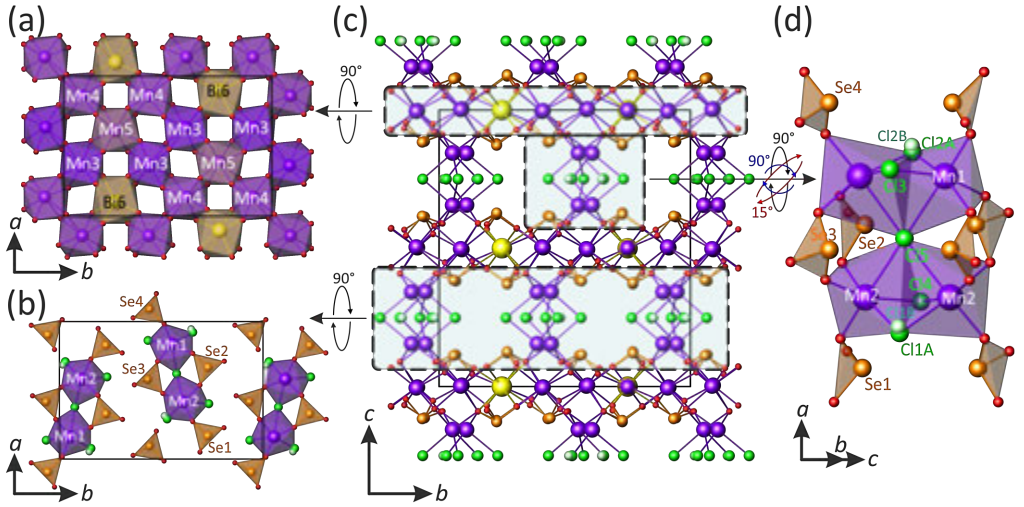

FIGURE 5.4 Projection of the crystal structure of $Mn_4(Mn_5,Bi)(SeO_3)_8Cl_5$ (**c5.4**) along [100] – (c), the sheet of square antiprisms – (a), the tetrameric unit – (d), and their arrangement in the structure – (b)

The tetrameric units are connected to the *2D* sheets *via* sharing of O–O edges of octahedra and selenite pyramids with the square antiprisms resulting in a complex *3D* framework with large pseudo-tetragonal empty channels occupied by lone electron pairs of Se^{4+} cations along the *a*-axis (Figure 5.4c).

$Bi_6(SeO_3)_4Cl_{10}$

The crystal structure of $Bi_6(SeO_3)_4Cl_{10}$ (**c5.5**) is formed by six distorted oxochloride polyhedra of bismuth, $Bi(1)O_3Cl_4$, $Bi(2)O_5Cl_4$, $Bi(3)O_3Cl_5$, $Bi(4)O_5Cl_4$, $Bi(5)O_5Cl_4$, and $Bi(6)O_5Cl_4$, linked to four crystallographically inequivalent Se^{4+} cations resulting in a *3D* framework. The stereoactive behaviour of the lone electron pairs on the Bi^{3+} cations is manifested by the particularly asymmetric coordination environments around these cations. Coordination polyhedra of Bi share their edges and corners to build $Bi_6(SeO_3)_4Cl_{10}$ blocks linked together in such a way as to create an open structure with some kind of empty channels bordered by the anions (essentially Cl^-) and parallel to the *b*-axis (Figure 5.5).

In the structure of **c5.5**, the cavities are around 9.7 Å long and 3.8 Å wide. The close inspection of a Fourier difference electron-density map showed a high residual peak (8.71 $e/Å^3$) at a distance of 0.86 Å from the Se(3) site indicating its possible splitting

into two satellite positions. The coupled refinement of the occupancies of the Se(3)/Se(3)' sites resulted in the 0.95/0.05 ratio. While the Se–O distances for Se(3) are plausible (1.71–1.74 Å), those for the Se(3)' site are too long (2.09–2.41 Å), which suggested its occupation by Bi^{3+}. The final Bi(3)a/Bi(3)b and Se(3)a/Se(3)b occupancies were refined to the ratio of 0.96/0.04. Detailed description of the crystal structure of **c5.5** can be found can be in the article **A-III** (*see* Included Articles).

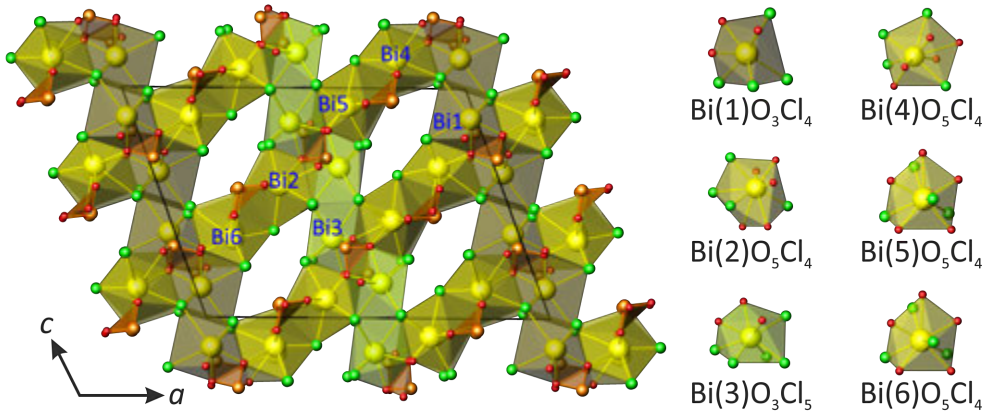

FIGURE 5.5 Projection of the crystal structure of $Bi_6(SeO_3)_4Cl_{10}$ (**c5.5**) on the (010) plane, showing BiO_xCl_y polyhedra (yellow) and SeO_3 groups (orange) sharing their edges and corners

β–Bi(SeO₃)Cl with giant unit cell

The crystal structure of β–$Bi(SeO_3)Cl$ (**c5.6**) is very unusual and complex. Noteworthy, beyond its NCS character, the volume cell is strikingly large (19792 $Å^3$). A total of 48 bismuth, 48 selenium, and 48 chlorine crystallographically independent atoms have been localized. The structure of **c5.6** can be described as built from two blocks, $[Bi_8Cl_{16}]^{8+}$ (Figure 5.6d) and $[Bi_{12}Cl_{32}]^{4+}$ (Figure 5.6c), regularly sandwiched between $[Bi_{14}(SeO_3)_{24}]^{6-}$ sheets (Figure 5.6b). In Figure 5.6a, the BiO_x polyhedra are shown by yellow colour, whereas, for the sake of clarity, the $[Bi_8Cl_{16}]^{8+}$ and $[Bi_{12}Cl_{32}]^{4+}$ sheets are represented as an arrangement of Bi (yellow) and Cl (green) atoms (Figure 5.6b). It should to be note that similar halide layers with the composition $[Bi_8Cl_{16}]^{8+}$ have also been found in the new compound $PbBi_{10}(SeO_3)_{12}Cl_8$ (**c5.7**) described below. The $[Bi_{14}(SeO_3)_{24}]^{6-}$ structural unit is built by the association of Bi^{3+} cations and SeO_3 pyramids. In BiO_x units with x in between 8 and 10, all the Bi-centered polyhedra are

asymmetric, which is typical of the bismuth coordination due to the stereoactive behaviour of the $6s^2$ lone pairs on Bi^{3+} cations.

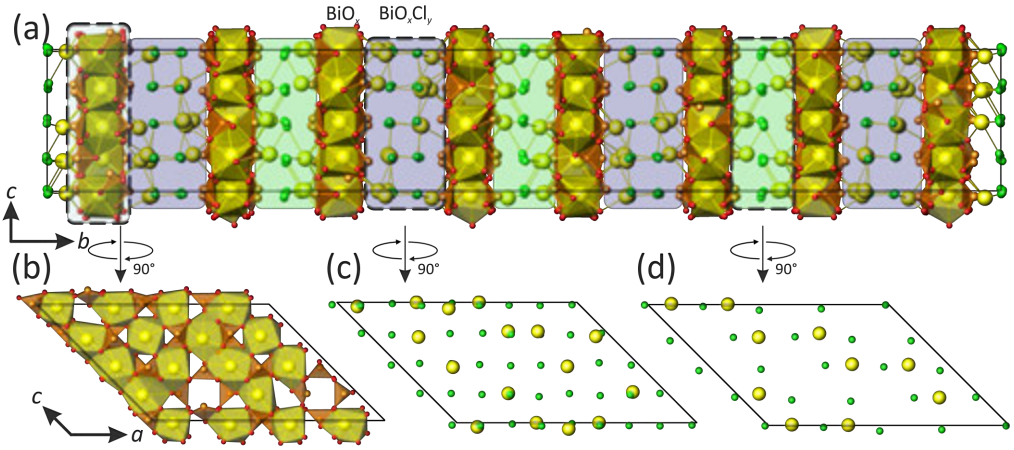

FIGURE 5.6 Projection of the crystal structure of β–$Bi(SeO_3)Cl$ (**c5.6**) along [100] – (a). An alternation of three different parallel layers: $[Bi_{14}(SeO_3)_{24}]^{6-}$ – (b), $[Bi_{12}Cl_{32}]^{4+}$ – (c), and $[Bi_8Cl_{16}]^{8+}$ – (d)

The large value of the *b*-parameter (~76 Å) can be explained by the variety of different modules stacked along the *b*-axis. In other words, the ordering between the $[Bi_8Cl_{16}]^{8+}$ and $[Bi_{12}Cl_{32}]^{4+}$ cationic units sandwiched between the $[Bi_{14}(SeO_3)_{24}]^{6-}$ anionic sheets is the key factor for the formation of a giant cell and responsible for the doubling of *b*-parameter. Detailed examination of the crystal structure of **c5.6** and the analysis of the α → β → γ phase transitions associated with a dramatic fluctuation of structural complexity together with the transitional character of the β phase can be found in the article **A-III** (*see* Included Articles).

$PbBi_{10}(SeO_3)_{12}Cl_8$

The crystal structure of $PbBi_{10}(SeO_3)_{12}Cl_8$ (**c5.7**) contains five independent sites occupied by heavy cations. One of them, Bi(1), is fully occupied by Bi^{3+}, while a refinement of the four others indicated the same mixed Bi^{3+}/Pb^{2+} occupancy of 0.9/0.1. Taking into account Bi/Pb–O and Bi–Cl bond lengths smaller than 3.10 Å, the following irregular coordination polyhedra of heavy cations can be observed: $Bi(1)O_8$, $Bi(2)O_{10}$, $Bi(3)O_{10}$, $Bi(4)O_{10}$, and $Bi(5)O_4Cl_4$. Three crystallographically inequivalent triangular

pyramidal selenite groups are connected to the *2D* structural units composed of $Bi(1)O_8$, $Bi(2)O_{10}$, $Bi(3)O_{10}$, and $Bi(4)O_{10}$ polyhedra by sharing of common O–O edges (Figure 5.7). Generally, the structure of **c5.7** can be described as a *2D* network, with the $[(Pb,Bi)_{14}(SeO_3)_{24}]^{n-}$ sheet (Figure 5.7b) sandwiched between the $[(Pb,Bi)_8Cl_{16}]^{n+}$ layers (Figure 5.7c) laying parallel to the (010) plane. The structural architecture of **c5.7** is closely related to that observed in the crystal structure of $CaNd_{10}(SeO_3)_{12}Cl_{18}$ [Berdonosov et al. 2007]. Detailed description of the crystal structure of **c5.7** can be found can be in the article **A-III** (*see* Included Articles).

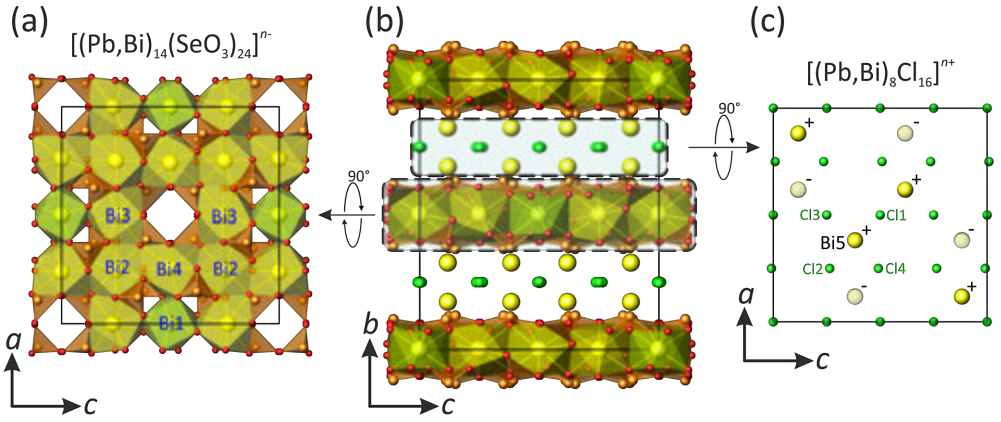

FIGURE 5.7 Projection of the crystal structure of $PbBi_{10}(SeO_3)_{12}Cl_8$ (**c5.7**) along the *a*-axis – (b), two parallel cationic and anionic layers: $[(Pb,Bi)_{14}(SeO_3)_{24}]^{n-}$ – (a) and $[(Pb,Bi_8)Cl_{16}]^{n+}$ – (c)

2.6 Crystal chemical studies of uranyl selenates and selenite-selenates

Crystallographic data and experimental parameters for the crystal structures of 16 novel compounds listed below are summarized in Table 6.1 and Table 6.2.

c6.1 –	$[CH_6N]_2[(UO_2)(SeO_4)_2(H_2O)](H_2O)$	**c6.9** –	$[C_2H_8N]_2[(UO_2)(SeO_4)_2(H_2O)]$
c6.2 –	$[CH_6N]_2[(UO_2)(SeO_4)_2(H_2O)]$	**c6.10** –	$[C_2H_8N]_2[(UO_2)_2(SeO_4)_3(H_2O)]$
c6.3 –	$[CH_6N]_2[(UO_2)_2(SeO_4)_3]$	**c6.11** –	$[C_4H_{15}N_3][H_3O]_{0.5}[(UO_2)_2(SeO_4)_{2.93}(SeO_3)_{0.07}(H_2O)](NO_3)_{0.5}$
c6.4 –	$[CH_6N](H_3O)[(UO_2)_2(SeO_4)_3(H_2O)](H_2O)$	**c6.12** –	$[C_2H_8N]_3[H_5O_2][(UO_2)_2(SeO_4)_3(H_2O)_2]_2(H_2O)_5$
c6.5 –	$[CH_6N]_4[(UO_2)_3(SeO_4)_5](H_2O)_4$	**c6.13** –	$[C_2H_8N]_2[H_3O][(UO_2)_3(SeO_4)_4(HSeO_3)(H_2O)](H_2SeO_3)_{0.2}$
c6.6 –	$[CH_6N](H_5O_2)(H_3O)_2[(UO_2)_3(SeO_4)_5](H_2O)_4$	**c6.14** –	$[C_4H_{12}N]_3[H_3O][(UO_2)_3(SeO_4)_5(H_2O)]$
c6.7 –	$[CH_6N]_4(H_3O)_2[(UO_2)_5(SeO_4)_8(H_2O)](H_2O)_4$	**c6.15** –	$[C_2H_8N]_3(C_2H_7N)[(UO_2)_3(SeO_4)_4(HSeO_3)(H_2O)]$
c6.8 –	$[CH_6N]_{1.5}(H_5O_2)_{1.5}(H_3O)_3[(UO_2)_5(SeO_4)_8(H_2O)](H_2SeO_4)_{2.6}(H_2O)_3$	**c6.16** –	$[C_2H_8N][(H_5O_2)(H_2O)][(UO_2)_2(SeO_4)_3(H_2SeO_3)](H_2O)$

TABLE 6.1 Crystallographic data and refinement parameters for **c6.1**, **c6.2**, **c6.3**, **c6.4**, **c6.5**, **c6.6**, **c6.7**, and **c6.8**

	c6.1	**c6.2**	**c6.3**	**c6.4**	**c6.5**	**c6.6**	**c6.7**	**c6.8**
M_r, (g mol^{-1})	639.99	623.99	1020.98	1042.96	1692.97	1678.91	2709.91	2946.25
sp. gr.	*Pnma*	$P2_1/c$	$P2_1$	$P2_1/c$	*Pnna*	*Ibca*	$Pca2_1$	*Pnma*
a (Å)	7.5496(7)	8.2366(10)	8.583(1)	8.4842(10)	16.422(1)	20.956(2)	31.505(2)	30.973(2)
b (Å)	12.014(1)	7.5888(6)	10.073(1)	10.2368(8)	18.4773(9)	34.767(8)	10.369(1)	37.022(2)
c (Å)	15.836(1)	22.260(2)	10.095(1)	24.228(2)	10.3602(5)	18.663(2)	16.242(1)	10.417(1)
β (°)	90	104.566(9)	95.98(1)	102.803(9)	90	90	90	90
V (Å^3)	1436.3(2)	1346.7(2)	867.7(2)	2051.9(3)	3143.7(3)	13597(4)	5305.9(6)	11945(1)
Z	4	4	2	4	4	16	4	8
ρ (g/cm^3)	2.960	3.078	3.908	3.376	3.577	3.280	3.392	3.277
μ (mm^{-1})	16.423	17.507	25.012	21.166	21.319	19.720	20.814	20.086
λ (MoK_α) (Å)	0.71073	0.71073	0.71073	0.71073	0.71073	0.71073	0.71073	0.71073

TABLE 6.1 *Continued*

	c6.1	**c6.2**	**c6.3**	**c6.4**	**c6.5**	**c6.6**	**c6.7**	**c6.8**
total rflns	10099	12119	5477	12326	18468	32094	27846	61466
indep rflns	1605	3656	2931	3602	2774	4913	8463	10116
R_{int}	0.0875	0.0828	0.1271	0.1698	0.1191	0.3280	0.2070	0.2139
R_1 [$I > 2\sigma(I)$]	0.0467	0.0466	0.1072	0.0674	0.0541	0.1040	0.0852	0.0858
wR_2 [$I > 2\sigma(I)$]	0.0860	0.0637	0.2712	0.1551	0.1119	0.1867	0.1901	0.1736
R_1 [all data]	0.0566	0.0785	0.1126	0.0957	0.0790	0.2138	0.1305	0.1556
wR_2 [all data]	0.0882	0.0688	0.2766	0.1693	0.1216	0.2287	0.2150	0.2083
GOF	1.334	0.996	1.083	1.049	1.104	0.968	0.997	1.055
$\Delta\rho_{max}$, $\Delta\rho_{min}$ (e Å^{-3})	1.44, −3.13	1.59, −2.21	8.61, −3.16	2.84 −1.99	2.23, −1.82	2.58, −1.43	2.44, −1.84	2.90, −1.49
CCDC #	866552	866549	866547	866553	866546	866551	866548	866550

TABLE 6.2 Crystallographic data and refinement parameters for **c6.9**, **c6.10**, **c6.11**, **c6.12**, **c6.13**, **c6.14**, **c6.15**, and **c6.16**

	c6.9	**c6.10**	**c6.11**	**c6.12**	**c6.13**	**c6.14**	**c6.15**	**c6.16**
M_r, (g mol^{-1})	666.15	1079.14	2256.03	2267.28	1685.05	1770.70	1685.07	1217.08
sp. gr.	$P2_12_12_1$	$P2_12_12_1$	$P2_1/c$	$P2_1/c$	$P2_1/m$	$P2_1/m$	*Pnma*	$P2_1/n$
a (Å)	7.5363(7)	11.2154(5)	11.1679(4)	12.451(5)	8.3116(4)	8.941(2)	11.659(1)	14.7979(8)
b (Å)	12.202(1)	11.2263(5)	10.9040(4)	31.126(5)	18.6363(8)	19.300(4)	14.956(2)	10.0238(6)
c (Å)	16.760(2)	16.9138(8)	17.9913(6)	14.197(4)	11.5623(5)	11.377(3)	22.194(2)	16.4176(9)
β (°)	90.00	90.00	98.019(1)	120.39(2)	97.582(1)	97.510(4)	90.00	111.628(1)
V (Å^3)	1541.2(2)	2129.6(2)	2169.6(2)	4746(2)	1775.3(1)	1946.5(7)	3870.0(7)	2263.8(2)
Z	4	4	2	4	2	2	4	4
ρ (g/cm^3)	2.871	3.366	3.457	3.173	3.152	3.021	2.892	3.571
μ (mm^{-1})	15.306	20.394	20.036	18.323	19.286	17.217	17.310	20.822
λ (MoK_α) (Å)	0.71073	0.71073	0.71073	0.71073	0.71073	0.71073	0.71073	0.71073
total rflns	13644	17184	23671	34682	23753	18435	10911	25431
indep rflns	4492	6112	4988	10896	5323	4597	1680	5476
R_{int}	0.056	0.065	0.072	0.096	0.076	0.120	0.112	0.073
R_1 [$I > 2\sigma(I)$]	0.031	0.029	0.033	0.048	0.036	0.040	0.060	0.027
wR_2 [$I > 2\sigma(I)$]	0.063	0.048	0.074	0.106	0.097	0.058	0.096	0.052
R_1 [all data]	0.035	0.038	0.049	0.104	0.055	0.099	0.095	0.041
wR_2 [all data]	0.064	0.050	0.077	0.122	0.102	0.066	0.105	0.054

TABLE 6.2 *Continued*

	c6.9	**c6.10**	**c6.11**	**c6.12**	**c6.13**	**c6.14**	**c6.15**	**c6.16**
GOF	0.940	0.934	0.964	0.875	0.979	0.737	1.127	0.928
$\Delta\rho_{max}$, $\Delta\rho_{min}$, (e Å^{-3})	2.34, −1.45	1.10, −1.20	2.82, −2.00	4.61, −4.34	2.79, −2.23	1.65, −1.38	1.05, −1.21	2.39, −1.81
CCDC #	901940	901941	901942	901943	901944	901945	901946	824406

2.6.1 Synthetic procedures

Single crystals of all novel uranyl selenates and selenite-selenates were prepared by isothermal evaporation under ambient conditions from aqueous solutions of uranyl nitrate hexahydrate, 40%–solution of selenic acid, the respective amine, and distilled water. Yellow-green homogeneous liquid solutions in the vials were left open to the air in a fume hood at the room temperature for several days, after which they were capped and left standing at room temperature. Experimental details containing various molar ratios of initial reagents for syntheses of 16 novel phases are summarized in Table 6.3.

TABLE 6.3 Experimental details of the isothermal evaporation syntheses of novel uranyl selenates and selenite-selenates (temperature: 23°C; time of crystal growth: 72 hours)

molar ratios:	**c6.1**	**c6.2**	**c6.3**	**c6.4**	**c6.5**	**c6.6**	**c6.7**	**c6.8**
SeO_2	0.5	0.4	0.7	0.4	0.8	0.7	0.4	0.7
$UO_2(NO_3)_2{\cdot}6H_2O$ [1]	0.1	0.1	0.1	0.1	0.1	0.2	0.1	0.2
CH_5N [2]	0.4	0.5	0.2	0.5	0.1	0.1	0.5	0.1
H_2O (ml)	2	2	2	2	2	2	2	2

molar ratios:	**c6.9**	**c6.10**	**c6.11**	**c6.12**	**c6.13**	**c6.14**	**c6.15**	**c6.16**
SeO_2	4.1	4.1	0.7	0.7	0.7	4.7	0.5	0.8
$UO_2(NO_3)_2{\cdot}6H_2O$ [1]	0.4	0.4	0.2	0.1	0.1	0.1	0.1	0.1
C_2H_7N [3]				0.2	0.2		0.4	0.1
$C_4H_{11}N$ [4]						0.1		
$C_4H_{13}N_3$ [5]			0.1					
C_3H_7NO [6]	1.3	1.3						
H_2O (ml)	2	2	2	2	2	2	2	2

[1] uranium materials used in these experiments were depleted; [2] methylamine (MA); [3] dimethylamine (DMA); [4] diethylamine (DEA); [5] diethylenetriamine (DETA); [6] *N*,*N*-dimethylformamide (DMF).

2.6.2 Structural description of sixteen novel phases

All novel phases of organically templated uranyl selenates and selenite-selenates presented in this work can be diversified as belonging to several groups according to different U^{6+}: $Se^{6+/4+}$ ratios of inorganic structural units: 1 : 2 – **c6.1**, **c6.2**, **c6.9**, **c6.16**;

2 : 3 – **c6.3**, **c6.4**, **c6.10-c6.12**; 3 : 5 – **c6.5**, **c6.6**, **c6.13 – c6.15**; and 5 : 8 – **c6.7**, **c6.8**. The crystal structures of all phases contain uranyl $(UO_7)^{8-}$ pentagonal bipyramids, selenate $(Se^{6+}O_4)^{2-}$ tetrahedra, or/and selenite $(Se^{4+}O_3)^{2-}$ triangular pyramids with a stereochemically active lone pair of electrons as a complementary ligand. The polyhedra are linked into inorganic structural units with relatively open architectures (those where corner-linkage of polyhedra dominates over edge-linkage). In the crystal structures, U^{6+} cations form approximately linear uranyl ions, $[UO_2]^{2+}$, with the average <U=O> bond length of 1.756 Å among all the structures presented in this study. These basic uranyl entities are coordinated in their equatorial planes by five oxygen atoms (or four O and one H_2O molecule) to form UO_7 (or $UO_6(H_2O)$) pentagonal bipyramids with the average $<U–O_{eq}>$ bond length equal to 2.390 Å. Generally, the $U–O_{eq}H_2$ bond lengths are longer and lie in range of 2.42–2.54 Å. The average <Se–O> bond distance in selenate and selenite groups equals to 1.628 Å. In the structures, the *1D* and *2D* inorganic structural units are separated and templated by organic species and water molecules. Detailed description of all the crystal structures of novel synthesized uranyl selenates and selenite-selenates can be found in the articles **A-I** (**c6.16**), **A-II** (**c6.1 – c6.8**), and **A-VI** (**c6.9 – c6.15**) (*see* Included Articles). Only topological features of the structures are discussed below in this chapter.

Topology of uranyl selenate and selenite-selenate units in the structures under consideration can be visualized using the nodal representation. Within this approach [Krivovichev 2004; Krivovichev 2009; Krivovichev 2010], the U^{6+} and $Se^{6+/4+}$ coordination polyhedra are symbolized by black and white nodes, respectively. The vertices are linked by an edge if two respective polyhedra share a common oxygen atom. The resulting graph is used to investigate topological relations between similar structures. Figure 6.1 shows a whole topological diversity of inorganic structural units in the crystal structures of novel compounds **c6.1 – c6.16**.

Compounds with U : Se = 1 : 2

Crystal structures of $[CH_6N]_2[(UO_2)(SeO_4)_2(H_2O)](H_2O)$ (**c6.1**), $[CH_6N]_2[(UO_2)(SeO_4)_2(H_2O)]$ (**c6.2**), and $[C_2H_8N]_2[(UO_2)(SeO_4)_2(H_2O)]$ (**c6.9**), are based upon structural units with composition $[(UO_2)(SeO_4)_2(H_2O)]^{2-}$. In the structures of **c6.1** and **c6.9** the $(UO_6(H_2O))^{6-}$ pentagonal bipyramids share corners with two adjacent $(SeO_4)^{2-}$ tetrahedra to form $[(UO_2)(SeO_4)_2(H_2O)]^{2-}$ *1D* chains arranged into the

pseudo sheets parallel (Figure 6.1a, b), while the structure of **c6.2** is based upon *2D* sheets of the same composition (Figure 6.1c, d). The chains have been observed first in the structure of $Mn[(UO_2)(SO_4)_2(H_2O)](H_2O)_5$ [Tabachenko et al. 1975] and later in a number of amine-templated uranyl oxysalts. The layered topology of **c6.2** is common for a large number of sheet topologies with the composition $[A_nO_2(SO_4)_2(H_2O)]$ [Krivovichev 2009].

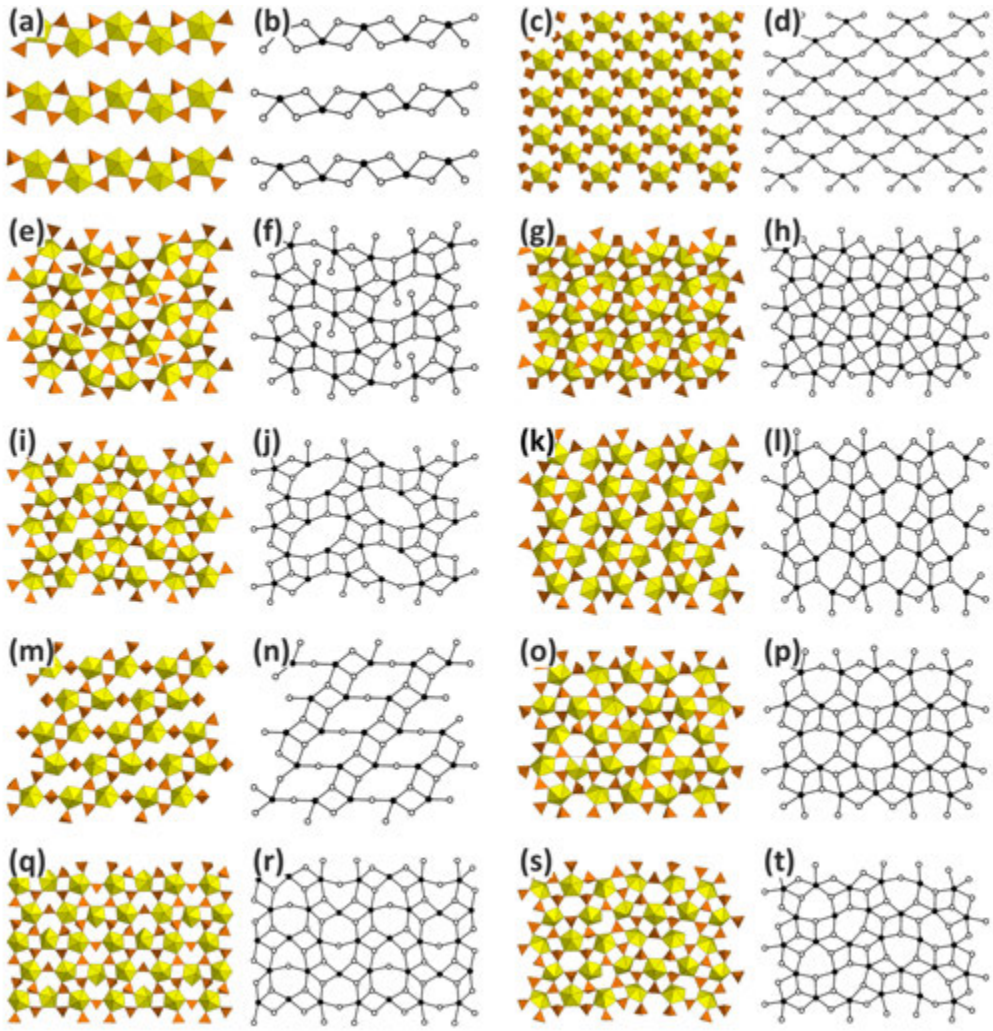

FIGURE 6.1 Topological diversity of inorganic structural units in the crystal structures of novel compounds. Uranyl pentagonal bipyramids and selenate/selenite groups are shown by yellow and orange in polyhedral representation and by black and white vertices in graphs

The crystal structure of $[C_2H_8N][(H_5O_2)(H_2O)][(UO_2)_2(SeO_4)_3(H_2SeO_3)](H_2O)$ (**c6.16**) is based upon $[(UO_2)_2(SeO_4)_3(H_2SeO_3)]^{2-}$ sheets formed as a result of condensation of the $(UO_7)^{8-}$, $(Se^{6+}O_4)^{2-}$, and $(Se^{4+}O(OH)_2)^0$ coordination units by sharing common oxygen atoms. In topological structure of the sheet (Figure 6.1e, f), the selenate group coordinates three uranyl ions, whereas diprotonated selenite groups coordinate one uranyl ion each. This topology has never been observed in any other inorganic oxysalts.

Compounds with U : Se = 2 : 3

In the crystal structures with a U:Se ratio of 2:3, $[CH_6N]_2[(UO_2)_2(SeO_4)_3]$ (**c6.3**), $[CH_6N](H_3O)[(UO_2)_2(SeO_4)_3(H_2O)](H_2O)$ (**c6.4**), $[C_2H_8N]_2[(UO_2)_2(SeO_4)_3(H_2O)]$ (**c6.10**), $[C_4H_{15}N_3][H_3O]_{0.5}[(UO_2)_2(SeO_4)_{2.93}(SeO_3)_{0.07}(H_2O)](NO_3)_{0.5}$ (**c6.11**), and $[C_2H_8N]_3[H_5O_2][(UO_2)_2(SeO_4)_3(H_2O)_2]_2(H_2O)_5$ (**c6.12**), coordination polyhedra of U^{6+} and $Se^{6+/4+}$ share common ligands to produce *2D* sheets with the chemical compositions $[(UO_2)_2(SeO_4)_{3-x}(SeO_3)_x(H_2O)_n]^{2-}$ (n = 0, 1, 2; x = 0, 0.07). Topology of the sheet with n = 0 observed in **c6.3** is based only upon 4-membered rings of alternating uranyl and selenate polyhedra (Figure 6.1g, h). It was already reported *e.g.* in $[CH_6N_3]_2[(UO_2)_2(SeO_4)_3]$ [Krivovichev et al. 2009].

Crystal structures of **c6.4**, **c6.10**, and **c6.11** with n = 1 are based upon structural units with same composition $[(UO_2)_2(SeO_4)_3(H_2O)]^{2-}$, but with different topologies of linkage of U and Se polyhedra. The structure of **c6.4** contains *2D* sheets (Figure 6.1i, j) similar to those found in the structure of **c6.16**. The important difference between these two topologies is related to the presence of additional selenite polyhedra coordinated uranyl group and located in large 8-membered rings of the sheet in the crystal structure of **c6.16**. The topology of the sheet in **c6.4** is rare and has been observed in unique uranyl selenate $K(H_3O)[(UO_2)_2(SeO_4)_3(H_2O)](H_2O)_6$ [Ling et al. 2010].

In the sheets of **c6.10** and **c6.11** (Figure 6.1k, l), 6-membered rings share edges to form chains separated by complex chains of dense 4-membered rings. This type of structural unit was observed in half dozen organically templated crystal structures with protonated molecules as counter ions [Krivovichev 2009]. The analysis of the topology of the sheets of **c6.10** and **c6.11** indicates that non-shared corners of selenate groups may have either up-, down- or disordered (up-or-down) orientations relative to the plane of the sheet. This ambiguity gives rise to geometric isomers with various

orientations of the selenium polyhedra. To identify and classify the isomers of this type, *Krivovichev and Burns* proposed a geometrical approach based on orientation matrices of the isomers [Krivovichev and Burns 2003]. According to this approach, the symbols **u** (up), **d** (down), **m** (orientation up-down topologically equivalent) or □ (white vertex is missing in the graph) are assigned to each white vertex. Interestingly, the orientation matrices of the sheets in the crystal structures of **c6.10** and **c6.11** are equivalent and can be written in row as (**u□dd**)(**uu□d**). Thus, the uranyl selenate sheets observed in these crystal structures correspond to the same geometrical isomers.

The topology of the $[(UO_2)_2(SeO_4)_3(H_2O)_n]^{2-}$ sheet with $n = 2$ in **c6.12** contains columns of edge-shared large hollow 8-membered rings and dense 4-membered rings (Figure 6.1m, n). This topology has never been observed in uranyl selenates.

Compounds with U : Se = 3 : 5

The crystal structures of $[CH_6N]_4[(UO_2)_3(SeO_4)_5](H_2O)_4$ (**c6.5**) and $[CH_6N](H_5O_2)(H_3O)_2[(UO_2)_3(SeO_4)_5](H_2O)_4$ (**c6.6**) are based upon topologically similar inorganic sheets with the composition $[(UO_2)_3(SeO_4)_5]^{4-}$ (Figure 6.1o, p). The sheets are built from 4- and 6-membered rings. This topology of uranyl was observed in some uranyl selenate and chromate compounds [Krivovichev 2009]. Using the geometrical approach based on determination of the orientation of non-shared vertices of selenate tetrahedra, the orientation rows for the sheets in **c6.5** and **c6.6** may be written as (□**uu**□**dd**)(**mddmuu**) and (□**ud**□**ud**)(**duuddd**)(□**du**□**du**)(**ddddud**), respectively. Thus, the uranyl selenate and selenite-selenate sheets observed in these crystal structures correspond to different geometrical isomers.

The crystal structures of $[C_2H_8N]_2[H_3O][(UO_2)_3(SeO_4)_4(HSeO_3)(H_2O)](H_2SeO_3)_{0.2}$ (**c6.13**), $[C_4H_{12}N]_3[H_3O][(UO_2)_3(SeO_4)_5(H_2O)]$ (**c6.14**), and $[C_2H_8N]_3(C_2H_7N)[(UO_2)_3(SeO_4)_4(HSeO_3)(H_2O)]$ (**c6.15**) have the same topology of inorganic sheets (Figure 6.1q, r) built up from 4- and 6-membered rings. This topology of inorganic complexes is typical for uranyl selenite-selenates, and it was observed *e.g.* in $[C_5H_{14}N]_4[(UO_2)_3(SeO_4)_4(HSeO_3)(H_2O)](H_2SeO_3)(HSeO_4)$ [Krivovichev et al. 2006].

The orientation matrices for **c6.13**, **c6.14** and **c6.15** have dimensions 6×2. The series of symbols written in row (**duuudd**)(**ud□du□**), (**dumudm**)(**ud□du□**), and (**ududud**)(**ud□du□**) for their inorganic sheets completely characterizes the topological structure of the geometric isomers **c6.13**, **c6.14** and **c6.15**.

Compounds with U : Se = 5 : 8

The crystal structures of $[CH_6N]_4(H_3O)_2[(UO_2)_5(SeO_4)_8(H_2O)](H_2O)_4$ (**c6.7**) and $[CH_6N]_{1.5}(H_5O_2)_{1.5}(H_3O)_3[(UO_2)_5(SeO_4)_8(H_2O)](H_2SeO_4)_{2.6}(H_2O)_3$ (**c6.8**) are based upon sheets with the chemical composition $[(UO_2)_5(SeO_4)_8(H_2O)]^{6-}$ (Figure 6.1s, t). They contain 4- and 6-membered rings: 6-membered rings share vertices to form corner-sharing pairs separated by chains of edge-sharing 4-membered rings. The pairs are stretched alternatively along mutual perpendicular directions. The compounds **c6.7** and **c6.8** are the first examples of this topology for uranyl selenates.

Using the geometrical approach based on determination of the orientation of non-shared vertices of selenate tetrahedra, the orientation rows for the sheets in **c6.7** and **c6.8** may be written as (**uu□uu**)(**ddud□**) and (**dd□dd**)(**duuu□**), respectively. Thus, the uranyl selenate and selenite-selenate sheets observed in these crystal structures correspond to different geometrical isomers.

2.6.3 Dimensional reduction

In order to investigate the chemistry-structure relationships, we employed the dimensional reduction principle [Long et al. 1996; Tulsky and Long 2001]. Here, the whole range of the compounds with the general formula $A_n(UO_2)_p(TO_4)_q(H_2O)_r$ (A^+ = monovalent cation, and T^{6+} = Se, S, Cr, Mo) has been analysed. It was supposed that the basic highly-polymerized *3D* parent structure is that of $(UO_2)(TO_4)$, whereas the role of reducing agents is played by $A_2(TO_4)$ and H_2O. Consequently, the relationships between different compositions and structures may be visualized using the UO_2TO_4 – A_2TO_4 – H_2O compositional diagram (Figure 6.2). List of all relevant compounds and dimensional characteristics of their structures can be found in the article **A-II** (*see* Included Articles). The diagram shown in Figure 6.2 may be divided into regions, where structures have the same dimensionality values (0 = finite clusters, 1 = chains, 2 = sheets, 3 = frameworks). Definition of the borders between the fields is not unambiguous and is rather tentative in character. For instance, due to the presence of only one point (**36**) corresponding to the *0D* phases, the borders between the *0D* and *1D* fields are hypothetical. We suppose these borders are subparallel to the borders between *1D*-and-*2D*, *2D*-and-*3D* fields, and are in agreement with the principle of dimensional reduction for inorganic oxysalts.

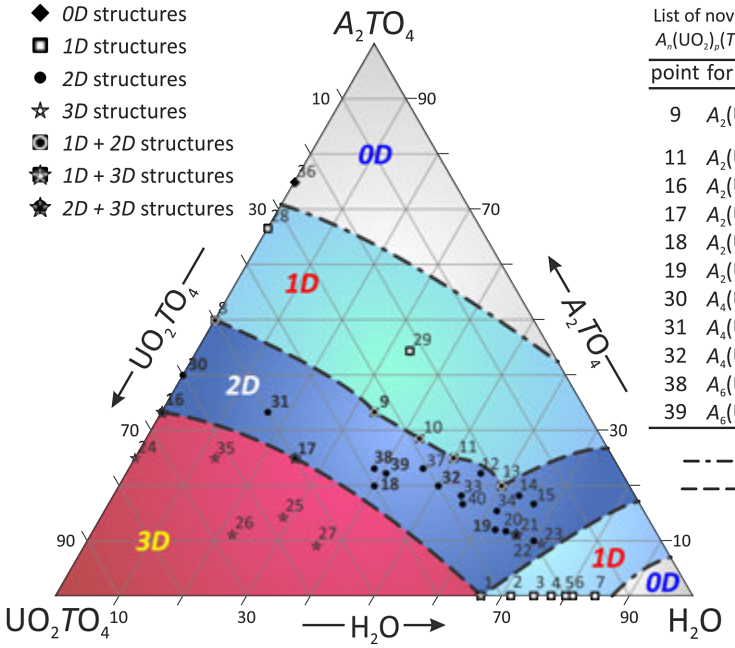

List of novel compounds with general formula $A_n(UO_2)_p(TO_4)_q(H_2O)_r$ (A^+ = amine, H_3O; $T = Se^{6+}$)

point	formula	type	dim.	comp.
9	$A_2(UO_2)(TO_4)_2(H_2O)$	1	1	**c6.9**
		2	2	**c6.2**
11	$A_2(UO_2)(TO_4)_2(H_2O)_2$	1	1	**c6.1**
16	$A_2(UO_2)_2(TO_4)_3$	2	2	**c6.3**
17	$A_2(UO_2)_2(TO_4)_3(H_2O)$	2	2	**c6.10**
18	$A_2(UO_2)_2(TO_4)_3(H_2O)_2$	2	2	**c6.4**
19	$A_2(UO_2)_2(TO_4)_3(H_2O)_5$	2	2	**c6.12**
30	$A_4(UO_2)_3(TO_4)_5$	2	2	**c6.5**
31	$A_4(UO_2)_3(TO_4)_5(H_2O)$	2	2	**c6.14**
32	$A_4(UO_2)_3(TO_4)_5(H_2O)_5$	2	2	**c6.6**
38	$A_6(UO_2)_5(TO_4)_8(H_2O)_5$	2	2	**c6.7**
39	$A_6(UO_2)_5(TO_4)_8(H_2O)_{5.5}$	2	2	**c6.8**

theoretical borders
experimental borders

FIGURE 6.2 Dimensional fields on the compositional diagram of the UO_2TO_4 – A_2TO_4 – H_2O (A = monovalent cation, T = S, Se, Cr, Mo) system.

However, some deviations are observed. The points **21** and **23** are located within the *2D* field, but correspond to the *3D* framework structures with the $A_6(UO_2)_2(TO_4)_3(H_2O)_6$ and $A_6(UO_2)_2(TO_4)_3(H_2O)_{7.5}$ compositions, respectively. We attribute these deviations to the double role of H_2O: in most cases, it acts as reducing agent, whereas, in the cases of **21** and **23**, it simply fills cavities of the uranyl-based framework.

For more detailed demonstration of the principle of dimensional reduction in the system, one may consider the line originating from the left and ending at the top corner of the diagram. The line describes compounds with the composition $A_n(UO_2)_p(TO_4)_q$. The points **24**, **30**, **28**, and **36** correspond to the structures with dimensionalities equal to 3, 2, 1, and 0, respectively. The points **16** and **8** are located on the borders between *2D*-and-*3D*, *1D*-and-*2D* fields, respectively. Thus, the dimensionality of the structural unit is decreasing from the points **24** to **36**, which is in agreement with the principle of dimensional reduction.

2.7 Analogy between electron lone pairs of selenites and H–P bonds phosphites

In this section, we present the fascinating results obtained at the end of this co-tutorial thesis project, with original evidence of negatively charged hydrogen in phosphites. The $(HPO_3)^{2-}$ anions, which are resulted from phosphonic acid $HPO(OH)_2$ upon deprotonation, are commonly encountered as a tridentate tetrahedral ligands in solids. The H–P bond in $(HPO_3)^{2-}$ is commonly viewed as resulting from protonation of the phosphorus lone pair. Although the phosphite groups in solution have been subject of a number of spectroscopic studies [Loub 1991], there has been no clear characterization of the H–P bond of phosphite anions in crystalline solids.

In the context of the present studies, we have synthesized two isotypic compounds, $Fe_2(SeO_3)_3$ and $Fe_2(HPO_3)_3$. The tunnel crystal structures of those clearly show an analogy between lone electron pairs of selenite groups and H–P bonds in phosphite anions. It demonstrates that in solids containing $(HPO_3)^{2-}$ and $(ESeO_3)^{2-}$ anions, the H–P bond in phosphites has the same role as does the lone pair *E* in selenites (Figure 7.1), suggesting that the H atom is negatively charged and the H–P bond possesses some hydridic character in $(HPO_3)^{2-}$ anions.

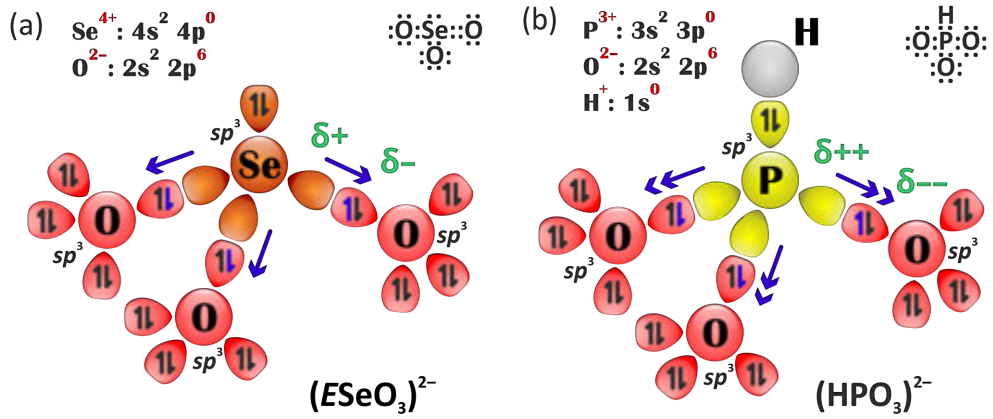

FIGURE 7.1 Lewis structures and simplified artistic representation of orbital models of $(ESeO_3)^{2-}$ (a) and $(HPO_3)^{2-}$ (b) anions, which highlights the similar geometrical role of H_{HPO3} and E_{SeO3}.

2.7.1 Synthesis and structural characterization of iron selenite and phosphite

Single crystals of $Fe_2(SeO_3)_3$ (**c7.1**) and $Fe_2(HPO_3)_3$ (**c7.2**) have been prepared by hydrothermal techniques. The reagents $FeCl_3{\cdot}6H_2O$, Li_2CO_3 and SeO_2/H_3PO_3 were mixed in a molar ratio of 1 : 1.5 : 2.5, and then dissolved the mixture in 6 ml of distilled water. The hydrothermal reactions were performed in 23 ml Teflon-lined autoclaves that were heated to 160 °C in ovens. The temperature of autoclaves was held constant for two days, followed by cooling to room temperature during 48 hours. It should to be note that another way for synthesis of $Fe_2(HPO_3)_3$ was reported in [Sghyar et al. 1991], where the crystalline compound was obtained by an isothermal slow evaporation from the aqueous solution containing 20% of Fe_2O_3, 30% of H_3PO_3, and 50% of distilled water at 90 °C. Crystallographic data and experimental parameters for the crystal structures of the compounds are summarized in Table 7.1.

TABLE 7.1 Crystallographic data and refinement parameters for $Fe_2(SeO_3)_3$ (**c7.1**) and $Fe_2(HPO_3)_3$ (**c7.2**).

	c7.1	**c7.2**
M_r (g mol^{-1})	492.58	351.63
space group	$P6_3/m$	$P6_3/m$
a (Å)	7.8720(9)	8.0195(2)
c (Å)	7.3258(10)	7.3700(2)
V (Å^3)	393.15(10)	410.48(2)
Z	2	2
ρ (g/cm^3)	4.161	2.845
μ (mm^{-1})	17.603	4.144
λ (MoK_α) (Å)	0.71073	0.71073
total rflns	3894	8590
indep rflns	472	475
R_{int}	0.0303	0.0325
R_1 [$I > 2\sigma(I)$]	0.0141	0.0133
wR_2 [$I > 2\sigma(I)$]	0.0308	0.0413
R_1 [all data]	0.0157	0.0154
wR_2 [all data]	0.0311	0.0433
GOF	1.098	1.249
$\Delta\rho_{max}$,$\Delta\rho_{min}$ (e Å^{-3})	0.451, –0.426	0.423, –0.309

The crystal structures of $Fe_2(SeO_3)_3$ (**c7.1**) and $Fe_2(HPO_3)_3$ (**c7.2**) contain $[Fe_2O_9]^{12-}$ dimers of face-sharing $Fe^{3+}O_6$ octahedra. The average Fe–O bond lengths of $Fe_2(SeO_3)_3$ and $Fe_2(HPO_3)_3$ are nearly the same, and so are their Fe···Fe distances (2.987 Å and 2.980 Å, respectively). The $[Fe_2O_9]^{12-}$ dimers share all their six vertices with

(ESeO$_3$)$^{2-}$or (HPO$_3$)$^{2-}$ tetrahedra, forming hexagonal channels along the c-axis (Figure 7.2). The H–P bonds are pointed toward the axis of each tunnel as do the lone pairs in of (ESeO$_3$)$^{2-}$. The Se–O bonds (1.676–1.722 Å) are longer than the P–O bonds (1.513–1.540 Å), but the tunnel is larger in diameter for Fe$_2$(HPO$_3$)$_3$ than for Fe$_2$(SeO$_3$)$_3$. The H–P bond is 1.310 Å, whereas the centre of each lone pair of selenite anion is at a distance of ≈0.260 Å from the Se (calculated using the program HYBRIDE based on a theory developed by *Verbaere* and co-workers. [Verbaere et al. 1978]).

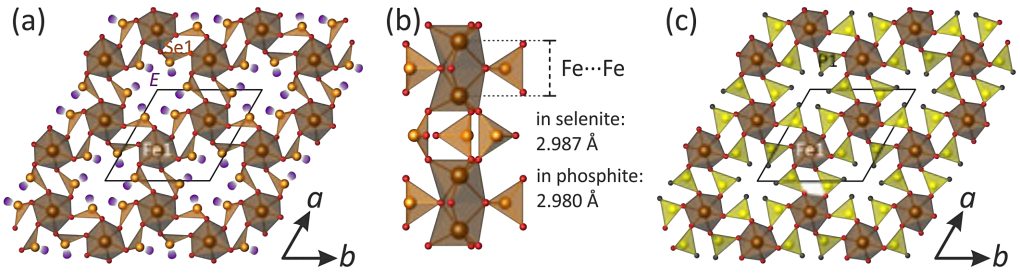

FIGURE 7.2 View of the crystal structures of Fe$_2$(SeO$_3$)$_3$ (**c7.1**) and Fe$_2$(HPO$_3$)$_3$ (**c7.2**) along the c-axis – (a) and (c), respectively; mode of linkage of iron (brown) and selenite (orange) polyhedra in **c7.1** – (b).

2.7.2 Calculation of partial charges

For a number of phases of already reported phosphite phases with various crystal structures of different dimensionalities, the partial charges on P and H were calculated using the Henry's method [Henry 2002; Henry 2008] in order to find systematic residual partial negative charges on the H atoms (Table 7.2). The latter indicates a weak but significant hydride character, *e.g.* the weakly negative charge of –0.024 electron units (*e.u.*) found for the H atoms in Fe$_2$(HPO$_3$)$_3$, and –0.108 *e.u.* and –0.099 *e.u.* for the H atoms of two inequivalent phosphite groups in Sr(H$_2$O)$_2$[(UO$_2$)(HPO$_3$)$_2$] [Villa et al. 2013].

In Fe$_2$(HPO$_3$)$_3$, the calculated partial charges for O and P atoms are $\delta_O \approx -0.34$ *e.u.* and $\delta_P \approx +0.17$ *e.u.*, respectively. Dealing with bigger ligands, *e.g.* chlorides in PCl$_3$, the bond P^{3+}–Cl$^-$ polarization is displaced in favor of high partial positive charge on the phosphorus atom ($\delta_{Cl} = -0.11$ and $\delta_P = +0.34$), which is not suitable for the formation of a H–P bond.

TABLE 7.2 Calculated partial charges for featured selected compounds.

	partial charges, ±*q*			
	H	P / Se / As	O / Cl	ref.
$Fe_2(HPO_3)_3$	–0.024	+0.170	–0.382 (×2), –0.293	[1], **c7.2**
$Sc_2(HPO_3)_3$	–0.068	+0.304	–0.602 (×2), –0.695	[2]
$Al_2(HPO_3)_3$	–0.042	+0.454	–0.504 (×2), –0.573	[3]
$Ga_2(HPO_3)_3$	–0.032	+0.479	–0.437 (×2), –0.483	[3]
$Fe_2(HPO_3)F_2$	–0.048	+0.401	–0.453 (×2), –0.452	[4]
$Sr(H_2O)_2[(UO_2)(HPO_3)_2]$	–0.108	+0.170	–0.539, –0.707, –0.695	[5]
	–0.099	+0.199	–0.666, –0.585, –0.676	
$Ni_{11}(HPO_3)_2(OH)_6$	–0.045	+0.478	–0.420 (×3)	[6]
	–0.048	+0.459	–0.432 (×3)	
PCl_3		+0.340	–0.114 (×2), –0.113	[7]
$Fe_2(SeO_3)_3$		+0.056	–0.353 (×2), –0.280	**c7.1**
$Sc_2(SeO_3)_3$		+0.088	–0.558 (×2), –0.661	[8]
$Zn_3(AsO_3)_2$		+0.231	–0.468 (×2), –0.467	[9]
		+0.206	–0.469 (×2), –0.470	

[1] – [Sghyar et al. 1991]; [2] – [Ewald et al. 2003]; [3] – [Morris et al. 1994]; [4] – [Liu et al. 2009]; [5] – [Villa et al. 2013]; [6] – [Marcos et al. 1993]; [7] – [Enjalbert et al. 1980]; [8] – [Wontcheu and Schleid 2003]; [9] – [Ghose et al. 1977].

Similar effects can be expected in arsenites by lowering the metal electronegativity ($\chi_P > \chi_{As}$), which play in favour of stereoactive "free" lone pairs in AsO_3 groups. A more electronegative selenium cation ($\chi_{Se} >> \chi_P$) generates less polarized Se–O bonds, as in $Fe_2(SeO_3)_3$, leading to $\delta_{Se} \approx +0.056$ *e.u.*, which is also not suitable for the formation of H–Se bonds and is responsible for $(ESeO_3)^{2-}$ ions in solids.

In fact, complementary *ab-initio* molecular calculations performed in collaboration with the group of Prof. Dr. M. Whangbo have validated the partial negative charge of the H atom due to the almost zero participation of *p*-states and strong contribution of H in the HOMO molecular orbital. We have also proved that due to its geometry and charge the HPO_3 groups are very weak magnetic connectors between two magnetic centres, *e.g.* PO_4, SeO_3… This work is still in preparation.

3 CONCLUSION AND PERSPECTIVES

The exploration of several metal-oxide chemical systems containing selenium with various metals ($Cu^{+/2+}$, Ni^{2+}, Co^{2+}, $V^{4+/5+}$, $Mn^{2+/3+}$, Fe^{3+}, Pb^{2+}, Bi^{3+}, U^{6+}) were presented in this work. Crystal chemistry of a large group of novel oxide compounds of Se^{4+} and Se^{6+} was mainly investigated by means of X-ray single crystal structural analysis. Further characterizations have not been detailed in this manuscript but can be found in the appended published articles. From the crystallographic viewpoint, most of the phases present a very well ordered assembly composed of distinct units leading to very good quality crystals. Only compounds described on the basis of oxocentered $O(Bi/Mn)_4$ units show a tendency for disorder. This is a general situation favoured in the Bi^{3+} case, because O–Bi bonds based on the sums of ionic radii give a contribution of 0.596 valence unit, greater than the 0.5 needed, which leads to distortion or Bi substitution, like in the described cases.

This thesis is one of the first dedicated to the synthesis of the series of novel metal-oxide compounds using the "geo-inspired" approach assumed emulation of natural crystal growth processes in order to obtain complex functional materials with a potential in terms of specific physical properties. A large variety of resulted novel compounds clearly shows the appropriateness of using this approach for prospecting of new functional materials. The good results obtained from the CVT and in solution validate that selenite and selenate groups are very suitable structural templating agents for the crystal growth of minerals in various geochemical environments.

In the context of this work, eight novel copper oxoselenites were obtained by the chemical vapour transport reactions. This result proves the efficiency of the CVT

method for the synthesis of unique mixed Cu^{+}–Cu^{2+} oxyhalide compounds. The compounds described herein are based upon oxocentered (μ_4–O)Cu_4 tetrahedral units that polymerize to form structural complexes of different dimensionality.

The PbO–NiO–SeO_2 ternary system was scrupulously investigated in hydrothermal conditions. Three novel lead nickel selenites and one novel lead cobalt selenite were synthesized and characterized. According to the experimental results, the pH values of the solution play the essential role in hydrolysis and condensation processes by hydrothermal reactions in the studied system, and determine structural architectures of resulted products of the syntheses.

Three novel compounds were prepared in the course of the investigation of the ternary systems with lead, vanadium, and selenium. Two of them are new polymorphic modifications of already known compounds. Discussion of polymorphism demonstrated a large diversity of geometries of structural units in the crystal structures of vanadate selenites, which can be caused in part by the presence of chemically differ bonds in ($V^{5+}O_n$) polyhedra. Also contributing is the fact that the asymmetric selenite groups with stereochemically active lone electron pairs could form structural cavities leading to materials with open architectures.

Seven novel Se compounds containing manganese and bismuth were synthesized by using various techniques: evaporation from aqueous solution, hydrothermal reactions, and chemical vapour transport reactions. Three phases of them represent the first examples of oxoselenites containing both bismuth and manganese cations.

Sixteen novel selenium-containing uranyl oxysalts templated by organic amines were reported. The observed topologies of the structural units of new compounds have been investigated using a graph theory, and a special approach based upon construction of orientation matrices has been applied to distinguish different geometrical isomers of uranyl selenates and selenite-selenates with the same structural topologies. Analysis of known $A_n(UO_2)_p(TO_4)_q(H_2O)_r$ compounds (A^+ = monovalent cation, and T^{6+} = Se, S, Cr, Mo) using the principle of dimensional reduction combined with the composition-structure diagram allowed to separate on it dimensional fields corresponding to the formation of uranyl structures with specific dimensionalities of their structural units.

The given analogy between lone electron pairs of selenite groups and H–P bonds of phosphite anions at the examples of isotypic selenite and phosphite compounds supported by calculations of partial charges, suggested that the H atom is negatively

charged and the H–P bond possesses some hydridic character in $(HPO_3)^{2-}$. It offers promising potentialities for synthesis of open structures decorated by polarized P–H or Se–*E* units, *i.e.* for cationic intercalation materials, molecular sieves, catalysis *etc*…

Overall results of the present study contribute to the fundamental knowledge of the crystal chemistry of synthetic and natural oxide compounds of selenium in the oxidation states of +4 and +6. The "geo-inspired" approach used for the synthesis of novel metal-oxide compounds is innovative and can be used within the framework of renewal of modern inorganic chemistry and purposeful design of novel complex functional materials with a potential in terms of specific physical properties. The number of discovered Se oxocompounds allows to predict possible mineral phases that may form in various geochemical environments. Observed open architectures in most of the new compounds give an opportunity to use their cavities for the intercalation/extraction of mobile organic ions into/out of them for catalysis and ion exchange chemistry in perspective. Further elaboration of more condensed Se structures with transition metals can lead to interesting magnetic properties. The only limitation is synthetic methods due to high volatility of selenium oxysalts.

REFERENCES

Abraham, F.; Cousin, O.; Mentré, O.; Ketatni, E. M. Crystal Structure Approach of the Disordered New Compounds $Bi_{\sim 1.2}M_{\sim 1.2}PO_{5.5}$ (*M*=Mn, Co, Zn): The Role of Oxygen-Centered Tetrahedra Linkage in the Structure of Bismuth–Transition Metal Oxy-phosphates // J. Solid State Chem. 2002. Vol. 167. P. 168–181.

Alekseev, E. V.; Krivovichev, S. V.; Armbruster, T.; Depmeier, W.; Suleimanov, E. V.; Chuprunov, E. V.; Golubev, A. V. Dimensional Reduction in Alkali Metal Uranyl Molybdates: Synthesis and Structure of $Cs_2[(UO_2)O(MoO_4)]$ // Z. Anorg. Allg. Chem. 2007. Vol. 633. P. 1979–1984.

Alekseev, E. V.; Krivovichev, S. V.; Depmeier, W. A crown ether as template for microporous and nanostructured uranium compounds // Angew. Chem. Int. Ed. Engl. 2008. Vol. 47. P. 549–551.

Aliev, A.; Endara, D.; Huvé, M.; Colmont, M.; Roussel, P.; Delevoye, L.; Tran, T. T.; Halasyamani, P. S.; Mentré, O. Labile degree of disorder in bismuth-oxophosphate compounds: Illustration through three new structural types // Inorg. Chem. 2014. Vol. 53. P. 861–871.

Aliev, A.; Huvé, M.; Colis, S.; Colmont, M.; Dinia, A.; Mentré, O. Two-Dimensional Antiferromagnetism in the $[Mn_{3+x}O_7][Bi_4O_{4.5-y}]$ Compound with a Maple-Leaf Lattice // Angew. Chem. Int. Ed. Engl. 2012. Vol. 51. P. 9393–9397.

Aliev, A.; Olchowka, J.; Colmont, M.; Capoen, E.; Wickleder, C.; Mentré, O. New $[PbBi_2O_4][Bi_2O_2]Cl_2$ and $[Pb_nBi_{10-n}O_{13}][Bi_2O_2]_nCl_{4+n}$ Series by Association of Sizable Subunits: Relationship with Arppe's Compound $Bi_{24}O_{31}Cl_{10}$ and Luminescence Properties // Inorg. Chem. 2013. Vol. 52. P. 8427–8435.

Amorós, P.; Marcos, M. D.; Roca, M.; Beltrán-Porter, A.; Beltrán-Porter, D. Synthetic Pathways for New Tubular Transition Metal Hydroxo- and Fluoro-Selenites: Crystal Structures of $M_{12}(X)_2(SeO_3)_8(OH)_6$ (*M*=Co^{2+}, Ni2+; X=OH^-, F^-) // J. Solid State Chem. 1996. Vol. 126. P. 169–176.

Berdonosov, P. S.; Olenev, A. V.; Dolgikh, V. A.; Lightfoot, P. The synthesis and crystal structures of the first rare-earth alkaline-earth selenite chlorides $MNd_{10}(SeO_3)_{12}Cl_8$ (*M*=Ca and Sr) // J. Solid State Chem. 2007. Vol. 180. P. 3019–3025.

Binnewies, M.; Glaum, R.; Schmidt, M.; Schmidt, P. Chemical Vapor Transport Reactions - A Historical Review // Z. Anorg. Allg. Chem. 2013. Vol. 639. P. 219–229.

Boudin, S.; Guesdon, A.; Leclaire, A.; Borel, M.-M. Review on vanadium phosphates with mono and divalent metallic cations: syntheses, structural relationships and classification, properties // Int. J. Inorg. Mater. 2000. Vol. 2. P. 561–579.

Burns, P. C.; Krivovichev, S. V.; Filatov, S. K. New Cu^{2+} Coordination Polyhedra in the Crystal Structure of Burnsite, $KCdCu_7O_2(SeO_3)_2Cl_9$ // Can. Mineral. 2002. Vol. 40. P. 1587–1595.

Burrows, A. D.; Mahon, M. F.; Sebestyen, V. M.; Lan, Y.; Powell, A. K. Synthesis, structures, and magnetic behavior of new anionic copper(II) sulfate aggregates and chains. // Inorg. Chem. 2012. Vol. 51. P. 10983–9.

Cao, X.-L.; Kong, F.; Hu, C.-L.; Xu, X.; Mao, J.-G. $Pb_4V_6O_{16}(SeO_3)_3(H_2O)$, $Pb_2VO_2(SeO_3)_2Cl$, and $PbVO_2(SeO_3)F$: New Lead(II)-Vanadium(V) Mixed-Metal Selenites Featuring Novel Anionic Skeletons. // Inorg. Chem. 2014. Vol. 53. P. 8816–8824.

Choppin, G. Radiochemistry and Nuclear Chemistry / G. Choppin, J. Rydberg, J.-O. Liljenzin. – Woburn, MA : Butterworth-Heinemann, 2001. – 1-720 p.

Choudhury, A.; Kumar, U.; Rao, C. N. R. Three-dimensional organically templated open-framework transition metal selenites // Angew. Chem. Int. Ed. Engl. 2002. Vol. 41. P. 158–161.

Colmont, M.; Endara, D.; Aliev, A.; Terryn, C.; Huvé, M.; Mentré, O. Bi_2O_3–CuO–P_2O_5 system: Two novel compounds built from the intergrowths oxocentered polycationic 1D-ribbons // J. Solid State Chem. 2013. Vol. 203. P. 266–272.

Colmont, M.; Huvé, M.; Ketatni, E. M.; Mentré, O. Polymorphism and anionic vacancies in the $Bi6(M,Bi)_1P_2(O,F)_{16-x}$ Aurivillius derivatives // Solid State Sci. 2008. Vol. 10. P. 533–543.

Darriet, J.; Galy, J. Tellurium (IV) Vanadium (V) Oxide, $Te_2V_2O_9$ // Cryst. Struct. Commun 1973. Vol. 2. P. 237–238.

David, R.; Kabbour, H.; Pautrat, A.; Touati, N.; Whangbo, M.-H.; Mentré, O. Two-orbital three-electron stabilizing interaction for direct Co^{2+}-As^{3+} bonds involving square-planar CoO_4 in $BaCoAs_2O_5$ // Angew. Chem. Int. Ed. Engl. 2014. Vol. 53. P. 3111–3114.

De, A. K. A text book of inorganic chemistry / A.K. De. – New Delhi : New Age International, 2003. – 914 p.

Effenberger, H. $Cu(SeO_2OH)_2$: Synthesis and crystal structure // Z. Kristallogr. 1985. Vol. 173. P. 267–272.

Effenberger, H.; Pertlik, F. Die Kristallstrukturen der Kupfer(II)-oxo-selenite $Cu_2O(SeO_3)$ (kubisch und monoklin) und $Cu_4O(SeO_3)_3$ (monoklin und triklin) // Monatsh. Chem. 1986. Vol. 117. P. 887–896.

Engelen, B.; Bäumer, U.; Hermann, B.; Müller, H.; Unterderweide, K. Zur Polymorphie und Pseudosymmetrie der Hydrate $M SeO_3 \cdot H_2O$ (M=Mn, Co, Ni, Zn, Cd) // Z. Anorg. Allg. Chem. 1996. Vol. 622. P. 1886–1892.

Enjalbert, R.; Savariault, J. M.; Legros, J. P. Etude structurale a 123 K du trichlorure de phosphore PCl_3 // C. R. Acad. Sci. II C 1980. Vol. C290. P. 239–241.

Evans, H. T. J.; Hughes, J. M. Crystal chemistry of the natural vanadium bronzes // Am. Mineral. 1990. Vol. 75. P. 508–521.

Ewald, B.; Prots, Y.; Kniep, R. Crystal structure of discandium tris-monohydrogenphosphate (III), $Sc_2(HPO_3)_3$ // Z. Kristallogr. 2003. Vol. 218. P. 377–378.

Filatov, S. K.; Semenova, T. F.; Vergasova, L. P. Types of polymerization of $[OCu_4]^{6+}$ in inorganic compounds with "additional" oxygen atoms // Dokl. Akad. Nauk (in Russ.) 1992. Vol. 322. P. 539–539.

Fischer, R. Die Kristallstruktur von Molybdomenit, $PbSeO_3$ // TMPM Tschermaks Mineral. Petrogr. Mitt 1972. Vol. 17. P. 196–207.

Ghose, S.; Boving, P.; La Chapelle, W. A.; Wan, C. Reinerite, $Zn_3(AsO_3)_2$: an arsenite with a novel type of Zn-tetrahedral double chain // Am. Mineral. 1977. Vol. 62. P. 1129–1134.

Henry, M. Nonempirical Quantification of Molecular Interactions in Supramolecular Assemblies // ChemPhysChem 2002. Vol. 3. P. 561–569.

Henry, M. Non-covalent interactions in solid-state molecular tectonics // M. V. Putz. *In*: Advances in quantum chemical bonding structures. Transworld Research Network, Kerala, India, pp 153–211

Hsu, F.-C.; Luo, J.-Y.; Yeh, K.-W.; Chen, T.-K.; Huang, T.-W.; Wu, P. M.; Lee, Y.-C.; Huang, Y.-L.; Chu, Y.-Y.; Yan, D.-C.; Wu, M.-K. Superconductivity in the PbO-type structure -FeSe // Proc. Natl. Acad. Sci. 2008. Vol. 105. P. 14262–14264.

Huvé, M.; Colmont, M.; Mentré, O. Bi^{3+}/M^{2+} oxyphosphate: a continuous series of polycationic species from the 1D single chain to the 2D planes. Part 1: From HREM images to crystal-structure deduction. // Inorg. Chem. 2006. Vol. 45. P. 6604–11.

Jo, V.; Kim, M. K.; Shim, I.-W.; Ok, K. M. Synthesis, Structure, and Characterization of a Layered Mixed Metal Oxychloride, $PbVO_3Cl$ // Bull. Korean Chem. Soc. 2009. Vol. 30. P. 2145–2148.

Johnston, M. G.; Harrison, W. T. A. Two new octahedral/pyramidal frameworks containing both cation channels and lone-pair channels: syntheses and structures of $Ba_2Mn^{II}Mn_2^{III}(SeO_3)_6$ and $PbFe_2(SeO_3)_4$ // J. Solid State Chem. 2004. Vol. 177. P. 4680–4686.

Jörg, G.; Bühnemann, R.; Hollas, S.; Kivel, N.; Kossert, K.; Van Winckel, S.; Gostomski, C. L. V. Preparation of radiochemically pure ^{79}Se and highly precise determination of its half-life // Appl. Radiat. Isot. 2010. Vol. 68. P. 2339–2351.

Kersten, C. Ueber mehrere neue Vorkommnisse des Selens // Ann. der Phys. und Chemie 1839. Vol. 122. P. 265–280.

Koskenlinna, M.; Valkonen, J. Lead selenite, $PbSeO_3$ // Cryst. Struct. Commun. 1977. Vol. 6. P. p813–816.

Kozin, M. S.; Aliev, A.; Colmont, M.; Mentré, O.; Siidra, O. I.; Krivovichev, S. V. Novel bismuth oxophosphate halides $[Bi_8O_8][BiO_2](PO_4)_2X$ (X=Cl, Br) based on oxocentered 2D blocks and their relationships to the Aurivillius phases // J. Solid State Chem. 2013. Vol. 199. P. 56–61.

Krivovichev, S. V. Structural Crystallography of Inorganic Oxysalts / S. V. Krivovichev. – Oxford : Oxford University Press, 2009. – 320 p.

Krivovichev, S. V. Combinatorial topology of salts of inorganic oxoacids: zero-, one- and two-dimensional units with corner-sharing between coordination polyhedra // Crystallogr. Rev. 2004. Vol. 10. P. 185–232.

Krivovichev, S. V. On the algorithmic complexity of crystals // Mineral. Mag. 2014. Vol. 78. P. 415–435.

Krivovichev, S. V. Crystal chemistry of selenates with mineral-like structures. IV. Crystal structure of $Zn(SeO_4)(H_2O)_2$, a new compound with a mixed framework of the variscite type // Geol. Ore Depos. 2007. Vol. 49. P. 542–546.

Krivovichev, S. V. Actinyl compounds with hexavalent elements (S, Cr, Se, Mo) - Structural diversity, nanoscale chemistry, and cellular automata modeling // Eur. J. Inorg. Chem. 2010. Vol. 2010. P. 2594–2603.

Krivovichev, S. V.; Burns, P. C. Geometrical isomerism in uranyl chromates II. Crystal structures of $Mg_2[(UO_2)_3(CrO_4)_5](H_2O)_{17}$ and $Ca_2[(UO_2)_3(CrO_4)_5](H_2O)_{19}$ // Z. Kristallogr. 2003. Vol. 218. P. 683–690.

Krivovichev, S. V.; Filatov, S. K.; Vergasova, L. P. The crystal structure of ilinskite, $NaCu_5O_2(SeO_3)_2Cl_3$, and review of mixed-ligand CuO_mCl_n coordination geometries in minerals and inorganic compounds // Mineral. Petrol. 2013a. Vol. 107. P. 235–242.

Krivovichev, S. V.; Gurzhiy, V. V.; Tananaev, I. G.; Myasoedov, B. F. Uranyl selenates with organic templates: Principles of structure and characteristics of self-organization // Russ. J. Gen. Chem. 2009. Vol. 79. P. 2723–2730.

Krivovichev, S. V.; Kahlenberg, V.; Kaindl, R.; Mersdorf, E.; Tananaev, I. G.; Myasoedov, B. F. Nanoscale tubules in uranyl selenates // Angew. Chem. Int. Ed. Engl. 2005a. Vol. 44. P. 1134–1136.

Krivovichev, S. V.; Kahlenberg, V.; Tananaev, I. G.; Kaindl, R.; Mersdorf, E.; Myasoedov, B. F. Highly porous uranyl selenate nanotubules // J. Am. Chem. Soc. 2005b. Vol. 127. P. 1072–3.

Krivovichev, S. V.; Mentré, O.; Siidra, O. I.; Colmont, M.; Filatov, S. K. Anion-Centered Tetrahedra in Inorganic Compounds // Chem. Rev. 2013b. Vol. 113. P. 6459–6535.

Krivovichev, S. V.; Tananaev, I. G.; Kahlenberg, V.; Myasoedov, B. F. Synthesis and crystal structure of a new uranyl selenite(IV)-selenate(VI), $[C_5H_{14}N]_4[(UO_2)_3(SeO_4)_4(HSeO_3)(H_2O)](H_2SeO_3)(HSeO_4)$ // Radiochemistry 2006. Vol. 48. P. 217–222.

Krivovichev, S. V.; Vergasova, L. P.; Starova, G. L.; Filatov, S. K.; Britvin, S. N.; Roberts, A. C.; Steele, I. M. Burnsite, $KCdCu_7O_2(SeO_3)_2Cl_9$, a New Mineral Species from the Tolbachik Volcano, Kamchatka Peninsula, Russia // Can. Mineral. 2002. Vol. 40. P. 1171–1175.

Lafront, A.-M.; Trombe, J.-C. "Layered hydrogenselenite" I. Synthesis, structure redetermination of $[Cu(HSeO_3)_2(H_2O)_2]$ and determination of $[Cu(HSeO_3)_2(NO_3)_2]^{2-}\cdot 2NH_4^+, NH_4NO_3$. Structural relationships of these complexes with $[Cu(HSeO_3)_2]$ // Inorganica Chim. Acta 1995. Vol. 234. P. 19–25.

Leclaire, A.; Chahboun, H.; Groult, D.; Raveau, B. Concerning the intersecting tunnel structure of a novel vanadyldiphosphate $K_2(VO)_3(P_2O_7)_2$ and its structural relationships with other V(V) and V(IV) phosphates and relatives // J. Solid State Chem. 77:170–179.

Lee, K.-S.; Kwon, Y.-U. Crystal structure of $V_2Se_2O_9$ and phase relations in the V_2O_5-SeO_2 system // J. Korean Chem. Soc. 1996. Vol. 40. P. 379–383.

Li, P.-X.; Kong, F.; Hu, C.-L.; Zhao, N.; Mao, J.-G. A Series of New Phases Containing Three Different Asymmetric Building Units // Inorg. Chem. 2010. Vol. 49. P. 5943–5952.

Lii, K.-H.; Wang, Y.-P.; Chneg, C.-Y.; Wang, S.-L.; Ku, H.-C. Crystal Structure and Magnetic Properties of a Vanadium (IV) Pyrophosphate: $Rb_2V_3P_4O_{17}$ // J. Chinese Chem. Soc. 1990. Vol. 37. P. 141–149.

Ling, J.; Sigmon, G. E.; Ward, M.; Roback, N.; Carman Burns, P. Syntheses, structures, and IR spectroscopic characterization of new uranyl sulfate/selenate 1D-chain, 2D-sheet and 3D-framework // Z. Kristallogr. 2010. Vol. 225. P. 230–239.

Liu, L.; Wang, X.; Xu, L.; Liu, X.; Liu, L.; Bi, B.; Pang, W. Synthesis, characterization and magnetic properties of a novel fluorinated iron phosphite $Fe_2(HPO_3)F_2$ with infinite –Fe–F–Fe–O–Fe– linkage and –Fe–F–Fe– layer // Inorganica Chim. Acta 2009. Vol. 362. P. 3881–3884.

Long, J. R.; McCarty, L. S.; Holm, R. H. A Solid-State Route to Molecular Clusters: Access to the Solution Chemistry of $[Re_6Q_8]^{2+}$ (*Q*=S, Se) Core-Containing Clusters via Dimensional Reduction // J. Am. Chem. Soc. 1996. Vol. 118. P. 4603–4616.

Loub, J. Crystal chemistry of inorganic phosphites // Acta Crystallogr. 1991. Vol. B47. P. 468–473.

Lü, M.; Aliev, A.; Olchowka, J.; Colmont, M.; Huvé, M.; Wickleder, C.; Mentré, O. Multidimensional Open-Frameworks: Combinations of One-Dimensional Channels and Two-Dimensional Layers in Novel Bi/*M* Oxo-Chlorides // Inorg. Chem. 2014. Vol. 53. P. 528–536.

Mandarino, J. A. Natural and synthetic selenites and selenates and their Gladstone-Dale compatibility // Eur. J. Mineral. 1994. Vol. 6. P. 337–349.

Marcos, M. D.; Amorós, P.; Beltrán-Porter, A.; Martinez-Manez, R.; Attfield, J. P. Novel crystalline microporous transition-metal phosphites $M_{11}(HPO_3)_8(OH)_6$ (*M*=Zn, Co, Ni). X-ray powder diffraction structure determination of the cobalt and nickel derivatives // Chem. Mater. 1993. Vol. 5. P. 121–128.

Mcmanus, A. V. P.; Harrison, W. T. A.; Cheetham, A. K. The synthesis and crystal structure of a new nickel selenite hydrate, $Ni_3(SeO_3)_3{\cdot}H_2O$ // J. Solid State Chem. 1991. Vol. 92. P. 253–260.

Mertens, B.; Müller-Buschbaum, H. Synthese und röntgen-strukturuntersuchung von $Rb_4Cd(VO)(V_2O_7)_2Cl$ und $Tl_4Cd(VO)(V_2O_7)_2Cl$ // Z. Naturforsch., B: Chem. Sci. 1997. Vol. 52. P. 453–456.

Millet, P.; Galy, J.; Johnsson, M. Crystal growth and structure of $V_2Se_2O_9$; comparison with $V_2Te_2O_9$ // Solid State Sci. 1999. Vol. 1. P. 279–286.

Morris, R. E.; Attfield, M. P.; Cheetham, A. K. Synthesis and structures of two isostructural phosphites, $Al_2(HPO_3)_3$ and $Ga_2(HPO_3)_3$ // Acta Crystallogr. 1994. Vol. C50. P. 473–476.

Palatinus, L.; Chapuis, G. SUPERFLIP – a computer program for the solution of crystal structures by charge flipping in arbitrary dimensions // J. Appl. Crystallogr. 2007. Vol. 40. P. 786–790.

Petříček, V.; Dušek, M.; Palatinus, L. Crystallographic Computing System JANA2006: General features // Z. Kristallogr. 2014. Vol. 229. P. 345–352.

Popovkin, B. A.; Cheremisinov, V. P.; Simanov, Y. P. Study of the crystal structure and vibration spectrum of lead selenite // J. Struct. Chem. 1963. Vol. 4. P. 38–43.

Pourbaix, M. Atlas of electrochemical equilibria in aqueous solutions / M. Pourbaix. – Houston, Tex : National Association of Corrosion Engineers, 1974. – 644 p.

Puranen, A.; Johnsson, M.; Dähn, R.; Cui, D. Reduction of selenite and selenate on anoxically corroded iron and the synergistic effect of uranyl reduction // J. Nucl. Mater. 2010. Vol. 406. P. 230–237.

Pyrzynska, K. Speciation analysis of some organic selenium compounds. A review // Analyst 1996. Vol. 121. P. 77R–83R.

Qu, L.; Peng, X. Control of Photoluminescence Properties of CdSe Nanocrystals in Growth // J. Am. Chem. Soc. 2002. Vol. 124. P. 2049–2055.

Rayman, M. P. The importance of selenium to human health // Lancet 2000. Vol. 356. P. 233–241.

Richter, K. L.; Mattes, R. Preparation, raman-spectra, and crystal structures of $V_2O_3(SO_4)_2$, $K[VO(SO_4)_2]$, and $NH_4[VO(SO_4)_2]$ // Z. Anorg. Allg. Chem. 1992. Vol. 611. P. 158–164.

Schindler, M.; Hawthorne, F. C.; Baur, W. H. Crystal chemical aspects of vanadium: Polyhedral geometries, characteristic bond valences, and polymerization of (VOn) polyhedra // Chem. Mater. 2000. Vol. 12. P. 1248–1259.

Scordari, F.; Stasi, F. The crystal structure of euchlorine, $NaKCu_3O(SO_4)_3$ // N. Jb. Mineral. Abh. 1990. Vol. 161. P. 241–253.

Séby, F.; Potin-Gautier, M.; Giffaut, E.; Borge, G.; Donard, O. F. . A critical review of thermodynamic data for selenium species at 25°C // Chem. Geol. 2001. Vol. 171. P. 173–194.

Sghyar, M.; Durand, J.; Cot, L.; Rafiq, M. Structure du phosphite de fer: $Fe_2(PO_3H)_3$ // Acta Crystallogr. 1991. Vol. C47. P. 2515–2517.

Sheldrick, G. M. A short history of SHELX. // Acta Crystallogr. 2008. Vol. A64. P. 112–22.

Shuvalov, R. R.; Vergasova, L. P.; Semenova, T. F.; Filatov, S. K.; Krivovichev, S. V.; Siidra, O. I.; Rudashevsky, N. S. Prewittite, $KPb_{1.5}Cu_6Zn(SeO_3)_2O_2Cl_{10}$, a new mineral from Tolbachik fumaroles, Kamchatka peninsula, Russia: Description and crystal structure // Am. Mineral. 2013. Vol. 98. P. 463–469.

Spek, A. L. Structure validation in chemical crystallography // Acta Crystallogr. 2009. Vol. D65. P. 148–155.

Starova, G. L.; Filatov, S. K.; Vergasova, L. P. The Crystal Structure of Fedotovite, $K_2Cu_3O(SO_4)_3$ // Mineral. Mag. 1991. Vol. 55. P. 613–616.

Tabachenko, V. V.; Serezhkin, V. N.; Serezhkina, L. B.; Kovba, L. M. Crystal structure of manganese sulfatouranylate $MnUO_2(SO_4)_2 \cdot 5H_2O$ // Koord. Khim. 1975. Vol. 5. P. 1563–1568.

Takeno, N. Atlas of Eh-pH diagrams. Geological Survey of Japan Open File Report No. 419 / N. Takeno. – Tsukuba : National Institute of Advanced Industrial Science and Technology, Research Center for Deep Geological Environments, 2005. – 1-287 p.

Tapiero, H.; Townsend, D.; Tew, K. The antioxidant role of selenium and seleno-compounds // Biomed. Pharmacother. 2003. Vol. 57. P. 134–144.

Tudo, J.; Jolibois, B.; Laplace, G. Préparation et étude des sulfates de vanadium V: $V_2O_5 \cdot 2SO_3$ et $V_2O_5 \cdot 4SO_3 \cdot 3H_2O$ // C. R. Acad. Sci. II C 1969. Vol. 269. P. 978–980.

Tulsky, E. G.; Long, J. R. Dimensional Reduction: A Practical Formalism for Manipulating Solid Structures // Chem. Mater. 2001. Vol. 13. P. 1149–1166.

Tyutyunnik, A. P.; Krasil'nikov, V. N.; Zubkov, V. G.; Perelyaeva, L. A.; Baklanova, I. V. Synthesis, structure, and properties of $V_2O_3(XO_4)_2$ (X=S, Se) // Russ. J. Inorg. Chem. 2010. Vol. 55. P. 501–507.

Verbaere, A.; Marchand, R.; Tournoux, M. Localisation du doublet solitaire dans les composés oxygènés cristallisés du thallium^{I} // J. Solid State Chem. 1978. Vol. 23. P. 383–390.

Vergasova, L. P.; Semenova, T. F.; Shuvalov, R. R.; Filatov, S. K.; Ananiev, V. V. Ilinskite $NaCu_5O_2(SeO_3)_2Cl_3$ - a new mineral of volcanic exhalations // Dokl. Akad. Nauk (in Russ.) 1997. Vol. 353. P. 641–644.

Verma, V. P. A review of synthetic, thermoanalytical, IR, Raman and X-ray studies on metal selenites // Thermochim. Acta 1999. Vol. 327. P. 63–102.

Villa, E. M.; Diwu, J.; Alekseev, E. V.; Depmeier, W.; Albrecht-Schmitt, T. E. Structural changes within the alkaline earth uranyl phosphites // Dalton Trans. 2013. Vol. 42. P. 9637–9644.

Wickleder, M. S.; Hamida, M. Ben $CoSm(SeO_3)_2Cl$, $CuGd(SeO_3)_2Cl$, $MnSm(SeO_3)_2Cl$, $CuGd_2(SeO_3)_4$ und $CuSm_2(SeO_3)_4$: Übergangsmetallhaltige Selenite von Samarium und Gadolinum // Z. Anorg. Allg. Chem. 2003. Vol. 629. P. 556–562.

Wildner, M. Crystal structures of $Co_3(SeO_3)_3 \cdot H_2O$ and $Ni_3(SeO_3)_3 \cdot H_2O$, two new isotypic compounds // Monatsh. Chem. 1991. Vol. 122. P. 585–594.

Wontcheu, J.; Schleid, T. $Tb_2Se_2O_7$: Terbium(III) Oxide Oxoselenate(IV) according to $Tb_2O[SeO_3]_2$ with a "Lone—Pair" Channel Structure // Z. Anorg. Allg. Chem. 2002. Vol. 628. P. 1941–1945.

Wontcheu, J.; Schleid, T. $Tb_3O_2Cl[SeO_3]_2$ and $Tb_5O_4Cl_3[SeO_3]_2$: Oxide Chloride Oxoselenates(IV) of Trivalent Terbium with "Lone-Pair" Channel or Layer Structures // Z. Anorg. Allg. Chem. 2005. Vol. 631. P. 309–315.

Wontcheu, J.; Schleid, T. $Sc_2Se_3O_9$: Scandium(III) Oxoselenate(IV) According to $Sc_2[SeO_3]_3$ with a Hexagonal "Lone-Pair" Channel Structure // Z. Anorg. Allg. Chem. 2003. Vol. 629. P. 1463–1465.

Yeon, J.; Kim, S.; Nguyen, S. D.; Lee, H.; Halasyamani, P. S. New Vanadium Selenites: Centrosymmetric $Ca_2(VO_2)_2(SeO_3)_3(H_2O)_2$, $Sr_2(VO_2)_2(SeO_3)_3$, and $Ba(V_2O_5)(SeO_3)$, and Noncentrosymmetric and Polar $A_4(VO_2)_2(SeO_3)_4(Se_2O_5)$ (A=Sr^{2+} or Pb^{2+}) // Inorg. Chem. 2012. Vol. 51. P. 609–619.

Zitzer, S.; Schleifenbaum, F.; Schleid, T. Synthesis, crystal structure and spectroscopic properties of $Y_3O_2Cl[SeO_3]_2$: Eu^{3+} // Z. Kristallogr. 2011. Vol. 226. P. 651–656.

APPENDIX

INCLUDED ARTICLES

Кристаллохимия новых кислородных соединений четырех- и шестивалентного селена
(Russian translation)

INCLUDED ARTICLES

A-I
Unprecedented layer topology in the crystal structure of a new organically templated uranyl selenite-selenate

Vadim M. Kovrugin, Vladislav V. Gurzhiy, Sergey V. Krivovichev, Ivan G. Tananaev, and Boris F. Myasoedov

Published in: *Mendeleev Communications*, 2012, Vol. 22 (1), p. 11–12.
DOI: 10.1016/j.mencom.2012.01.003

Available online at www.sciencedirect.com
ScienceDirect
Mendeleev Commun., 2012, **22**, 11–12
Mendeleev Communications

Unprecedented layer topology in the crystal structure of a new organically templated uranyl selenite-selenate

Vadim M. Kovrugin,*[a] Vladislav V. Gurzhiy,[a,b] Sergey V. Krivovichev,[a] Ivan G. Tananaev[c] and Boris F. Myasoedov[c]

[a] *Department of Geology, St. Petersburg State University, 199034 St. Petersburg, Russian Federation. Fax: +7 812 328 9647; e-mail: kovrugin_vm@hotmail.com*
[b] *Department of Chemistry, St. Petersburg State University, 198504 St. Petersburg, Russian Federation*
[c] *A. N. Frumkin Institute of Physical Chemistry and Electrochemistry, Russian Academy of Sciences, 119991 Moscow, Russian Federation*

DOI: 10.1016/j.mencom.2012.01.003

The crystal structure of the new organically templated uranyl selenite-selenate $[C_2H_8N][(H_5O_2)(H_2O)][(UO_2)_2(SeO_4)_3(H_2SeO_3)](H_2O)$ is based upon complex layers with a unique topology, which was not observed previously in inorganic compounds.

The oxo salt compounds of uranyl have been intensively studied owing to their importance in radioactive waste management, uranium mineralogy, catalysis, ion-exchange, *etc*.[1] Special attention was attracted to organically templated uranyl compounds as promising materials for separation and extraction technologies. A variety of compounds of this class, including organically templated uranium sulfates,[2–6] selenites,[7] molybdates,[8–12] vanadates[13,14] and silicates,[15] have been prepared recently. Uranyl selenates,[16–21] which can form nanotubular structures[22–24] that have no analogues among well-known inorganic oxo salts, are of special interest. Here, we report on the synthesis[†] and structural characterization of a new uranyl selenite-selenate, $[C_2H_8N][(H_5O_2)(H_2O)][(UO_2)_2(SeO_4)_3(H_2SeO_3)](H_2O)$ **1**, with an unprecedented layer topology.

The crystal structure of **1**[‡] contains two independent U atoms that form the linear uranyl cation $[O=U=O]^{2+}$. The U=O bond lengths are 1.751(5)–1.765(4) Å. Both uranyl cations formed by the U(1) and U(2) atoms are surrounded in the equatorial plane by five O_{eq} atoms to form the pentagonal bipyramids $[UO_7]^{8-}$. In the crystal structure of **1**, the U–O_{eq} bond lengths vary from 2.378(4) to 2.414(5) Å. In the structure of **1**, three sites [Se(1), Se(2) and Se(3)] of four independent Se positions correspond to Se^{VI}, whereas the Se(4) site is occupied by Se^{IV}. The Se^{VI} positions are surrounded by four O atoms each with the average ⟨Se–O⟩ bond lengths of 1.638, 1.636 and 1.642 Å for Se(1), Se(2) and Se(3), respectively. The Se(4) site has a trigonal pyramidal coordination with an apex occupied by the Se^{IV} atom. This coordination is typical of the Se^{IV} atom with a stereoactive lone electron pair. The $Se(4)O_3$ trigonal pyramid is strongly distorted with one short Se(4)–O(17) bond [1.661(4) Å], and the Se(4)–O(18) and Se(4)–O(19) bonds being appreciably longer [1.713(5) and 1.735(5) Å, respectively]. Such a distorted coordination geometry is typical of biprotonated selenite groups (H_2SeO_3); in particular, it was observed in the structure of $[C_5H_{14}N]_4(UO_2)_3(SeO_4)_4(HSeO_3)(H_2O)(H_2SeO_3)(HSeO_4)$.[27]

The crystal structure of **1** is based upon $[(UO_2)_2(SeO_4)_3(H_2SeO_3)]^{2-}$ layers formed as a result of the condensation of $[UO_7]^{8-}$, $[SeO_4]^{2-}$ and (H_2SeO_3) coordination units by sharing common oxygen atoms. The $[(UO_2)_2(SeO_4)_3(H_2SeO_3)]^{2-}$ layers are parallel to (101) (Figure 1). Protonated dimethylamine molecules, $[C_2H_8N]^+$, and $[H_5O_2]^+$ hydroxonium complexes are located in the interlayer space and form hydrogen bonds to the O atoms of uranyl groups and selenium oxo complexes.

Figure 2(*a*) shows the structure of the $[(UO_2)_2(SeO_4)_3(H_2SeO_3)]^{2-}$ layer in more detail. The selenate tetrahedra and (H_2SeO_3) trigonal pyramids coordinate uranyl ions in a mono-

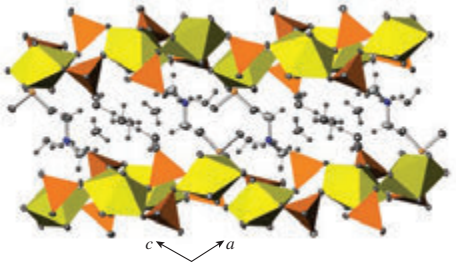

Figure 1 Crystal structure of **1** projected along the *b* axis. Displacement ellipsoids are drawn at a 50% probability level.

† The yellowish green transparent plates of **1** were prepared by evaporation from aqueous solutions. A mixture of 0.0503 g (0.1 mmol) of $UO_2(NO_3)_2·6H_2O$, 0.0045 g (0.1 mmol) of dimethylamine, 0.1160 g (0.8 mmol) of 40% H_2SeO_4, and 2 ml of distilled water was stirred until complete homogenization, poured onto a watch glass, and kept in a fume hood at room temperature. The crystals of **1** crystallized on the bottom of the vessel after three days.

‡ *Crystallographic data*. Crystals of **1** ($C_2H_{19}NO_{23}Se_4U_2$, M = 1217.08) are monoclinic, space group $P2_1/n$, at 293 K: a = 14.7979(8), b = 10.0238(6) and c = 16.4176(9) Å, β = 111.628(1)°, V = 2263.8(2) Å^3, Z = 4, d_{calc} = 3.571 g cm^{-3}, μ(MoKα) = 20.822 cm^{-1}, F(000) = 2168. Intensities of 25431 reflections were measured with a Bruker SMART APEX II CCD diffractometer [λ(MoKα) = 0.71073 Å, $2\theta_{max}$ = 58°] and 5476 independent reflections (R_{int} = 0.0734) were used in further refinement. The structure was solved by direct method and refined by the full-matrix least-squares technique against F^2 in the anisotropic-isotropic approximation. Hydrogen atoms of H_2O groups were located from the Fourier synthesis of the electron density. The H(C,N) atom positions were calculated. The refinement converged to wR_2 = 0.0538 and GOF = 0.928 for all independent reflections [R_1 = 0.0265 was calculated against F for 4285 observed reflections with $I > 2\sigma(I)$]. All calculations were performed using SHELXTL PLUS 5.0.16.

CCDC 824406 contains the supplementary crystallographic data for this paper. These data can be obtained free of charge from The Cambridge Crystallographic Data Centre *via* www.ccdc.cam.ac.uk/data_request/cif. For details, see 'Notice to Authors', *Mendeleev Commun.*, Issue 1, 2012.

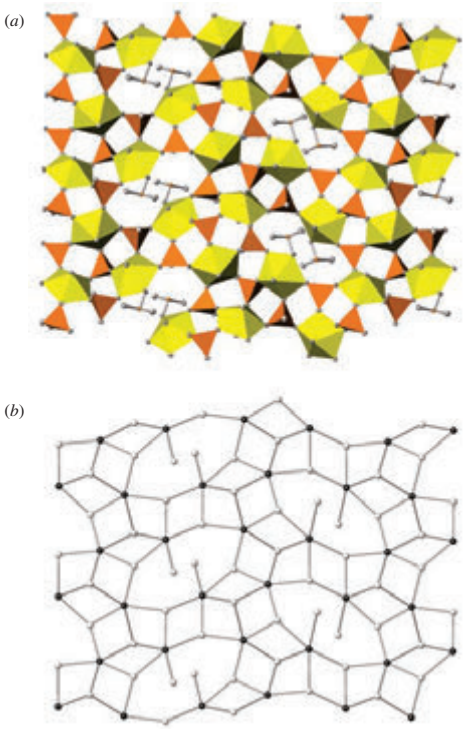

Figure 2 (*a*) Projection of the uranyl selenite-selenate layer in the crystal structure of **1** (displacement ellipsoids at 50% probability level) and (*b*) its topology shown as a graph (U and Se polyhedra are symbolized by black and white nodes, respectively).

dentate fashion; however, their topological roles are remarkably distinct. The selenate group coordinates three uranyl ions, whereas protonated selenite groups coordinate one uranyl ion each. This is in agreement with the empirical rule formulated previously that, in uranyl selenite-selenate complexes, the connectivity of selenite is lower than that of selenate anions.[28] The linkage topology of the U and Se polyhedra can be described in terms of the graph theory[29] if U and Se atoms are symbolized by black and white nodes. The nodes are linked by a line if the corresponding atoms are bonded to the same bridging O atom. An idealized version of the black-and-white graph for the uranyl selenite-selenate complex in **1** is shown in Figure 2(*b*). This topology is unprecedented for both the chemistry of uranium and the structural chemistry of uranyl oxo salts in general. The topology is remarkable due to the presence of 1-connected branches inside eight-membered rings; this feature has been observed in just two other organically templated uranyl oxo salt compounds[21,30] and has never been observed in other inorganic oxo salts.

This work was supported by the Federal Target Programme ‘Scientific and Scientific-Pedagogical Personnel of the Innovative Russia’ (contract no. 02.740.11.0326) and the St. Petersburg State University (grant no. 3.37.84.2011).

References

1 T. E. Albrecht-Schmitt, P. C. Burns and S. V. Krivovichev, in *The Chemistry of the Actinide and Transactinide Elements*, eds. L. R. Morss, N. M. Edelstein and J. Fuger, Springer, Dordrecht, 2010, vol. 6, pp. 4157–4191.
2 A. J. Norquist, M. B. Doran, P. M. Thomas and D. O’Hare, *Inorg. Chem.*, 2003, **42**, 5949.
3 A. J. Norquist, M. B. Doran, P. M. Thomas and D. O’Hare, *Dalton Trans.*, 2003, 1168.
4 M. B. Doran, B. E. Cockbain, A. J. Norquist and D. O’Hare, *Dalton Trans.*, 2004, 3810.
5 M. B. Doran, B. E. Cockbain and D. O’Hare, *Dalton Trans.*, 2005, 1774.
6 M. S. Bharara and E. V. Gorden, *Dalton Trans.*, 2010, **39**, 3557.
7 P. M. Almond and T. E. Albrecht-Schmitt, *Inorg. Chem.*, 2003, **42**, 5693.
8 P. S. Halasyamani, R. J. Francis, S. M. Walker and D. O’Hare, *Inorg. Chem.*, 1999, **38**, 271.
9 S. V. Krivovichev and P. C. Burns, *J. Solid State Chem.*, 2003, **170**, 106.
10 S. V. Krivovichev, T. Armbruster, D. Yu. Chernyshov, P. C. Burns, E. V. Nazarchuk and W. Depmeier, *Micropor. Mesopor. Mater.*, 2005, **78**, 225.
11 S. V. Krivovichev, P. C. Burns, T. Armbruster, E. V. Nazarchuk and W. Depmeier, *Micropor. Mesopor. Mater.*, 2005, **78**, 217.
12 S. V. Krivovichev, C. L. Cahill, E. V. Nazarchuk, P. C. Burns and T. Armbruster, W. Depmeier, *Micropor. Mesopor. Mater.*, 2005, **78**, 209.
13 L. Jouffret, Z. Shao, M. Rivenet and F. Abraham, *J. Solid State Chem.*, 2010, **183**, 2290.
14 L. Jouffret, M. Rivenet and F. Abraham, *J. Solid State Chem.*, 2010, **183**, 84.
15 X. Wang, J. Huang and A. J. Jacobson, *J. Am. Chem. Soc.*, 2002, **124**, 15190.
16 S. V. Krivovichev, V. V. Gurzhiy, I. G. Tananaev and B. F. Myasoedov, *Russ. J. Gen. Chem.*, 2009, **79**, 2723.
17 S. V. Krivovichev, V. V. Gurzhiy, I. G. Tananaev and B. F. Myasoedov, *Z. Kristallogr.*, 2009, **224**, 316.
18 J. Ling, G. E. Sigmon and P. C. Burns, *J. Solid State Chem.*, 2009, **182**, 402.
19 J. Ling, G. E. Sigmon, M. Ward, N. Roback and P. C. Burns, *Z. Kristallogr.*, 2010, **225**, 230.
20 V. V. Gurzhiy, S. V. Krivovichev, P. C. Burns, I. G. Tananaev and B. F. Myasoedov, *Radiokhimiya*, 2010, **52**, 3 [*Radiochem.* (*Engl. Transl.*), 2010, **52**, 1].
21 S. V. Krivovichev, V. V. Gurzhiy, I. G. Tananaev and B. F. Myasoedov, *Radiokhimiya*, 2010, **52**, 8 [*Radiochem.* (*Engl. Transl.*), 2010, **52**, 7].
22 S. V. Krivovichev, V. Kahlenberg, R. Kaindl, E. Mersdorf, I. G. Tananaev and B. F. Myasoedov, *Angew. Chem. Int. Ed.*, 2005, **44**, 1134.
23 S. V. Krivovichev, V. Kahlenberg, I. G. Tananaev, R. Kaindl, E. Mersdorf and B. F. Myasoedov, *J. Am. Chem. Soc.*, 2005, **127**, 1072.
24 E. V. Alekseev, S. V. Krivovichev and W. Depmeier, *Angew. Chem. Int. Ed.*, 2008, **47**, 549.
25 A. Altomare, G. Cascarano, C. Giacovazzo, A. Guagliardi, M. C. Burla, G. Polidori and M. Camalli, *J. Appl. Crystallogr.*, 1994, **27**, 435.
26 G. M. Sheldrick, *Acta Crystallogr.*, 2008, **A64**, 112.
27 S. V. Krivovichev, I. G. Tananaev, V. Kahlenberg and B. F. Myasoedov, *Radiokhimiya*, 2006, **48**, 197 [*Radiochem.* (*Engl. Transl.*), 2006, **48**, 217].
28 S. V. Krivovichev, I. G. Tananaev, V. Kahlenberg and B. F. Myasoedov, *Dokl. Akad. Nauk*, 2005, **403**, 349 [*Dokl. Phys. Chem.* (*Engl. Transl.*), 2005, **403**, 124].
29 S. V. Krivovichev, *Structural Crystallography of Inorganic Oxysalts*, Oxford University Press, Oxford, 2008.
30 E. V. Alekseev, S. V. Krivovichev and W. Depmeier, *Radiokhimiya*, 2008, **50**, 385 [*Radiochem.* (*Engl. Transl.*), 2008, **50**, 445].

Received: 13th May 2011; Com. 11/3725

A-II
Structural topology and dimensional reduction in uranyl oxysalts: eight novel phases in the methylamine–$(UO_2)(NO_3)_2$–H_2SeO_4–H_2O system

Vadim M. Kovrugin, Vladislav V. Gurzhiy, and Sergey V. Krivovichev

Published in: *Structural Chemistry*, 2012, Vol. 23 (6), p. 2003–2017.

DOI: 10.1007/s11224-012-0001-7

Struct Chem (2012) 23:2003–2017
DOI 10.1007/s11224-012-0001-7

ORIGINAL RESEARCH

Structural topology and dimensional reduction in uranyl oxysalts: eight novel phases in the *methylamine*–$(UO_2)(NO_3)_2$–H_2SeO_4–H_2O system

Vadim M. Kovrugin · Vladislav V. Gurzhiy · Sergey V. Krivovichev

Received: 19 February 2012 / Accepted: 21 March 2012 / Published online: 6 May 2012

Abstract Single crystals of eight novel uranyl selenates, $(CH_3NH_3)_2[(UO_2)(SeO_4)_2(H_2O)](H_2O)$ (**I**) and $(CH_3NH_3)_2[(UO_2)(SeO_4)_2(H_2O)]$ (**II**), $(CH_3NH_3)_2[(UO_2)_2(SeO_4)_3]$ (**III**) and $(CH_3NH_3)(H_3O)[(UO_2)_2(SeO_4)_3(H_2O)](H_2O)$ (**IV**), $(CH_3NH_3)_4[(UO_2)_3(SeO_4)_5](H_2O)_4$ (**V**) and $(CH_3NH_3)(H_5O_2)(H_3O)_2[(UO_2)_3(SeO_4)_5](H_2O)_4$ (**VI**), $(CH_3NH_3)_4(H_3O)_2[(UO_2)_5(SeO_4)_8(H_2O)](H_2O)_4$ (**VII**), and $(CH_3NH_3)_{1.5}(H_5O_2)_{1.5}(H_3O)_3[(UO_2)_5(SeO_4)_8(H_2O)](H_2SeO_4)_{2.6}(H_2O)_3$ (**VIII**), have been prepared by isothermal evaporation from aqueous solutions and structurally characterized. The observed structural topologies of uranyl selenate units have been investigated using graph theory. The principle of dimensional reduction has been used for analysis of the uranyl oxysalts with general chemical formula $A_n(UO_2)_p(TO_4)_q(H_2O)_r$ (A = monovalent cation, and T = S, Se, Cr, Mo), which allowed to construct three-component composition-structure diagram with separate dimensionality fields for different chemical compositions.

Keywords Uranium · Selenium · Methylamine · Uranyl oxysalts · Crystal structure · Single crystal X-ray diffraction · Topology · Dimensional reduction

V. M. Kovrugin · V. V. Gurzhiy · S. V. Krivovichev (✉)
Department of Crystallography, Faculty of Geology,
St. Petersburg State University, University Emb. 7/9,
Saint Petersburg, Russia 199034
e-mail: skrivovi@mail.ru

S. V. Krivovichev
Institute of Silicate Chemistry, Russian Academy of Sciences,
Makarova Emb. 6, Saint Petersburg, Russia 199034

Introduction

Mathematical and topological models of inorganic chemical structures are of particular importance for understanding relations between their chemical composition and structural geometry and topology [1]. Simple topological models allowed to establish some important regularities, relationships and hierarchy among known simple and complex structure types [2–5]. In this paper, we report on structural topologies of eight novel uranium selenates and structure–composition relationships in complex uranyl compounds in general. It should be noted that structural chemistry of inorganic uranium compounds has had many important advances over the last 15 years partially summarized in [6–9]. In particular, introduction of two-dimensional tilings (so-called anion topologies [10]) and graphs [11, 12] led to deeper understanding of topological organization in uranium-based systems, including nanoscale structures such as uranium peroxide nanospheres [13–15] and uranyl selenate nanotubules [16–18]. The use of novel synthesis techniques allowed to prepare whole series of novel uranium compounds, e.g., mixed-valent uranium silicates [19–21] and uranyl borates [22–24]. Owing to their environmental and technological importance, uranyl oxysalts containing tetrahedral oxyanions of VIth group of the Periodic Table received particular attention [25]. Alekseev et al. [26] rationalized "composition–structure" relationships in uranyl molybdates using the principle of dimensional reduction proposed by Long et al. [27] for the description of decreasing dimensionality of chalcogenide structural units in Re sulfides and selenides. This principle was applied to various materials, including a wide class of ternary compounds [28], organic–inorganic composites [29], and some inorganic-oxysalt-based systems [12]. The principle of dimensional reduction states that incorporation of an ionic reagent and water into parent salts results in derivative compounds with decreasing

dimensionality of the structural unit. In addition to new experimental data on uranyl selenates, the present paper reports further extension of the dimensional reduction principle onto wide class of uranyl oxysalts containing monovalent organic and inorganic cations that play the role of reduction agents in complex systems.

Experimental

Caution

Although all uranium materials used in these experiments are depleted, extra care should always be used when handling uranium-containing materials.

Materials

Methylamine (40 wt% in H_2O, Sigma-Aldrich), selenic acid (40 wt% in H_2O, 99.95 %, Aldrich), and $UO_2(NO_3)_2{\cdot}6H_2O$ (Vekton) were used as received. Deionized distilled water was also used in these syntheses.

Synthesis

Crystals of new eight organic–inorganic compounds $(CH_3NH_3)_2[(UO_2)(SeO_4)_2(H_2O)](H_2O)$ (**I**), $(CH_3NH_3)_2[(UO_2)(SeO_4)_2(H_2O)]$ (**II**), $(CH_3NH_3)_2[(UO_2)_2(SeO_4)_3]$ (**III**), $(CH_3NH_3)(H_3O)[(UO_2)_2(SeO_4)_3(H_2O)](H_2O)$ (**IV**), $(CH_3NH_3)_4[(UO_2)_3(SeO_4)_5](H_2O)_4$ (**V**), $(CH_3NH_3)(H_5O_2)(H_3O)_2[(UO_2)_3(SeO_4)_5](H_2O)_4$ (**VI**), $(CH_3NH_3)_4(H_3O)_2[(UO_2)_5(SeO_4)_8(H_2O)](H_2O)_4$ (**VII**) and $(CH_3NH_3)_{1.5}(H_5O_2)_{1.5}(H_3O)_3[(UO_2)_5(SeO_4)_8(H_2O)](H_2SeO_4)_{2.6}(H_2O)_3$ (**VIII**) have been prepared by evaporation from aqueous solutions of uranyl nitrate, 40 %—solution of selenic acid, 40 %—solution of methylamine, and deionized distilled water. Yellow–green homogeneous liquid solutions were left in a fume hood at room temperature. The crystals of compound **I** were synthesized through the reaction of 0.0502 g (0.1 mmol) of uranyl nitrate, 0.0124 g (0.4 mmol) of methylamine, 0.0725 g (0.5 mmol) of selenic acid, and 2.0031 g (111.3 mmol) of deionized distilled water. The solid products were formed after 2 days in small amount. The crystals of compounds **II**, **IV**, and **VII** were synthesized through the reaction of 0.0504 g (0.1 mmol) of uranyl nitrate, 0.0155 g (0.5 mmol) of methylamine, 0.0580 g (0.4 mmol) of selenic acid, and 2.0067 g (111.5 mmol) of deionized distilled water. The solid products were formed after 3 days in small amount. The crystals of compound **III** were synthesized through the reaction of 0.0498 g (0.1 mmol) of uranyl nitrate, 0.0061 g (0.2 mmol) of methylamine, 0.1015 g (0.7 mmol) of selenic acid, and 1.9954 g (110.9 mmol) of deionized distilled water. The solid products were formed after 2 days in small amount. The crystals of compound **V** were synthesized through the reaction of 0.0505 g (0.1 mmol) of uranyl nitrate, 0.0031 g (0.1 mmol) of methylamine, 0.1160 g (0.8 mmol) of selenic acid, and 1.9986 g (111.0 mmol) of deionized distilled water. The solid products were formed after 2 days in small amount. The compounds **VI** and **VIII** were synthesized through the reaction of 0.1004 g (0.2 mmol) of uranyl nitrate, 0.0030 g (0.1 mmol) of methylamine, 0.1014 g (0.7 mmol) of selenic acid, and 2.0023 g (111.2 mmol) of deionized distilled water. The solid products were formed after 3 days in small amount.

X-ray crystallographic analysis

Single crystals selected for data collection were examined under an optical microscope, encased in epoxy and mounted on a glass fiber. Data were collected by means of a STOE IPDS II diffractometer using monochromated MoK_α radiation and frame widths of 2° in ω. The unit-cell parameters were refined by least-squares techniques. The data were corrected for Lorentz, polarization, and background effects. An analytical absorption correction based on the indexed faces was applied. The structures were solved by direct methods and refined by means of the programs SHELXL–97 [30] and SIR–92 [31]. Attempts to refine anisotropic parameters of several oxygen atoms positions and positions of atoms in organic methylamine molecules resulted in physically unrealistic values. Due to the low quality of crystals of most phases, their metastability and sensitivity to air, only relatively rough structural models could be obtained. As a consequence, crystallographic agreement index (R_1) values for some crystals are not of the same order as those obtained from perfect crystals. Due to these reasons, we were unable to localize the positions of H atoms as well, and the details of the hydrogen bonding system remain unclear. However, some approximate schemes can be derived from O–O contacts involving sites occupied by the H_2O molecules and hydronium cations. Relevant crystallographic data are listed in Tables 1 and 2. Selected interatomic distances are given in Table 3. CCDC files 866553, 866549, 866547, 866553, 866546, 866551, 866548, and 866550 contain the supplementary crystallographic data for the compounds **I**, **II**, **III**, **IV**, **V**, **VI**, **VII**, and **VIII** reported in this paper. These data can be obtained free of charge from The Cambridge Crystallographic Data Centre via www.ccdc.cam.ac.uk/data_request/cif.

Results

Compounds with U:Se = 1:2

Compounds with U:Se = 1:2 can be described by the general formula $(CH_3NH_3)[(UO_2)(SeO_4)_2(H_2O)](H_2O)_n$,

Table 1 Crystallographic Data for **I–V** in the system $UO_2(NO_3)_2$–H_2SeO_4–methylamine–H_2O

Compound	**I**	**II**	**III**	**IV**
Empirical formula	$(CH_3NH_3)_2[(UO_2)(SeO_4)_2(H_2O)](H_2O)$	$(CH_3NH_3)_2[(UO_2)(SeO_4)_2(H_2O)]$	$(CH_3NH_3)_2[(UO_2)_2(SeO_4)_3]$	$(CH_3NH_3)(H_3O)[(UO_2)_2(SeO_4)_3(H_2O)](H_2O)$
fw	639.99	623.99	1020.98	1042.96
Crystal system	Orthorhombic	Monoclinic	Monoclinic	Monoclinic
Space group	*Pnma*	$P2_1/c$	$P2_1$	$P2_1/c$
a (Å)	7.5496(7)	8.2366(10)	8.5827(13)	8.4842(10)
b (Å)	12.0135(9)	7.5888(6)	10.0730(15)	10.2368(8)
c (Å)	15.8362(13)	22.260(2)	10.0915(14)	24.228(2)
α (deg)	90.00	90.00	90.00	90.00
β (deg)	90.00	104.566(9)	95.980(12)	102.803(9)
γ (deg)	90.00	90.00	90.00	90.00
V (Å^3)	1436.3(2)	1346.7(2)	867.7(2)	2051.9(3)
Z	4	4	2	4
D_c (g cm^{-1})	2.960	3.078	3.908	3.376
μ (mm^{-1})	16.423	17.507	25.012	21.166
2θ range (deg)	4.26–53.66	3.78–58.64	4.06–50.00	3.44–50.00
Reflections collected	10099	12119	5477	12326
Independent reflections	1605 [R(int) = 0.0875]	3656 [R(int) = 0.0828]	2931 [R(int) = 0.1271]	3602 [R(int) = 0.1698]
gof[a]	1.334	0.996	1.083	1.049
R_1, wR_2 [$I > 2\sigma(I)$][a]	0.0467, 0.0860	0.0466, 0.0637	0.1072, 0.2712	0.0674, 0.1551
R_1, wR_2 [all data]	0.0566, 0.0882	0.0785, 0.0688	0.1126, 0.2766	0.0957, 0.1693

$wR_2 = [\Sigma[w(F_o^2 - F_c^2)^2/\Sigma w(F_o^2)^2]^{1/2}$

[a] gof $= [\Sigma w(F_o^2 - F_c^2)^2/(n_{obs} - n_{param})]^{1/2}$

[b] $R_1 = \Sigma(|F_o| - |F_c|)/\Sigma|F_o|$

where $n = 1$ (**I**) and 0 (**II**). These compounds are probably the most stable in the system, which is manifested by their frequent occurence in the experiments and relatively high quality of their crystals. The crystal structures of **I** and **II** contain one symmetrically independent U^{6+} cation each that forms two short U^{6+}–O^{2-} bonds [1.755(10)–1.775(6) Å] resulting in formation of nearly linear uranyl cations, $[UO_2]^{2+}$. This basic uranyl entity is coordinated in the equatorial plane by four oxygen atoms and one H_2O molecule, which forms pentagonal bipyramids with the U^{6+}–O_{eq} bond lengths in range of 2.331(9)–2.360(7) Å. There are two independent Se atoms per formula unit in each structure. The Se^{6+} cations in the structures are tetrahedrally coordinated by four O atoms, forming $[SeO_4]^{2-}$ tetrahedra. The interpolyhedral Se–O_{br} bonds are longer (1.628(9)–1.656(6) Å; O_{br} = O atom bridging between U and Se polyhedra) than the Se–O_t bonds (1.593(10)–1.624(7) Å; O_t = terminal O atom in selenate group).

Crystal structures of **I** and **II** are based upon complex units with composition $[(UO_2)(SeO_4)_2(H_2O)]^{2-}$, but with different topologies of linkage of U and Se polyhedra for different values of n. For $n = 1$, the structure contains 1D chains, for $n = 0$ the structure is based upon 2D sheets (Fig. 1). The $[UO_6(H_2O)]^{6-}$ pentagonal bipyramids share corners with two $[SeO_4]^{2-}$ tetrahedra to form $[(UO_2)(SeO_4)_2(H_2O)]^{2-}$ chains running parallel to the c axis in the structure of **I**, and $[(UO_2)(SeO_4)_2(H_2O)]^{2-}$sheets which are parallel to $(10\bar{1})$ in the structure of **II**. The chains of **I** are arranged into sheets parallel to (010) plane.

In both structures, protonated $[CH_3NH_3]^+$ methylamine cations and water molecules are arranged between the chains and the sheets and provide their linkage into a three-dimensional structures.

Compounds with U:Se = 2:3

In the crystal structures of **III** and **IV**, there are two symmetrically independent U positions. They have typical pentagonal bipyramidal coordination. The uranyl bond lengths are in the range of 1.746(9)–1.771(10) Å. In the equatorial plane, both uranyl cations are coordinated by five O^{2-} anions of the selenate groups in the crystal structure of **III**, whereas, in the structure of **IV**, the U(2) site is coordinated by four O^{2-} anions and one $H_2O(17)$ group. The average $\langle U–O_{eq}\rangle$ bond length is 2.34 Å in **III**. In the crystal structure of **IV**, the U–O_{eq} bond lengths are in the range of 2.32(1)–2.41(1) Å, and the U–$H_2O(17)$ bond length is 2.494(16) Å. Each structure contains three

Table 2 Crystallographic Data for **VI–IX** in the system $UO_2(NO_3)_2$–H_2SeO_4–methylamine–H_2O

Compound	V	VI	VII	VIII
Empirical formula	$(CH_3NH_3)_4[(UO_2)_3(SeO_4)_5](H_2O)_4$	$(CH_3NH_3)(H_5O_2)(H_3O)_2[(UO_2)_3(SeO_4)_5](H_2O)_4$	$(CH_3NH_3)_4(H_3O)_2[(UO_2)_5(SeO_4)_8(H_2O)](H_2O)_4$	$(CH_3NH_3)_{1.5}(H_5O_2)_{1.5}(H_3O)_3[(UO_2)_5(SeO_4)_8(H_2O)](H_2SeO_4)_{2.6}(H_2O)_3$
fw	1692.97	1678.91	2709.91	2946.25
Crystal system	Orthorhombic	Orthorhombic	Orthorhombic	Orthorhombic
Space group	*Pnna*	*Ibca*	$Pca2_1$	*Pnma*
a (Å)	16.4221(14)	20.956(2)	31.505(2)	30.9728(19)
b (Å)	18.4773(9)	34.767(8)	10.3688(6)	37.022(2)
c (Å)	10.3602(5)	18.663(2)	16.2424(11)	10.4171(5)
α (deg)	90.00	90.00	90.00	90.00
β (deg)	90.00	90.00	90.00	90.00
γ (deg)	90.00	90.00	90.00	90.00
V (Å^3)	3143.7(3)	13597(4)	5305.9(6)	11945.0(11)
Z	4	16	4	8
D_c (g cm^{-1})	3.577	3.280	3.392	3.277
μ (mm^{-1})	21.319	19.720	20.814	20.086
2*θ* range (deg)	4.40–50.00	2.34–47.00	2.58–49.00	2.20–49.00
Reflections collected	18,468	32,094	27,846	61,466
Independent reflections	2774 [R(int) = 0.1191]	4913 [R(int) = 0.3280]	8463 [R(int) = 0.2070]	10116 [R(int) = 0.2139]
gof[a]	1.104	0.968	0.997	1.055
R_1, wR_2 [$I > 2\sigma(I)$][b]	0.0541, 0.1119	0.1040, 0.1867	0.0852, 0.1901	0.0858, 0.1736
R_1, wR_2 [all data]	0.0790, 0.1216	0.2138, 0.2287	0.1305, 0.2150	0.1556, 0.2083

$wR_2 = [\Sigma[w(F_o^2 - F_c^2)^2/\Sigma w(F_o^2)^2]^{1/2}$

[a] gof $= [\Sigma w(F_o^2 - F_c^2)^2/(n_{obs} - n_{param})]^{1/2}$

[b] $R_1 = \Sigma(|F_o| - |F_c|)/\Sigma|F_o|$

symmetrically independent $[SeO_4]^{2-}$ tetrahedra. The ⟨Se–O⟩ bond lengths are 1.66 and 1.62 Å for **III**, and the compound **IV**, respectively.

In both structures, the $[UO_7]^{8-}$, $[UO_6(H_2O)]^{6-}$ and $[SeO_4]^{2-}$ coordination polyhedra share common ligands to produce 2D sheets with the chemical compositions $[(UO_2)_2(SeO_4)_3]^{2-}$ in **III** and $[(UO_2)_2(SeO_4)_3(H_2O)]^{2-}$ in **IV**. The sheets are parallel to (100) and (10$\bar{1}$) in the compounds **III** and **IV**, respectively (Fig. 2). The interpolyhedral Se–O_{br}–U angles are in the range of 136(2)–146(3)°, with the average value of 140° in **III**, and 133.9(8)–144.8(9)°, with the average value of 138.5° in **IV**, which is in general agreement with the average value of 136.8° reported in [32].

The structure of **III** contains two protonated linear methylamine molecules $[CH_3NH_3]^+$ as interlayer species. In the interlayer space of **IV**, there are two protonated $[CH_3NH_3]^+$ cations and one H_2O molecule.

Compounds with U:Se = 3:5

The crystal structures of **V** and **VI** contain three crystallographically independent U atoms each. All the U^{6+} sites adopt the pentagonal bipyramidal coordination geometry with two short uranyl bonds (⟨U–O_{Ur}⟩ = 1.75 Å in both **V** and **VI**). In the equatorial plane, the uranyl cations are surrounded by five O atoms (⟨U–O_{eq}⟩ = 2.40 Å). There are five tetrahedrally coordinated Se sites in each structure (⟨Se–O⟩ = 1.64 and 1.62 Å in **V** and **VI**, respectively). In the structure of **VI**, one of the tetrahedra is disordered in terms of the O(13) and O(14) sites, which have 50 % occupancy each.

In both structures, the $[UO_7]^{8-}$ pentagonal bipyramids and $[SeO_4]^{2-}$ tetrahedra are linked through common vertices to form sheets with the composition $[(UO_2)_3(SeO_4)_5]^{4-}$. In the structure of **V**, the uranyl selenate sheets are corrugated and oriented parallel to (100). In the structure of **VI**, the inorganic two-dimensional complexes are more or less planar and run parallel to (010) (Fig. 3).

Both structures contain protonated methylamine molecules $[CH_3NH_3]^+$ and water molecules that provide three-dimensional linkage of the uranyl selenate sheets via hydrogen bonding. In the interlayer space of the crystal structure of **VI** there is one independent $[H_5O_2]^+$ cation (the respective O(33)–O(34) interatomic distance is 2.30(12) Å) and two hydronium cations $[H_3O]^+$.

Table 3 Selected bond distances (Å) and angles (deg) in the structures of **I**–**VIII**

	$U–O_{Ur}$	$U–O_{eq}$	$U–H_2O_{eq}$	$Se–O_{nr}$	$Se–O_t$	$U–O_{nr}–Se$
I	⟨1.762⟩	⟨2.336⟩	2.482(13)	⟨1.630⟩	⟨1.602⟩	⟨139.8⟩
	1.755(10)–1.769(12)	2.331(9)–2.340(9)		1.628(9)–1.632(8)	1.593(10)–1.610(8)	138.2(5)–141.3(5)
II	⟨1.767⟩	⟨2.347⟩ 2.335(6)–2.360(7)	2.513(6)	⟨1.646⟩ 1.638(7)–1.656(6)	⟨1.614⟩ 1.610(6)–1.624(7)	⟨140.4⟩
	1.759(6)–1.775(6)					132.5(4)–147.7(4)
III	⟨1.770⟩	⟨2.34⟩	–	⟨1.66⟩	⟨1.65⟩	⟨140⟩
	1.769(10)–1.771(10)	2.22(5)–2.44(6)		1.59(3)–1.74(6)	1.65(3)–1.65(4)	136(2)–146(3)
IV	⟨1.751⟩	⟨2.375⟩	2.494(16)	⟨1.628⟩	⟨1.597⟩	⟨138.5⟩
	1.746(9)–1.758(9)	2.316(14)–2.407(14)		1.608(15)–1.654(14)	1.583(16)–1.605(19)	133.9(8)–144.8(9)
V	⟨1.753⟩	⟨2.403⟩	–	⟨1.643⟩	⟨1.609⟩	⟨135.2⟩
	1.740(14) –1.759(15)	2.369(11) –2.43(2)		1.44(2) –1.657(14)	1.608(13) –1.95(3)	127.0(6) –145.1(13)
VI	⟨1.75⟩	⟨2.40⟩	–	⟨1.62⟩	⟨1.60⟩	⟨136.8
	1.67(3)–1.81(3)	2.33(4)–2.45(3)		1.55(3)–1.68(3)	1.54(4)–1.66(4)	129.6(19)–146.2(19)
VII	⟨1.758⟩	⟨2.39⟩	2.54(3)	⟨1.61⟩	⟨1.55⟩	⟨136.8⟩
	1.751(10)–1.764(10)	2.31(2)–2.48(3)		1.55(4)–1.66(3)	1.50(5)–1.62(3)	129(2)–152.9(13)
VIII	⟨1.72⟩	⟨2.396⟩	2.51(2)	⟨1.619⟩	⟨1.587⟩	⟨137.6⟩
	1.69(2)–1.77(2)	2.364(18)–2.421(19)		1.575(19)–1.652(17)	1.56(2)–1.61(2)	126.3(13)–150.2(14)

In brackets given are average value in the crystal structures

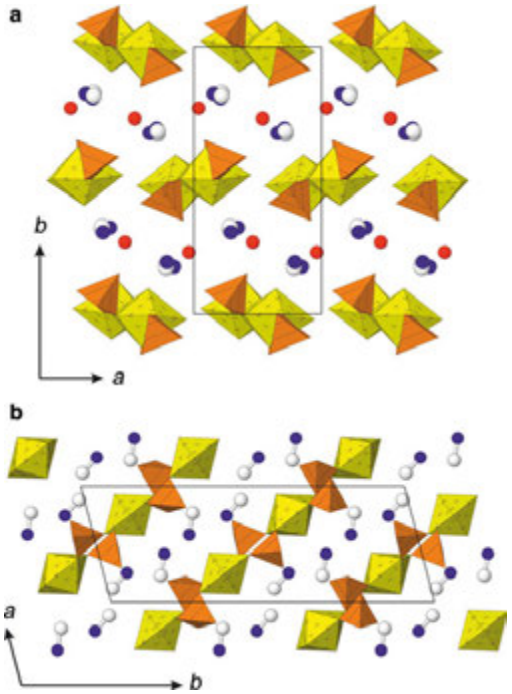

Fig. 1 The crystal structures of **I** and **II** projected along the *c* (**a**), and *b* (**b**) axes, respectively. Legend: U polyhedra = *yellow*; Se polyhedra = *orange*; C and N atoms are *white* and *blue*, respectively; *red circles* = H_2O groups (Color figure online)

Compounds with U:Se = 5:8

Five symmetrically independent uranium positions were observed in the crystal structures of **VII** and **VIII**. All U sites have typical seven-coordinate pentagonal bipyramidal coordination geometries with the average $\langle U^{6+}–O_{Ur}\rangle$ uranyl bond lengths equal to 1.76 and 1.73 Å for **VII** and **VIII**, respectively. The uranyl cations are equatorially coordinated by five O atoms, which leads to the formation of pentagonal bipyramids with the $U^{6+}–O_{eq}$ bond lengths in the range of 2.31(2)–2.48(3) Å for **VII** and 2.36(2)–2.42(2) Å for **VIII**. In both structures, four out of the five equatorial oxide ligands of $[U(1)O_2]^{2+}$ cations belong to the $[SeO_4]^{2-}$ groups; the fifth is an H_2O molecule. The U(1)–H_2O bond length is 2.54(3) and 2.51(2) Å in **VII** and **VIII**, respectively. The Se atoms in both structures are tetrahedrally coordinated by four O atoms each, forming $[SeO_4]^{2-}$ tetrahedra. The ⟨Se–O⟩ bond lengths of tetrahedra are 1.61 and 1.62 Å for **VII** and **VIII**, respectively.

The structures of **VII** and **VIII** are based upon sheets with the chemical composition $[(UO_2)_5(SeO_4)_8(H_2O)]^{6-}$. The sheets are formed by corner sharing between $[U\varphi_7]^{n-}$

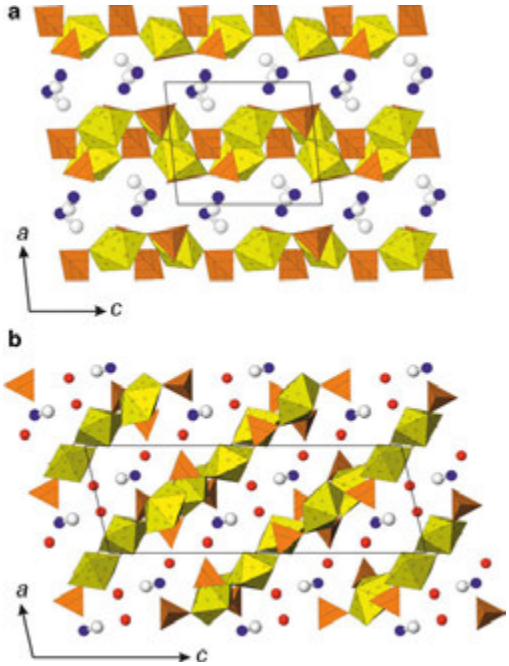

Fig. 2 The crystal structures of **III** and **IV** projected along the *b* axes (**a**, **b**, respectively). Legend is as in Fig. 1

(φ = O, H_2O; n = 6, 8) pentagonal bipyramids and $[SeO_4]^{2-}$ tetrahedra. In the structure of **VII**, the uranyl selenate sheets are slightly corrugated and arranged in parallel with the (001) plane (Fig. 4a). In the structure of **VIII**, the uranyl selenate sheets are planar and run parallel to (010) (Fig. 4b). The interpolyhedral Se–O_{br}–U angles in **VII** and **VIII** have the average values of 136.8° and 137.6°, respectively, which are in general agreement with the average value of 136.8° reported in [32].

The compounds **VII** and **VIII** contain as interlayer species protonated methylamine $[CH_3NH_3]^+$ cations, hydronium $[H_3O]^+$ and $[H_5O_2]^+$ cations and water molecules as interlayer species. Assignment of the interlayer sites to the $[H_3O]^+$ cations was based upon the presence of three $H_3O^{+\cdots}O$ contacts in the range of 2.6–2.9 Å. The $[H_5O_2]^+$ cations are characterized by the presence of a short O···O contact of 2.3–2.4 Å corresponding to a strong hydrogen bond within the cation and two additional O···O contacts in the range of 2.7–2.9 Å for each O atom of the $[H_5O_2]^+$ cation. In contrast, H_2O groups form from two to three weak hydrogen bonds to adjacent O atoms with the O···O interatomic distances longer than 2.9 Å. In the interlayer space of **VIII**, there are also three disordered electroneutral (H_2SeO_4) groups.

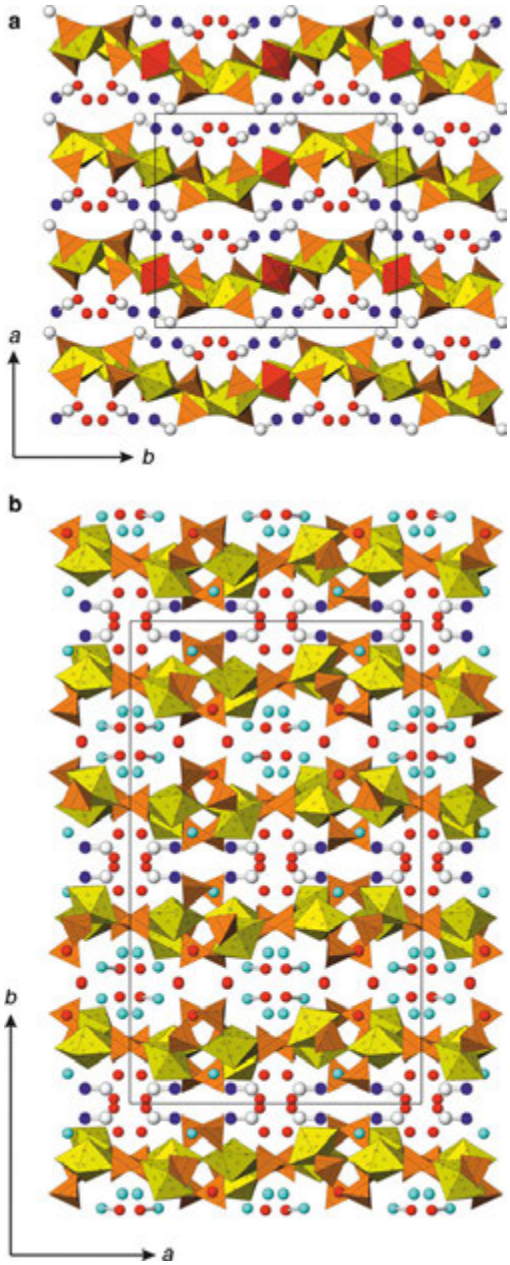

Fig. 3 The crystal structures of **V** and **VI** projected along the *c* axes (**a**, **b**, respectively). Legend is as in Fig. 1; the selenate tetrahedra in **V** with disordered orientations are shown in *red*; *cyan circles* = $[H_3O]^+$ groups (Color figure online)

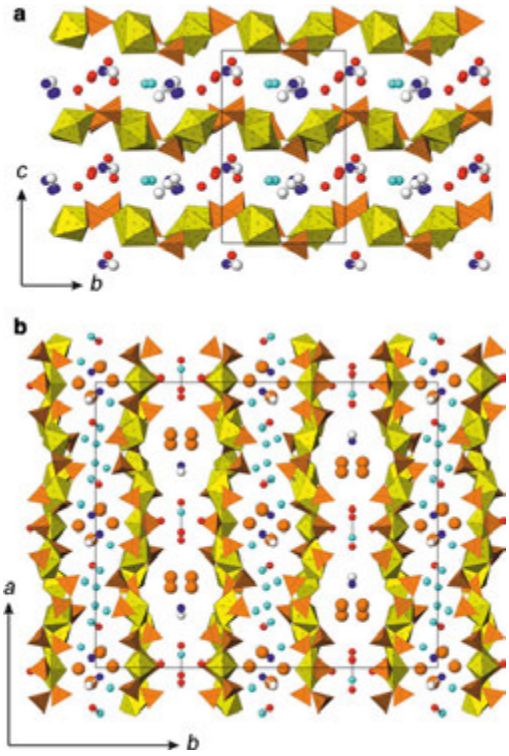

Fig. 4 The crystal structures of **VII** and **VIII** projected along the *a* (**a**) and *c* (**b**) axes, respectively. Legend is as in Fig. 1; *cyan circles* = $[H_3O]^+$ groups; *orange circles* indicate positions of disordered Se atoms in the interlayer space (Color figure online)

Discussion

Topological analysis

Topological structure of uranyl selenate units in the structures under consideration here can be visualized using the nodal representation. Within this approach [11, 12, 25], the U and Se coordination polyhedra are symbolized by black and white nodes, respectively. The vertices are linked by an edge if two respective polyhedra share a common oxygen atom. The resulting graph is used to investigate topological relations between similar structures.

Figure 5c and d show black-and-white graphs corresponding to the topological structures of the 1D- and 2D-units of **I** and **II**. The $[(UO_2)(SeO_4)_2(H_2O)]^{2-}$ chain observed in the structure of **I** corresponds to the simple 1D graph. Chains of this type are quite common for uranyl compounds with $[TO_4]^{n-}$ tetrahedra (T = S, Se, P, As). They have been observed first in the structure of $Mn[(UO_2)(SO_4)_2(H_2O)](H_2O)_5$ [33] and later in a number of amine-templated uranyl sulfates [34–39] and other compounds, including $[(UO_2)(H_2PO_4)_2(H_2O)](H_2O)_2$ [40], $[(UO_2)(H_2AsO_4)_2(H_2O)]$ [41], $M[(UO_2)(SeO_4)_2(H_2O)](H_2O)_4$ (M = Mg, Zn) [42], $[C_5H_{16}N_2]_2[(UO_2)(SeO_4)_2(H_2O)](NO_3)_2$ [43]. The black-and-white graph of the sheet observed in the structure of **II** (Fig. 5d) consists of four-connected black and two-connected white vertices. This graph corresponds to the topology observed in a number of layered uranyl selenates: $[C_5H_{14}N_2]_2[(UO_2)(SeO_4)_2(H_2O)]_2(H_2O)$, $[C_4H_{12}N]_2[(UO_2)(SeO_4)_2(H_2O)]$ [9], $(H_3O)_2[(UO_2)(SeO_4)_2(H_2O)](H_2O)$ [44], and $K_2(H_5O_2)(H_3O)[(UO_2)_2(SeO_4)_4(H_2O)_2](H_2O)_4$ [45]. The graph contains tight four-membered rings and extended voids of about 3×15 Å^2 in dimensions.

Figure 6a, b show uranyl selenate sheets in the structures of **III**, and **IV**, respectively. The corresponding black-and-white graphs are depicted in Fig. 6c, d, respectively. The topology of **III** is based only upon four-membered rings of alternating black and white nodes. The graph has been observed in uranyl selenates $(H_3O)[C_3H_5N_2][(UO_2)_2(SeO_4)_3]$ [9] and $[CH_6N_3]_2[(UO_2)_2(SeO_4)_3]$ [46]. Topology of the $[(UO_2)_3(SeO_4)_5]^{2-}$ sheet in **IV** contains four- and eight-membered rings. This topology is relatively rare and has previously been observed in $K(H_3O)[(UO_2)_2(SeO_4)_3(H_2O)](H_2O)_6$ [47] and $[N_8C_{26}H_4]_{0.5}[(UO_2)_2(SO_4)_3(H_2O)](H_2O)_2$ [48].

The crystal structures of **V** and **VI** are based upon topologically similar inorganic sheets with the composition $[(UO_2)_3(SeO_4)_5]^{4-}$ (Fig. 7a, b). Their graphs (Fig. 7c, d) are built from four- and six-membered rings. This topology of uranyl was observed in some selenate and chromate compounds, e.g., in $Mg_2[(UO_2)_3(SeO_4)_5](H_2O)_{16}$ [49] and $Mg_2[(UO_2)_3(CrO_4)_5](H_2O)_{17}$ [50].

The black-and-white graphs corresponding to the topological structures of the $[(UO_2)_5(SeO_4)_8(H_2O)]^{6-}$ sheet in **VII** and **VIII** are shown in Fig. 8a, b. They contain both four- and six-membered rings. Six-membered rings share vertices to form corner–sharing pairs separated by chains of edge–sharing four-membered rings. The pairs are stretched alternatively along [120] and [$\bar{1}$20]. All white vertices are three-connected, whereas black vertices are either four- or five-connected, which correspond to the $[UO_6(H_2O)]^{6-}$ and $[UO_7]^{8-}$ pentagonal bipyramids, respectively. This topology has previously been observed in $[N_3C_6H_{18}]_2[(UO_2)_5(SO_4)_8(H_2O)]$ [51], but **VII** and **VIII** are the first examples of this topology for uranyl selenates.

Geometrical isomerism

To define topology of a structure by means of its nodal representation is not always enough to define its complete

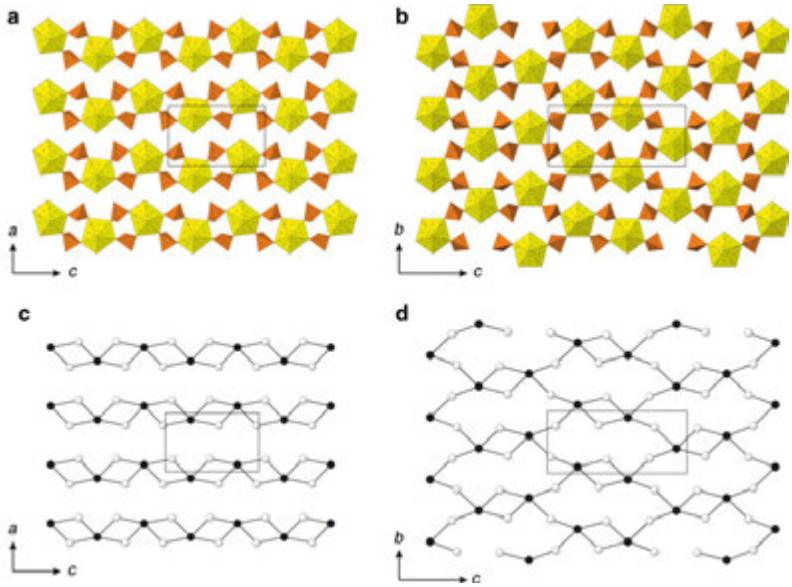

Fig. 5 The $[(UO_2)(SeO_4)_2(H_2O)]^{2-}$ chains in the crystal structure of **I** (**a**) and $[(UO_2)(SeO_4)_2(H_2O)]^{2-}$ sheets (**b**) in the crystal structure of **II** in polyhedral representations (legend as in Fig. 1), and their graphs (**c**, **d**, respectively). See text for details

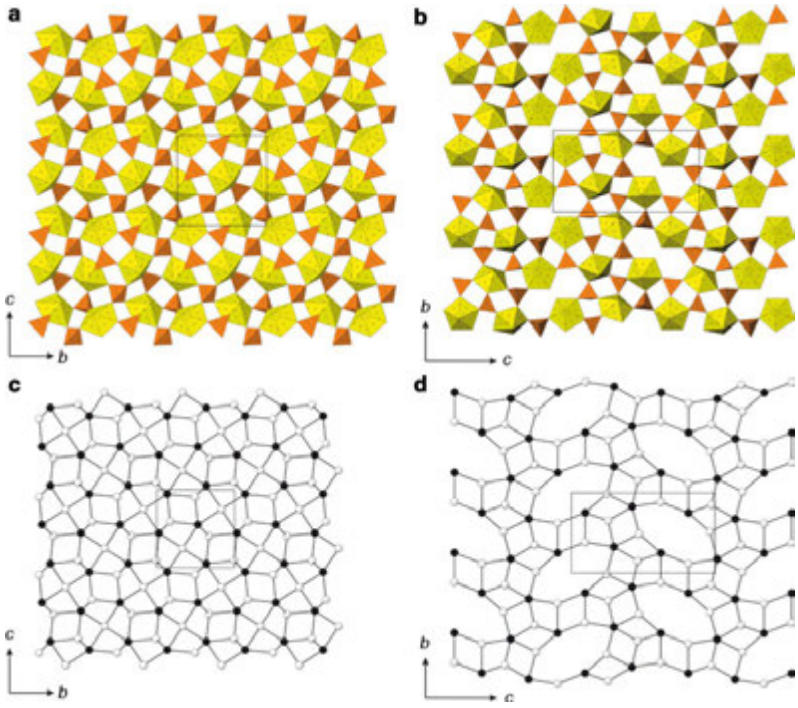

Fig. 6 The two-dimensional uranyl selenate sheets in the crystal structures of **III** (**a**) and **IV** (**b**) and their *black*-and-*white* graphs (**c**, **d**, respectively) (Color figure online)

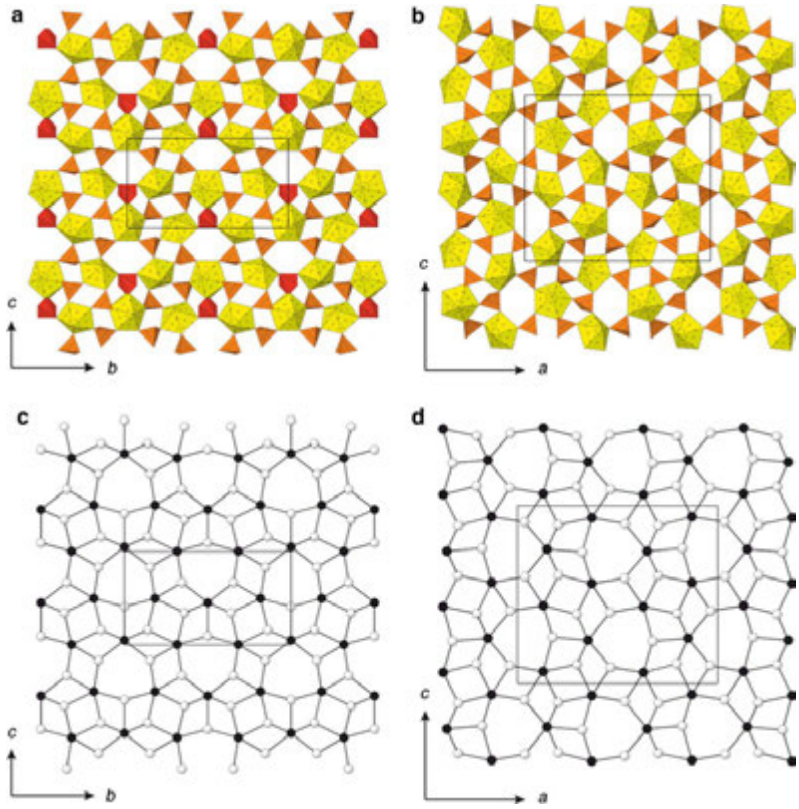

Fig. 7 The $[(UO_2)_3(SeO_4)_5(H_2O)]^{2-}$ sheets in the crystal structure of **V** (**a**) and **VI** (**b**) and their *black*-and-*white* graphs (**c**, **d**, respectively). The selenate tetrahedra in **V** with disordered orientations are shown in *red* (Color figure online)

topological structure. This is particularly true for compounds, which contain tetrahedra with terminal O atoms not involved in an interpolyhedral bonding. In this case, detailed examination of orientations of tetrahedra may reveal geometrical difference between the sheets with the same black-and-white graph, which led Krivovichev and Burns [50] to the definition of geometrical isomerism. It is important to note that geometrical isomers cannot be transformed into each other by simple rotations of tetrahedra and such a transformation is impossible without breaking of chemical bonds. To distinguish between the $[(UO_2)_3(SeO_4)_5]^{2-}$ sheets with the same graph observed in the structures of **IV**, $K(H_3O)[(UO_2)_2(SeO_4)_3(H_2O)](H_2O)_6$ [47], and $[N_8C_{26}H_4]_{0.5}[(UO_2)_2(SO_4)_3(H_2O)](H_2O)_2$ [48], one has to analyze orientations of tetrahedra relative to the plane of the sheet. As can be seen in the black-and-white graph of the topology (Fig. 6d), each $[TO_4]^{2-}$ (T = Se, S) tetrahedron in the sheet is three-connected, i.e., it shares three of its corners with adjacent either four- or five-connected $[UO_6(H_2O)]^{6-}$ and $[UO_7]^{8-}$ pentagonal bipyramids. The fourth corner is non-shared and may have either up-, down- or disordered (up-or-down) orientation relative to the plane of the sheet. This ambiguity gives rise to geometric isomers with various orientations of the tetrahedra. To identify and classify the isomers of this type, we use their orientation matrices [50]. According to this approach, as applied to the structures in hand, symbols **u** (up), **d** (down), **m** (disordered up-or-down orientation), or □ (white vertex is missing in the graph) are assigned to each white vertex.

The graphs shown in Fig. 9 have the **u** and **d** symbols written near white vertices. It can be seen that the systems of the **u** and **d** symbols are different for the sheets, which therefore should be considered as different geometrical isomers. The isomers can be distinguished by their orientation matrices that provide short notations of the translationally independent rectangular system of the **u**, **d**, and □ symbols. The orientation matrix for the sheet of the crystal structure of **IV** shown in Fig. 9c has 8 × 2 dimensions and can be written in row as (**uududd**□□)(**dd**□□**uudu**). It is noteworthy that the crystal structure of $K(H_3O)[(UO_2)_2(SeO_4)_3(H_2O)](H_2O)_6$ [47] has the same orientation matrix

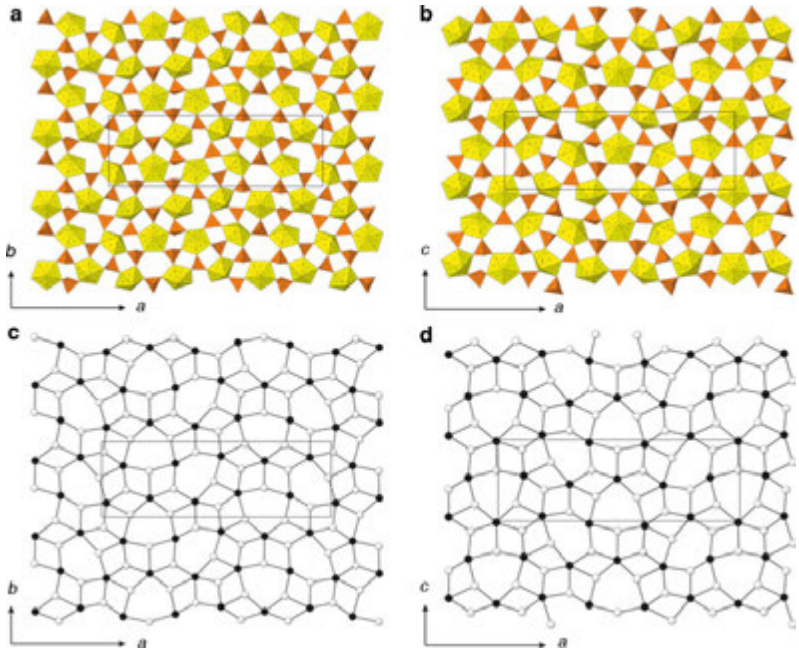

Fig. 8 Two-dimensional sheets in the crystal structures of **VII** (**a**) and **VIII** (**b**) and their *black*-and-*white* graphs (**c**, **d**, respectively) (Color figure online)

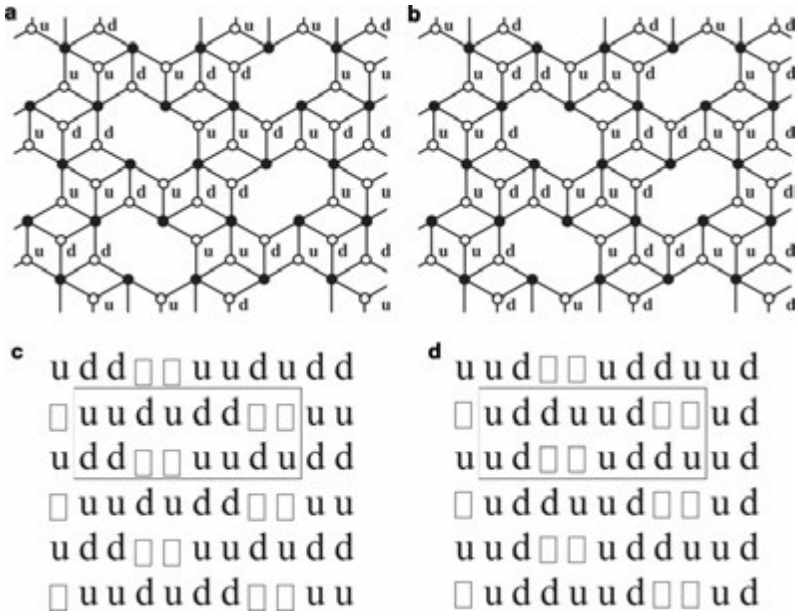

Fig. 9 *Black*-and-*white* graphs of the uranyl selenate sheets in the structures of **IV** and $K(H_3O)[(UO_2)_2(SeO_4)_3(H_2O)](H_2O)_6$ (**a**) and in the structure of $[N_8C_{26}H_4]_{0.5}[(UO_2)_2(SO_4)_3(H_2O)](H_2O)_2$ (**b**) with the orientation symbols of tetrahedra; extended tables of orientation symbols (**c**, **d**, respectively). Translationally independent orientation matrices of tetrahedra are selected in (**c**) and (**d**) by *rectangular* areas (Color figure online)

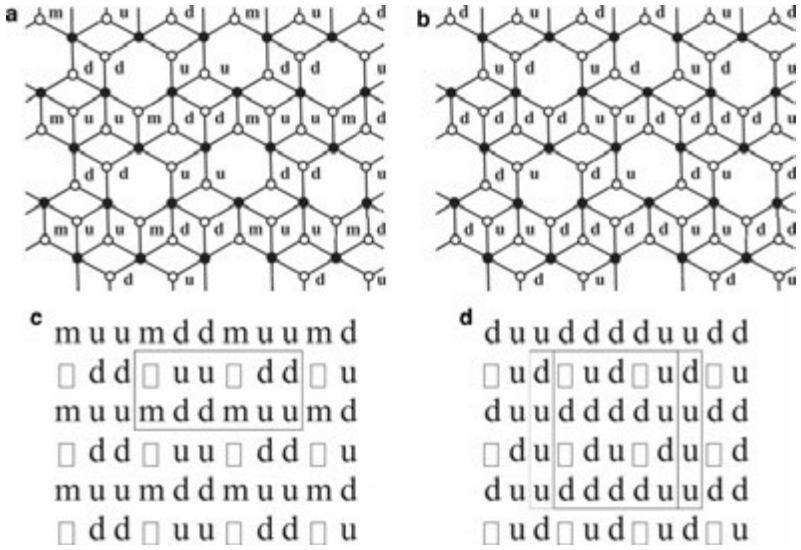

Fig. 10 *Black*-and-*white* graphs of uranyl selenate sheets in the structures of **V** (**a**) and **VI** (**b**) with the orientation symbols of tetrahedra; extended tables of orientation symbols (**c**, **d**, respectively). Translationally independent orientation matrices of tetrahedra are selected in (**c**) and (**d**) by *rectangular* areas (Color figure online)

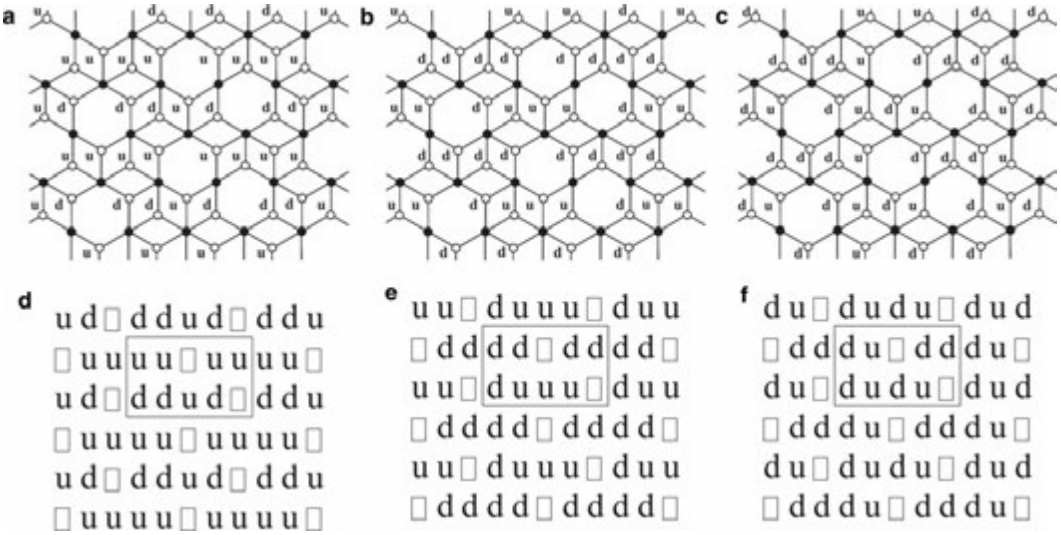

Fig. 11 *Black*-and-*white* graphs of uranyl selenate sheets in the structures of **VII** (**a**), **VIII** (**b**), and $[N_3C_6H_{18}]_2[(UO_2)_5(SO_4)_8(H_2O)]$ (**c**) with the orientation symbols of tetrahedra; extended tables of orientation symbols (**d**–**f**, respectively). Translationally independent orientation matrices of tetrahedra are selected in (**d**–**f**) by *rectangular* areas (Color figure online)

of the inorganic sheet. The orientation matrix of the sheet of the crystal structure of $[N_8C_{26}H_4]_{0.5}[(UO_2)_2(SO_4)_3(H_2O)](H_2O)_2$ [48] shown in Fig. 9d can be written as (**uddduud□□**)(**ud□□uddu**).

The black-and-white graph corresponding to the inorganic $[(UO_2)_3(SeO_4)_5]^{4-}$ sheets in **V**, and **VI** are shown in Fig. 10a, b, respectively, with the orientation symbol indicated at each white vertex. The orientation matrices (Fig. 10c, d) have dimensions 6 × 2 and 6 × 4 for **V** and **VI**, respectively. The series of symbols written in row (**□uu□dd**)(**mddmuu**) and (**□ud□ud**)(**duuddd**) (**□du□du**)(**ddddud**) for the inorganic sheets completely characterizes the topological structure of the geometric isomers **V** and **VI**. It should be noted that the matrix of **VI**

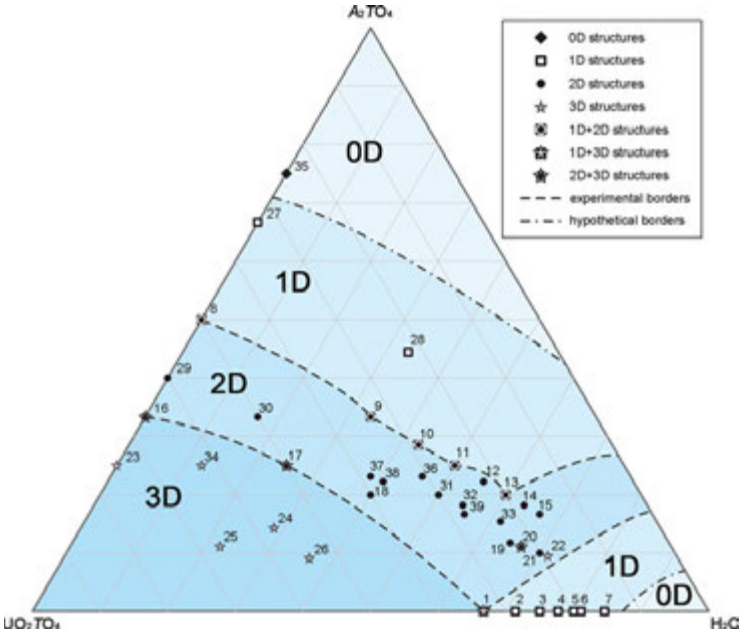

Fig. 12 Dimensional fields on the compositional diagram of the UO_2TO_4–A_2TO_4–H_2O (A = monovalent cation, T = S, Se, Cr, Mo) system. See Table 4 for the list of compounds and references

contain the **m** symbol, which symbolizes selenate tetrahedron that has no preferred orientation due to its disordered arrangement.

The black-and-white graphs for the $[(UO_2)_5(H_2O)(SO_4)_8]^{6-}$ sheets in **VII**, **VIII**, and $[N_3C_6H_{18}]_2[(UO_2)_5(SO_4)_8(H_2O)]$ with the **u**, **d** and □ symbols written near the white vertices are shown in Fig. 11. Orientation matrices for these sheets may be written as (**uu**□**uu**)(**ddud**□), (**dd**□**dd**)(**duuu**□), and (**du**□**dd**)(**dudu**□), respectively (Fig. 11a–c).

Dimensional reduction in uranyl oxysalts with general formula $A_n(UO_2)_p(TO_4)_q(H_2O)_r$

The eight novel compounds reported herein can be described by the general formula $[CH_3NH_3]_n(UO_2)_p(TO_4)_q(H_2O)_r$. In order to investigate the chemistry–structure relationships, we employ the dimensional reduction principle [26–29]. In order to put the study in more general context, the whole range of the compounds with the general formula $A_n(UO_2)_p(TO_4)_q(H_2O)_r$ (A = monovalent cation, and T = S, Se, Cr, Mo) has been analyzed. It was supposed that the basic highly-polymerized three-dimensional parent structure is that of $(UO_2)(TO_4)$, whereas the role of reducing agents is played by $A_2(TO_4)$ and H_2O. As a consequence, the relationships between different compositions and structures may be visualized using the UO_2TO_4–A_2TO_4–H_2O compositional diagram (Fig. 12). Table 4 summarizes formulas and dimensional characteristics of the structures of respective compounds.

The diagram shown in Fig. 12 may be divided into regions, where structures have the same dimensionality values (0 = finite clusters, 1 = chains, 2 = sheets, 3 = frameworks). Definition of the borders between the fields is not unambiguous and is rather tentative in character. For instance, due to the presence of only one point (**35**) corresponding to the 0D phases, the borders between the 0D and 1D fields are hypothetical. We suppose these borders are subparallel to the borders between 1D-and-2D, 2D-and-3D fields, and are in agreement with the principle of dimensional reduction for inorganic oxysalts. However, some deviations are observed. The points **20** and **22** are located within the 2D field, but correspond to the 3D framework structures with the $A_6(UO_2)_2(TO_4)_3(H_2O)_6$ and $A_6(UO_2)_2(TO_4)_3(H_2O)_{7.5}$ compositions, respectively. We attribute these deviations to the double role of H_2O: in most cases, it acts as reducing agent, whereas, in the cases of **20** and **22**, it simply fills cavities of the uranyl-based framework.

For more detailed demonstration of the principle of dimensional reduction in the system, one may consider the line originating from the left and ending at the top corner of the diagram. The line describes compounds with the composition $A_n(UO_2)_p(TO_4)_q$. The points **23**, **29**, **27**, and **35** correspond to the structures with dimensionalities equal to

Table 4 Phases of inorganic oxysalts with general formula $A_n(UO_2)_p(TO_4)_q(H_2O)_r$ in the UO_2TO_4–A_2TO_4–H_2O system

Point	Formula type	n	p	q	r	D^a	T	A	References
1	$(UO_2)(TO_4)(H_2O)_2$	0	1	1	2	1	Se, Cr	–	[52, 53]
						3	Mo	–	[54]
2	$(UO_2)(TO_4)(H_2O)_{2,5}$	0	2	2	5	1	S	–	[55]
3	$(UO_2)(TO_4)(H_2O)_3$	0	1	1	3	1	Cr	–	[52]
4	$(UO_2)(TO_4)(H_2O)_{3,5}$	0	2	2	7	1	S	–	[56, 57]
5	$(UO_2)(TO_4)(H_2O)_4$	0	1	1	4	1	Se	–	[58]
6	$(UO_2)(TO_4)(H_2O)_{4,3}$	0	1	1	4.3	1	Cr	–	[52]
7	$(UO_2)(TO_4)(H_2O)_{5,5}$	0	2	2	11	1	Cr	–	[59]
8	$A_2(UO_2)(TO_4)_2$	2	1	2	0	1	Mo	Li	[60]
						2	Mo	Na, K, Rb, Cs	[61–64]
						2	Cr, Mo	Tl	[65]
9	$A_2(UO_2)(TO_4)_2(H_2O)$	2	1	2	1	1	Se	Amine, H_3O	[66]
						2	S, Se	Amine, H_3O	[67], **II**
						2	Mo	K, Rb, Cs, NH_4	[63, 64, 68–70]
10	$A_2(UO_2)(TO_4)_2(H_2O)_{1.5}$	4	2	4	3	1-2	Se	Amine	[25]
11	$A_2(UO_2)(TO_4)_2(H_2O)_2$	2	1	2	2	1	S, Se	Amine	[47]
						2	S, Se	K, Rb, Cs, NH_4	[71–76]
						2	Se	Amine, H_3O	[77–79], **I**
12	$A_2(UO_2)(TO_4)_2(H_2O)_{2,5}$	4	2	4	5	2	Se	Amine	[80]
13	$A_2(UO_2)(TO_4)_2(H_2O)_3$	2	1	2	3	1	Se	Amine	[66]
						2	S, Se	Amine, H_3O	[81]
14	$A_2(UO_2)(TO_4)_2(H_2O)_{3,5}$	4	2	4	7	2	Se	K, H_3O	[82]
15	$A_2(UO_2)(TO_4)_2(H_2O)_4$	2	1	2	4	2	Se, Mo	Na	[83, 84]
16	$A_2(UO_2)_2(TO_4)_3$	2	2	3	0	2	S, Se	Amine, H_3O	[9, 66, 85], **III**
						2	S, Mo	Cs	[86, 87]
						3	Mo	Rb, Cs	[87]
						3	Mo	Tl	[88]
17	$A_2(UO_2)_2(TO_4)_3(H_2O)$	2	2	3	1	2	Se	Amine	[9, 75, 89]
						3	Se	H_3O	[77]
18	$A_2(UO_2)_2(TO_4)_3(H_2O)_2$	2	2	3	2	2	Se	K, H_3O	[45]
						2	Se	Amine, H_3O	[66, 89], **IV**
19	$A_2(UO_2)_2(TO_4)_3(H_2O)_{5,5}$	4	2	6	11	2	Se	H_3O	[90]
20	$A_2(UO_2)_2(TO_4)_3(H_2O)_6$	2	2	3	6	2	Se, Cr	K, Rb, NH_4	[73, 91, 92]
						3	Se	Rb, H_3O	[93, 94]
21	$A_2(UO_2)_2(TO_4)_3(H_2O)_7$	2	2	3	7	2	Se	K, H_3O	[47]
22	$A_2(UO_2)_2(TO_4)_3(H_2O)_{7,5}$	4	4	6	15	3	Se	Na	[95]
23	$A_2(UO_2)_3(TO_4)_4$	2	3	4	0	3	Mo	Na, K	[9]
24	$A_2(UO_2)_4(TO_4)_5(H_2O)_2$	2	4	5	2	3	Mo	Amine	[96]
25	$A_2(UO_2)_6(TO_4)_7(H_2O)_2$	2	6	7	2	3	S	Amine	[97]
						3	Mo	Rb, Cs, NH_4	[63, 98]
26	$A_2(UO_2)_6(TO_4)_7(H_2O)_4$	2	6	7	4	3	Mo	Amine	[99]
27	$A_4(UO_2)(TO_4)_3$	4	1	3	0	1	Cr	Na	[100]
28	$A_4(UO_2)(TO_4)_3(H_2O)_{1,5}$	8	2	6	3	1	Mo	Na, Tl	[83]
29	$A_4(UO_2)_3(TO_4)_5$	4	3	5	0	2	Se	Amine, H_3O	**V**
30	$A_4(UO_2)_3(TO_4)_5(H_2O)$	4	3	5	1	2	Se	Rb	[73]
31	$A_4(UO_2)_3(TO_4)_5(H_2O)_5$	4	3	5	5	2	Se	Amine, H_3O	**VI**
32	$A_4(UO_2)_3(TO_4)_5(H_2O)_6$	4	3	5	6	2	Se	Amine, H_3O	[66]
33	$A_4(UO_2)_3(TO_4)_5(H_2O)_8$	4	3	5	8	2	Cr	K	[91]

Table 4 continued

Point	Formula type	n	p	q	r	D[a]	T	A	References
34	$A_4(UO_2)_5(TO_4)_7(H_2O)$	4	5	7	1	3	Mo	NH_4	[101]
35	$A_6(UO_2)(TO_4)_4$	6	1	4	0	0	Mo	Na, Rb, Cs, Tl	[63, 83, 102, 103]
36	$A_6(UO_2)_4(TO_4)_7(H_2O)_6$	6	4	7	6	2	Cr	K	[104]
37	$A_6(UO_2)_5(TO_4)_8(H_2O)_5$	6	5	8	5	2	Se	Amine, H_3O	**VII**
38	$A_6(UO_2)_5(TO_4)_8(H_2O)_{5,5}$	12	10	16	11	2	Se	Amine, H_3O	**VIII**
39	$A_6(UO_2)_5(TO_4)_8(H_2O)_{10}$	6	5	8	10	2	Se	H_3O	[105]

T = S, Se, Cr, Mo; A = monovalent cation

[a] D dimensionality of structural unit

3, 2, 1, and 0, respectively. The points **16** and **8** are located on the borders between 2D-and-3D, 1D-and-2D fields, respectively. Thus, the dimensionality of the structural unit is decreasing from the points **23** to **35**, which is in agreement with the principle of dimensional reduction.

Conclusions

In this study, we have reported eight novel phases in the methylamine–$(UO_2)(NO_3)_2$–H_2SeO_4–H_2O system. Structural topologies of these phases are conveniently described using nodal representation, which provides essential tools for topological description and classification of complex inorganic structures. However, some structural complications such as the presence of 3-connected tetrahedra may lead to loss of information about precise topological arrangement. In this case, additional techniques have to be applied to distinguish different geometrical isomers, e.g., the approach based upon construction of orientation matrices. The structures of the eight new phases are thus completely characterized by combination of graph and orientation matrices. Analysis of the $A_n(UO_2)_p(TO_4)_q(H_2O)_r$ compounds (A = monovalent cation, and T = S, Se, Cr, Mo) using the principle of dimensional reduction and composition-structure diagram allowed to separate specific fields corresponding to the formation of structures with specific dimensionalities of their structural units.

Acknowledgments This study was supported by RFBR (Grant 12-03-90711 to VVG) and St. Petersburg State University through the internal grant 3.37.84.2011 and the X-Ray Diffraction Resource Center.

References

1. Hyde BG, Andersson S (1989) Inorganic crystal structures. Wiley, New York
2. Hansen S, Andersson S, Fälth L (1982) Z Kristallogr 160:9
3. Andersson S, Hyde BG (1982) Z Kristallogr 158:119
4. Andersson S (1983) Angew Chem Int Ed 22:69
5. Nyman H, Hyde BG, Andersson S (1984) Acta Crystallogr B40:441
6. Burns PC, Miller ML, Ewing RC (1996) Can Miner 34:845
7. Burns PC (1999) Rev Miner 38:23
8. Burns PC (2005) Can Miner 43:1839
9. Krivovichev SV, Burns PC, Tananaev IG (eds) (2007) Structural chemistry of inorganic compounds. Elsevier, Amsterdam
10. Miller ML, Finch RJ, Burns PC, Ewing RC (1996) J Mater Res 11:3048
11. Krivovichev SV (2004) Crystallogr Rev 10:185
12. Krivovichev SV (2008) Structural crystallography of inorganic oxysalts. Oxford University Press, Oxford
13. Burns PC, Hughes Kubatko KA, Sigmon G, Fryer BJ, Gagnon JE, Antonio MR, Soderholm L (2005) Angew Chem Int Ed 44:2135
14. Sigmon G, Unruh DK, Ling J, Weaver B, Ward M, Pressprich L, Simonetti A, Burns PC (2009) Angew Chem Int Ed 48:2737
15. Burns PC (2010) C R Chim 13:737
16. Krivovichev SV, Kahlenberg V, Kaindl R, Mersdorf E, Tananaev IG, Myasoedov BF (2005) Angew Chem Int Ed 44:1134
17. Krivovichev SV, Kahlenberg V, Tananaev IG, Kaindl R, Mersdorf E, Myasoedov BF (2005) J Am Chem Soc 127:1072
18. Alekseev EV, Krivovichev SV, Depmeier W (2008) Angew Chem Int Ed 47:549
19. Chen CS, Lee SF, Lii KH (2005) J Am Chem Soc 127:12208
20. Lin C, Chen C, Shiryaev AA, Zubavichus YV, Lii KH (2008) Inorg Chem 47:4445
21. Lee CS, Wang SL, Lii KH (2009) J Am Chem Soc 131:15116
22. Wang S, Alekseev EV, Miller HM, Depmeier W, Albrecht-Schmitt TE (2010) Inorg Chem 49:9755
23. Wang S, Alekseev EV, Stritzinger JT, Depmeier W, Albrecht-Schmitt TE (2010) Inorg Chem 49:6690
24. Wang S, Alekseev EV, Stritzinger JT, Depmeier W, Albrecht-Schmitt TE (2010) Inorg Chem 49:2948
25. Krivovichev SV (2010) Eur J Inorg Chem 2010:2594
26. Alekseev EV, Krivovichev SV, Armbruster T, Depmeier W, Suleimanov EV, Chuprunov EV, Golubev AV (2007) Z Anorg Allg Chem 633:1979
27. Long JR, McCarty LS, Holm RH (1996) J Am Chem Soc 118:4603
28. Tulsky EG, Long JR (2001) Chem Mater 13:1149
29. Haddad S, Awwadi F, Willet RD (2003) Cryst Growth Des 3:501
30. Sheldrick GM (2008) Acta Crystallogr A64:112
31. Altomare A, Cascarano G, Giacovazzo C, Guagliardi A, Burla MC, Polidori G, Camalli M (1994) J Appl Crystallogr 27:435
32. Krivovichev SV (2004) Radiochemistry 46:434
33. Tabachenko VV, Serezhkin VN, Serezhkina LB, Kovba LM (1979) Koord Khim 5:1563

34. Mikhailov YUN, Gorbunova YUE, Demchenko EA, Serezhkina LB, Serezhkin VN (2000) Zh Neorg Khim 45:1711
35. Norquist AJ, Thomas PM, Doran MB, O'Hare D (2002) Chem Mater 14:5179
36. Norquist AJ, Doran MB, Thomas PM, O'Hare D (2003) Dalton Trans 2003:1168
37. Norquist AJ, Doran MB (2003) Solid State Sci 5:1149
38. Thomas PM, Norquist AJ, Doran MB (2003) J Mater Chem 13:88
39. Stuart CL, Doran MB, Norquist AJ, O'Hare D (2003) Acta Crystallogr E59:m446
40. Mercier R, Pham TM, Colomban P (1985) Solid State Ion 15:113
41. Gesing TM, Rüscher CH (2000) Z Anorg Chem 626:1414
42. Krivovichev SV, Kahlenberg V (2005) Z Naturforsch 60b:538
43. Krivovichev SV, Kahlenberg V (2005) Z Anorg Allg Chem 631:2352
44. Krivovichev SV (2008) Zap Vseross Miner Ova 137(1):54
45. Gurzhiy VV, Tyumentseva OS, Krivovichev SV, Tananaev IG, Myasoedov BF (2011) Radiochemistry 53:569
46. Krivovichev SV, Gurzhiy VV, Tananaev IG, Myasoedov BF (2009) Russ J Gen Chem 79:2723
47. Ling J, Sigmon GE, Ward M, Roback N, Burns PC (2010) Z Kristallogr 225:230
48. Doran MB, Norquist AJ, Stuart CL, O'Hare D (2004) Acta Crystallogr E60:m996
49. Krivovichev SV, Kahlenberg V (2004) Z Anorg Allg Chem 630:2736
50. Krivovichev SV, Burns PC (2003) Z Kristallogr 218:683
51. Norquist AJ, Doran MB, Thomas PM, O'Hare D (2003) Inorg Chem 42:5949
52. Krivovichev SV, Burns PC (2003) Z Kristallogr 218:568
53. Marukhnov AV, Serezhkin VN, Pushkin DV, Smirnov OP, Plakhtii VP (2008) Russ J Inorg Chem 53:1283
54. Serezhkin VN, Efremov VA, Trunov VK (1980) Crystallogr Rep 25:494
55. Van den Putten N, Loopstra BO (1974) Cryst Struct Commun 3:377
56. Zalkin A, Ruben H, Templeton DH (1978) Inorg Chem 17:3701
57. Brandenburg NP, Loopstra BO (1973) Cryst Struct Commun 2:243
58. Serezhkin VN, Soldatkina MA, Efremov VA (1981) Zh Strukt Khim 22:171
59. Serezhkin VN, Trunov VK (1981) Crystallogr Rep 26:301
60. Krivovichev SV, Burns PC (2003) Solid State Sci 5:481
61. Sadikov GG, Krasovskaya TI, YuA Polyakov, Nikolaev VP (1998) Izv Akad Nauk SSSR Neorg Mater 24:109
62. Krivovichev SV, Burns PC (2002) J Solid State Chem 168:245
63. Krivovichev SV, Burns PC (2005) Can Miner 43:713
64. Krivovichev SV, Finch R, Burns PC (2002) Can Miner 40:193
65. Krivovichev SV, Locock AJ, Burns PC (2005) Z Kristallogr 220:10
66. Gurzhiy VV, Krivovichev SV, Tananaev IG (2012) Radiochemistry (in prep)
67. Medrish IV, Vologzhanina AV, Starikova ZA, Antipin MYU, Serezhkina LB, Serezhkin VN (2005) Russ J Inorg Chem 50:360
68. Rastsvetaeva RK, Barinova AV, Fedoseev AM, Budantseva NA, Nikolaev YUV (1999) Dokl Ross Akad Nauk 365:68
69. Andreev GB, MYu Antipin, Fedoseev AM, Budantseva NA (2001) Russ J Coord Chem 27:208
70. Khrustalev VN, Andreev GB, Antipin MYU, Fedoseev AM, Budantseva NA, Shirokova IB (2000) Russ J Inorg Chem 45:1845
71. Niinisto L, Toivonen J, Valkonen J (1979) Acta Chem Scand A33:621
72. Mikhailov YUN, Gorbunova YUE, Shishkina OV, Serezhkina LB, Serezhkin VN (2001) Russ J Inorg Chem 46:1661
73. Krivovichev SV, Kahlenberg V (2005) Z Anorg Allg Chem 631:739
74. Mikhailov YUN, Gorbunova YUE, Serezhkina LB, Demchenko EA, Serezhkin VN (1997) Zh Neorg Khim 42:1413
75. Serezhkin VN, Verevkin AG, Smirnov OP, Plahtii VP (2010) Russ J Inorg Chem 55:1600
76. Niinisto L, Toivonen J, Valkonen J (1978) Acta Chem Scand A32:647
77. Ling J, Sigmon GE, Burns PC (2009) J Solid State Chem 182:402
78. Krivovichev SV (2008) Geol Ore Depos 50:789
79. Krivovichev SV (2008) Geol Ore Depos 50:795
80. Krivovichev SV, Kahlenberg V (2005) Z Anorg Allg Chem 631:2358
81. Baggio RF, de Benyacar MAR, Perazzo BO, de Perazzo PK (1977) Acta Crystallogr B33:3495
82. Gurzhiy VV, Tyumentseva OS, Krivovichev SV, Tananaev IG, Myasoedov BF (2012) Radiochemistry 54:43
83. Krivovichev SV, Burns PC (2003) Can Miner 41:707
84. Mikhailov YUN, Gorbunova YUE, Baeva EE, Serezhkina LB, Serezhkin VN (2001) Russ J Inorg Chem 46:2017
85. Norquist AJ, Doran MB, Thomas PM, O'Hare D (2003) Dalton Trans 2003:1168
86. Ross M, Evans HT Jr (1960) J Inorg Nucl Chem 15:338
87. Krivovichev SV, Cahill CL, Burns PC (2002) Inorg Chem 41:34
88. Nazarchuk EV, Krivovichev SV, Burns PC (2005) Radiochemistry 47:447
89. Krivovichev SV, Gurzhii VV, Tananaev IG, Myasoedov BF (2006) Dokl Phys Chem 409:228
90. Krivovichev SV, Kahlenberg V (2005) Radiochemistry 47:452
91. Krivovichev SV, Burns PC (2003) Z Kristallogr 218:725
92. YuN Mikhailov, YuE Gorbunova, Serezhkina LB, Serezhkin VN (1997) Zh Neorg Khim 42:734
93. Blatov VA, Serezhkina LB, Serezhkin VN, Trunov VK (1988) Russ J Coord Chem 14:1705
94. Kuchumova NV, Shtokova IP, Serezhkina LB, Serezhkin VN (1989) Zh Neorg Khim 34:1029
95. Baeva EE, Virovets AV, Peresypkina EV, Serezhkina LB (2006) Russ J Inorg Chem 51:210
96. Krivovichev SV, Cahill CL, Nazarchuk EV, Burns PC, Armbruster T, Depmeier W (2005) Micropor Mesopor Mater 78:225
97. Doran M, Norquist AJ, O'Hare D (2002) Chem Commun 2002:2946
98. Krivovichev SV, Burns PC (2001) Can Miner 39:207
99. Krivovichev SV, Armbruster T, DYu Chernyshov, Burns PC, Nazarchuk EV, Depmeier W (2005) Micropor Mesopor Mater 78:225
100. Krivovichev SV, Burns PC (2003) Z Anorg Allg Chem 629:1965
101. Krivovichev SV, Cahill CL, Burns PC (2003) Inorg Chem 42:2459
102. Krivovichev SV, Burns PC (2002) Can Miner 40:210
103. Krivovichev SV, Burns PC (2001) Can Miner 39:197
104. Sykora RE, McDaniel SM, Albrecht–Schmitt TE (2004) J Solid State Chem 177:1431
105. Krivovichev SV, Kahlenberg V (2005) Radiochemistry 47:415

A-III
Revised bismuth chloroselenite system: evidence of a noncentrosymmmetric structure with a giant unit cell

Almaz Aliev, Vadim M. Kovrugin, Marie Colmont, Christine Terryn, Marrielle Huvé, Oleg I. Siidra, Sergey V. Krivovichev, and Olivier Mentré

Published in: *Crystal Growth & Design*, 2014, Vol. 14 (6), p. 3026–3034.
DOI: 10.1021/cg500293w

CRYSTAL GROWTH & DESIGN

Article

pubs.acs.org/crystal

Revised Bismuth Chloroselenite System: Evidence of a Noncentrosymmmetric Structure with a Giant Unit Cell

Almaz Aliev,[†] V. M. Kovrugin,[†,§] Marie Colmont,*[,†] Christine Terryn,[‡] Marielle Huvé,[†] O. I. Siidra,[§] S. V. Krivovichev,[§] and Olivier Mentré[†]

[†]Université Lille 1, Université Lille Nord France, ENSCL, CNRS, UCCS, UMR 8181, F-59652 Villeneuve d'Ascq, France

[‡]Plateforme Imagerie Cellulaire et Tissulaire, 51 rue Cognacq-Jay, 51100 Reims, France

[§]St. Petersburg State University, Department of Crystallography, University Emb. 7/9, 199034 St. Petersburg, Russia

Supporting Information

ABSTRACT: The reactions between PbO, Bi_2O_3 (or BiOCl), and SeO_2 by the chemical vapor transport method using HCl as a transporting agent afforded three novel bismuth/lead chloroselenites, namely, β-$BiSeO_3Cl$ (**1**), $Bi_6(SeO_3)_4Cl_{10}$ (**2**), and $PbBi_{10}(SeO_3)_{12}Cl_8$ (**3**). Compound **1** is noncentrosymmetric (space group *Cc*, SHG active) and has a giant unit cell (V = 19792(2) Å^3). In the context of the complex $BiSeO_3Cl$ phase diagram reported by Oppermann et al., it was assigned to the undescribed β-form on the basis of its IR spectra and powder X-ray diffraction pattern. The comparison between the α-, β-, and γ-forms suggests their formation via the condensation of volatile $Bi(SeO_3)Cl$ molecules. Analysis of the structures of the α-, β-, and γ-forms indicates that the $\alpha \rightarrow \beta \rightarrow \gamma$ phase transitions are associated with a dramatic fluctuation of structural complexity together with the transitional character of the β phase. Compounds **1** and **3** are layered compounds with identical ($[M_8Cl_{16}]^{8+}$ and $[M_{14}(SeO_3)_{24}]^{6-}$) layers, where M stands for Bi in **1** and Pb/Bi in **3**. There are additional $[Bi_{12}Cl_{32}]^{4+}$ layered subunits in **1**. The crystal structure of **2** consists of the $[Bi_6(SeO_3)_4Cl_{10}]$ building blocks forming an open framework with six-membered-ring channels. These three compounds complete the poorly known bismuth selenium oxochloride panorama.

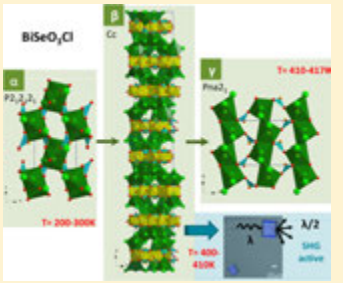

INTRODUCTION

The search for noncentrosymmetric (NCS) compounds is an important field for solid state chemists due to their promising properties for nonlinear optics (NLO) including second harmonic generation (SHG) and dielectrics including piezoelectricity, pyroelectricity, and ferroelectricity.[1,2] In particular, NLO materials have become tremendously important and are drawing more and more attention owing to their promising applications in laser science and technology. However, the search for the new compounds with NLO coefficients remains a chemical challenge. It can be resolved using a rational "design" approach but appears rather limited to particular chemical systems together with the controlled association of well-defined building units such as OBi_4 oxocentered tetrahedra[3,4] or oxofluoride metal units.[5] The lone-pair (LP) polyanions, such as EO_3 where E stand for the external s^2 electrons, also favorably arrange in NCS crystal structures, as for instance, in the compound $BiO(IO_3)$ with efficient SHG,[6] E allowing asymmetric or one-side coordination around the polyanion. In this context, selenite oxides are also promising materials with complex crystal structures.[7,8] As poorly involved in the creation of chemical bonds, the terminal LP could form voids in the structure, up to their segregation into cavities, channels, or layered interleaves. The use of halide ions as additional anions enhances this tendency, as recently shown in several examples of bismuth oxochloride structures, i.e., Arppe's compound derivatives[9] or multidimensional open frameworks.[10] Combining both NCS and low-dimensional specificities appear as a challenge for multifunctional materials.

The BiOCl–SeO_2 binary system studied here was poorly explored and consists of one single chemical composition, $Bi(SeO_3)Cl$, that crystallizes in three polymorphs.[11,12] As already discussed in other papers,[9] the combined use of bismuth, halide, and selenium may lead to the formation of materials related to the Sillen phases.

Here we used chemical vapor transport to evidence novel bismuth–selenium oxochlorides. This method is particularly well suited to the system because of the high volatility of SeO_2 and $BiCl_3$ at low temperatures. As a transport agent, HCl is used, though SeO_2 can be considered as playing the same role.[13]

In this paper, we report on the synthesis of three new bismuth selenite halides, **1**- β-$BiSeO_3Cl$, **2**- $Bi_6(SeO_3)_4Cl_{10}$, and **3**- $PbBi_{10}(SeO_3)_{12}C_{18}$ and describe their structural peculiarities. For the layered β-$BiSeO_3Cl$ that has a noncentrosymmetric

Received: February 27, 2014
Revised: April 18, 2014
Published: April 23, 2014

Table 1. Crystal Data, Measurement and Structural Refinement Parameters for β-$BiSeO_3Cl$, $Bi_6(SeO_3)_4Cl_{10}$, and $PbBi_{10}(SeO_3)_{12}Cl_8$

	β-$BiSeO_3Cl$	$Bi_6(SeO_3)_4Cl_{10}$	$PbBi_{10}(SeO_3)_{12}Cl_8$
	Crystal Data		
crystal symmetry	monoclinic	monoclinic	orthorhombic
space group	*Cc*	$P2_1/c$	*Ccca*
a (Å)	22.7052(3)	21.460(2)	15.819(6)
b (Å)	76.785(4)	8.4012(9)	17.871(7)
c (Å)	16.0550(3)	15.3370(18)	15.857(6)
β (deg)	135.000(2)	110.639(5)	
V (Å^3)	19792(2)	2587.7 (5)	4483 (3)
Z	192	4	4
D_x (g/cm^3)	5.470	5.432	6.079
μ (mm^{-1}) (for λ Kα = 0.71073 Å)	52.04	47.37	53.17
appearance	colorless platelet	colorless needle	colorles platelet
crysral size (mm^3)	0.13 × 0.09 × 0.05	0.81 × 0.37 × 0.13	0.16 × 0.15 × 0.06
	Data Collection		
λ(Mo Kα) (Å)	0.71073	0.71073	0.71073
scan mode	ω and φ	ω and φ	ω and φ
θ(min−max) (deg)	1.1−26.5	2.0−30.5	2.2−26.4
R(int) (%)	0.096	0.045	0.050
recording reciprocal space	$-28 \le h \le 28$	$-30 \le h \le 30$	$-15 \le h \le 19$
	$-96 \le k \le 96$	$-11 \le k \le 7$	$-22 \le k \le 21$
	$-20 \le l \le 20$	$-20 \le l \le 21$	$-19 \le l \le 19$
	Refinement		
measured, independent obs[a] refl	242854, 35097, 20 337	34697, 7843, 6363	10469, 2253, 1504
no. of refined parameters	1637	298	115
refinement method	F^2	F^2	F^2
$R_1(F^2)$(obs)/$R_1(F^2)$(all)	0.0612/0.1124	0.0299/0.0427	0.0667/0.1057
$wR_2(F^2)$(obs)/$wR_2(F^2)$ (all)	0.0645/0.0694	0.0330/0.0442	0.0639/0.0859
GOF(obs)/GOF(all)	1.32/1.63	1.46/1.76	0.84/0.92
$\Delta\rho_{max}/\Delta\rho_{min}$ (e·Å^{-3})	5.39/−4.51	3.42/−2.97	5.38/−7.01
extinction coefficient		0.0070(13)	0.0022(13)

[a]obs = $[I > 3\sigma(I)]$.

crystal structure and a giant unit cell (V = 19783 Å^3), the SHG properties have been quantified.

EXPERIMENTAL SECTION

Syntheses. The crystals of the three compounds reported here were obtained by the chemical vapor transport (CVT) method. The precursors were ground together and loaded into a quartz tube (ca. 20 cm). The evacuated and sealed ampules were placed into tubular furnace with precursors' side of the ampules being in the center and other side being close to the edge of the furnace. The central part of the furnace was heated at 450 °C for 14 days. The temperature difference between the hot and cold ends of the ampule is about 50 °C.

1- β-$BiSeO_3Cl$. Transparent colorless square platelet crystals of **1** were found on the walls of the cold side of the quartz ampule with the precursor mixture 1BiOCl + 1SeO_2 + 1MnO_2 and a drop of concentrated solution of HCl. An energy-dispersive spectroscopy (EDS) analysis indicated the absence of manganese in the obtained crystals.

2- $Bi_6(SeO_3)_4Cl_{10}$. The transparent colorless needles of **2** were found on the walls of the cold side of the quartz ampule with the mixture of 2$BiCl_3$ + 1 Bi_2O_3 + 4SeO_2 + 1Mn_2O_3 in the absence of HCl. An EDS analysis showed no Mn in the obtained crystals.

For **1** and **2**, attempts to incorporate manganese was tested in order to induce transport/magnetic properties. However, using chemical transport it is clear that Mn species are poorly mobile.

3- $PbBi_{10}(SeO_3)_{12}Cl_8$. The crystals of **3** are the transparent colorless platelets which were picked out from the walls of the cold side of the quartz ampule with the mixture of 1PbO + 1BiOCl + 1SeO_2 and a drop of concentrated solution of HCl. The presence of lead was evidenced by an electron probe microanalyzer (EPMA) analysis, and the ratio Pb/Bi was found to be 0.8:15.5.

The synthesis of the corresponding polycrystalline samples by a solid state route for the three compounds failed, due to the rather low temperature at which selenium oxide becomes volatile (close to 350 °C).

Single crystal X-ray Diffraction. Crystals of **1** (colorless platelet), **2** (colorless needle), and **3** (colorless platelet) were mounted on glass fibers and studied on a Bruker X8 APEX II diffractometer equipped with a microfocus X-ray tube with the Mo Kα radiation at 50 kV and 40 mA. The collected data were integrated using the Bruker program Saint Plus 6.025.[14] The unit-cell parameters were refined from the full data set. Multiscan absorption correction was performed for the three compounds using SADABS.[15] The structures were solved by Superflip method.[16] Jana 2006 program was used for structure refinements.[17] All relevant details of the data collection and evaluation for the three new structures are listed in Table 1. Atomic coordinates and anisotropic displacement parameters as well as the results of bond-valence calculations[18,19] are given in Supporting Information.

Transmission Electron Microscopy TEM. EDS studies were performed on a FEI Tecnai G220 transmission electron microscope. The material was crushed and dropped in the form of alcohol suspensions on carbon-supported copper grids followed by evaporation under ambient conditions. The EDS analysis was performed in order to validate the refined stoichiometry of the obtained single crystals.

Infrared Spectroscopy. Infrared spectra of **1** were measured between 4000 and 400 cm^{-1} with a Perkin−Elmer Spectrum Two spectrometer equipped with a diamond attenuated total reflectance

dx.doi.org/10.1021/cg500293w | Cryst. Growth Des. 2014, 14, 3026−3034

(ATR) accessory. It was compared to the IR spectra reported for previously known $BiSeO_3Cl$ forms.

Multiphoton SHG Microscopy. In this study, a laser scanning microscope LSM 710 NLO Zeiss (Iena, Germany) was used as implemented at the Plateforme d'Imagerie Cellulaire et Tissulaire, Reims, France. Excitation was provided by a CHAMELEON femtosecond Titanium-Sapphire laser (Coherent, Santa Clara, USA) set at 860 nm, tuning the power until SHG was detected (→ 16% maximal power, ~0.55 mW) on selected single crystal of **1** deposited on a glass plate. Samples were imaged with a 20×, 0.8 NA objective lens. Emitted signal of SHG was collected with a bandpass filter (420–440 nm) and compared to emission for KDP crystals collected in the same conditions.

$BiSeO_3Cl$ Phase Diagram. The compounds with the $BiSeO_3Cl$ composition have already been reported in the literature as three different polymorphic modifications, α, β, and γ (Figure 1). The γ-

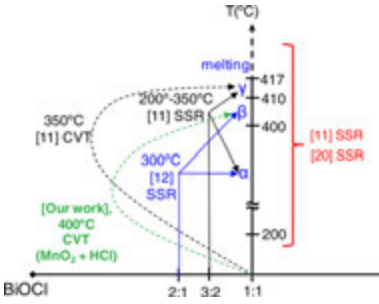

Figure 1. Phase relationships for $BiSeO_3Cl$ depending on temperature and stoichiometric amounts of BiOCl and SeO_2. Figure is built on information's taken from our work and refs 11, 12, and 20. SSR stands for solid state reaction and CVT is for chemical vapor transport.

form (space group $Pna2_1$, a = 11.707(2), b = 7.047(1), c = 5.315(1) Å) was prepared in evacuated (10^{-2} Pa) silica tubes from the 3:2 mixtures of BiOCl and SeO_2 by Ibragimov et al.[11] The mixtures were placed in the tubes in a dry chamber under a nitrogen atmosphere. The phase composition of the reaction products was determined by X-ray diffraction. Solid-state reactions were run at 200 °C, 250 °C, 300 °C, and 350 °C for 240 h, followed by a furnace-cooling or quenching in ice water. Using a starting mixture enriched in BiOCl, the product was systematically the γ-form. Single crystals of the α-$BiSeO_3Cl$ (space group $P2_12_12_1$, a = 6.353(2), b = 7.978(3), c = 8.651(4) Å) was obtained by Berdonosov et al.[12] by heating of the evacuated quartz tube with BiOCl and SeO_2 in 2:1 ratio at 300 °C for 240 h. According to them, if the starting mixture was enriched in BiOCl, the reaction products occasionally contained yellow BiOCl platelets and colorless parallelepipedal crystals of γ-$BiSeO_3Cl$. Oppermann et al.[20] reported the sequence of phase transitions occurring with temperature starting from the α-form as follows: $\alpha \rightarrow \beta$ at 400 °C/2 °C and $\beta \rightarrow \gamma$ at 410 °C/2 °C and going until melting point at 417 °C/2 °C. This was deduced from differential thermal analysis performed by Oppermann et al.[20]

The crystal structure of the α- and γ-forms are shown in Figure 2 according to the crystallographic data reported in refs 11 and 12. Optical properties as well as dielectric properties of the NCS γ-form have been investigated.[11] Optical conclusions are that dielectric relaxation due to ions jumping over the defect vacancies in the crystal lattice occurs. The β-$BiSeO_3Cl$ polymorph was announced as stable in a very narrow thermal domain from the high temperature transformation of α-$BiSeO_3Cl$ between 400 and 410 °C.[20] However, the crystal structure of the β phase was not solved at this temperature from the powder XRD data. Thus, there are only very few data available (XRD powder pattern and IR spectra) for the β-form.[20] Therefore, the

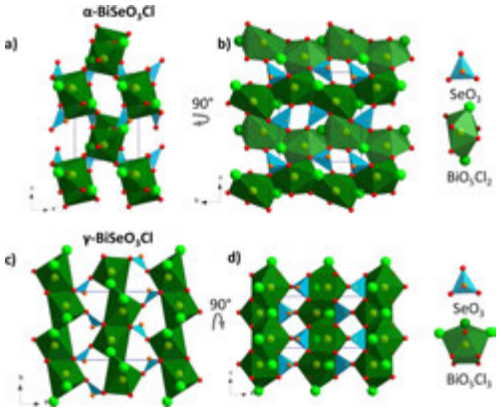

Figure 2. Crystal structure of α-$BiSeO_3Cl$: (a) projection along the b-axis, (b) along the a-axis. The crystal structure of γ-$BiSeO_3Cl$: (c) projection along the c-axis, (d) along the b-axis.

formal identification of the phase is rather difficult. Here we report on the synthesis and crystal structure of this phase.

Crystal Structure of β-$BiSeO_3Cl$. Colorless platelet single crystals have been isolated from the CVT products. An EDS analysis performed on single crystals shows evidence of Bi, Se, and Cl with a ratio of the elements 1.0/1.1/0.9. The majority of the tested crystals correspond to the phase with the lattice parameters, a = 22.7052(3) Å, b = 76.785(4) Å, c = 16.0550(3) Å, and β = 135.000(2)°, space group Cc. Beyond its NCS character, the volume cell is strikingly large, and the structure is very complex. A total of 48 bismuth, 48 selenium, and 48 chlorine independent atoms have been located. The positions of the oxygen atoms were derived by the inspection of the local Fourier-difference electron-density maps. Because of the high number of refined parameters, anisotropic thermal parameters were refined for the Bi and Se atoms only. The final cycles of least-squares refinement including atomic coordinates and anisotropic thermal parameters for all cations and isotropic thermal parameters of anions converged to R_1 = 0.0612, wR_2 = 0.0645 (racemic twinning domains 91%, 9%). The crystal data and selected bond lengths are given in Tables S1–S8 of Supporting Information, respectively. The crystal-structure data for β-$BiSeO_3Cl$ phase were deposited with the depository number CSD-426283. It is noteworthy that residual electronic density remains quite high (5.39 e Å^{-3}) at the end of the refinement. This is not surprising in the case of giant cell in the presence of heavy elements For example, other referenced bismuth selenites show similar electronic density; see refs 11 and 12. The same phenomenon was also observed for crystals **2** and **3**.

The crystal structures of the α- and γ-$BiSeO_3Cl$ structures are shown in Figure 2. The BiO_5Cl_2 polyhedra in the former and the BiO_3Cl_3 polyhedra in the latter are interconnected via SeO_3 triangular pyramids by sharing respective edges and corners. The Bi^{3+} cations can be considered as interstitial ions in the $[ClSeO_3]^{3-}$ anionic sublattice, so that both compounds can be considered as three-dimensional (3D).

The β-$BiSeO_3Cl$ crystal structure can be described as 2D (Figure 3a,b), which is of interest from the viewpoint of the reported $\alpha \rightarrow \beta \rightarrow \gamma$ sequence of transitions. The crystal structure is built from two blocks, $[Bi_8Cl_{16}]^{8+}$ (Figure 3c) and $[Bi_{12}Cl_{32}]^{4+}$ (Figure 3d), regularly sandwiched between $[Bi_{14}(SeO_3)_{24}]^{6-}$ layers (Figure 3d). In Figure 3a, the BiO_xCl_y polyhedra are shown in green, whereas, for the sake of clarity, the $[Bi_8Cl_{16}]^{8+}$ and $[Bi_{12}Cl_{32}]^{4+}$ layers are represented as an arrangement of Bi (yellow) and Cl (green) atoms (Figure 3b). Similar halide layers with the composition $[Bi_8Cl_{16}]^{8+}$ have been already observed in the structure $Bi_8(SeO_3)_3Br_6$[21] and have also been found in the new compound $PbBi_{10}(SeO_3)_{12}Cl_8$ described below.

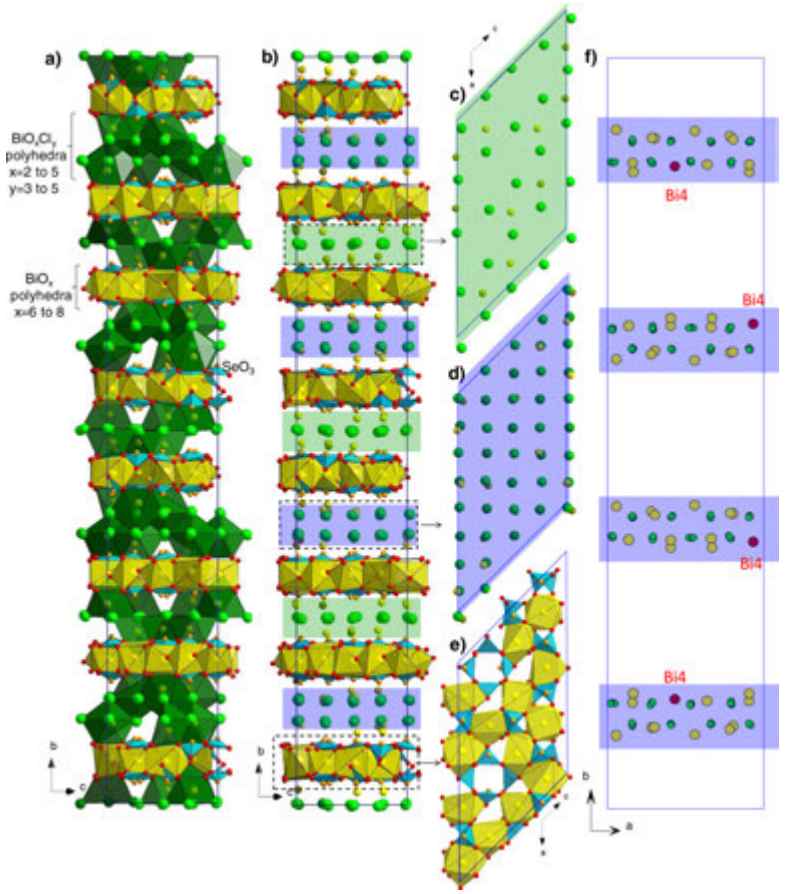

Figure 3. (a) The crystal of β-BiSeO$_3$Cl projected along the *a* axis. BiO$_x$ polyhedra are shown in yellow and BiO$_x$Cl$_y$ in green; (b) the same projection without the interlayer BiO$_x$Cl$_y$ polyhedra. It shows an alternation of three different parallel layers: (c) $[Bi_8Cl_{16}]^{8+}$ (green), (d) $[Bi_{12}Cl_{32}]^{4+}$ (blue), and (e) $[Bi_{14}(SeO_3)_{24}]^{6-}$ presented as an association of distorted Bi−O$_x$ polyhedra and SeO$_3$ by sharing edges and corners. (f) Focus on $[Bi_{12}Cl_{32}]^{4+}$ layers enhances the complex stacking along *b*∼76 Å, through the Bi$_4$ atom position.

The Se^{4+} cations form SeO_3 triangular pyramids with the lone electron pairs pointing externally. The Se−O bond lengths and the O−Se−O bond angles are in the typical range from 1.65 to 1.75 Å and from 92.8° to 106.4, respectively (see Tables S7 and S8, Supporting Information). The $[Bi_{14}(SeO_3)_{24}]^{6-}$ layer is built by the association of Bi^{3+} cations and the SeO_3 triangles. In BiO$_x$ units (shown in yellow in Figure 3d) with *x* in between 8 and 10, all the bi-centered polyhedra are asymmetric, which is typical of the bismuth coordination due to the stereoactive behavior of the $6s^2$ lone pairs on Bi^{3+} cations. The BVS for the 48 independent Bi atoms is in the 2.7−3.6 range (see Table S9, Supporting Information).

The large value of the *b*-parameter (∼76 Å) can be explained by the variety of different modules stacked along the *b*-axis. In other words, the ordering between the $[Bi_{12}Cl_{32}]^{4+}$ and $[Bi_8Cl_{16}]^{8+}$ cationic units sandwiched between the $[Bi_{14}(SeO_3)_{24}]^{6-}$ anionic layers is the key factor for the formation of a giant cell and responsible for the doubling of *b*-parameter (Figure 3f).

Structural complexity of the BiSeO$_3$Cl polymorphs may be quantified using Shannon information theory.[22−24] According to this theory, structural complexity may be quantitatively evaluated from the Shannon information encoded in the atomic arrangement of the unit cell. The structural information amounts, $I_{G,total}$, for the α- and γ-forms are identical and equal to 62.039 bits per unit cell (bits/u.c.),[25] which allows classification of their structures as simple.[24] In contrast, the structure of the β-form is very complex, as its structural information equals 4705.880 bits/u.c. This value is quite high, and, on average, only 0.02% of inorganic structures are classified as very complex as detailed in ref 25. The reason for such an explosive increase in structural complexity can be seen in the transitional character of the β-phase. In order to understand structural reconstructions during the $\alpha \rightarrow \beta \rightarrow \gamma$ transition, one may consider the arrangements (packing) of the heavy Bi atoms in the three structures. As it can be seen from Figure 4a that the arrangement of Bi atoms in the structure of the α-phase is three-dimensional and is of the diamond type with the coordination number of each Bi atom equal to four (only Bi−Bi contacts <5.5 Å are considered; Figure 4d). The average <Bi−Bi> interatomic distance is 4.344 Å. The arrangement of the Bi atoms in the γ-form is 2D (Figure 4c) and corresponds to the simple planar hexagonal net with each Bi atom surrounded by six neighbors (Figure 4e). The average <Bi−Bi> interatomic distance is 4.823 Å. The arrangement of the Bi atoms in

dx.doi.org/10.1021/cg500293w | *Cryst. Growth Des.* 2014, 14, 3026−3034

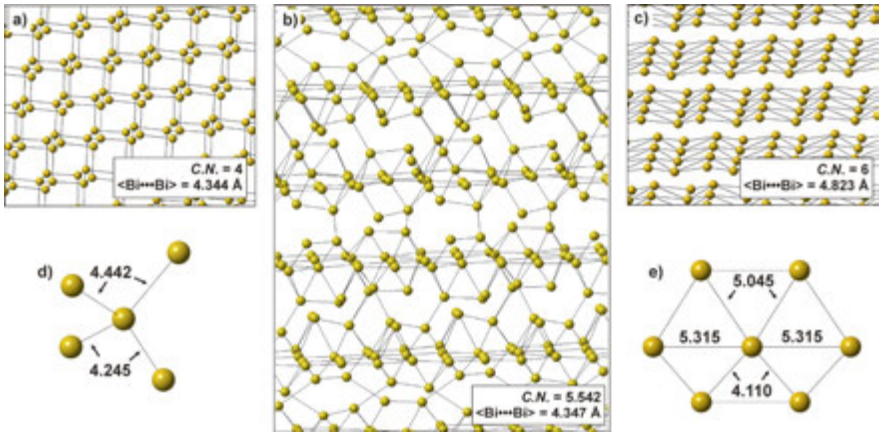

Figure 4. Arrangement of the Bi atoms in the structures of the α-, β-, and γ-polymorphs of $BiSeO_3Cl$ (a, b, and c, respectively) and the local coordination environments of Bi atoms in the structures of the α- and γ-phases (d and e, respectively). Only Bi−Bi contacts shorter than 5.5 Å are taken into account. The boxes in a, b, and c contain average Bi coordination numbers (CN) and the average <Bi−Bi> interatomic distances.

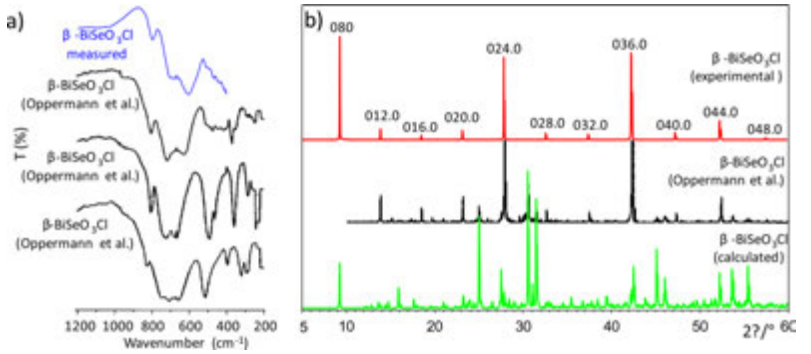

Figure 5. (a) Infrared red spectrum of the prepared β'-$BiSeO_3Cl$ (in blue) compared to the spectrum of β-$BiSeO_3Cl$, α-$BiSeO_3Cl$ and γ-$BiSeO_3Cl$ (in black) (from Oppermann et al.[20]). (b) XRD patterns of experimental β-$BiSeO_3Cl$ (red), β-$BiSeO_3Cl$ from Oppermann's work (black) and of XRDP calculated from data of the crystal structure (green). Our β-$BiSeO_3Cl$ reassembles the β-form mentioned by Oppermann et al.[20] Differences between simulated and experimental XRD powder patterns for β-$BiSeO_3Cl$ imply preferred orientation (along $(0n0)$) as the X-ray diagram was measured using single crystals on a silicium sample holder.

the structure of transitional β-phase is intermediate between three- and two-dimensional with Bi atoms segregated into planes perpendicular to the b axis (Figure 4b). The average coordination number of Bi atoms is 5.542, i.e., intermediate between 4 (as in α-phase) and 6 (as in γ-phase). The <Bi−Bi> distance is 4.347 Å. The $\alpha \rightarrow \beta \rightarrow \gamma$ transition is therefore associated with the regrouping of the Bi atoms from a three-dimensional (diamond-like) to two-dimensional (simple hexagonal) arrangement with the surprising narrow-range stabilization of the intermediate highly complex structure. This complexity-generating mechanism seems to be relatively abundant in inorganic compounds. Perhaps, the most simple example is the temperature-driven phase transition from the high-temperature SiO_2 with the cristobalite structure ($I_{G,total}$ = 5.510 bits/u.c.) to the room-temperature quartz structure (8.265 bits/u.c.) through the transitional tridymite topology with the higher complexity (17.510 bits/u.c.) compared to cristobalite and quartz polymorphs. The unusually high complexity of β-$BiSeO_3Cl$ can thus be assigned to its existence as an intermediate phase between the structurally simple α- and γ-forms.

In order to check whether the phase under study is indeed the β-phase reported previously, the infrared (IR) spectra of β-$BiSeO_3Cl$ were measured between 4000 and 400 cm^{-1} using crushed crystals. On Figure 5a, the IR spectrum is compared to those reported for the α-, β-, and γ-forms in ref 20. At first glance, the IR spectrum matches rather well. However, on this basis only, it remains rather difficult to make a definite conclusion, since the vibrational spectra for all the polymorphs include the Se−O, Bi−O, and Bi−Cl bands that are not expected to be drastically shifted (cf. strong similarities between the IR spectra of the α-, β-, and γ-forms). In Figure 5b, the theoretical X-ray diffraction pattern is compared to the experimental patterns reported for the β-form[20] and for the phase presented above. Taking into account significant preferred orientation effects along the β- [010] directions, a good compatibility is confirmed. Finally, we presume that our refined model indeed corresponds to the mysterious β-form. This assessment involves first order $\alpha \rightarrow \beta$ and $\beta \rightarrow \gamma$ reconstructive transitions through a complex intermediate β-phase with extraordinary complexity and the giant unit cell (V = 19792 $Å^3$).

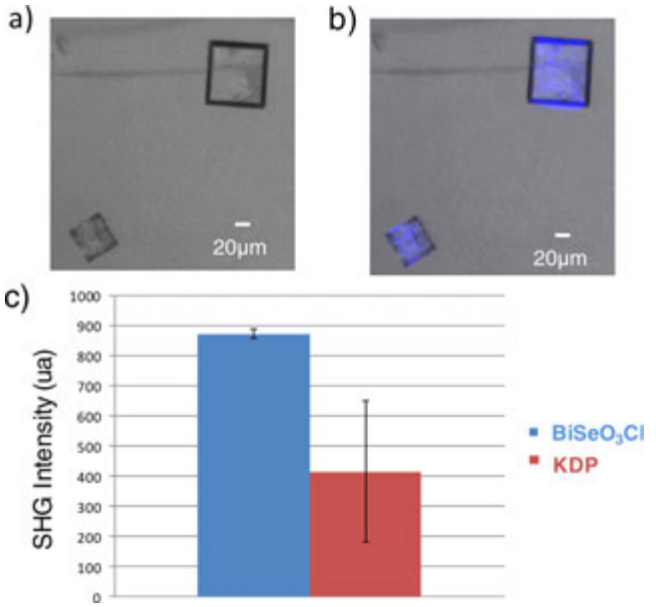

Figure 6. (a) Transmission image of a crystal of $BiSeO_3Cl$, (b) color: emitting surface (λ_{em} = 420−440 nm, λ_{em} = 860 nm), (c) SHG intensity of $BiSeO_3Cl$ single crystals compared to KDP with experimental error bars.

For β-$BiSeO_3Cl$, only the noncentrosymmetric structure model with the space group *Cc* leads to an acceptable convergence of the least-squares refinement. This noncentrosymmetric behavior arises from the fact that no inversion centers have been found in any of the three distinct layered subunits, probably the result of the stereoactive behavior of the LP on Bi^{3+} cations. The second harmonic generation effect was therefore tested for the single crystals of **1** by means of a laser scanning microscope (selected λ = 860 nm). Figure 6 shows the crystal of **1** in the absence and in the presence of emission. The color at the surface of the single crystals shows an intrinsic homogeneous distribution of the emitted doubled frequency light collected with a band-pass filter (420−440 nm). Recent quantitative data collected on single crystal of compound **1** give an efficiency doubled from KDP (KH_2PO_4) (wavelength: 860 nm, frequency 80 MHz) as presented on Figure 6c). It is noteworthy that errors on measurement of KDP efficiency are quite large, although it was registered on three different samples. It is due to the large thickness of the crystals.

Oppermann et al. have concluded that volatile $BiSeO_3Cl$ molecules are formed during the CVT process.[20] We have tried to figure out the configurations of these imaginary molecules by analyzing the structures of the α-, β-, and γ-forms of $BiSeO_3Cl$. With that purpose in mind, for each Bi atom the closest Cl atom and SeO_3 group was selected, leading to the individual $BiSeO_3Cl$ molecules shown in the Figure7a for the α-form and Figure7b for the γ-form. Selection of this kind is more complicated in β-$BiSeO_3Cl$ due to the high number of independent atomic positions: Bi (48), Se (48), and Cl (48), that all display versatile coordination environments. In fact, the full structure can be divided into individual $BiSeO_3Cl$ groups, in agreement with the proposed real existence of such molecules and their reorganization across phase transitions observed upon heating.[20] Only two extreme geometries with the shortest (Figure 7c) and longest (Figure 7d) Bi−Cl bonds are shown in this paper.

The Crystal Structure of $Bi_6(SeO_3)_4Cl_{10}$. Colorless needle-like single crystals of $Bi_6(SeO_3)_4Cl_{10}$ have been isolated after another CVT synthesis involving the initial composition $2BiCl_3$ + 1 Bi_2O_3 + $4SeO_2$ + $1Mn_2O_3$ as detailed above. The pertinent data of the diffraction-data collection and structural solution and refinement are summarized in Table 1. Ten Bi atoms were localized using the charge-flipping method, whereas the remaining atoms (4 Se, 10 Cl, and 12 O) were deduced from the inspection of the difference Fourier maps. The structure refinement rapidly converged to a reasonable reliability factor.

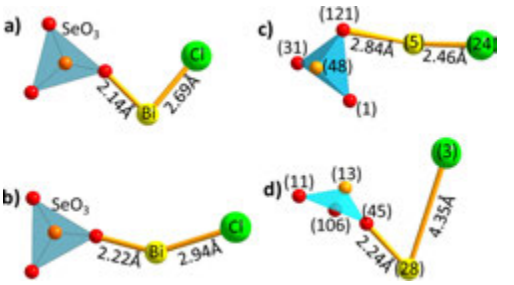

Figure 7. $BiSeO_3Cl$ "molecules" in the structures of (a) α-$BiSeO_3Cl$ and (b) γ-$BiSeO_3Cl$. $BiSeO_3Cl$ "molecules" with (c) shortest and (d) longest Bi−Cl bonds which are the two extreme representatives of 48 Bi atoms in β-$BiSeO_3Cl$.

The crystal structure is shown in Figure 8a,b. It can be considered as formed from six distorted bicentered oxochloride polyhedra: $Bi(1)O_5Cl_4$, $Bi(2)O_3Cl_5$, $Bi(3)O_3Cl_4$, $Bi(4)O_5Cl_4$, $Bi(5)O_4Cl_4$, and $Bi(6)O_4Cl_4$, linked to four Se atoms with the Bi−O, Bi−Cl, and Se−O distances in the same range as those observed for the compound **1**, leading to a 3D network. The BVS values for the Bi atoms are in the range of 2.9−3.1. The stereoactive behavior of the lone electron pairs on the Bi^{3+} and Se^{4+} cations is manifested by the particularly asymmetric coordination environments around these cations. Bi coordination polyhedra share edges and corners to build $Bi_6(SeO_3)_4Cl_{10}$ blocks linked together in such a way as to create an

dx.doi.org/10.1021/cg500293w | *Cryst. Growth Des.* 2014, 14, 3026−3034

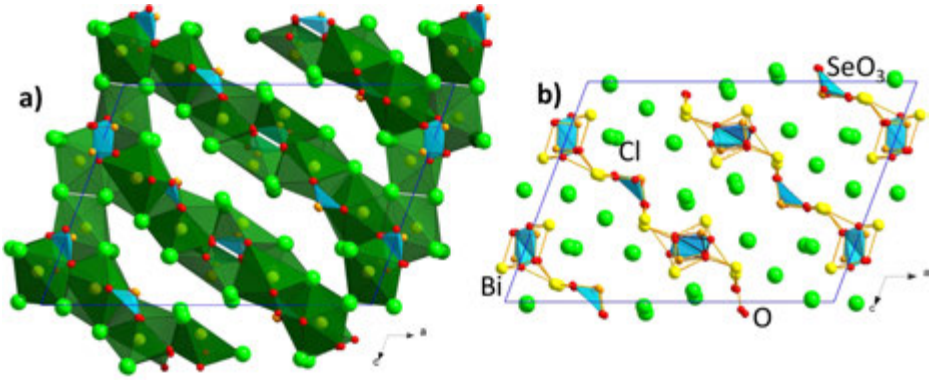

Figure 8. (a) The crystal structure of $Bi_6(SeO_3)_4Cl_{10}$ projected along the *b* axis, showing BiO_xCl_y polyhedra (dark green) and SeO_3 groups (blue) sharing edges and corners. (b) The same projection with omission of the BiO_xCl_y polyhedra for clarity.

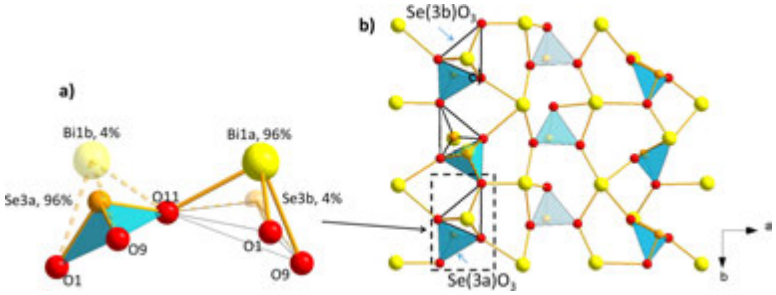

Figure 9. (a) Oxygen coordination of the Bi1a and Se3a atoms, (b) part of the structure of $Bi_6(SeO_3)_4Cl_{10}$ projected along the *c* axis.

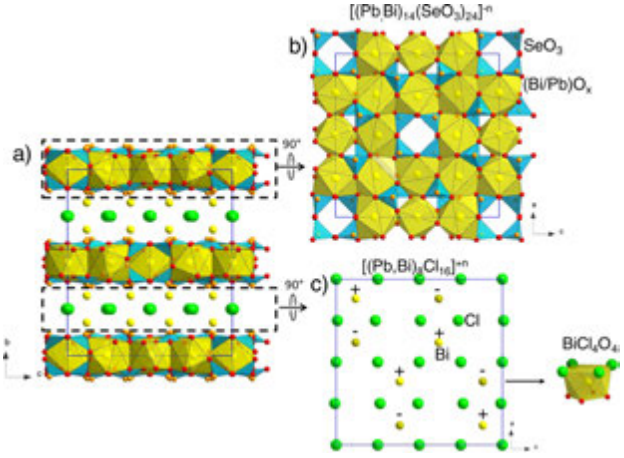

Figure 10. (a) The crystal structure of $PbBi_{10}(SeO_3)_{12}Cl_8$ projected along the *a* axis with two parallel cationic and anionic layers: (b) $[(Pb,Bi)_{14}(SeO_3)_{24}]^{n-}$ built on association of distorted BiO_x polyhedra (yellow) and SeO_3 groups (blue) (c) $[(Pb,Bi_8)Cl_{16}]^{n+}$ layers parallel to the *ac* plane. The labels ± stand for Bi *y* coordinate above or below the chloride planes.

open structure with some kind of empty cavities bordered by the anions (essentially Cl^-) and parallel to the *b* axis. These cavities are delimited by 12 edges (1- edges: Cl−Cl and Cl−O and faces: Cl−Cl−Cl) as shown on Figure 8a. The cavities are around 9.7 Å long and 3.8 Å wide. The presence of such tunnels with *n*-membered rings (MRs; here $n = 12$) was already observed in other selenites and especially in

dx.doi.org/10.1021/cg500293w | *Cryst. Growth Des.* 2014, 14, 3026−3034

the structure of $Bi_2(V^VO_2)_2(SeO_3)_4$ (8-MR).[26] Focusing on the chloride arrangement, it reveals a 2D character of the structure with Cl^- crenel-layered (Figure 8b).

The close inspection of a Fourier difference electron-density map showed a high residual peak (8.71 $e/Å^3$) 0.86 Å away from the Se3 site indicating its possible splitting into two satellite positions. The coupled refinement of the occupancies of the Se3/Se3′ sites resulted in the 0.95/0.05 ratio. While the Se−O distances for Se3 are plausible (1.71−1.74 Å), those for the Se3′ site are too long (2.09−2.41 Å), which suggested its occupation by Bi. The final Bi1a/Bi1b and Se3a/Se3b occupancies were refined to the ratio of 0.96/0.04 (Figure 9a). The weak statistical Bi/Se disorder occurs within the chains formed by edge-sharing -$OSeO_2$BiO- dimers running along the *b*-axis (Figure 9b).

The atomic positions, isotropic and anisotropic displacement parameters, and principal distances are given in Tables S9−S11 of Supporting Information. The crystal-structure data for $Bi_6(SeO_3)_4Cl_{10}$ phase were deposited with the depository number CSD-426286.

The Crystal Structure of $PbBi_{10}(SeO_3)_{12}Cl_8$. Colorless platelet crystals of **3** were mounted on a glass fiber for the X-ray diffraction analysis. The unit-cell parameters and systematic absences were consistent with the orthorhombic space group *Ccca*. Seven independent Bi sites were found from charge flipping, while other sites have been deduced from the inspection of difference electron-density maps. At this stage, the formula was established as $Bi_{11}(SeO_3)_{12}Cl_8$, which is not electroneutral. Taking into account the presence of Pb during in the synthesis, an elemental analysis was performed. The EPMA microprobe analysis provided the ratio Pb/Bi of 0.8:15, which is reasonably close to the expected 1:10 ratio for an electroneutral structure. The mixed Bi/Pb occupancy of 1/9 has been considered for the Bi2, Bi3, Bi4, and Bi5, since their bond-valence sum values are 2.77, 2.59, 2.52, 2.47 v.u., respectively. The resulting electroneutral formula is $PbBi_{10}(SeO_3)_{12}Cl_8$, and the structure is shown on Figure 10a. If all Bi/Pb−O and Bi−Cl bond lengths smaller than 3.10 Å are taken into account, the following irregular coordination polyhedra can be observed: $Bi(1)O_8$, $Bi(2)O_{10}$, $Bi(3)O_{10}$, $Bi(4)O_{10}$, and $Bi(5)O_4Cl_4$. The Bi−O bond lengths vary from 2.37 to 2.75 Å, whereas the Bi−Cl bond lengths are in the range from 2.96 to 3.10 Å.

In the SeO_3 groups, Se^{4+}−O bond lengths and O−Se^{4+}−O bond angles are between 1.65 and 1.75 Å, and 92.8 and 106.4°, respectively, as expected. The structure can be described as a 2D network, with the $[(Pb,Bi)_{14}(SeO_3)_{24}]^{n-}$ layer (Figure 10b) sandwiched between the $[(Pb,Bi)_8Cl_{16}]^{n+}$ (Figure 10c) layers parallel to the *ac* plane. This structure is polystructural with $CaNd_{10}(SeO_3)_{12}Cl_{18}$ crystal structure published by Berdonosov et al. in 2007.[27]

Technical details of the data acquisition and refinement parameters are gathered in Table 1. The crystal-structure data for $PbBi_{10}(SeO_3)_{12}Cl_8$ are deposited with the depository number CSD-426285. The atomic coordinates, displacement parameters, and selected bond-lengths are gathered in Tables S12−S14 of Supporting Information.

CONCLUSIONS

The discovery of new bismuth selenite halides (Cl, Br, or I) remains occasional, while our study sheds light on three new architectures with structural similarities arising from the asymmetric coordinations of the Bi^{3+}, Se^{4+}, and/or Pb^{2+} lone pair cations. As expected from the likely interleave role of halogen anions, two of the three obtained structures are layered. These compounds were obtained as small single crystals only. Up to now, our attempts to scale the preparation into larger amounts of material were unsuccessful. This is a common limitation regarding the works previously reported for several selenites, which remains problematic for further characterization of such complex structural architectures. This blank gap could be filled by using soft chemistry processes, such solvothermal routes currently tested by our research group in the selenite chemical systems. In summary, even if CVT is shown here as a powerful tool to access complex (i.e., giant) crystal structures, alternative synthesis routes must be developed. At least in the case of $BiSeO_3Cl$, the role of preformed molecules could be the key parameter for the stabilization of particular polymorphs forms using high temperature methods. Finally, it is worth concluding that, in this work, we have prepared and characterized the mysterious β-$BiSeO_3Cl$ phase shown reported previously as stable only in a narrow thermal range (ΔT = 7 °C). The structure of this phase can be described as very complex, and the complexity-generating mechanism can be assigned to its role as a transitional phase between structurally simple α- and γ-polymorphs.

ASSOCIATED CONTENT

Supporting Information

Tables of fractional atomic coordinates and isotropic or equivalent isotropic displacement parameters, atomic displacement parameters, selected bond distances and angles and interatomic distances, and bond sum valence values. This material is available free of charge via the Internet at http://pubs.acs.org.

AUTHOR INFORMATION

Corresponding Author

*Email: marie.colmont@ensc-lille.fr. Fax: (+) 33 3 20 43 64 34.

Notes

The authors declare no competing financial interest.

ACKNOWLEDGMENTS

The Fonds Européen de Développement Régional (FEDER), CNRS, Région Nord Pas-de-Calais, and Ministère de l'Education Nationale de l'Enseignement Supérieur et de la Recherche are acknowledged for funding the X-ray diffractometers. Laurence Burylo and Nora Djellal are thanked for their precious technical help. This work was carried out under the framework of the Multi-InMaDe project supported by the ANR (Grant ANR 2011-JS-08 003 01). S.V.K. acknowledges financial support from St. Petersburg State University (Internal Grant 3.38.136.2014).

REFERENCES

(1) Ok, K. M.; Chi, E. O.; Halasyamani, P. S. *Chem. Soc. Rev.* **2006**, *35*, 710−717.

(2) Halasyamani, P. S. In *Functional Oxides*; Bruce, D. W.; O'Hare, D.; Walton, R. I., Eds.; John Wiley & Sons, Ltd: New York, 2010; pp 1−39.

(3) Endara, D.; Colmont, M.; Huvé, M.; Capet, F.; Lejay, J.; Aschehoug, P.; Mentré, O. *Inorg. Chem.* **2012**, *51*, 9557−9562.

(4) Colmont, M.; Endara, D.; Aliev, A.; Terryn, C.; Huvé, M.; Mentré, O. *J. Solid State Chem.*.

(5) Lu, H.; Gautier, R.; Donakowski, M. D.; Tran, T. T.; Edwards, B. W.; Nino, J. C.; Halasyamani, P. S.; Liu, Z.; Poeppelmeier, K. R. *J. Am. Chem. Soc.* **2013**, *135*, 11942−11950.

(6) Nguyen, S. D.; Yeon, J.; Kim, S.-H.; Halasyamani, P. S. *J. Am. Chem. Soc.* **2011**, *133*, 12422−12425.

(7) Krivovichev, S. V.; Filatov, S. K.; Vergasova, L. P. *Mineral. Petrol.* **2013**, *107*, 235−242.

(8) Zhang, S.-Y.; Hu, C.-L.; Li, P.-X.; Jiang, H.-L.; Mao, J.-G. *Dalton Trans. Camb. Engl. 2003* **2012**, *41*, 9532−9542.

(9) Aliev, A.; Olchowka, J.; Colmont, M.; Capoen, E.; Wickleder, C.; Mentré, O. *Inorg. Chem.* **2013**.

(10) Lü, M.; Aliev, A.; Olchowka, J.; Colmont, M.; Huvé, M.; Wickleder, C.; Mentré, O. *Inorg. Chem.* **2014**, *53*, 528−536.

A-IV
pH-Controlled pathway and systematic hydrothermal phase diagram for elaboration of synthetic lead nickel selenites

Vadim M. Kovrugin, Marie Colmont, Christine Terryn, Silviu Colis, Oleg I. Siidra, Sergey V. Krivovichev, and Olivier Mentré

Published in: *Inorganic Chemistry*, 2015, Vol. 54 (5), p. 2425–2434.
DOI: 10.1021/ic503055v

Inorganic Chemistry

Article

pubs.acs.org/IC

pH Controlled Pathway and Systematic Hydrothermal Phase Diagram for Elaboration of Synthetic Lead Nickel Selenites

Vadim M. Kovrugin,[†,‡] Marie Colmont,[†] Christine Terryn,[§] Silviu Colis,[∥] Oleg I. Siidra,[‡] Sergey V. Krivovichev,[‡] and Olivier Mentré*[,†]

[†]Université Lille Nord de France, UMR 8181 CNRS, Unité de Catalyse et de Chimie du Solide (UCCS USTL), 59655 Villeneuve d'ASCQ, France

[‡]Department of Crystallography, Saint-Petersburg State University, Universitetskaya nab. 7/9, 199034 St. Petersburg, Russia

[§]Plateforme Imagerie Cellulaire et Tissulaire, 51 rue Cognacq-Jay, 51100 Reims, France

[∥]Institut de Physique et Chimie des Matériaux de Strasbourg (IPCMS), UMR 7504 CNRS and Université de Strasbourg (UDS-ECPM), F-67034 Cedex 2 Strasbourg, France

Supporting Information

ABSTRACT: The PbO−NiO−SeO_2 ternary system was fully studied using constant hydrothermal conditions at 473 K. It yields the establishment of the corresponding phase diagram using a systematic assignment of reaction products by both powder and single-crystal X-ray diffraction. It leads to the preparation of three novel lead nickel selenites, α-$PbNi(SeO_3)_2$ (**I**), β-$PbNi(SeO_3)_2$ (**II**), and $PbNi_2(SeO_2OH)_2(SeO_3)_2$ (**III**), and one novel lead cobalt selenite, α-$PbCo(SeO_3)_2$ (**IV**), which have been structurally characterized. The crystal structures of the α-forms **I**, **IV**, and **III** are based on a 3D complex nickel selenite frameworks, whereas the β-$PbNi(SeO_3)_2$ modification (**II**) consists of nickel selenite sheets stacked in a noncentrosymmetric structure, second-harmonic generation active. The pH value of the starting solution was shown to play an essential role in the reactive processes. Magnetic measurements of **I**, **III**, and **IV** are discussed.

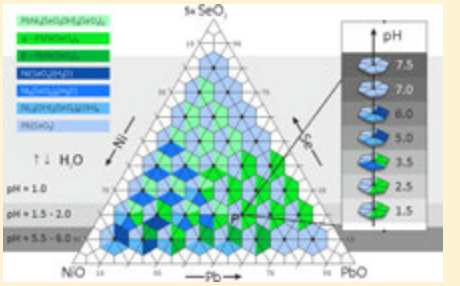

INTRODUCTION

The demand for specific noncentrosymmetric (NCS) crystal structures is very strong because interesting physical properties, such as second-harmonic generation (SHG),[1] piezoelectricity,[2] ferroelectricity,[3] and pyroelectricity,[4] can be expected. In particular, nonlinear optic materials have become tremendously important and are drawing more and more attention owing to their promising applications in laser science and technology. The NCS compounds are commonly observed when dealing with (Ti^{4+}, V^{5+}, Mo^{6+}) octahedrally coordinated d^0 transition metals susceptible to second-order Jahn−Teller (SOJT) effects. Typical SOJT asymmetric coordination environments are also favored for cations with a stereoactive lone pair of electrons (As^{3+}, Se^{4+}, Sb^{3+}, Pb^{2+}, and Bi^{3+}, etc.) in more drastic manner leading to a diversity of unusual polyhedral coordination. The crystal chemistry of metal selenites is very rich as first reviewed by Verma.[5] The incorporation of heavy lone pair cations such as Pb^{2+}/Bi^{3+} with selenite groups increases the chance to achieve asymmetric building units or NCS crystal structures as demonstrated in several earlier works dedicated to the exploration of PbO/Bi_2O_3−MO_x−SeO_2 (M = Cu^{2+}, V^{3+}, Ge^{4+}, Nb^{5+}, V^{5+}, Mo^{6+}, W^{6+}; x = 1, 2; y = 1, 2, 3, 5) ternary systems.[6−11] From the experimental viewpoint, due to the low and close melting and sublimation temperatures (340 and 350 °C, respectively), the crystal growth of selenites is generally achieved using either chemical transport routes,[12,13] recently leading to original bismuth selenites, including giant cell compounds,[14] or hydrothermal methods due to the good solubility and reactivity of $(SeO_3)^{2-}$ anions. However, as recently demonstrated by the evidence of a number of phases in competition in the $CoSeO_3$−SeO_2−H_2O phase diagram[15] and other hybrid inorganic−organic systems,[16,17] a systematic approach may be preferred for exhaustive search of novel crystal structures. Thus, research was not yet carried out on ternary systems with lead and nickel/cobalt as transition metals constituents. Herein, we present a scrupulous investigation of the PbO−NiO−SeO_2 system in hydrothermal conditions. It leads to the synthesis of four novel lead selenites, α-$PbNi(SeO_3)_2$ (**I**), β-$PbNi(SeO_3)_2$ (**II**), $PbNi_2(SeO_2OH)_2(SeO_3)_2$ (**III**), and α-$PbCo(SeO_3)_2$ (**IV**), that have been structurally characterized by single-crystal X-ray diffraction (XRD). Their magnetic properties will be also discussed in this Article.

Received: December 22, 2014
Published: February 17, 2015

DOI: 10.1021/ic503055v
Inorg. Chem. 2015, 54, 2425−2434

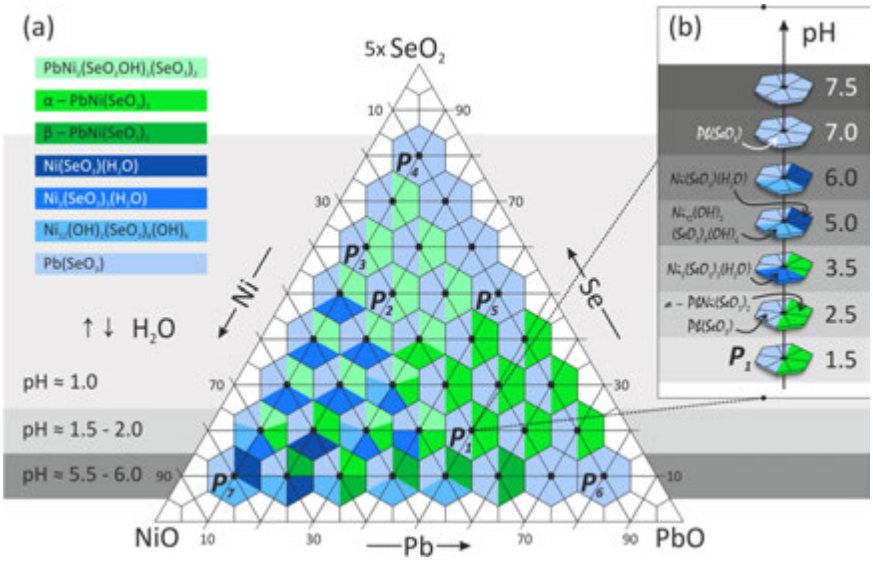

Figure 1. Experimental crystallization diagram of the PbO–NiO–SeO_2–H_2O system at 423 K with the pH zones shown in the background by gray colors (a), and the series of experiments with a PbO:NiO:SeO_2 molar ratio of 5:3:10 corresponding to the P_1 point with various pH values (b). The black points indicate the experimental combinations of the molar ratios of precursors. The compositions of various phases synthesized in each experimental point are shown by hexagons of different colors..

Table 1. Crystallographic Data for the compounds α- $PbNi(SeO_3)_2$ (I), β-$PbNi(SeO_3)_2$ (II), $PbNi_2(SeO_2OH)_2(SeO_3)_2$ (III), and α-$PbCo(SeO_3)_2$ (IV)

	I	II	III	IV
M_r (g mol^{-1})	519.82	519.82	834.47	520.04
cryst syst	orthorhombic	orthorhombic	monoclinic	orthorhombic
space group	*Pnma*	$Cmc2_1$	$P2/c$	*Pnma*
a (Å)	12.7476(4)	5.4715(4)	13.6824(10)	12.8208(4)
b (Å)	5.4562(2)	9.1963(6)	5.2692(5)	5.4902(2)
c (Å)	7.8332(2)	11.4436(9)	19.3476(13)	7.9085(2)
α (deg)	90	90	90	90
β (deg)	90	90	129.524(4)	90
γ (deg)	90	90	90	90
V (Å^3)	544.83(3)	575.81(7)	1075.94 (16)	556.67(3)
Z	4	4	4	4
ρ (g/cm^3)	6.337	5.996	5.151	6.205
μ (mm^{-1})	47.637	45.074	32.668	46.221
λ(Mo Kα) (Å)	0.71073	0.71073	0.71073	0.71073
$\theta_{min-max}$ (deg)	3.1–29.6	3.6–28.0	1.9–28.0	3.0–28.0
reflns collected	10212	2345	5454	3226
indep reflns (R_{int})	823 (0.0336)	686 (0.0260)	2083 (0.0459)	742 (0.0260)
R_1 ($I > 2\sigma(I)$)	0.0139	0.0141	0.0496	0.0186
wR_2 ($I > 2\sigma(I)$)	0.0360	0.0346	0.0992	0.0429
R_1 (all data)	0.0165	0.0142	0.0783	0.0203
wR_2 (all data)	0.0387	0.0346	0.1104	0.0439
GOF	1.090	1.109	1.187	1.142
$\Delta\rho_{max}/\Delta\rho_{min}$ (e Å^{-3})	1.573/−1.110	1.310/−1.073	2.916/−2.912	0.971/−1.887

EXPERIMENTAL SECTION

Syntheses. Commercial PbO (99,999%, Aldrich), SeO_2 (99%, Alfa Aesar), NiO (99%, Sigma-Aldrich), and CoO (95%, Alfa Aesar) were used as received. After weighing and grinding, the reagents were mixed in 6 mL of distilled water. When necessary, sodium hydroxide solution was used to adjust the pH to its desired value. Our exploration of the crystal growth in the PbO–NiO–SeO_2–H_2O system consisted of examination of 36 possible combinations of molar ratios of the solid precursors within the Gibbs's triangle (Figure 1a). In all syntheses the mPbO + nNiO + (k/5)SeO_2 (m, n, k = 1, 2, ..., 8) molar sum was fixed as constant equal to 10 mmol, and the mixture was completed with 6 mL of

DOI: 10.1021/ic503055v
Inorg. Chem. 2015, 54, 2425–2434

distilled water. It has been experimentally established that only acidic conditions favor the crystallization of structural varieties. In our study, the reactive medium self-acidifies by solubilization of SeO_2 into selenous acid according to the following reactions:

$$SeO_2 + H_2O \rightarrow H_2SeO_3 \quad (1)$$

$$H_2SeO_3 \leftrightarrow H^+ + (HSeO_3)^- \quad (pK_a = 2.62) \quad (2)$$

$$(HSeO_3)^- \leftrightarrow H^+ + (SeO_3)^{2-} \quad (pK_a = 8.32) \quad (3)$$

Then a large stoichiometric excess of SeO_2 was necessary to achieve reactions as shown in Figure 1a, where the amount of selenium dioxide is multiplied by five. The pH values increase from ∼1 to ∼5.5−6.0 on decreasing the SeO_2 content in our experimental range. The solid products were systematically analyzed by powder XRD (PXRD) analysis (after grinding), while representative crystals of each of the present phases were also selected by morphology and colors and tested by single-crystal XRD analysis. It leads to the phase distribution given in Figure 1a, where the crystallization domains of phases are illustrated by different colors.

The chemical reactions were performed during 36 h in 23 mL Teflon-lined Parr reaction vessels heated in an oven at 473 K. At the end of the experiment time, the vessels were cooled during 48 h. The precipitate was filtered through filter paper. Single crystals of three novel lead selenites with nickel, α-$PbNi(SeO_3)_2$ (**I**), β-$PbNi(SeO_3)_2$ (**II**), and $PbNi_2(SeO_2OH)_2(SeO_3)_2$ (**III**), have been prepared by the hydrothermal techniques. They have been observed in the mixtures already reported: $Ni(SeO_3)(H_2O)$,[18] $Ni_3(SeO_2)_3(H_2O)$,[19,20] $Ni_{12}(OH)_6(SeO_3)_8(OH)_2$,[21] and $Pb(SeO_3)$.[22−25] Single crystals of the cobalt selenite, α-$PbCo(SeO_3)_2$ (**IV**) were obtained by the reaction analogous to that used to obtain compound **I**. Attempts to synthesize the Co analogue of compounds **II** and **III** using similar techniques proved unsuccessful. In general, out of **IV** our hydrothermal conditions using cobalt precursors rarely lead to crystal growth, which is one motivation of our study. The novel lead selenite crystals occur as yellow needles (**I**), yellow prisms (**II**), green plates (**III**), and purple needles (**IV**) up to 300 μm in maximal dimension.

X-ray Diffraction. Powder X-ray diffraction analyses of all of the powder samples were performed at room temperature in a 2θ range of 10−60° with a scan step width of 0.02° using a D8 Advance Bruker AXS diffractometer (Cu Kα radiation, λ = 1.5418 Å). Single crystals selected for data collection were examined under an optical microscope and mounted on a glass fiber. Data were collected by means of a Bruker DUO four-circle diffractometer equipped with an APEX II CCD detector and monochromated Mo Kα radiation. Unit-cell parameters were refined by the least-squares techniques using the full recorded data set. The data were integrated and corrected for absorption using a multiscan type model implemented in the Bruker programs APEX[26] and SADABS.[27] The structures were solved by direct methods and refined by means of the program SHELXL-2013.[28] Crystallographic data are summarized in Table 1. The visible difference in the quality of the crystallographic data of compound **III** is a result of the relatively poor quality and small size of the collected crystal. Fractional atomic coordinates, atomic displacement parameters, and selected bond distances are listed in Tables S1−S12 of the Supporting Information. The crystal structure data for α-$PbCo(SeO_3)_2$, α-$PbNi(SeO_3)_2$, β-$PbNi(SeO_3)_2$, and $PbNi_2(SeO_2OH)_2(SeO_3)_2$ were deposited with the depository numbers CSD-428904, CSD-428905, CSD-428906, and CSD-428907, respectively.

SQUID. The magnetic properties of the samples were analyzed using a MPMS SQUID-VSM (Quantum Design) magnetometer in a temperature and field range of 1.8−300 K and 0−7 T, respectively. The temperature dependence variation of the magnetization was carried out under a magnetic field of 0.1 T after cooling the sample in a field of 0.1 T (FC, field cooling) or in zero field (ZFC, zero-field cooling). Using these variations, χ and χ^{-1} vs T could be obtained that could inform on the magnetic interactions. All measurements were carried out on nonaligned samples (random crystallites orientation).

Multiphoton SHG Microscopy. For compound **II**, a laser scanning microscope LSM 710 NLO Zeiss (Jena, Germany) was used as implemented at the Plateforme d'Imagerie Cellulaire et Tissulaire, Reims, France. Excitation was provided by a CHAMELEON femtosecond titanium−sapphire laser (Coherent, Santa Clara, CA, USA) set at 860 nm, tuning the power until SHG was detected. Samples were imaged with a 20× , 0.8 NA objective lens. The emitted signal of SHG was collected with a bandpass filter (420−440 nm). The analyzed zone is performed by pixels of 0.55 × 0.55 μm^2.

Partial Charge and Dipole Moment Calculations. We have chosen to follow Henrýs model for determination of partial charges using scales of atomic nonempirical electronegativity and hardness (to measure the resistance the atom can oppose to the flow of electronic density) implemented in the program PACHA. This software uses a nonempirical method to determine partial charges using crystal structure data and two parameters per chemical element: configuration energy and the radius of the most diffuse valence orbital to avoid any unphysical aspects.[29]

RESULTS AND DISCUSSION

Phases in Competition. The analysis of the different solid phases in competition allows a rough rationalization on the basis of the starting stoichiometry and pH value. First, we note that the $Pb(SeO_3)$ compound is the most frequent phase in the system, and it has been observed as a solid product with variable degree of

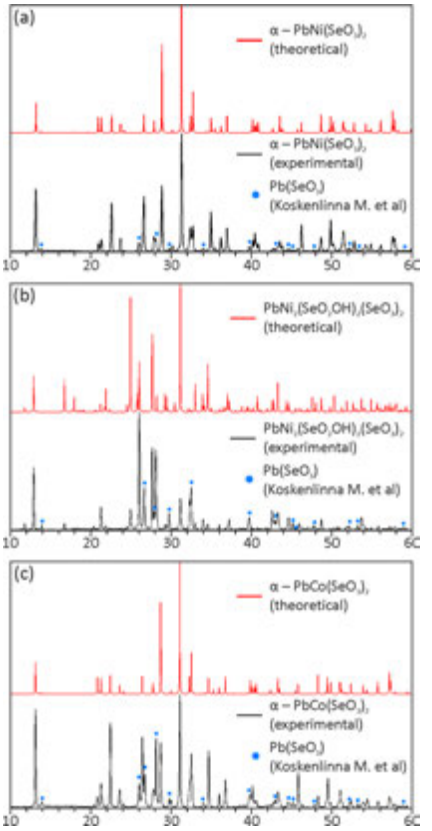

Figure 2. Theoretical (red) and experimental (black) PXRD patterns for the crystal structures of α-$PbNi(SeO_3)_2$ (a), $PbNi_2(SeO_2OH)_2(SeO_3)_2$ (b), and α-$PbCo(SeO_3)_2$ (c).

DOI: 10.1021/ic503055v
Inorg. Chem. 2015, 54, 2425−2434

Table 2. Solid Products of the Experiments with a PbO/NiO/SeO_2 Molar Ratio of 5:3:10 (Point P_1 in Figure 1a)

no.	pH before reaction	pH after reaction	solid products
P_1	1.0	1.5	$Pb(SeO_3)$; α-$PbNi(SeO_3)_2$ (**I**)
1	1.5	2.5	$Pb(SeO_3)$; α-$PbNi(SeO_3)_2$ (**I**)
2	2.0	3.5	$Pb(SeO_3)$; α-$PbNi(SeO_3)_2$ (**I**); $Ni_3(SeO_3)_3(H_2O)$
3	3.0	5.0	$Pb(SeO_3)$; $Ni(SeO_3)(H_2O)$; $Ni_{12}(OH)_6(SeO_3)_8(OH)_2$
4	4.0	6.0	$Pb(SeO_3)$; $Ni(SeO_3)(H_2O)$; $Ni_{12}(OH)_6(SeO_3)_8(OH)_2$
5	5.0	7.0	$Pb(SeO_3)$
6	6.0	7.5	$Pb(SeO_3)$

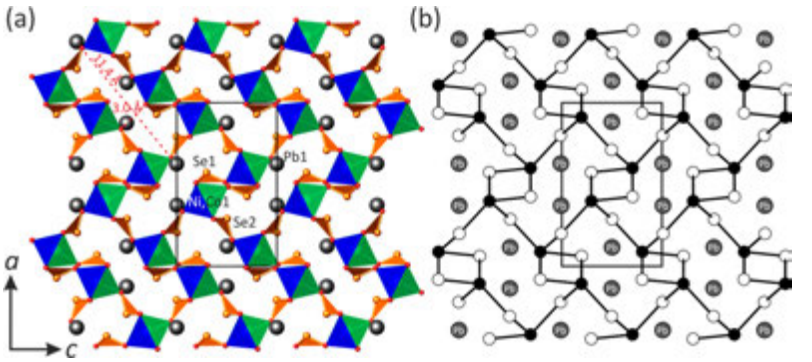

Figure 3. General projection of the crystal structures of α-$PbM(SeO_3)_2$ (M = Ni^{2+} (**I**), Co^{2+} (**IV**)) along the *b* axis (a) and the corresponding black-and-white graph (b). Legend, panel a: MO_6 octahedra, blue-green; SeO_3 trigonal pyramids, orange; Pb^{2+}, gray balls. Legend panel b: M^{2+}, black circles; Se^{4+}, white circles.

crystallinity in each hydrothermal experiment, sometimes found as a predominant white powder. This proves a preferred complexation of Pb^{2+} by $(SeO_3)^{2-}$ and enhanced precipitation independently of the pH. Second, about the cationic stoichiometry, rich lead compounds appear in the right zone of the diagram while lead-free nickel selenites ($Ni(SeO_3)(H_2O)$[18] and $Ni_3(SeO_2)_3(H_2O)$[19,20]) have been obtained at the left side with low Pb concentrations. This result, even though expected, demonstrates formation mechanisms controlled by the solution concentrations of each species. Finally, occulting the systematic presence of $Pb(SeO_3)$,[22−25] low pH values favor reactivity of $(HSeO_3)^-$ groups (e.g., in $PbNi_2(SeO_2OH)_2(SeO_3)_2$), while selenite groups predominate at higher pH values (e.g., $PbNi(SeO_3)$ polymorphs) in good agreement with the acidic reactions and pK_as given earlier (eqs 2 and 3).

Experimental (black) and theoretical (red) PXRD patterns for new phases described later, α-$PbNi(SeO_3)_2$ (**I**), $PbNi_2(SeO_2OH)_2(SeO_3)_2$ (**III**), and α-$PbCo(SeO_3)_2$ (**IV**), are represented in Figure 2, leading to a mixture with diamagnetic $Pb(SeO_3)$. It enables the measurement of their magnetic properties. Intensities of the reflections in the PXRD patterns are affected by relatively strong preferred orientation, due to anisotropic crystallite shape related to the crystal structures. . Theoretical patterns were generated with PowderCell 2.4 from the single-crystal data without taking into account the preferred orientation. The PXRD patterns of **I** and **III** correspond to the samples performed for the P_1 point (PbO:NiO:SeO_2 = 5:3:10) and P_2 point (PbO:NiO:SeO_2 = 2:3:25) of Figure 1a, respectively. The solid products of **IV** for the powder X-ray diffraction analysis have been obtained with stoichiometry to analogous **I** by replacing NiO by CoO. For other stoichiometries, PXRD patterns corresponding to the P_3, P_4, P_5, P_6, and P_7 points in Figure 1a are provided as examples in the Supporting Information (Figures S1−S5).

Influence of the pH. To gain more information about the reaction processes in the PbO−NiO−SeO_2−H_2O phase diagram, an in-depth investigation was carried out for the particular P_1 (PbO:NiO:SeO_2 molar ratio of 5:3:10) stoichiometric mixture at various pH values up to 7.5 (in order to prevent the reduction of SeO_2 to γ-Se metal[30,31]). The reagents were mixed with 1.75 M aqueous NaOH solution until the required pH values. Then, the hydrothermal treatment was applied. The resulted products of these series as a function of the pH values are listed in Table 2 and shown in Figure 1b. Experimental PXRD patterns are provided in the Supporting Information (Figures S6−S11).

The results obtained in the course of the hydrothermal experiments demonstrated an essential role of the pH values, especially dealing with the influence of the degree of condensation of the ionic species. Once more at all pH the $Pb(SeO_3)$ is revealed as very stable. For the other products, we observe that water molecules and, subsequently, hydroxide anions are progressively incorporated into the compound structures on increasing the pH. In particular, at low pH of 1.5−2.5 only condensed compounds, α-$PbNi(SeO_3)_2$ (**I**) and $Pb(SeO_3)$,[22−25] are formed. The reaction occurring with pH value of 3.5 leads to reported compound $Ni_3(SeO_3)_3(H_2O)$[20] with one-third of Ni^{2+} coordinated by water molecules. Increasing the pH to 5.0−6.0 markedly increases the incorporation of water molecules and/or hydroxyl groups leading to $Ni_{12}(OH)_2(SeO_3)_8(OH)_6$[21] and $Ni(SeO_3)(H_2O)$.[18] The crystal structure of the latter is only composed of

DOI: 10.1021/ic503055v
Inorg. Chem. 2015, 54, 2425−2434

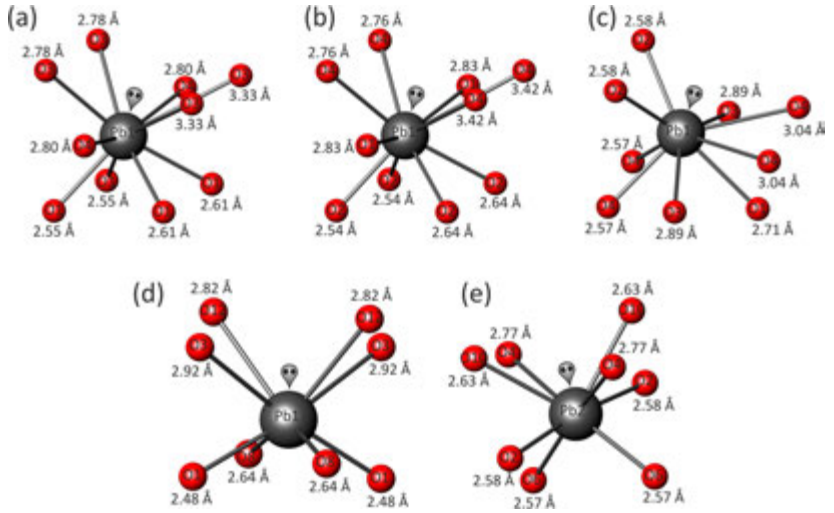

Figure 4. Coordination environment of Pb^{2+} cations in the crystal structures of **I** (a), **IV** (b), **II** (c), and **III** (d and e).

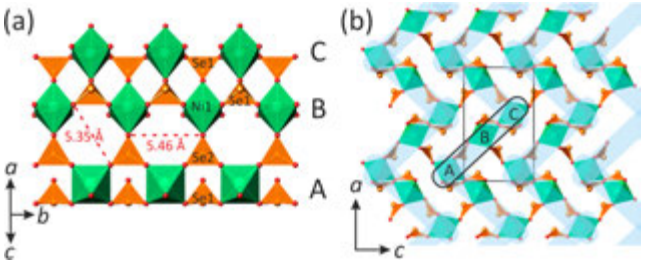

Figure 5. Polyhedral representation of the channel walls in α-$PbNi(SeO_3)_2$ (a) and its projection along the *b* axis as a combination of the pseudoribbons cross-linked into a 3D framework (Pb^{2+} cations are omitted for clarity) (b). Legend: NiO_6 octahedra, green; SeO_3 trigonal pyramids, orange.

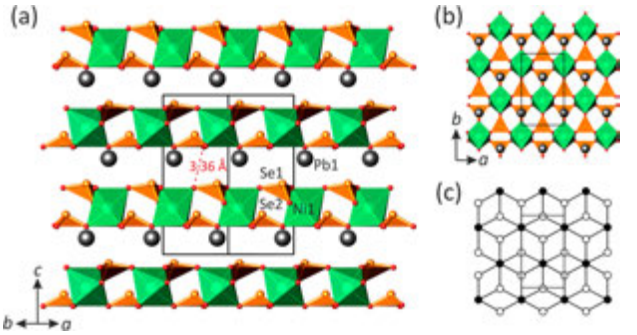

Figure 6. Crystal structure of β-$PbNi(SeO_3)_2$ in two different projections (a and b), and the black-and-white graph corresponding to the Ni−Se sheet in the structure (Pb^{2+} cations are omitted for clarity) (c). Designations as in Figure 4.

$NiO_5(H_2O)$ polyhedra, while the tubular crystal structure of $Ni_{12}(OH)_2(SeO_3)_8(OH)_6$[21] contains half of the protonated $(NiO_5(OH))^{9-}$ octahedra. With pH values greater than 7.0, only the very stable solid products $Pb(SeO_3)$[22−25] phase is observed.

STRUCTURAL DESCRIPTION

α-$PbM(SeO_3)_2$ (M = Ni^{2+}, Co^{2+}). The isotypic compounds **I** and **IV** crystallize in orthorhombic symmetry (space group *Pnma*). They are built up from a 3D framework composed of

DOI: 10.1021/ic503055v
Inorg. Chem. 2015, 54, 2425−2434

Table 3. Calculated Partial Charges for I (α-PbNi$(SeO_3)_2$), II (β-PbNi$(SeO_3)_2$), III ($PbNi_2(SeO_2OH)_2(SeO_3)_2$), and IV ($\alpha$-PbCo$(SeO_3)_2$)

α-PbNi$(SeO_3)_2$	
atom	charge ± q
Pb1	+0.74952
Se1	+0.24784
Se2	+0.24417
Ni1	+0.93022
O1	−0.37204
O2	−0.33946
O3	−0.36119
O4	−0.36583

β-PbNi$(SeO_3)_2$	
atom	charge ± q
Pb1	+0.77033
Se1	+0.25253
Se2	+0.22790
Ni1	+0.90996
O1	−0.35484
O2	−0.35920
O3	−0.35784
O4	−0.36482

α-PbCo$(SeO_3)_2$	
atom	charge ± q
Pb1	+0.73096
Se1	+0.23494
Se2	+0.23527
Co1	+1.00606
O1	−0.37077
O2	−0.37602
O3	−0.35183
O4	−0.36630

$PbNi_2(SeO_2OH)_2(SeO_3)_2$	
atom	charge ± q
Pb1	+0.81193
Pb2	+0.82647
Se1	+0.27735
Se2	+0.27396
Se3	+0.28956
Se4	+0.28127
Ni1	+0.99233
Ni2	+0.96340
O1	−0.36194
O2	−0.35874
O3	−0.35630
O4	−0.35919
O5	−0.33540
O6	−0.35710
O7	−0.33391
O8	−0.35640
O9	−0.38723
O10	−0.35713
O11	−0.38634
O12	−0.35635
H1	+0.20398
H2	+0.20493

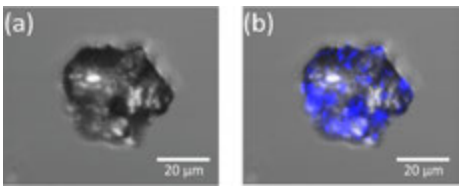

Figure 7. Transmission image of a crystal of β-PbNi$(SeO_3)_2$ (a); emitting surface (λ_{em} = 420−440 nm, λ_{em} = 860 nm), blue color (b).

anionic $(SeO_3)^{2-}$ and $(MO_6)^{10-}$ building units sharing common corners (Figure 3). We find one symmetrically independent M^{2+} position with rather regular $(MO_6)^{10-}$ octahedral coordination. The average bonding ⟨M−O⟩ distances are 2.077 Å for **I** and 2.113 Å for **IV**. There are two independent Se atoms per formula unit where Se^{4+} cations form typical $(SeO_3)^{2-}$ triangular pyramids with Se located at its apical corner and a stereoactive lone pair acting as a complementary external ligand. The average ⟨Se−O⟩ distance is 1.704 Å for both compounds, M = Ni^{2+} (**I**) and Co^{2+} (**IV**). The unique Pb^{2+} site is surrounded by O anions shared by $(SeO_3)^{2-}$ and $(MO_6)^{10-}$ groups, forming asymmetric polyhedra. In both compounds the Pb^{2+} cations demonstrate eight short strong Pb−O bonds (2.552−2.802 and 2.539−2.827 Å in **I** and **IV**, respectively) in one coordination hemisphere, and two longer weaker bonds (3.332 and 3.418 Å in **I** and **IV**, respectively) in the other hemisphere (Figure 4a,b) with a clear location of the stereochemically active lone pair. In Figure 3b a 3D metal cationic framework of the crystal structures of **I** and **IV** is represented as a black-and-white graph with black-and-white nodes symbolizing coordination polyhedra of M^{2+} and Se^{4+}, respectively. It highlights the topological connectivity of the SeO_3 and MO_6 polyhedra in complex 3D framework with stretched rectangular channels extending along the [010] direction occupied by the lead cations and the Se^{4+} lone pairs with a dimension of 3.1 × 11.4 $Å^2$, measured as the shortest and longest O···O distances across the channels (Figure 3b). In the (010) plane, their sections are arranged in a crossed manner with alternate of the two orientations [201] and the [20$\bar{1}$] with respect to the *Pnma* symmetry. The channels are bordered by six MO_6 and six SeO_3 polyhedra (Figure 3a). The projection of the channel walls is given in the figure resulting in a three M-octahedra-wide pseudoribbons (Figure 5a). Within the pseudoribbon, there are void spaces that are bounded by six-membered rings with a dimension of 5.35 × 5.46 $Å^2$. The pseudoribbons are further cross-linked into a 3D $[M(SeO_3)_2]^{2-}$ framework through common SeO_3 trigonal pyramids (Figure 5b). Divalent lead cations reside in the cavities and balance the charge of the framework of compounds **I** and **IV**. In general, it is typical for heteropolyhedral frameworks in inorganic oxysalts to be based upon interconnecting chains oriented parallel to each other.[32] The framework topology found out for α-PbM$(SeO_3)_2$ (M = Ni^{2+} and Co^{2+}) has been observed previously, e.g., in the structures of $(H_3O)[Fe(HPO_4)_2]$,[33] $Na_3[In(PO_4)_2]$,[34] and $Pb[Fe(AsO_4)(AsO_3OH)$.[35]

***β*-PbNi$(SeO_3)_2$.** The crystal structure of **II** adopts an orthorhombic symmetry (noncentrosymmetric space group, $Cmc2_1$). It contains one symmetrically independent Ni^{2+} cation that forms a slightly distorted NiO_6 octahedron: the trans O−Ni−O bond angles fall in the range of 155.82−172.69°, whereas the cis angles range from 80.91° to 102.94°. The Ni−O bond lengths are 2.045(5)−2.148(6) Å. Two independent Se^{4+} sites have a trigonal pyramidal coordination with an apex occupied by the selenium cation as already mentioned previously. The average ⟨Se−O⟩ bond lengths of the trigonal pyramids are 1.698 and 1.707 Å for Se1 and Se2 sites, respectively. In the crystal structure of **II** a unique Pb^{2+} ion has seven short Pb−O bonds (2.569−2.885 Å) in the first coordination hemisphere, whereas the second hemisphere is occupied by two longer bonds (3.035 Å) (Figure 4c). Once again, the coordination polyhedra of the lead cation is asymmetric and obviously indicates that the $6s^2$ lone pair is stereochemically active. In contrast, we have recently described the crystal structure of $PbBi_4O_6Cl_2$ in which the Pb^{2+} lone pair activity is fully quenched.[36]

Similarly to what was found in the α-PbNi$(SeO_3)_2$ form (**I**), the β-form is built up from isolated NiO_6 octahedra interlinked by SeO_3 groups via common oxygen corners. However, the linkage modes differ in both structures. The crystal structure of **II** (Figure 6a) is essentially two-dimensional (2D) and is based upon $[Ni(SeO_3)_2]^{2-}$ sheets. They are shown in Figure 6b and lay parallel to (001). The lone pairs of electrons of Se^{4+} cations are shifted in the [001] direction toward the vacant part of the interlayer space. The sheets in **II** are very similar to 2D pseudoribbons delimiting the channels of **I** and **IV**. Same cavities are filled by the Pb^{2+} cations, which serve to balance charge and achieve the cohesion between the sheets. The shortest interlayer O···O contacts across the interlayer is about 3.36 Å, much greater than the sum of van der Waals radii and involves a true 2D-

DOI: 10.1021/ic503055v
Inorg. Chem. 2015, 54, 2425−2434

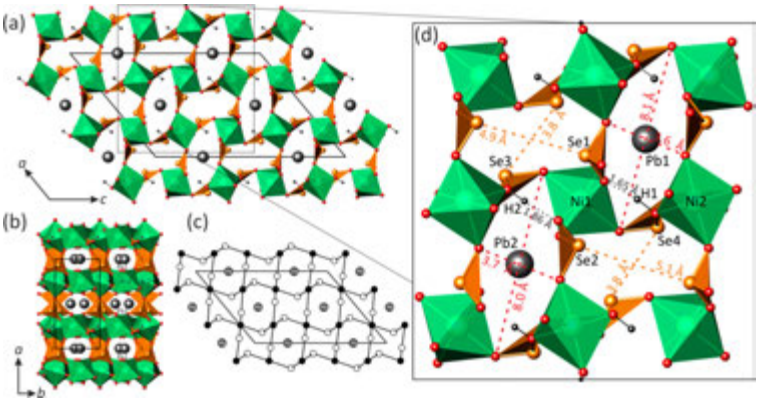

Figure 8. General projection of the crystal structure of $PbNi_2(SeO_2OH)_2(SeO_3)_2$ along the *b* and *c* axes (a and b), respectively; its black-and-white graph (c); and more detailed fragment of the structure (d). Legend as in Figure 4.

character. The black-and-white graph corresponding to the layered nickel selenite structural units is shown in Figure 6c. This kind of layer topology is one of the most common in inorganic oxysalts[32,37] and has been recently observed, for instance, in the crystal structure of steklite, $K[Al(SO_4)_2]$,[38] where (AlO_6) octahedra are linked by (SO_4) tetrahedra. In selenites, it has been reported for the crystal structures of $K_2[M(SeO_3)_2]$ (M = Mn and Co).[39,40] The NCS character of **II** is well evidenced on Figure 6a where only "*up*" SeO_3 orientations are found in the crystal structure. Dipole moments were calculated for **II** due to its noncentrosymmetricity. In this calculation performed using Pacha,[29] local charges given in Table 3 have been used. In general, it is noteworthy that the charge distribution is very similar in the four new selenites, due to similar concomitant groups. Ni^{2+} and Co^{2+} show a similar degree of covalence leading to a residual covalence charge close to ~+1. As expected the Se−O bonds are very strong leading to a residual charge around +0.25. Finally, the shortest Pb−O distances also bring a strong degree of covalence leading to Pb partial charge close to +1. For **II**, all SeO_3 groups stand in to bring local dipole moments that do not cancel each other. The moments are mainly oriented along the [001] direction with values of 1.87 and 2.07 Debyes for $Se(1)O_3$ and $Se(2)O_3$, respectively. Other local dipoles arise from distorted NiO_6 octahedra and Pb^{2+} complex coordination polyhedra that also lead to a net nonzero polarization due to the $Cmc2_1$ symmetry. Finally each individual layer shown on Figure 6a brings its own total dipole, mainly parallel to *c* but with different (*a*, *b*) components. Our calculations performed on the $[Pb_4Ni_4(SeO_3)_8]$ unit-cell content containing two layers lead to M = 21.51 Debyes almost parallel to *c* (negative charge barycenter (1.157, −0.111, 2.197), positive charge barycenter (−1.189, −0.256, −1.617)). This important value is expected to lead to strong SHG effects. Our analysis was performed on three different crystals of **II** as detailed in the Experimental Section. Dealing with a rather thick crystal, only some areas of the crystal surface show a significant SHG signal as shown in blue color in Figure 7. This feature is rather common and was observed recently in $[Bi_{12}O_{15}][Li_2(SO_4)_4]$.[41] It is noteworthy that in the experimental setting the detected SHG signal is maximal in the horizontal plane (below the crystal), which reduces the detection for thick and irregular absorbing samples In addition the refinement of racemic twinned domains (ratio ~ 60:40) suggests the possibility for local SHG quenching at the antiphase boundary.

Polymorphism in $PbNi(SeO_3)_2$. In our experiments, we have observed two modifications of $PbNi(SeO_3)_2$ that differ in both crystallographic parameters and structural topology. The *α*-phase has a notably smaller unit-cell volume (544.83 $Å^3$) than the *β*-phase (575.81 $Å^3$) and, as a consequence, a remarkably higher density (6.337 versus 5.996 g/cm^3, respectively). In terms of structural complexity expressed as a Shannon information amount per unit cell,[42,43] the *β*-phase is considerably more simple (58.439 bits per unit cell) than the *α*-phase (116.877 bits per unit cell). It is a general observation that a high-temperature polymorph is structurally simpler than its low-temperature counterpart (due to the increase in both vibrational and configurational entropies),[44] which, together with the data on density and unit-cell volumes, strongly suggest that the *α*- and *β*-modifications of $PbNi(SeO_3)_2$ are low- and high-temperature polymorphs, respectively. This conclusion agrees well with the 3D and 2D characters of their structures, respectively, which is frequently observed in inorganic compounds (that is, structural dimensionality of a low-temperature polymorph is higher than that of its high-temperature counterpart[45]).

$PbNi_2(SeO_2OH)_2(SeO_3)_2$. The crystal structure of **III** adopts a monoclinic symmetry (space group, $P2/c$). There are two symmetrically independent Ni^{2+} sites with rather regular octahedral coordination with the average ⟨Ni−O⟩ bond lengths equal to 2.064 and 2.077 Å for Ni1 and Ni2 sites, respectively. The four crystallographically inequivalent Se^{4+} atoms are asymmetrically coordinated by three oxygen atoms in a trigonal pyramidal geometry. However, two of them are protonated leading to strongly distorted $(Se(3)O_2OH)^-$ and $(Se(4)O_2OH)^-$ trigonal pyramids with one long Se−O bond (1.810 and 1.785 Å for Se(3) and Se(4), respectively) and two shorter Se−O bonds (1.659−1.676 and 1.649−1.675 Å for Se3 and Se4, respectively). Similarly distorted coordination geometry is typical of hydroxide ligands, as reported for instance in the crystal structure of $Ni(HSeO_3)\cdot 4H_2O$.[46] The average ⟨Se−O⟩ bond lengths are equal to 1.695, 1.693, 1.715, and 1.703 Å for $Se(1)O_3$, $Se(2)O_3$, $Se(3)O_2OH$, and $Se(4)O_2OH$, respectively. The two independent Pb^{2+} cations are 8-fold oxygen coordinated (Figure 3d,e) with Pb−O distances in the ranges of 2.481−2.916 and 2.567−2.765 Å for Pb1 and Pb2, respectively. They both

DOI: 10.1021/ic503055v
Inorg. Chem. 2015, 54, 2425−2434

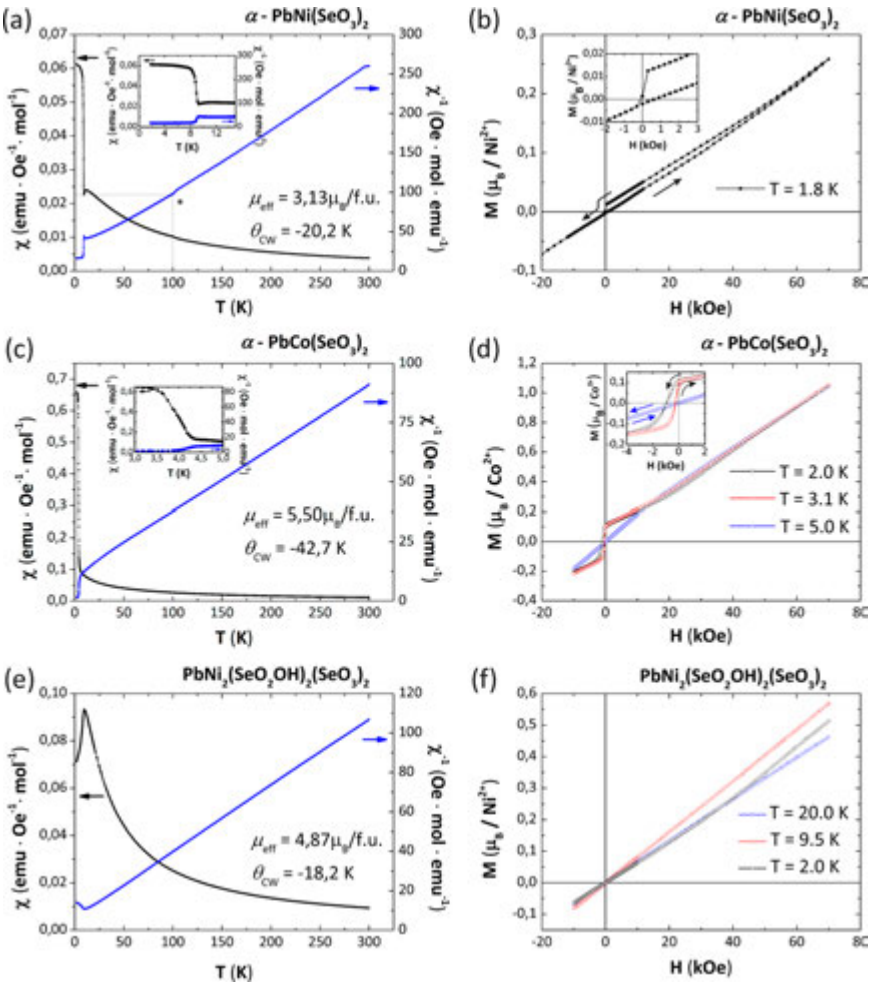

Figure 9. Thermal evolution of the magnetic susceptibility for **I** (a), **IV** (c), and **III** (e). Magnetization as a function of applied field for **I** (b), **IV** (d), and **III** (f).

show a distorted square antiprismatic arrangement with lone pairs of electrons oriented toward the longest oxygen neighbors, similarly to lead coordination in $PbMo_2O_5(SeO_3)_2$.[10]

In the crystal structure of **III**, the NiO_6 octahedra are sharing their vertices with SeO_3 groups, forming a 3D framework encapsulating channels propagating along the [010] direction (Figure 8a). Four independent channels are occupied alternately by divalent lead cations and lone pairs of electrons of the Se^{4+} cations. The channels containing Pb^{2+} are bordered by O^{2-} ions and have a cross-section of maximum of ~3.6 × 8.1 Å^2 taking into account the shortest O···O separations. Those bordered by Se^{4+} ions Se···Se are ~3.8 × 5.1 Å^2 large on the basis of the Se···Se distances (Figure 8d). It is striking that in the (a,b) projection the similitude between Pb1 and Pb2 channels suggests a $V/2$ subcell. In fact the projection in the (a,b) plane evidences channels growing along the c-axis with a clear distinction between Pb2 and Pb1 sites (Figure 8b).

Figure 8c shows the black-and-white graph corresponding to a 3D metal cationic framework of **III**. Its structural architecture is closely related to that observed in the crystal structure of $PbFe_2(SeO_3)_4$[47] and represents an interesting topological variation of the primitive cubic (pcu) network.[48]

MAGNETIC PROPERTIES

The powder samples selected for magnetic measurements have been prepared from stoichiometries corresponding to the P_1 (**I** and **IV** (replacing NiO by CoO)) and P_2 (**III**) points in Figure 1a. After Rietveld refinement though strong preferred orientation effects, the refined phase weight fractions of impurity (diamagnetic $Pb(SeO_3)$) are 0.17, 0.42, and 0.15 for the powder samples of **I**, **III**, and **IV**, respectively. Magnetic data were

DOI: 10.1021/ic503055v
Inorg. Chem. 2015, 54, 2425−2434

normalized taking into account the massic contribution of the second phase. PXRD patterns are shown in Figure 2.

The FC magnetic susceptibility χ and χ^{-1} versus temperature are plotted in Figure 9a,c for α-$PbNi(SeO_3)_2$ (**I**) and α-$PbCo(SeO_3)_2$ (**IV**). In the high-temperature range, $\chi^{-1}(T)$ could be fitted using a Curie–Weiss law $\chi = C/(T - \theta_{CW})$. Both compounds show very similar behavior dominated by antiferromagnetic exchanges as given by the negative Curie–Weiss temperatures, $\theta_{CW} = -20.2$ and -42.7 K, respectively. The deduced effective moments are 3.13 μ_B and 5.50 μ_B per formula unit, respectively. It indicates significant spin–orbit couplings (SOC) compared to calculated spin-only values, i.e., 2.83 μ_B/Ni^{2+} and 3.87 μ_B/Co^{2+}. One should also note that the exaggerated value measured in the cobalt compound compared to the commonly observed $\mu_{eff} \sim 4.5$ μ_B probably denote an approximate determination of the **IV** compound's weight fraction in the biphasic sample, due to preferred orientation effects mentioned previously.

For **I** the broad peak below 100 K and the upturn of the susceptibility below 9 K suggests the setting of short-range antiferromagnetic correlations but is immediately masked by the appearing of a magnetic moment. In **IV** a similar, but even more abrupt, phenomenon occurs below 4.5 K. In both compounds, it is accompanied by a ZFC/FC divergence at low temperature, as shown in Supporting Information Figure S12. It is ascribed to intrinsic spin-canting due to favored antisymmetric exchanges (Dzyaloshinski–Moriya interactions) in this crystal structure with strong SOC ions. As expected from the strongest SOC for Co^{2+}, the M(H) magnetization plot indicates a largest remanent moment for **IV** compared to **I**, i.e., 0.1 μ_B/Co^{2+} against 0.01 μ_B/Ni^{2+} as shown on the Figures 9b,d. In the mean-field approximation, the Curie–Weiss temperature is given as $\theta_{CW} = 2zJS(S+1)/3k_b$ where the z-number of neighbors interact with the same J force with a central M^{2+} ion. Theoretically, this approximation is available in the Heisenberg case but could lead to an approximated value for Co^{2+} and Ni^{2+} ions where spin–orbit coupling should favor anisotropic spins (XY or Ising).

Dealing with similar crystal structures of **I** and **IV**, one can derive $J_{(I)}/J_{(IV)} = \theta_{CW(I)}(S_{Co^{2+}})(S_{Co^{2+}} + 1)/\theta_{CW(IV)}(S_{Ni^{2+}})(S_{Ni^{2+}} + 1) = 0.89$. This involves very similar J coupling values. Taking into account that each metal center is surrounded by z = 8 other metals with plausible M–O–O–M superexchange paths (4.8 Å < M–M < 6.2 Å and O–O distance smaller than the sum of their ionic radii), one can also estimate the mean J value to $J/k_b \sim -1.9$ and -2.1 K, respectively.

$\chi(T)$ and $\chi^{-1}(T)$ of compound **III** are shown on Figure 9e. It shows a paramagnetic regime above the setting of an antiferromagnetic transition at T_N = 10 K. The Curie–Weiss law above T_N yields $\mu_{eff} = 4.87$ μ_B/(formula unit (f.u.)). (3.44 μ_B/Ni^{2+}) and $\theta_{CW} = -18.2$ K in good agreement with predominant antiferromagnetic exchanges between Ni^{2+} ions with strong SOC. Once more, in a mean-field approximation can we deduce a mean J_{Ni-Ni}/k_b of -1.71 K from the θ_{CW} value, taking into account z equals eight Ni neighbors around each Ni^{2+} with efficient geometrical SSE paths under conditions given previously. This low value is nearly similar to the one found for compound **I** and gives an indication for weak but comparable Ni–O–O–Ni negative exchanges mediated by SeO_3 corners in both compounds.

CONCLUSION

In this work, the PbO–NiO–SeO_2 ternary system in hydrothermal conditions at 473 K was investigated. Three novel lead nickel selenites and one novel lead cobalt selenite were synthesized and characterized. The $PbNi(SeO_3)_2$ compound crystallizes in two polymorphic orthorhombic modifications, α (**I**) and β (**II**). The $PbCo(SeO_3)_2$ phase (**IV**) is isotypic with **I**. According to the experimental results, the pH values of the solution play the essential role in hydrolysis and condensation processes by hydrothermal reactions in the studied system and determine structural architectures of resulted products of the syntheses. The observed dependence of the structural variety and the structural units upon the pH values is remarkable and can be used for preparation of new transition metal oxoselenites and similar groups of heavy-element compounds with novel structural architectures.

ASSOCIATED CONTENT

Supporting Information

Tables listing fractional atomic coordinates, atomic displacement parameters, and selected bond distances, figures showing experimental XRD patterns and temperature dependences of magnetization, and crystallographic information files. This material is available free of charge via the Internet at http://pubs.acs.org.

AUTHOR INFORMATION

Corresponding Author

*E-mail: olivier.mentre@ensc-lille.fr.

Notes

The authors declare no competing financial interest.

ACKNOWLEDGMENTS

This work was carried out under the framework of the Multi-InMaDe project supported by the ANR (Grant ANR 2011-JS-08 00301). The Fonds Européen de Développement Régional (FEDER), CNRS, Région Nord Pas-de-Calais, and Ministère de l'Education Nationale de l'Enseignement Supérieur et de la Recherche are acknowledged for funding the X-ray diffractometers. V.M.K. thanks l'Ambassade de France en Russie and l'Agence Campus France (Contract Nos. 768231K, 779116K, 794852B, 808399A, and 808400J) for the partial support of this work. S.V.K. and O.I.S. acknowledge financial support from St. Petersburg State University (Internal Grant 3.38.136.2014).

REFERENCES

(1) Dadap, J. I.; Shan, J.; Heinz, T. F. *J. Opt. Soc. Am. B* **2004**, *21*, 1328–1347.
(2) Cady, W. G. *Piezoelectricity: An Introduction to the Theory and Applications of Electromechanical Phenomena in Crystals*; Dover Publications: New York, 1964; p 822.
(3) Jona, F.; Shirane, G. *Ferroelectric Crystals*; Pergamon Press: Oxford, U.K., 1962; p 402.
(4) Lang, S. B. *Sourcebook of Pyroelectricity*; Gordon and Breach Science: London, New York, 1974; p 562.
(5) Verma, V. P. *Thermochim. Acta* **1999**, *327*, 63–102.
(6) Effenberger, H. *J. Solid State Chem.* **1988**, *73*, 118–126.
(7) Li, P.-X.; Kong, F.; Hu, C.-L.; Zhao, N.; Mao, J.-G. *Inorg. Chem.* **2010**, *49*, 5943–5952.
(8) Yeon, J.; Kim, S.; Nguyen, S. D.; Lee, H.; Halasyamani, P. S. *Inorg. Chem.* **2012**, *51*, 609–619.
(9) Zhang, S.-Y.; Hu, C.-L.; Li, P.-X.; Jiang, H.-L.; Mao, J.-G. *Dalton Trans.* **2012**, *41*, 9532–9542.
(10) Oh, S.; Lee, D. W.; Ok, K. M. *Inorg. Chem.* **2012**, *51*, 5393–5399.
(11) Oh, S.-J.; Lee, D. W.; Ok, K. M. *Dalton Trans.* **2012**, *41*, 2995–3000.

DOI: 10.1021/ic503055v
Inorg. Chem. 2015, 54, 2425–2434

(12) Kovrugin, V. M.; Colmont, M.; Mentré, O.; Siidra, O. I.; Krivovichev, S. V. *Mineral. Mag.* **2015**, submitted for publication.
(13) Kovrugin, V. M.; Siidra, O. I.; Colmont, M.; Mentré, O.; Krivovichev, S. V. *Mineral. Petrol.* **2015**, submitted for publication.
(14) Aliev, A.; Kovrugin, V. M.; Colmont, M.; Terryn, C.; Huvé, M.; Siidra, O. I.; Krivovichev, S. V.; Mentré, O. *Cryst. Growth Des.* **2014**, *14*, 3026−3034.
(15) Vlaev, L. T.; Genieva, S. D.; Gospodinov, G. G. *J. Therm. Anal. Calorim.* **2005**, *81*, 469−475.
(16) Forster, P. M.; Stock, N.; Cheetham, A. K. *Angew. Chem., Int. Ed.* **2005**, *44*, 7608−7611.
(17) Sonnauer, A.; Stock, N. *Eur. J. Inorg. Chem.* **2008**, *2008*, 5038−5045.
(18) Engelen, B.; Bäumer, U.; Hermann, B.; Müller, H.; Unterderweide, K. *Z. Anorg. Allg. Chem.* **1996**, *622*, 1886−1892.
(19) Wildner, M. *Monatsh. Chem.* **1991**, *122*, 585−594.
(20) Mcmanus, A. V. P.; Harrison, W. T. A.; Cheetham, A. K. *J. Solid State Chem.* **1991**, *92*, 253−260.
(21) Amorós, P.; Marcos, M. D.; Roca, M.; Beltrán-Porter, A.; Beltrán-Porter, D. *J. Solid State Chem.* **1996**, *126*, 169−176.
(22) Popovkin, B. A.; Cheremisinov, V. P.; Simanov, Y. P. *J. Struct. Chem.* **1963**, *4*, 38−43.
(23) Fischer, R. *TMPM, Tschermaks Mineral. Petrogr. Mitt.* **1972**, *17*, 196−207.
(24) Koskenlinna, M.; Valkonen, J. *Cryst. Struct. Commun.* **1977**, *6*, 813−816.
(25) Pasero, M.; Rotiroti, N. *Neues Jahrb. für Mineral., Monatsh.* **2003**, *2003*, 145−152.
(26) *APEX*; Bruker AXS: Madison, WI, USA, 2007.
(27) *SADABS*; Bruker AXS: Madison, WI, USA, 2001.
(28) Sheldrick, G. M. *Acta Crystallogr.* **2008**, *A64*, 112−122.
(29) Henry, M. *ChemPhysChem* **2002**, *3*, 561−569.
(30) Pourbaix, M. *Atlas of electrochemical equilibria in aqueous solutions*; National Association of Corrosion Engineers: Houston, TX, USA, 1974; p 644.
(31) Takeno, N. *Atlas of Eh-pH diagrams*, Geological Survey of Japan Open File Report No.419; National Institute of Advanced Industrial Science and Technology, Research Center for Deep Geological Environments: Tsukuba, Japan, 2005; p 287.
(32) Krivovichev, S. V. *Structural Crystallography of Inorganic Oxysalts*; Oxford University Press: Oxford, U.K., 2009.
(33) Vencato, I.; Mattievich, E.; Moreira, L. F.; Mascarenhas, Y. P. *Acta Crystallogr.* **1989**, *C45*, 367−371.
(34) Lii, K.-H. *Eur. J. Solid State Inorg. Chem.* **1996**, *33*, 519−526.
(35) Effenberger, H.; Hejny, C.; Pertlik, F. *Monatsh. Chem.* **1996**, *127*, 127−133.
(36) Aliev, A.; Olchowka, J.; Colmont, M.; Capoen, E.; Wickleder, C.; Mentré, O. *Inorg. Chem.* **2013**, *52*, 8427−8435.
(37) Krivovichev, S. V. *Crystallogr. Rev.* **2004**, *10*, 185−232.
(38) Murashko, M. N.; Pekov, I. V.; Krivovichev, S. V.; Chernyatyeva, A. P.; Yapaskurt, V. O.; Zadov, A. E.; Zelensky, M. E. *Geol. Ore Deposits (Transl. of Geol. Rudn. Mestorozhd.)* **2013**, *55*, 594−600.
(39) Wildner, M. *Acta Crystallogr.* **1992**, *C48*, 595−595.
(40) Wildner, M. *Acta Crystallogr.* **1992**, *C48*, 410−412.
(41) Lü, M.; Colmont, M.; Huvé, M.; De Waele, I.; Terryn, C.; Aliev, A.; Mentré, O. *Inorg. Chem.* **2014**, *53*, 12058−12065.
(42) Krivovichev, S. V. *Acta Crystallogr.* **2012**, *A68*, 393−398.
(43) Krivovichev, S. V. *Angew. Chem., Int. Ed.* **2014**, *53*, 654−661.
(44) Krivovichev, S. V. *Mineral. Mag.* **2013**, *77*, 275−326.
(45) Krivovichev, S. V.; Cahill, C. L.; Burns, P. C. *Inorg. Chem.* **2002**, *41*, 34−39.
(46) Engelen, B.; Boldt, K.; Unterderweide, K.; Bäumer, U. *Z. Anorg. Allg. Chem.* **1995**, *621*, 331−339.
(47) Johnston, M. G.; Harrison, W. T. A. *J. Solid State Chem.* **2004**, *177*, 4680−4686.
(48) Krivovichev, S. V. *Mineral. Mag.* **2014**, *78*, 415−435.

DOI: 10.1021/ic503055v
Inorg. Chem. 2015, 54, 2425−2434

A-V
Oxocentered Cu(II) lead selenite honeycomb lattices hosting Cu(I)Cl_2 groups obtained by chemical vapor transport reactions

Vadim M. Kovrugin, Marie Colmont, Oleg I. Siidra, Olivier Mentré, Alexandr Al-Shuray, Vladislav V. Gurzhiy, and Sergey V. Krivovichev

Published in: *Chemical Communications*, 2015, Vol. 51 (46), p. 9563–9566.
DOI: 10.1039/c5cc01426c

ChemComm

COMMUNICATION

View Article Online
View Journal | View Issue

Oxocentered Cu(II) lead selenite honeycomb lattices hosting $Cu(I)Cl_2$ groups obtained by chemical vapor transport reactions†

Cite this: *Chem. Commun.*, 2015, 51, 9563

Received 15th February 2015,
Accepted 30th April 2015

DOI: 10.1039/c5cc01426c

www.rsc.org/chemcomm

Vadim M. Kovrugin,[ab] Marie Colmont,[b] Oleg I. Siidra,[a] Olivier Mentré,[b] Alexander Al-Shuray,[a] Vladislav V. Gurzhiy[a] and Sergey V. Krivovichev*[a]

Chemical vapor transport (CVT) reactions were used to prepare three modular mixed-valent Cu(I)–Cu(II) compounds, $(Pb_2Cu^{2+}{}_9O_4)(SeO_3)_4(Cu^{+}Cl^{2})Cl_5$ (1), $(PbCu^{2+}{}_5O_2)(SeO_3)_2(Cu^{+}Cl_2)Cl_3$ (2), and $(Pb_xCu^{2+}{}_{(6-x)}O_2)(SeO_3)_2(Cu^{+}Cl_2)K_{(1-x)}Cl_{(4-x)}$ (x = 0.20) (3). In their crystal structures chains of anion-centered $(OCu^{2+}{}_4)$ and $(OCu^{2+}{}_3Pb)$ tetrahedra form honeycomb-like double layers with cavities occupied by linear $[Cu^{+}Cl_2]^{-}$ groups.

Inorganic copper oxocompounds attract considerable attention due to their interesting structural and physical properties[1] as well as mineralogical and geochemical importance.[2] Of special interest are mixed-valent Cu(I)–Cu(II) systems with separate symmetrically independent monovalent and divalent copper sites due to their contrasted coordinations combined in one crystal structure. Herein we report on the synthesis and characterization of three novel Cu(I)–Cu(II) lead oxoselenite chlorides inspired by mineralogical discoveries in such unusual geological conditions as volcanic fumaroles.[2g,3] Here copper oxoselenites form from volcanic gases emanating from cooling magmatic chambers deep under the Earth's surface long after the period of eruptive activities. The formation of such Cu compounds in fumaroles provides a useful hint for their synthesis under laboratory conditions, in particular, the chemical vapor transport (CVT) method.[4] The specific feature of many Cu oxoselenites is the presence in their crystal structures of oxocentered $(\mu_4\text{–}O)Cu_4$ tetrahedral units that polymerize to form extended structural complexes.[2g,3] Likely, during these reactions the selenites and metal halides play the role of transport agents.[5] In order to reproduce natural exhalative chemistry, in this work, we investigate the formation of phases in the $PbO\text{–}Cu^{2+}Cl_2\text{–}Cu^{+}Cl\text{–}Cu^{2+}O\text{–}SeO_2$ system containing Pb^{2+} cations that possess stereochemically active $6s^2$ lone electron pairs favouring formation segregation of structural compartments occupied by these pairs.[6] In addition, the preference of Pb^{2+} ions for similar OPb_4 tetrahedral units is an asset for creation of more complex edifices.

Crystallographic information for three novel compounds synthesized by the CVT reaction method (Fig. 1a) is summarized in Table 1. Schematic representations of coordination environments of cations in the crystal structures of **1–3** are shown in

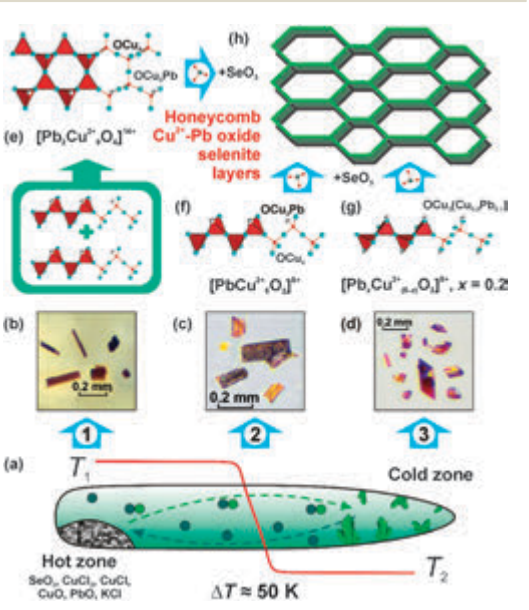

Fig. 1 General scheme of syntheses by the method of CVT reactions (a), the crystals of **1**, **2** and **3** (b–d), and the scheme of formation of honeycomb Cu^{2+}–Pb selenite layers (e–h). The types of oxo-centered 1-dimensional units (shown in red) formed by corner-sharing OCu_4 and OCu_3Pb tetrahedra in the structures of **1**, **2** and **3** are shown. (legend: Cu = cyan balls; Pb = grey balls). See text for details.

[a] *Department of Crystallography, St. Petersburg State University, University Emb. 7/9, 199034 St. Petersburg, Russia. E-mail: s.krivovichev@spbu.ru*

[b] *UCCS, UMR 8181, Université Lille Nord de France, USTL, F-59655 Villeneuve d'Ascq, France*

† Electronic supplementary information (ESI) available: CIF files, experimental section, IR spectra, and tables with bond-valence analysis for **1–3**. See DOI: 10.1039/c5cc01426c

Fig. S1, ESI.† In all the compounds, Cu^{+} cations form two relatively short Cu^{+}–Cl bonds (2.058–2.118 Å), which result in the formation of tightly bonded $[CuCl_2]^{-}$ anionic groups that can be considered as separate structural entities. The Cu^{2+} cations have mixed oxochloride coordinations that have previously been observed in Cu oxochloride compounds,[2a] with typical trends of Jahn–Teller d^9 ions. The Cu(1) and Cu(2) sites in **1**, the Cu(4) site in **2**, and Cu(3) site in **3** form $[CuO_4Cl_2]$ distorted octahedra with four short equatorial Cu–O and two long apical Cu–Cl bonds. The Cu(3) site in **1**, the Cu(2) and Cu(3) sites in **2**, and the Cu(1) site in **3** are octahedrally coordinated with $[CuO_3Cl]$ squares complemented by two long Cu–Cl bonds. The Cu(4) site in **1** forms a $[CuO_4Cl]$ trigonal bipyramid, whereas the Cu(1) site in **2** and the Cu(4) site in **3** form $[CuO_3Cl_2]$ trigonal bipyramids. The Pb atoms have asymmetrical coordinations consisting of three strong Pb–O bonds (2.356–2.420 Å) located in one coordination hemisphere and four long Pb–Cl in another. This coordination of Pb^{2+} cations is typical for lead oxohalide compounds[7] and is consistent with the presence of stereoactive lone electron pairs. In all the compounds under consideration, Se^{4+} cations form standard $(SeO_3)^{2-}$ selenite triangular pyramidal oxo-anions (Se–O = 1.688–1.726 Å). The structure of **3** has one symmetrically independent K site with the site-occupation factor (s.o.f.) equal to 0.8. Its coordination polyhedron can be described as a distorted hexagonal bipyramid. Bond-valence sums[8] calculated for all the sites in the crystal structures of **1–3** are in full agreement with their expected oxidations states (in valence units): Cu^{+} sites – 1.00–1.16, Cu^{2+} sites – 1.96–2.14, Pb^{2+} sites – 1.95–1.96, Se^{4+} sites – 4.03–4.16, and K^{+} site – 0.80.

The high variability of cation coordinations in the structures of **1–3** makes their uniform description in terms of cation coordination polyhedra a difficult task. It is therefore more reasonable to look for more mundane consideration, *e.g.* in terms of cation arrays or coordination of anions.[9] In addition to the O atoms associated with the SeO_3 groups, all three compounds contain additional O_a atoms (oxo-anions) not bonded to Se^{4+} cations and tetrahedrally coordinated by four metal atoms (Cu and Pb). In the crystal structure of **1** there are two additional O atoms, O(2) and O(4), that form $(OCu^{2+}{}_3Pb)$ and $(OCu^{2+}{}_4)$ tetrahedra, respectively. The oxo-centered tetrahedra share common corners to form $[O_4Pb_2Cu^{2+}{}_9]^{14+}$ double chains depicted in Fig. 1e. These chains are growing parallel to the *b*-axis, and its common value for the three compounds ($b \sim 6.2$ Å) denotes similar arrangement between the oxo-centered building units in the full series. These types of chains of anion-centered tetrahedra are original and have not been observed in inorganic compounds previously. The SeO_3 groups are attached to the triangular bases of oxo-centered tetrahedra that results in the formation of complex 1-dimensional $\{[O_4Pb_2Cu^{2+}{}_9](SeO_3)_4\}^{6+}$ interconnected *via* Pb–O bonds in 2-dimensional metal-oxide double layers (Fig. 2b). The projection of the layers in the (*bc*) plane leads to a honeycomb-like lattice of tetrahedra, even though this idealized vision neglects the disconnections occurring at the oxocentered-oxoanion contacts. In contrast, monometallic $[O_2Cu_5]$ honeycomb-layers are reported in several compounds based upon anion-centered tetrahedra.[9] The layers are surrounded by Cl^{-} anions in the interleaves and accommodate both linear $[Cu^{+}Cl_2]^{-}$ anions and Cl^{-} ions in the larger and smaller honeycomb-windows, respectively. The interactions between the Cl^{-} ions of the $[Cu^{+}Cl_2]^{-}$ groups and host cationic networks are restricted to rather weak Cu^{2+}–Cl^{-} (>2.975 Å), Pb^{2+}–Cl^{-} (>3.396 Å) and K^{+}–Cl^{-} (>3.478 Å) bonds with bond-valences not exceeding 0.08 valence units (Tables S1–S3, ESI†). Taking into account the relative strength of the Cu^{+}–Cl bonds and weak interactions between them and the rest of the structure, these units may be considered as guest anions embedded in the complex metal oxochloride matrix based upon anion-centered tetrahedra.

A very similar 'host–guest' principle is at work in the structures of **2** and **3** as well. Here the $(OCu^{2+}{}_3Pb)$ and $(OCu^{2+}{}_4)$ tetrahedra share corners to produce single chains extending along the common *b*-parameter that have $[O_2PbCu_5]^{8+}$ and $[O_2Pb_xCu^{2+}{}_{(6-x)}]^{8+}$

Table 1 Crystallographic data for **1**, **2**, and **3**

	1	**2**	**3**
Empirical formula	$(Pb_2Cu^{2+}{}_9O_4)(SeO_3)_4(Cu^{+}Cl_2)Cl_5$	$(PbCu^{2+}{}_5O_2)(SeO_3)_2(Cu^{+}Cl_2)Cl_3$	$(Pb_xCu^{2+}{}_{(6-x)}O_2)(SeO_3)_2(Cu^{+}Cl_2)K_{(1-x)}Cl_{(4-x)}$, $x = 0.20$
Crystal system		*C*2/*m*	
Space group		Monoclinic	
a (Å)	18.605(17)	18.4956(4)	15.116(1)
b (Å)	6.204(6)	6.1454(1)	6.1850(4)
c (Å)	12.673(11)	15.2985(4)	9.2672(9)
β (deg)	109.87(2)	119.311(1)	95.965(5)
V (Å^3)	1376(2)	1516.25(6)	861.72(12)
ρ_{calc} (g cm^{-3})	4.514	4.607	3.840
μ (mm^{-1})	25.78	25.02	15.52
Reflection collected	7722	6910	4817
Independent reflections (R_{int})	1301 (0.069)	1924 (0.024)	974 (0.029)
Goodness-of-fit	0.791	1.231	1.121
$R_1[I > 2\sigma(I)]^a$	0.0257	0.0260	0.0412
wR_2	0.0349	0.0761	0.1172
R_1 (all data)	0.0475	0.0267	0.0496
wR_2	0.0378	0.0761	0.1176
Largest diff. peak and hole [e Å^{-3}]	0.951, −0.988	3.783, −2.942	4.244, −1.592

^{a} $R_1 = \sum||F_o| - |F_c||/\sum|F_o|$; w$R_2 = \{\sum[w(F_o^2 - F_c^2)_2]/\sum[w(F_o^2)^2]\}^{1/2}$.

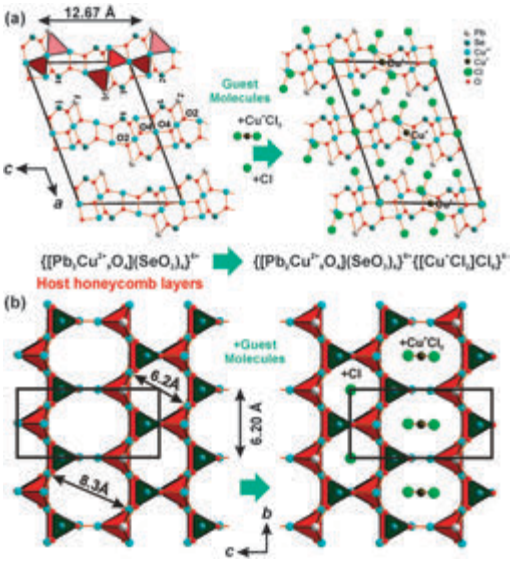

Fig. 2 General projections of the structure of **1** along the *b* and *a* axes – (a) and (b). Honeycomb layers of $\{[Pb_2Cu^{2+}{}_9O_4](SeO_3)_4\}^{6+}$ composition are hosts for the $[Cu^+Cl_2]^-$ guest species localized in the layer cavities. The $\{[Pb_2Cu^{2+}{}_9O_4](SeO_3)_4\}^{6+}$ layers are formed *via* interconnection of the $[Pb_2Cu^{2+}{}_9O_4]$ oxo-centered chains (red) and isolated SeO_3 groups (dark-green). The O(2) and O(4) designated in (a) are central oxygen atoms in OCu_4 and OCu_3Pb tetrahedra, respectively.

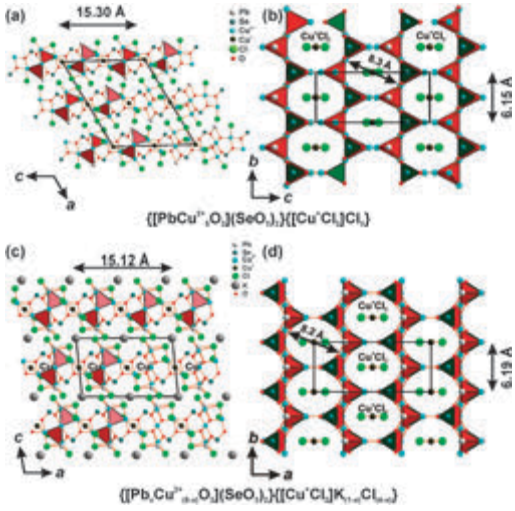

Fig. 3 General projections of the structure of **2** (a, b) and **3** (c, d). In **2**, the OCu_4 and OCu_3Pb tetrahedra (red) form single $[O_2PbCu_5]$ chains, which results in the enlargement of the *c*-parameter value from 12.67 Å (in **1**) to 15.30 Å (in **2**). In **3**, K atoms are located in the interlayer under and above the pseudohexagonal voids filled by the $[Cu^+Cl_2]$ groups. The layers (b, d) are characterized by only one type of pore with 8.3 Å and 8.2 Å diameter in **2** and **3**, respectively.

compositions, respectively (Fig. 1f and g). Together with SeO_3 groups, these chains form 1-dimensional $\{[O_2M_6](SeO_3)_2\}^{4+}$ metal-oxide (M = Cu or Pb) backbones of the structures that are arranged to form pseudo honeycomb layers. Due to the elementary single-chains, only large honeycomb windows are created that accommodate the $[Cu^+Cl_2]^-$ guest anions (Fig. 3) as observed in **1**. The structure of **3** contains additional K^+ cations located in the interlayer space between the metal oxoselenite chloride layers. In all three structures, lone electron pairs on the Pb^{2+} and Se^{4+} cations are oriented toward the interlayer space, thus conforming the 'chemical scissor' principle of structural organization in compounds with lone-electron-pair cations.[10]

It is noteworthy that compounds **1** and **2** are closely chemically related, which can be described by the equation:

$$(Pb_2Cu^{2+}{}_9O_4)(SeO_3)_4(Cu^+Cl_2)Cl_5\ (\mathbf{1}) + Cu^+Cu^{2+}Cl_3 \rightarrow 2(PbCu^{2+}{}_5O_2)(SeO_3)_2(Cu^+Cl_2)Cl_3\ (\mathbf{2})$$

From the structural viewpoint, transition from **1** to **2** is associated with the reconstruction of the metal-oxide backbone, *i.e.* in depolymerization of anion-centered tetrahedra and splitting of the double $[O_4Pb_2Cu^{2+}{}_9]^{14+}$ chains into single $[O_2PbCu_5]^{8+}$ chains. This kind of structural reconstruction accompanied by the inclusion of imaginary ionic component $Cu^+Cu^{2+}Cl_3$ into the metal-oxide matrix is in good agreement with the principle of dimensional reduction.[11] It should also be noted that **2** is a synthetic analogue of allochalcoselite, the mineral first described to be obtained from volcanic fumaroles of the Tolbachik volcano (Kamchatka peninsula, Russia).[3d]

To summarize, three novel Cu^{2+}–Cu^+ Pb oxoselenite chlorides were obtained by the chemical vapor transport reactions, which proves the efficiency of this method for the synthesis of new mixed Cu^{2+}–Cu^+ based oxyhalide compounds. These compounds described herein are based upon oxocentered mixed Pb–Cu^{2+} one-dimensional units of different architectures. These units determine basic topologies of the structures and influence their stability and properties. For instance, in the three compounds only corner-sharing OCu_4 and OCu_3Pb are found in chains and double chains forming hollow voids. It follows that in all the compounds, the role of the tightly bonded $[Cu^+Cl_2]^-$ anions is that of guest complexes incorporated inside metal oxide chloride units. The present study also points out that the Cu^+Cl_2 groups may serve as transport agents of Cu^+ in Cl-rich gaseous environments such as that observed in natural volcanic fumaroles.

This work was financially supported by the Russian Science Foundation through the grant 14-17-00071. Technical support by the SPbSU X-ray Diffraction Resource Centre is gratefully acknowledged. This work was carried out under the framework of the Multi-InMaDe project supported by the ANR (Grant ANR 2011-JS-08 003 01). V.M.K. thanks l'Ambassade de France en Russie and l'Agence Campus France (contracts no. 768231K, 779116K 794852B, 808399A, and 808400J) for the partial support of this work.

Notes and references

1 (*a*) N. V. Kuratieva, M. Banki, A. A. Tsirlin, J. Eckert, H. Ehrenberg and D. Mikhailova, *Inorg. Chem.*, 2013, **52**, 13974; (*b*) A. A. Tsirlin, O. Janson, S. Lebernegg and H. Rosner, *Phys. Rev. B: Condens. Matter Mater. Phys.*, 2013, **B87**, 064404; (*c*) S. Tamilarasan, D. Sarma, S. Bhattacharjee, U. V. Waghmare, S. Natarajan and J. Gopalakrishnan, *Inorg. Chem.*, 2013, **52**, 5757; (*d*) P. S. Berdonosov, O. Janson, A. V. Olenev, S. V. Krivovichev, H. Rosner, V. A. Dolgikh and A. A. Tsirlin, *Dalton Trans.*, 2013, **42**, 9547; (*e*) T.-T. Zhu, W. Sun, Y.-X. Huang, Z.-M. Sun, Y. Pan, L. Balents and J.-X. Mi, *J. Mater. Chem. C*, 2014, **2**, 8170; (*f*) H. L. Feng, M. Arai, Y. Matsushita, Y. Tsujimoto, Y. Yuan, C. I. Sathish, J. He, M. Tanaka and K. Yamaura, *J. Solid State Chem.*, 2014, **217**, 9; (*g*) S. Hu, A. Mace, M. Johnsson, V. Gnezdilov, P. Lemmens, J. Tapp and A. Moeller, *Inorg. Chem.*, 2014, **53**, 7661.

2 (*a*) S. V. Krivovichev, S. K. Filatov and L. P. Vergasova, *Mineral. Petrol.*, 2013, **107**, 235; (*b*) I. V. Pekov, M. E. Zelenski, V. O. Yapaskurt, Y. S. Polekhovsky and M. N. Murashko, *Eur. J. Mineral.*, 2013, **25**, 91; (*c*) I. V. Pekov, N. V. Zubkova, M. E. Zelenski, V. O. Yapaskurt, Y. S. Polekhovsky, O. A. Fadeeva and D. Y. Pushcharovsky, *Mineral. Mag.*, 2013, **77**, 107; (*d*) I. V. Pekov, O. I. Siidra, N. V. Chukanov, V. O. Yapaskurt, D. I. Belakovskiy, M. N. Murashko and E. G. Sidorov, *Eur. J. Mineral.*, 2014, **26**, 597; (*e*) I. V. Pekov, N. V. Zubkova, V. O. Yapaskurt, D. I. Belakovskiy, I. S. Lykova, M. F. Vigasina, E. G. Sidorov and D. Yu. Pushcharovsky, *Mineral. Mag.*, 2014, **78**, 905; (*f*) I. V. Pekov, N. V. Zubkova, V. O. Yapaskurt, P. M. Kartashov, Yu. S. Polekhovsky, M. N. Murashko and D. Yu. Pushcharovsky, *Eur. J. Mineral.*, 2014, **26**, 667; (*g*) L. P. Vergasova, T. F. Semenova, S. V. Krivovichev, S. K. Filatov, A. A. Zolotarev, Jr. and V. V. Ananiev, *Eur. J. Mineral.*, 2014, **26**, 439.

3 (*a*) S. V. Krivovichev, S. K. Filatov, T. F. Semenova and I. V. Rozhdestvenskaya, *Z. Kristallogr.*, 1998, **213**, 645; (*b*) S. V. Krivovichev, R. R. Shuvalov, T. F. Semenova and S. K. Filatov, *Z. Kristallogr.*, 1999, **214**, 135; (*c*) P. C. Burns, S. V. Krivovichev and S. K. Filatov, *Can. Mineral.*, 2002, **40**, 1587; (*d*) S. V. Krivovichev, S. K. Filatov, P. C. Burns and L. P. Vergasova, *Can. Mineral.*, 2006, **44**, 507; (*e*) S. V. Krivovichev, S. K. Filatov, P. C. Burns and L. P. Vergasova, *Can. Mineral.*, 2007, **45**, 929; (*f*) R. R. Shuvalov, L. P. Vergasova, T. F. Semenova, S. K. Filatov, S. V. Krivovichev, O. I. Siidra and N. S. Rudashevsky, *Am. Mineral.*, 2013, **98**, 463.

4 M. Binnewies, R. Glaum, M. Schmidt and P. Schmidt, *Z. Anorg. Allg. Chem.*, 2013, **639**, 219.

5 A. Aliev, V. M. Kovrugin, M. Colmont, C. Terryn, M. Huvé, O. I. Siidra, S. V. Krivovichev and O. Mentré, *Cryst. Growth Des.*, 2014, **14**, 3026.

6 O. I. Siidra, D. S. Zenko and S. V. Krivovichev, *Am. Mineral.*, 2014, **99**, 817.

7 (*a*) S. V. Krivovichev, O. I. Siidra, E. V. Nazarchuk, P. C. Burns and W. Depmeier, *Inorg. Chem.*, 2006, **45**, 3846; (*b*) O. I. Siidra, D. O. Zinyakhina, A. I. Zadoya, S. V. Krivovichev and R. W. Turner, *Inorg. Chem.*, 2013, **52**, 2799; (*c*) O. I. Siidra, S. V. Krivovichev, R. W. Turner, M. S. Rumsey and J. Spratt, *Am. Mineral.*, 2013, **98**, 248; (*d*) O. I. Siidra, S. V. Krivovichev, R. W. Turner, M. S. Rumsey and J. Spratt, *Am. Mineral.*, 2013, **98**, 256; (*e*) O. I. Siidra, D. S. Zenko, A. N. Suknotova and S. V. Krivovichev, *Mineral. Mag.*, 2013, **77**, 3239.

8 (*a*) N. E. Brese and M. O'Keeffe, *Acta Crystallogr.*, 1991, **B47**, 192; (*b*) S. V. Krivovichev and I. D. Brown, *Z. Kristallogr.*, 2001, **216**, 245.

9 S. V. Krivovichev, O. Mentré, O. I. Siidra, M. Colmont and S. K. Filatov, *Chem. Rev.*, 2013, **113**, 6459.

10 (*a*) R. Becker, M. Johnsson, R. K. Kremer and P. Lemmens, *Solid State Sci.*, 2003, **5**, 1411; (*b*) Z. Mayerova, M. Johnsson and S. Lidin, *Angew. Chem., Int. Ed.*, 2006, **45**, 5602; (*c*) V. Jo, M. K. Kim, D. W. Lee, I. W. Shim and K. M. Ok, *Inorg. Chem.*, 2010, **49**, 2990.

11 E. G. Tulsky and J. R. Long, *Chem. Mater.*, 2001, **13**, 1149.

A-VI
Topologically and geometrically flexible structural units in seven new organically templated uranyl selenates and selenite-selenates

Vladislav V. Gurzhiy, Vadim M. Kovrugin, Pavel A. Mikhaylenko,
Olga S. Tyumentseva, Sergey V. Krivovichev, and Ivan G. Tananaev
Published in: *Journal of Solid State Chemistry*, 2015, Vol. 229, 32–40.
DOI: 10.1016/j.jssc.2015.04.040

Journal of Solid State Chemistry 229 (2015) 32–40

Contents lists available at ScienceDirect

Journal of Solid State Chemistry

journal homepage: www.elsevier.com/locate/jssc

Topologically and geometrically flexible structural units in seven new organically templated uranyl selenates and selenite–selenates

Vladislav V. Gurzhiy [a,*], Vadim M. Kovrugin [a], Olga S. Tyumentseva [a], Pavel A. Mikhaylenko [a], Sergey V. Krivovichev [a], Ivan G. Tananaev [b]

[a] Department of Crystallography, St. Petersburg State University, University Emb. 7/9, 199034 St. Petersburg, Russia
[b] National Research Nuclear University MEPhI, pr. Pobedy 48, 456783 Ozersk, Russia

ARTICLE INFO

Article history:
Received 6 March 2015
Received in revised form
24 April 2015
Accepted 27 April 2015
Available online 8 May 2015

Keywords:
Uranyl
Selenate
Crystal structure
Topology
Isomerism
X-ray diffraction

ABSTRACT

Single crystals of seven novel uranyl oxysalts of selenium with protonated methylamine molecules, $[C_2H_8N]_2[(UO_2)(SeO_4)_2(H_2O)]$ (**I**), $[C_2H_8N]_2[(UO_2)_2(SeO_4)_3(H_2O)]$ (**II**), $[C_4H_{15}N_3][H_3O]_{0.5}[(UO_2)_2(SeO_4)_{2.93}(SeO_3)_{0.07}(H_2O)](NO_3)_{0.5}$ (**III**), $[C_2H_8N]_3[H_5O_2][(UO_2)_2(SeO_4)_3(H_2O)_2]_2(H_2O)_5$ (**IV**), $[C_2H_8N]_2[H_3O][(UO_2)_3(SeO_4)_4(HSeO_3)(H_2O)](H_2SeO_3)_{0.2}$ (**V**), $[C_4H_{12}N]_3[H_3O][(UO_2)_3(SeO_4)_5(H_2O)]$ (**VI**), and $[C_2H_8N]_3(C_2H_7N)[(UO_2)_3(SeO_4)_4(HSeO_3)(H_2O)]$ (**VII**) have been prepared by isothermal evaporation from aqueous solutions. Their crystal structures have been solved by direct methods and their uranyl selenate and selenite–selenate units investigated using black-and-white graphs from the viewpoints of topology of interpolyhedral linkages and isomeric variations. The crystal structure of **IV** is based upon complex layers with unique topology, which has not been observed previously in uranyl selenates. Investigations of the statistics and local distribution of the U–O_{br}–Se bond angles demonstrates that shorter angles associate with undulations, whereas larger angles correspond to planar areas of the uranyl selenite layers.

1. Introduction

Within the last decade actinide oxysalts attracted significant attention due to their importance in mineralogy, uranium mining technologies and studies related to the advanced nuclear fuel cycle. The diversity of polyhedral units found in uranyl compounds is unique, starting from isolated complexes [1–3] and clusters [4–7] to cage compounds [8–11] and nanotubules [12–14]. Selenium-containing uranyl oxysalts are known for both mono- and divalent inorganic cations [15–19], as well as for organic template molecules of various charge and structure [20–24]. The crystal structures of uranyl selenates and selenites are based upon a variety of complex units formed by polymerization of U and Se coordination polyhedra. The topology and geometry of these units is controlled by a number of factors, governing interactions between organic and inorganic substructures. The principles that describe these interactions include hydrophillic–hydrophobic interactions, charge-density matching and weak hydrogen bonding that nevertheless may induce distortions of particular geometries of U–O–Se links. Herein we report on the syntheses and structural characterization of seven novel Se-contaning uranyl oxysalts that contain protonated organic molecules as interlayer species.

2. Experimental

2.1. Synthesis

N,*N*-dimethylformamide (99%, Sigma-Aldrich), dimethylamine (40 wt% in H_2O, Aldrich), diethylenetriamine (99%, Sigma-Aldrich), diethylamine (99%, Sigma-Aldrich), selenic acid (40 wt% in H_2O, 99.95%, Aldrich), and $UO_2(NO_3)_2 \cdot 6H_2O$ (Vekton) were used as received. $[C_2H_8N]_2[(UO_2)(SeO_4)_2(H_2O)]$ (**I**), $[C_2H_8N]_2[(UO_2)_2(SeO_4)_3(H_2O)]$ (**II**), $[C_4H_{15}N_3][H_3O]_{0.5}[(UO_2)_2(SeO_4)_{2.93}(SeO_3)_{0.07}(H_2O)](NO_3)_{0.5}$ (**III**), $[C_2H_8N]_3[H_5O_2][(UO_2)_2(SeO_4)_3(H_2O)_2]_2(H_2O)_5$ (**IV**), $[C_2H_8N]_2[H_3O][(UO_2)_3(SeO_4)_4(HSeO_3)(H_2O)](H_2SeO_3)_{0.2}$ (**V**), $[C_4H_{12}N]_3[H_3O][(UO_2)_3(SeO_4)_5(H_2O)]$ (**VI**), and $[C_2H_8N]_3(C_2H_7N)[(UO_2)_3(SeO_4)_4(HSeO_3)(H_2O)]$ (**VII**) have been prepared by evaporation from aqueous solutions of uranyl nitrate, 40%—solution of selenic acid, *N*,*N*-dimethylformamide, 40%—solution of methylamine, diethylenetriamine, diethylamine, and deionized distilled water. Yellow–green homogeneous liquid solutions were left in a fumehood at the room temperature. The crystals of compound **I**, and **II** were synthesized through the reaction 0.198 g (0.4 mmol) of uranyl nitrate, 0.094 g (1.3 mmol) of *N*,*N*-dimethylformamide,

* Corresponding author. Tel.: +7 9119749592.
E-mail addresses: vladgeo17@mail.ru (V.V. Gurzhiy), vladgeo17@mail.ru (I.G. Tananaev).

http://dx.doi.org/10.1016/j.jssc.2015.04.040
0022-4596/

0.590 g (4.1 mmol) of selenic acid and 2.001 g (110.2 mmol) of deionized distilled water. The crystals of compound **IV**, and **V** were synthesized through the reaction 0.0502 g (0.1 mmol) of uranyl nitrate, 0.009 g (0.2 mmol) of dimethylamine, 0.102 g (0.7 mmol) of selenic acid and 2.002 g (110.2 mmol) of deionized distilled water. The crystals of compound **VII** were synthesized through the reaction 0.0502 g (0.1 mmol) of uranyl nitrate, 0.018 g (0.4 mmol) of dimethylamine, 0.072 g (0.5 mmol) of selenic acid and 2.001 g (110.2 mmol) of deionized distilled water. The crystals of compound **III** were synthesized through the reaction 0.100 g (0.2 mmol) of uranyl nitrate, 0.010 g (0.1 mmol) of diethylenetriamine, 0.102 g (0.7 mmol) of selenic acid and 2.002 g (110.2 mmol) of deionized distilled water. The crystals of compound **VI** were synthesized through the reaction 0.059 g (0.1 mmol) of uranyl nitrate, 0.010 g (0.1 mmol) of diethylamine, 0.679 g (4.7 mmol) of selenic acid and 2.002 g (110.2 mmol) of deionized distilled water. The solid products were formed after three days in small amount. The pH values of the solutions described above are in the range from 1 to 0, moreover for the newly prepared solutions the values tend closer to 1, whereas precipitation of crystals increases acidity.

2.2. Single crystal X-ray study

Single crystals of **I–VII** have been selected for data collection under an optical microscope, encased in epoxy and mounted on glass fibres. Data were collected using monochromatic Mo$K\alpha$ radiation (λ[Mo$K\alpha$]= 0.71073 Å) by means of a Bruker SMART APEX II CCD (**I–VI**) and STOE IPDS II (**VII**) diffractometers. The unit-cell parameters were refined by least-squares techniques. Data were integrated and corrected for background, Lorentz, and polarization effects using an empirical spherical model by means of the Bruker programs *APEX2* and *XPREP* (**I–VI**) and *STOE X-AREA* (**VII**). Absorption correction was applied using the *SADABS* program [25] for (**I–VI**) and *STOE X-RED* & *X-SHAPE* [26] for **VII**. The structures were solved by direct methods and refined using the SIR-92 [27] and *SHELXL*-97 programs [28] incorporated in the *OLEX2* program package [29]. Due to the low quality of crystals (especially phases **IV–VII**), their metastability and sensitivity to air, only rather rough structural models could be obtained, which is manifested in the presence of high residual electron-density peaks, low bond precision, and refinement of organic molecules in isotropic approximation only (**VII**), as well as in the impossibility to localize the positions of several H atoms. However, the hydrogen bonding system in such cases can be inferred from the short O–O contacts involving sites occupied by water and hydronium molecules. The final models included coordinates and anisotropic displacement parameters for all non-hydrogen atoms. The carbon-bound H atoms were placed in calculated positions and were included in the refinement in the 'riding' model approximation, with U_{iso}(H) set to 1.5U_{eq}(C) and C–H 0.96 Å for CH_3 groups, with U_{iso}(H) set to 1.2U_{eq}(C) and C–H 0.97 Å for CH_2 groups, U_{iso}(H) set to 1.2U_{eq}(N) and N–H 0.89 Å for the NH_3 groups, and U_{iso}(H) set to 1.2U_{eq}(N) and N–H 0.86 Å for the NH_2 groups. Positions of H atoms of H_2O molecules, hydronium cations and OH^- groups were localized from difference Fourier maps and kept fixed during refinement. Relevant crystallographic data are listed in Table 1. Selected interatomic distances are listed in Tables S1–S7. CCDC files 901940, 901941, 901942, 901943, 901944, 901945, and 901946 contain the supplementary crystallographic data for the compounds **I–VII**, respectively. These data can be obtained free of charge from The Cambridge Crystallographic Data Centre via www.ccdc.cam.ac.uk/data_request/cif

3. Results

3.1. Structural descriptions

The crystal structures of all seven compounds reported in this paper contain uranyl pentagonal bipyramids and selenate tetrahedra. The structures of **V** and **VII** also contain selenite trigonal pyramids. The polyhedra are linked into inorganic structural units. The structures contain one (**I**), two (**II**, **III**, **V**, **VI** and **VII**), or four (**IV**) crystallographically unique U^{VI} cations forming approximately linear uranyl ions, $[UO_2]^{2+}$, with the U=O bond lengths varying from 1.711(10) Å to 1.787(7) Å. These basic uranyl entities are coordinated in their equatorial planes by four oxygen atoms and one H_2O molecule to form UO_7 pentagonal bipyramids with the average $\langle U–O_{eq}\rangle$ bond lengths equal to 2.390 Å. The U–H_2O bond lengths lie in range of 2.424(12)–2.554(7) Å. In the structure of **I** there are two symmetrically independent Se^{VI} atoms. The structures of **II**, **III**, **IV**, and **VI** contain three Se^{VI} atoms each, whereas the structure of **IV** contains six

Table 1
Crystallographic data for **I**, **II**, **III**, **IV**, **V**, **VI** and **VII**.

Compound	I	II	III	IV	V	VI	VII
Formula mass	666.15	1079.14	2256.03	2267.28	1685.05	1770.70	1685.07
Space group	$P2_12_12_1$	$P2_12_12_1$	$P2_1/c$	$P2_1/c$	$P2_1/m$	$P2_1/m$	*Pnma*
a (Å)	7.5363(7)	11.2154(5)	11.1679(4)	12.451(5)	8.3116(4)	8.941(2)	11.6591(11)
b (Å)	12.2021(11)	11.2263(5)	10.9040(4)	31.126(5)	18.6363(8)	19.300(4)	14.9556(17)
c (Å)	16.7601(16)	16.9138(8)	17.9913(6)	14.197(4)	11.5623(5)	11.377(3)	22.194(2)
β (°)	90.00	90.00	98.019(1)	120.39(2)	97.582(1)	97.510(4)	90.00
V (Å^3)	1541.2(2)	2129.57(17)	2169.57(17)	4746(2)	1775.31(14)	1946.5(7)	3870.0(7)
Size (mm^3)	0.21 × 0.17 × 0.09	0.21 × 0.17 × 0.07	0.23 × 0.19 × 0.08	0.23 × 0.18 × 0.07	0.19 × 0.14 × 0.08	0.22 × 0.20 × 0.06	0.26 × 0.20 × 0.09
μ (mm^{-1})	15.306	20.394	20.036	18.323	19.286	17.217	17.310
Z	4	4	2	4	2	2	4
2θ range (°)	4.13–60.00	4.35–60.00	4.38–55.00	2.62–55.00	4.17–60.00	4.18–54.98	3.28–39.10
D_{calc} (g/cm^3)	2.871	3.366	3.457	3.173	3.152	3.021	2.892
Total ref.	13,644	17,184	23,671	34,682	23,753	18,435	10,911
Unique ref.	4492	6112	4988	10896	5323	4597	1680
Unique $\lvert F_o\rvert \geq 4\sigma_F$	4117	5340	3855	5379	3940	2459	1221
R_{int}	0.0564	0.0651	0.0723	0.0963	0.0762	0.1196	0.1116
R_σ	0.0562	0.0684	0.0574	0.0993	0.0605	0.1609	0.0714
R_1 ($\lvert F_o\rvert \geq 4\sigma_F$)	0.0311	0.0283	0.0330	0.0482	0.0362	0.0396	0.0602
wR_2 ($\lvert F_o\rvert \geq 4\sigma_F$)	0.0629	0.0484	0.0735	0.1060	0.0935	0.0583	0.0962
GOF	0.940	0.934	0.964	0.875	1.083	0.737	1.127
ρ_{min}, ρ_{min}, e (Å^3)	−1.497, 2.339	−1.199, 1.099	−1.997, 2.824	−4.340, 4.608	−2.216, 2.793	−1.383, 1.651	−1.210, 1.054
CCDC	901940	901941	901942	901943	901944	901945	901946

Note: $R_1 = \Sigma\lvert\lvert F_o\rvert - \lvert F_c\rvert\rvert/\Sigma\lvert F_o\rvert$; $wR_2 = \{\Sigma\ [w(F_o^2 - F_c^2)^2]/\Sigma[w(F_o^2)^2]\}^{1/2}$; $w = 1/[\sigma^2(F_o^2) + (aP)^2 + bP]$, where $P = (F_o^2 + 2F_c^2)/3$; GOF = $\{\Sigma[w(F_o^2 - F_c^2)]/(n-p)\}^{1/2}$ where n is the number of reflections and p is the number of refined parameters.

independent Se^{VI} atoms. In the structures of **V** and **VII** there are three independent Se positions of which two sites [Se1 and Se2] correspond to Se^{VI}, whereas the Se3 site is occupied by Se^{IV}. The Se^{VI} cations in each structure are tetrahedrally coordinated by four O atoms, forming $[SeO_4]^{2-}$ tetrahedra with the average ⟨Se–O⟩ bond length equals to 1.634 Å. In the structure of **V** and **VII**, the Se3 site has a trigonal pyramidal coordination with an apex occupied by the Se^{IV} atom. This coordination type is typical for Se^{IV} cations possessing stereoactive lone electron pairs. In the structure of **III**, the Se3 site is occupied by both Se^{VI} (site-occupation factor (s.o.f.)=0.93) and Se^{IV} (s.o.f.=0.07) atoms with the total s.o.f. equal to 1.0. The $Se3O_3$ trigonal pyramids in **V** and **VII** are strongly distorted: two short equivalent bonds [1.645(6) Å and 1.653(16) Å in **V** and **VII**, respectively] and one longer bond [1.78 (2) Å and 1.78(4) Å in **V** and **VII**, respectively]. The observed elongation is the result of relatively strong hydrogen bonding to the nearby terminal methyl cations of the protonated dimethylamine molecule in the structure of **V**, and by protonation of the selenite group in the structure of **VII**. The asymmetric $[SeO_3]^{2-}$ and $[HSeO_3]^{2-}$ selenite groups were observed, in particular, in the structures of $(NH_4)[UO_2(HSeO_3)(SeO_3)]$ [30], $M[(UO_2)(HSeO_3)(SeO_3)]$ (M=K, Rb, Cs, Tl) [31], $[C_5H_{14}N][(UO_2)(SeO_4)(SeO_2OH)]$ [32], and $[C_5H_{14}N]_4(UO_2)_3(SeO_4)_4(HSeO_3)(H_2O)(H_2SeO_3)(HSeO_4)$ [33].

In the crystal structure of **I**, the $[UO_6(H_2O)]^{6-}$ pentagonal bipyramids share corners with two adjacent $[SeO_4]^{2-}$ tetrahedra to form $[(UO_2)(SeO_4)_2(H_2O)]^{2-}$ chains running parallel to the *b* axis. The chains are arranged into the pseudo layers parallel to the (0 0 1) plane (Fig. 1a). Two protonated dimethylamine cations $[C_2H_8N]^+$ are arranged between the chains and provide their linkage into a three-dimensional structure.

The crystal structures of **II**, **IV** and **III**, are based upon complex 2D layers with the composition $[(UO_2)_2(SeO_4)_3(H_2O)_n]^{2-}$. The topology of the U and Se polyhedral linkage is different for the different values of *n*. The layers are parallel to (0 0 1) in **II** and **III**, and to (0 1 0) in **IV** (Figs. 2 and 3). The uranyl selenate layers present in **II** and **III** are slightly corrugated. The interpolyhedral U–O_{br}–Se angles in **II**, **III** and **IV** have the average values of 135.6°, 136.1° and 135.6 ×, respectively, which are in general agreement with the average value of 136.8° reported in [34]. The structure of **II** contains two protonated linear dimethylamine molecules $[C_2H_8N]^+$ as interlayer species. Diprotonated diethylenetriamine cation $[C_4H_{15}N_3]^{2+}$, hydronium cation $[H_3O]^+$ and disordered nitrate group $[NO_3]^-$ are arranged between the layers in the structure of **III**. In the interlayer space of **IV**, there are three crystallographically independent protonated $[C_2H_8N]^+$ cations, one Zundel $[H_5O_2]^+$ cation, and five water molecules.

The crystal structures of **V**, **VI**, and **VII** are based upon the layers with U:Se=3:5 formed as a result of condensation of the $[UO_2]^{2+}$, $[UO_2(H_2O)]^{2+}$, $[Se^{VI}O_4]^{2-}$, $[Se^{IV}O_3]^{2-}$ and $[HSe^{IV}O_3]^-$ coordination polyhedra by sharing common oxygen atoms. In the structures of **V** and **VI** the inorganic layers are parallel to (1 0 0) (Fig. 4). The layers in **VII** are parallel to (0 0 1) and are strongly undulated along the *c* axis (Fig. 5). The undulation vector is parallel to [0 1 0] and is equal to *b* (14.956 Å). The undulation amplitude is about 15 Å. The undulations in the adjacent sheets have an anti-phase character, which means that large elliptical channels are created along the *a* axis. The structure

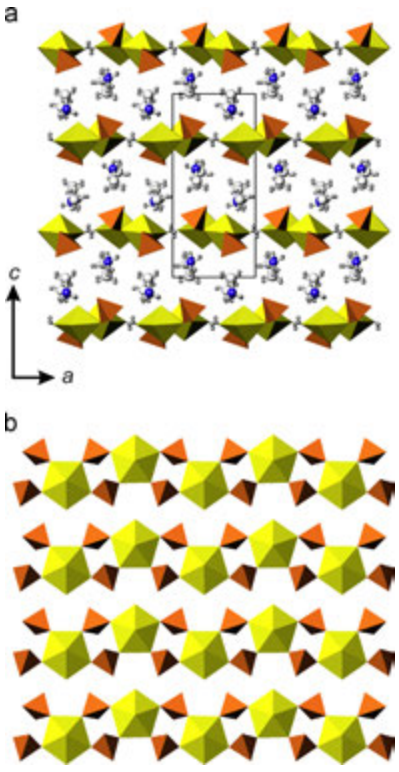

Fig. 1. The crystal structure of **I** projected along the *b* axis (**a**), and the $[(UO_2)(SeO_4)_2(H_2O)]^{2-}$ chains in the crystal structure of **I** (**b**). Legend: U polyhedra=yellow; Se polyhedra=orange; C and N atoms are white and blue, respectively; hydrogen atoms are small grey circles. (For interpretation of the references to color in this figure legend, the reader is referred to the web version of this article.)

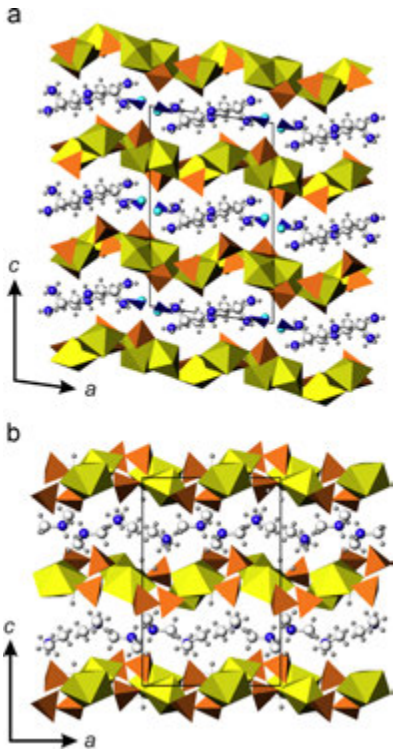

Fig. 2. The crystal structures of **II** and **III** projected along the *b* axis, (a) and (b), respectively. Legend is as in Fig. 1; $[H_3O]^+$ groups=cyan circles, $[NO_3]^-$=blue triangles. (For interpretation of the references to color in this figure legend, the reader is referred to the web version of this article.)

with similar undulated layers was observed previously [35]. In the structure of **V**, two protonated dimethylamine molecules $[C_2H_8N]^+$ and one hydronium cation $[H_3O]^+$ are located in the interlayer space, and form hydrogen bonds to the O atoms of uranyl groups and selenium oxyanions. The structure of **VI** contains three protonated diethylamine molecules $[C_4H_{12}N]^+$ and one hydronium cation $[H_3O]^+$ as interlayer species. The charge of the inorganic layer in **VII** is compensated by three disordered protonated dimethylamine molecules $[C_2H_8N]^+$ located in the interlayer space. It is of interest

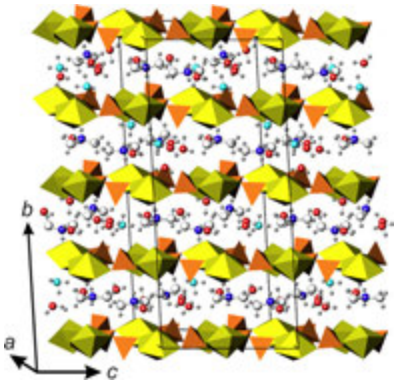

Fig. 3. The crystal structure of **IV**. Legend is as in Fig. 1; $[H_3O]^+$ groups and water molecules=cyan and red circles, respectively. (For interpretation of the references to color in this figure legend, the reader is referred to the web version of this article.)

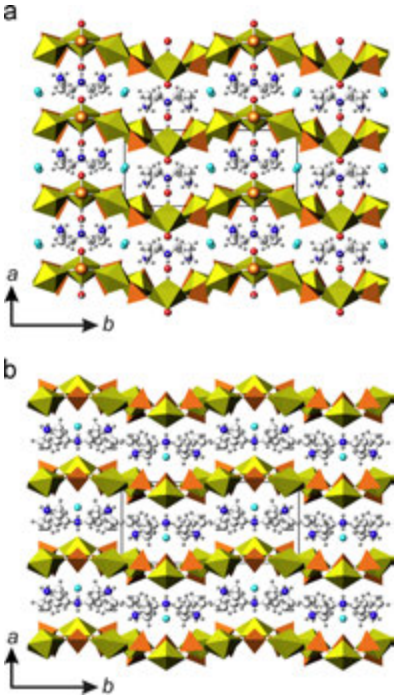

Fig. 4. The crystal structures of **V** and **VI** projected along the *b* axis, (a) and (b), respectively. Legend is as in Fig. 1. $[H_3O]^+$ groups and oxygen atoms=cyan and red circles; Se^{IV} atoms=big orange circles. (For interpretation of the references to color in this figure legend, the reader is referred to the web version of this article.)

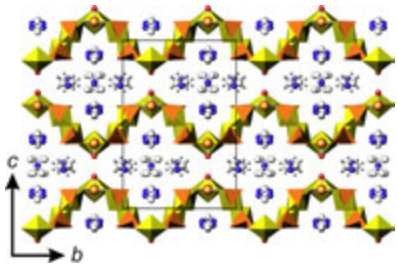

Fig. 5. The crystal structure of **VII** projected along the *b* axis. Legend is as in Fig. 1; oxygen atoms=circles; Se^{IV} atoms=big orange circles.

that there is also one electroneutral dimethylamine molecule $(C_2H_7N)^0$ in the centre of the elliptical channels.

3.2. Topological analysis

Topological structure of uranyl selenate units in the structures under consideration can be visualized using the nodal representation. In the framework of this approach [36–38], the U and Se coordination polyhedra are symbolized by black and white nodes, respectively. The vertices are linked by an edge if two respective polyhedra share a common oxygen atom. The resulting graph is used to investigate topological relations between similar structures.

Fig. 1b shows the topological structure of the 1D-units of **I**. The $[(UO_2)(SeO_4)_2(H_2O)]^{2-}$ chain observed in the structure of **I** corresponds to the simple 1D graph. Chains of this type are quite common for uranyl compounds with the $[TO_4]^{n-}$ tetrahedra (T=S, Se, P, As). They have been observed first in the structure of $Mn[(UO_2)(SO_4)_2(H_2O)](H_2O)_5$ [39] and later in a number of amine-templated uranyl sulfates [40–45] and other compounds, including $[(UO_2)(H_2PO_4)_2(H_2O)](H_2O)_2$ [46], $[(UO_2)(H_2AsO_4)_2(H_2O)]$ [47], $M[(UO_2)(SeO_4)_2(H_2O)](H_2O)_4$ (M=Mg, Zn) [48], $[C_5H_{16}N_2]_2[(UO_2)(SeO_4)_2(H_2O)](NO_3)_2$ [49], $[CH_3NH_3]_2[(UO_2)(SeO_4)_2(H_2O)](H_2O)$ [50].

Fig. 6a and b shows uranyl selenate layers in the structures of **II**, **III**, and **IV**. The corresponding black-and-white graphs are depicted in Fig. 6c and d. In the crystal structure of **II** and **III**, the topology of the $[(UO_2)_2(SeO_4)_3(H_2O)_n]^{2-}$ layers with n=1 is based upon 4- and 6-membered rings of alternating black and white nodes. The graph has been observed in uranyl sulfates $[N_2C_3H_{12}][(UO_2)_2(H_2O)(SO_4)_3]$ [44], $[N_2C_4H_{14}][(UO_2)_2(H_2O)(SO_4)_3](H_2O)$ [51], and uranyl selenates $[C_4H_{12}N]_2[(UO_2)_2(SeO_4)_3(H_2O)]$, $[C_4H_{14}N_2][(UO_2)_2(SeO_4)_3(H_2O)](H_2O)_2$, $[C_3H_{10}N]_2[(UO_2)_2(SeO_4)_3(H_2O)](H_2O)$, $[C_5H_{16}N_2][(UO_2)_2(SeO_4)_3(H_2O)](H_2O)$ [52], $K(H_5O_2)[(UO_2)_2(SeO_4)_3(H_2O)]$ [53]. The topology of the $[(UO_2)_2(SeO_4)_3(H_2O)_n]^{2-}$ layer with n=2 in **IV** contains 4- and 8-membered rings. This topology is rare and has previously been observed only in two uranyl chromates $(NH_4)_2(UO_2)_2(CrO_4)_3(H_2O)_6$ [54] and $K_2[(UO_2)_2(CrO_4)_3(H_2O)_2](H_2O)_4$ [55], but has never been observed in uranyl selenates.

The crystal structures of **V**, **VI**, and **VII** are based upon the layers with U:Se=3:5 (Fig. 7a). These structures have the same topology of inorganic layers. The corresponding graph (Fig. 7b) is built from 4- and 6-membered rings. This topology of inorganic complexes is typical for uranyl selenite–selenates such as $[C_5H_{14}N]_4[(UO_2)_3(SeO_4)_4(HSeO_3)(H_2O)](H_2SeO_3)(HSeO_4)$ [33], $(H_3O)[C_5H_{14}N]_2[(UO_2)_3(SeO_4)_4(HSeO_4)(H_2O)]$, $(H_3O)[C_5H_{14}N]_2[(UO_2)_3(SeO_4)_4(HSeO_4)(H_2O)](H_2O)$ [56], and has also been observed in some uranyl selenates: $Rb_4[(UO_2)_3(SeO_4)_5(H_2O)]$ [57], $(H_5O_2)_2(H_3O)_2[(C_{10}H_{20}O_5)_2][(UO_2)_3(SeO_4)_5(H_2O)]$ and $(H_5O_2)(H_3O)_3[C_{10}H_{20}O_5]_5[(UO_2)_3(SeO_4)_5(H_2O)]$ [58].

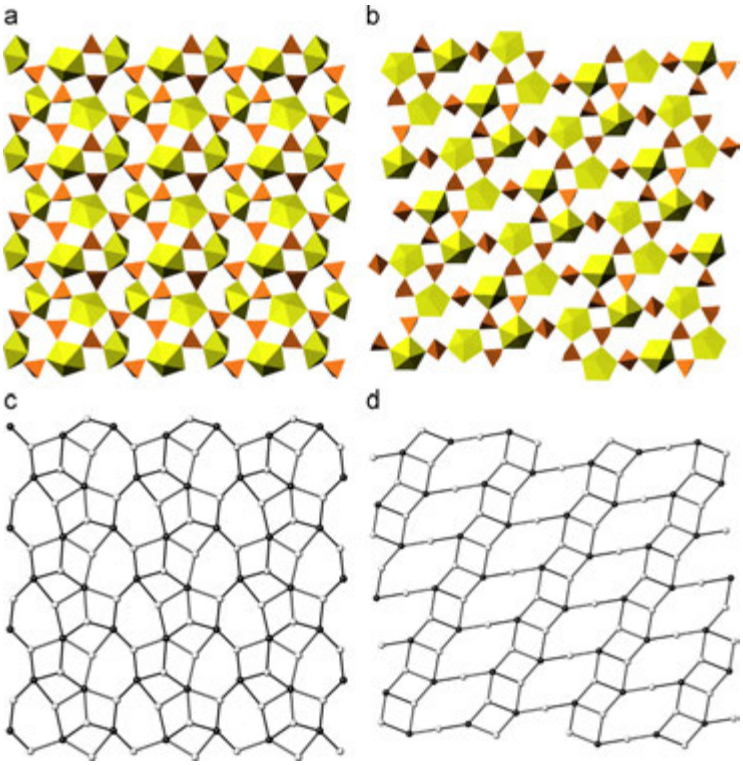

Fig. 6. The $[(UO_2)_2(SeO_4)_3(H_2O)_n]^{2-}$ layers in the crystal structures of **II**, **III**—(a) ($n=1$), and in the crystal structure of **IV**—(b) ($n=2$) in polyhedral representations; their graphs (c and d, respectively). Legend is as in Fig. 1; white vertices=Se, black vertices=U.

3.3. Geometrical isomerism

To define a topology of the layer by means of its nodal representation is not enough to define its complete topological structure. The detailed examination of orientations of structural units may reveal geometrical difference between the layers with the same black-and-white graph, which led Krivovichev and Burns [57] to the definition of geometrical isomerism. It is important to note that the isomers cannot be transformed one into another by simple rotations without breaking of chemical bonds. To distinguish between the layers with the same graph observed in the structures of **II**, **III**, and **V**, **VI**, **VII**, one has to analyse orientations of selenium polyhedra relative to the planes of the layers.

The analysis of the black-and-graph of the topology of layers of **V**, **VI** and **VII** (Fig. 7d–f) indicates that its white vertices are either 2- or 3-connected: 2-connected white vertices correspond to selenite trigonal pyramids, whereas 3-connected correspond to selenate tetrahedra. These selenite–selenate polyhedra share three of its corners with adjacent 4- or 5-connected uranyl pentagonal bipyramids. The non-shared corners may have either up-, down- or disordered (up-or-down) orientations relative to the plane of the layer. This ambiguity gives rise to geometric isomers with various orientations of the selenium polyhedra. To identify and classify the isomers of this type, we use their orientation matrices [58]. According to this approach, as applied to the structures in hand, the symbols **u** (up), **d** (down), **m** (orientation up-down topologically equivalent) or □ (white vertex is missing in the graph) are assigned to each white vertex.

The graphs shown in Fig. 8 have the **u**, **d** and **m** symbols written near white vertices. It can be seen that the systems of the **u**, **d** and **m** symbols are different for the layers, which therefore should be considered as different geometrical isomers. The isomers can be distinguished by their orientation matrices that provide short notations of the translational independent rectangular system of the **u**, **d**, **m** and □ symbols. The orientation matrices of the layers in the crystal structures of **V**, **VI** and **VII** shown in Figs. 8d–f have 6×2 dimensions and can be written in row as (**duuudd**)(**ud□du□**), (**dumudm**)(**ud□du□**) and (**ududud**)(**ud□du□**), respectively. Thus, the uranyl selenite layers observed in the crystal structures of **V**, **VI** and **VII** correspond to different geometrical isomers.

Using the above procedure, we can constitute the equivalence of the orientation matrices of the inorganic layers of the crystal structures of **II** and **III**. The same orientation matrix for these structures may be written as (**u□dd**)(**uu□d**) (Fig. 9).

3.4. Flexibility of structural units

An interesting feature of the substantial number of uranyl compounds [37,59], including seven structures reported herein, is the connection of adjacent coordination polyhedra through the common bridging vertices that can be depicted as a sort of a flexible ball-in-socket arrangement. This flexibility results in the relative ease of adaptation of layered $[(UO_2)_x(TO_4)_y]^{z-}$ systems to variable cations and other species present in the solutions during crystallization. As it has been observed in multiple experiments, there is no direct correlation between the size of the cation and the degree of the layer distortion (corrugation). The presence of large cations or molecules may lead to minor tiltings of coordination polyhedra at their connections, i.e.

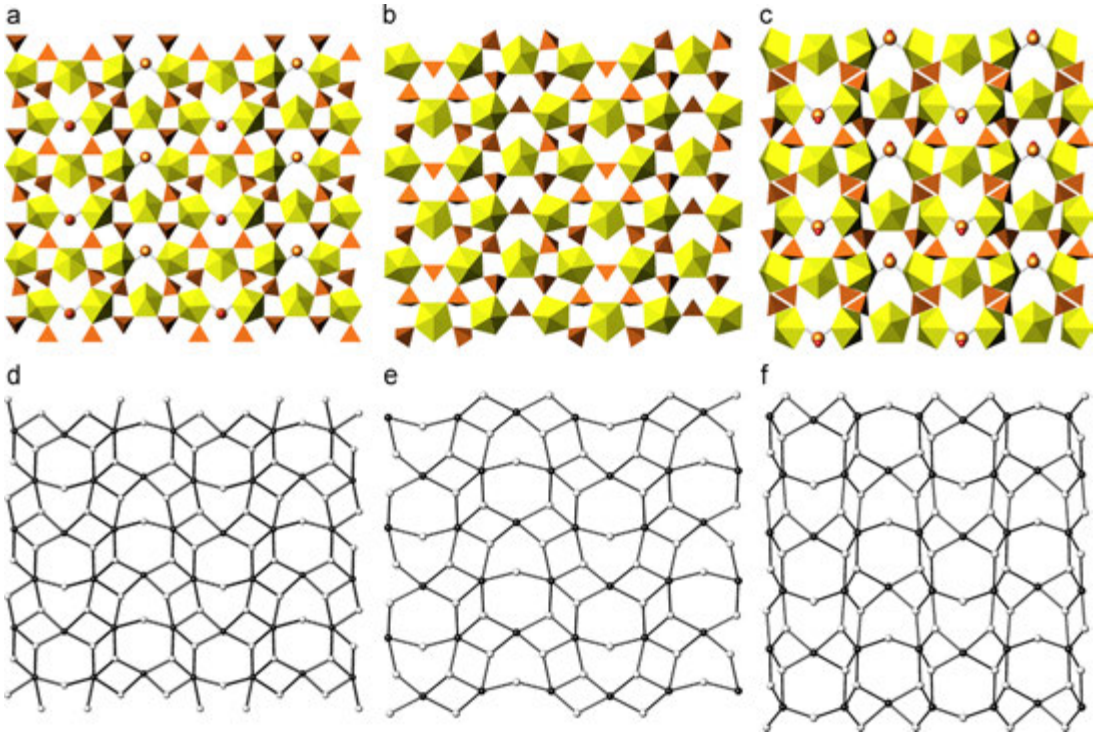

Fig. 7. The inorganic layers with U:Se=3:5 in the crystal structures of **V**, **VI**, and **VII**—(a), (b), and (c), respectively; their graphs—(d), (e) and (f), respectively. Legend is as in Fig. 5. See text for details.

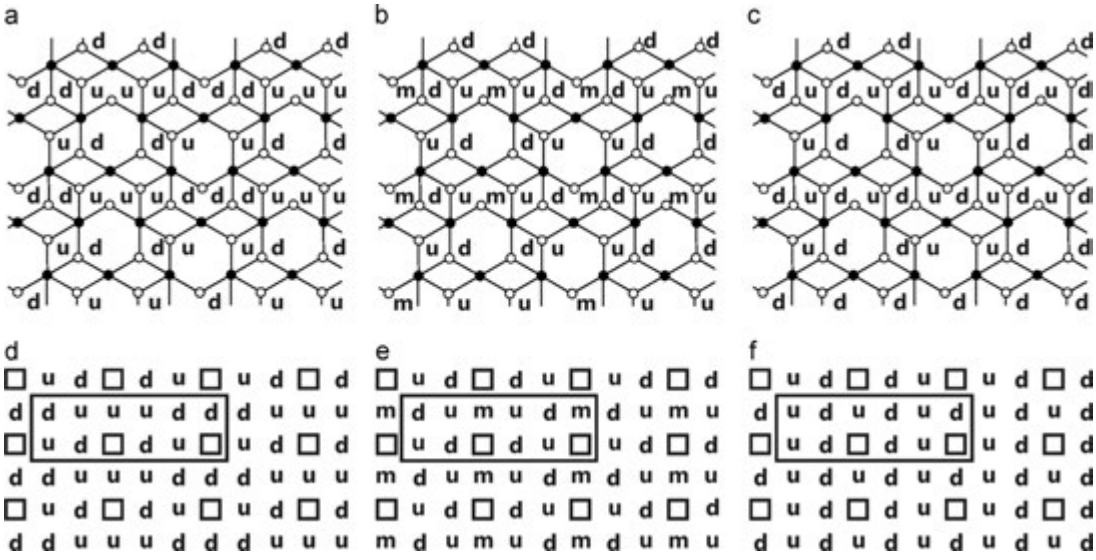

Fig. 8. Black-and-white graphs of the inorganic layers in the structures of **V**, **VI**, and **VII**—(a), (b) and (c), respectively, with the orientation symbols of selenium polyhedra; extended tables of orientation symbols (d), (e) and (f), respectively. Translational independent orientation matrices are selected in extended tables by rectangular areas.

around bridging oxygen atoms, to result in a symmetry reduction [60] compared to the ideal symmetry of structural units. In some cases, interactions between interlayer species and uranyl oxysalt units result in distortion of the layer planes and, in rare cases, formation of tubular structures [12–14]. The total effect of the 2-D unit bending includes rotation and displacements of individual U–O_{br}–T fragments (Fig. 10).

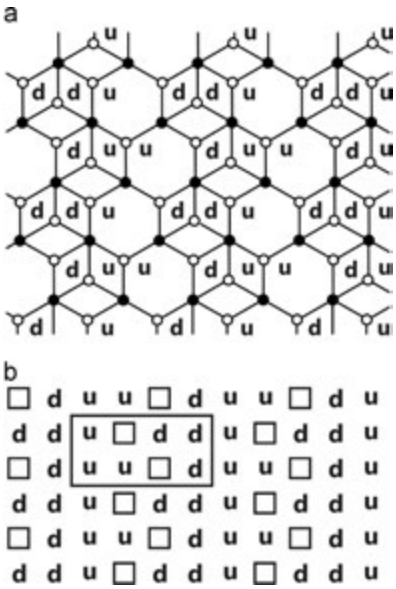

Fig. 9. Black-and-white graph of the inorganic layers in the structures of **II**, and **III** (a) with the orientation symbols of selenium polyhedra; extended tables of orientation symbols—(b). Translational independent orientation matrices are selected in (b) by rectangular areas.

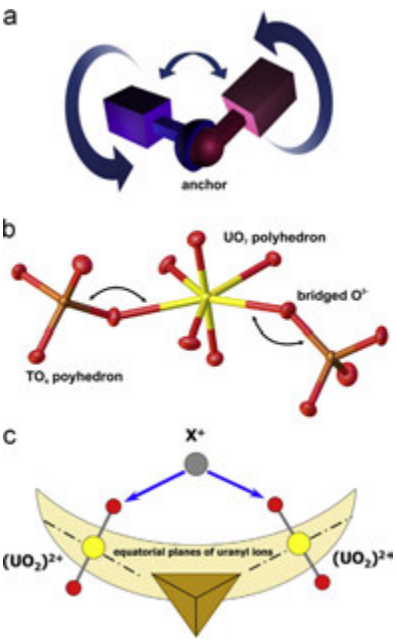

Fig. 10. Ball-in-socket joint model (a) and its working principle in the structures of uranyl containing compounds (b and c).

Therefore, it can be assumed that the value of the layer distortion can be determined by analyzing the bond angles at bridging oxygen atoms. This principle has a restricted application and works only locally, because of the fact that polyhedral tiltings are often occur in the layer plane. It might be assumed that the lower the average U–O–T angle, the higher the degree of the layer distortion. However, Table 2 and Fig. 11 show that the average value of the bridging angles for the most flat layers (**IV**) is less than the average value for the most distorted ones (**VII**). However, the smallest angle in the structure of **VII** [124.9(11) Å] matches the "wave's crest", while the biggest angle (157.2(13) Å) stretches along the "wave's wall" (Fig. 12). The same observation could be also attributed, for instance, to the structure of **II**, where the similar pair of angles [128.7(4) and 143.3(4) Å] arranged in the similar way. Thus, the local distribution of the U–O–Se links supports the suggestion that the lower U–O_{br}–T angles correspond to the direction of the higher layer undulation. Another point is that the average angles arranged in the middle part of the interval even for highly distorted layers, which could be explained by the tendency of the layer to flatten itself at least partially.

Table 2
The U–O_{br}–Se bond angles (°) in the structures of **I**–**VII**.

I		U3–O4–Se4	141.2 (6)
U1–O3–Se1	138.0 (4)	U3–O17–Se4	132.3 (6)
U1–O5–Se1	137.4 (4)	U3–O8–Se5	132.8 (6)
U1–O7–Se2	141.6 (3)	U3–O29–Se6	135.7 (6)
U1–O9–Se2	137.1 (4)	U4–O12–Se4	133.8 (6)
⟨U–O_{br}–Se⟩	138.5	U4–O5–Se5	132.2 (6)
		U4–O10–Se5	143.2 (7)
II		U4–O16–Se6	134.4 (6)
U1–O3–Se1	134.0 (4)	⟨U–O_{br}–Se⟩	135.6
U1–O5–Se1	143.3 (4)		
U1–O8–Se2	137.1 (4)	**V**	
U1–O9–Se2	133.8 (3)	U1–O1–Se1	134.3 (3)
U1–O16–Se3	132.5 (3)	U1–O4–Se2	141.3 (4)
U2–O6–Se1	128.7 (4)	U1–O12–Se1	131.4 (3)
U2–O10–Se2	133.8 (3)	U1–O8–Se2	142.9 (4)
U2–O14–Se3	143.6 (4)	U1–O9–Se3	136.8 (3)
U2–O15–Se3	134.0 (4)	U2–O2–Se1	142.9 (3)
⟨U–O_{br}–Se⟩	135.6	U2–O5–Se2	161.0 (5)
		⟨U–O_{br}–Se⟩	141.5
III			
U1–O4–Se1	140.9 (3)	**VI**	
U1–O5–Se1	143.6 (4)	U1–O4–Se1	150.3 (4)
U1–O6–Se2	133.8 (3)	U1–O14–Se2	136.1 (4)
U1–O3–Se3	132.9 (3)	U2–O5–Se1	133.7 (4)
U1–O7–Se3	133.4 (4)	U2–O6–Se1	132.7 (4)
U2–O13–Se1	131.2 (3)	U2–O10–Se2	134.5 (4)
U2–O10–Se2	138.1 (3)	U2–O12–Se2	153.4 (4)
U2–O11–Se2	136.5 (3)	U2–O11–Se3	135.3 (4)
U2–O12–Se3	134.6 (3)	⟨U–O_{br}–Se⟩	139.4
⟨U–O_{br}–Se⟩	136.1		
		VII	
IV		U1–O9–Se1	132.8 (10)
U1–O7–Se1	132.3 (5)	U1–O14–Se1	132.6 (13)
U1–O11–Se1	133.4 (6)	U1–O1–Se2	157.2 (13)
U1–O2–Se2	140.9 (6)	U1–O5–Se2	139.4 (10)
U1–O18–Se3	135.5 (6)	U1–O11–Se3	124.9 (11)
U2–O6–Se1	140.2 (7)	U2–O15–Se1	137.0 (11)
U2–O1–Se2	133.5 (6)	U2–O6–Se2	139.2 (11)
U2–O3–Se2	133.5 (6)	⟨U–O_{br}–Se⟩	137.6
U2–O13–Se3	134.0 (6)		

4. Conclusion

In this paper, we have reported seven new uranyl oxysalts with selenium and organic amines. The observed topologies of the structural units of new compounds have been investigated using graphs, and the special approach based upon construction of orientation matrices has been applied to distinguish different geometrical isomers of uranyl selenates and selenite–selenates with the same structural topologies. The statistical analysis of the U–O_{br}–Se bond angles in selenium polyhedra in the crystal structures showed the possibility for the specification of the undulation of crystal complexes. Further analysis of the data accumulated for uranyl oxysalts may

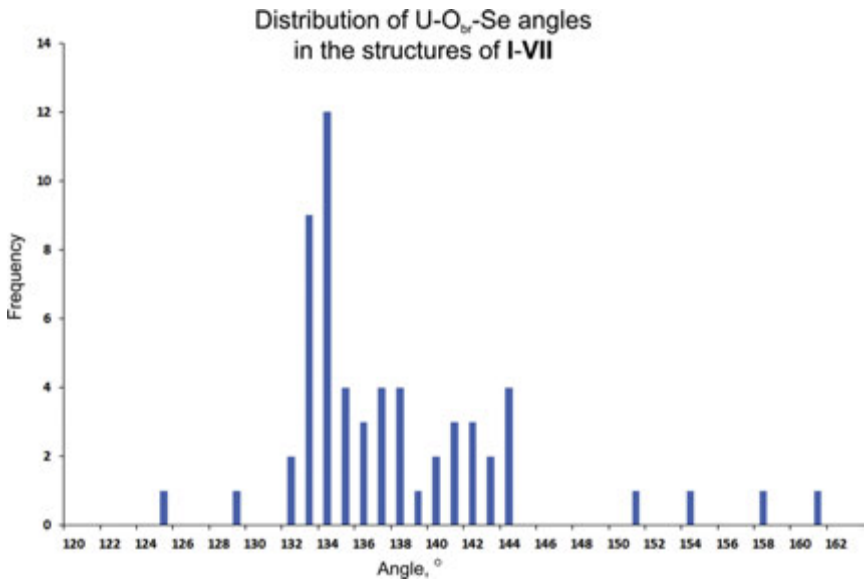

Fig. 11. Distribution of U–O_{br}–Se angles in the structures of **I–VII**.

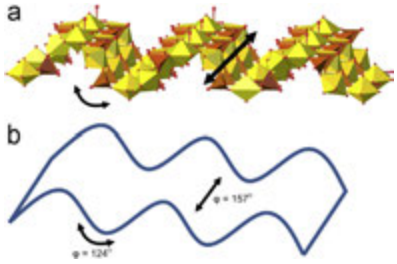

Fig. 12. The smallest angle (124.9(11) Å) in the structure of **VII** matches the "wave's crest" while the biggest angle (157.0(13) Å) stretches along the "wave's wall"; fragment of the structure of **VII** (a) and its schematic view (b).

provide more details for understanding of how cations of various shape and dimensionality influence topology and geometry of complex inorganic substructures.

Acknowledgments

This work was supported by St. Petersburg State University (internal grant 3.38.136.2014), President of Russian Federation grant for young scientists (no. MK-1737.2014.5 to VVG) and Russian Foundation for Basic Research (grant 12-05-33097 to VMK). X-ray diffraction studies were carried out in the X-ray Diffraction Centre of St. Petersburg State University.

Appendix A. Supporting information

Supplementary data associated with this article can be found in the online version at http://dx.doi.org/10.1016/j.jssc.2015.04.040.

References

[1] S.V. Krivovichev, P.C. Burns, Can. Mineral. 43 (2005) 713–720.
[2] S.V. Krivovichev, P.C. Burns, Can. Mineral. 41 (2003) 707–719.
[3] S.V. Krivovichev, P.C. Burns, Can. Mineral. 40 (2002) 201–209.
[4] G.E. Sigmon, P.C. Burns, J. Am. Chem. Soc. 133 (2011) 9137–9139.
[5] P.C. Burns, C.R. Chim. 13 (2010) 737–746.
[6] G.E. Sigmon, B. Weaver, K.A. Kubatko, P.C. Burns, Inorg. Chem. 48 (2009) 10907–10909.
[7] P.C. Burns, K.A. Kubatko, G.E. Sigmon, B.J. Fryer, J.E. Gagnon, M.R. Antonio, L. Soderholm, Angew. Chem. Int. Ed. 44 (2005) 2135–2139.
[8] J. Ling, M. Ozga, M. Stoffer, P.C. Burns, Dalton Trans. 41 (2012) 7278–7284.
[9] J. Ling, J. Qiu, P.C. Burns, Inorg. Chem. 51 (2012) 2403–2408.
[10] P.C. Burns, Mineral. Mag. 75 (2011) 1–25.
[11] J. Ling, J. Qiu, J.E.S. Szymanowski, P.C. Burns, Chem. Eur. J 17 (2011) 2571–2574.
[12] S.V. Krivovichev, V. Kahlenberg, R. Kaindl, E. Mersdorf, I.G. Tananaev, B.F. Myasoedov, Angew. Chem. Int. Ed. 44 (2005) 1134–1136.
[13] S.V. Krivovichev, V. Kahlenberg, I.G. Tananaev, R. Kaindl, E. Mersdorf, B.F. Myasoedov, J. Am. Chem. Soc. 127 (2005) 1072–1073.
[14] E.V. Alekseev, S.V. Krivovichev, W. Depmeier, Angew. Chem. Int. Ed. 47 (2008) 549–551.
[15] V.V. Gurzhiy, S.V. Krivovichev, . Vestn S.-Peterb. Univ., Ser. : Geol., Geogr. 7 vol. 3 (2008) 33–40.
[17] S.V. Krivovichev, V. Kahlenberg, J. Alloys Compd. 395 (2005) 41–47.
[18] S.V. Krivovichev, V. Kahlenberg, J. Alloys Compd. 389 (2005) 55–60.
[19] S.V. Krivovichev, V. Kahlenberg, Z. Anorg. Allg. Chem. 630 (2004) 2736–2742.
[20] L.J. Jouffret, E.M. Wylie, P.C. Burns, Z. Anorg. Allg. Chem. 638 (2012) 1796–1803.
[21] V.V. Gurzhiy, P.A. Mikhailenko, S.V. Krivovichev, I.G. Tananaev, B.F. Myasoedov, Russ. J. Gen. Chem. 82 (2012) 23–26.
[22] V.M. Kovrugin, V.V. Gurzhiy, S.V. Krivovichev, I.G. Tananaev, B.F. Myasoedov, Mendeleev Commun. 22 (2012) 11–12.
[23] S.V. Krivovichev, V.V. Gurzhiy, I.G. Tananaev, B.F. Myasoedov, Z. Kristallogr. 224 (2009) 316–324.
[24] S.V. Krivovichev, V.V. Gurzhiy, I.G. Tananaev, B.F. Myasoedov, Russ. J. Gen. Chem. 79 (2009) 2723–2730.
[25] G.M. Sheldrick, SADABS, Univ. Gottingen, Germany, 2004.
[26] Stoe & Cie, (Darmstadt, Germany): Stoe & Cie GmbH, 2005.
[27] A. Altomare, G. Cascarano, C. Giacovazzo, A. Guagliardi, M.C. Burla, G. Polidori, M. Camalli, J. Appl. Crystallogr. 27 (1994) 435.
[28] G.M. Sheldrick, Acta Crystallogr. A 64 (2008) 112–122.
[29] O.V. Dolomanov, L.J. Bourhis, R.J. Gildea, J.A.K. Howard, H. Puschmann, Appl. Crystallogr. 42 (2009) 339–341.
[30] M. Koskenlinna, I. Mutikainen, T. Leskela, M. Leskela, Acta Chem. Scand. 51 (1997) 264–269.
[31] P.M. Almond, T.E. Albrecht-Schmitt, Inorg. Chem. 41 (2002) 1177–1183.

[32] S.V. Krivovichev, I.G. Tananaev, V. Kahlenberg, B.F. Myasoedov, Dokl. Phys. Chem. 403 (2005) 124–127.
[33] S.V. Krivovichev, I.G. Tananaev, V. Kahlenberg, B.F. Myasoedov, Radiochemistry 48 (2006) 217–222.
[34] S.V. Krivovichev, Radiochemistry 46 (2004) 434–437.
[35] S.V. Krivovichev, V. Kahlenberg, E.Yu. Avdontseva, E. Mersdorf, R. Kaindl, Eur. J. Inorg. Chem. 2005 (2005) 1653–1656.
[36] S.V. Krivovichev, Crystallogr. Rev. 10 (2004) 185–232.
[37] S.V. Krivovichev, Structural Crystallography of Inorganic Oxysalts, Oxford University Press, Oxford, 2008.
[38] S.V. Krivovichev, Eur. J. Inorg. Chem. 2010 (2010) 2594–3437.
[39] V.V. Tabachenko, V.N. Serezhkin, L.B. Serezhkina, L.M. Kovba, Zh. Neorg. Khim. 5 (1979) 1563–1568.
[40] Yu.N. Mikhailov, Yu.E. Gorbunova, E.A. Demchenko, L.B. Serezhkina, V.N. Serezhkin, Zh. Neorg. Khim. 45 (2000) 1711–1713.
[41] A.J. Norquist, P.M. Thomas, M.B. Doran, D. O'Hare, Chem. Mater. 14 (2002) 5179–5184.
[42] A.J. Norquist, M.B. Doran, P.M. Thomas, D. O'Hare, Dalton Trans. 2003 (2003) 1168–1175.
[43] A.J. Norquist, M.B. Doran, Solid State Sci. 5 (2003) 1149–1158.
[44] P.M. Thomas, A.J. Norquist, M.B. Doran, J. Mater. Chem. 13 (2003) 88–92.
[45] C.L. Stuart, M.B. Doran, A.J. Norquist, D. O'Hare, Acta Crystallogr. E 59 (2003) m446–m448.
[46] R. Mercier, T.M. Pham, P. Colomban, Solid State Ionics 15 (1985) 113–126.
[47] T.M. Gesing, C.H. Rüscher, Z. Anorg. Chem. 626 (2000) 1414–1420.
[48] S.V. Krivovichev, V. Kahlenberg, Z. Naturforsch. 60b (2005) 538–542.
[49] S.V. Krivovichev, V. Kahlenberg, Z. Anorg. Chem 631 (2005) 2352–2357.
[50] V.M. Kovrugin, V.V. Gurzhiy, S.V. Krivovichev, Struct. Chem. 23 (2012) 2003–2017.
[51] M.B. Doran, A.J. Norquist, D. O'Hare, Inorg. Chem. 42 (2003) 6989–6995.
[52] S.V. Krivovichev, V.V. Gurzhii, I.G. Tananaev, B.F. Myasoedov, Dokl. Phys. Chem. 409 (2006) 228–232.
[53] V.V. Gurzhiy, O.S. Tyumentseva, S.V. Krivovichev, I.G. Tananaev, B.F. Myasoedov, Radiochemistry 54 (2012) 43–47.
[54] Y.u.N. Mikhailov, Y.u.E. Gorbunova, L.B. Serezhkina, V.N. Serezhkin, Zh. Neorg. Khim. 42 (1997) 734–738.
[55] S.V. Krivovichev, P.C. Burns, Z. Kristallogr. 218 (2003) 725–732.
[56] S.V. Krivovichev, I.G. Tananaev, B.F. Myasoedov, Radiochemistry 48 (2006) 552–560.
[57] S.V. Krivovichev, V. Kahlenberg, Z. Anorg. Allg. Chem. 631 (2005) 739–744.
[58] S.V. Krivovichev, P.C. Burns, Z. Kristallogr. 218 (2003) 683–690.
[59] S.V. Krivovichev, P.C. Burns, I.G. Tananaev, Structural Chemistry of Inorganic Actinide Compounds, Elsevier, The Netherlands (2007) 494.
[60] V.V. Gurzhiy, D.V. Tyshchenko, S.V. Krivovichev, I.G. Tananaev, Z. Kristallogr. 229 (2014) 368–377.

A-VII
Emulating exhalative chemistry: synthesis and structural characterization of ilinskite, $Na[Cu_5O_2](SeO_3)_2Cl_3$, and its K-analogue

Vadim M. Kovrugin, Oleg I. Siidra, Marie Colmont, Olivier Mentré, and Sergey V. Krivovichev

Published in: *Mineralogy and Petrology*, 2015, Vol. 109, 421–430.
DOI: 10.1007/s00710-015-0369-3

Miner Petrol (2015) 109:421–430
DOI 10.1007/s00710-015-0369-3

ORIGINAL PAPER

Emulating exhalative chemistry: synthesis and structural characterization of ilinskite, $Na[Cu_5O_2](SeO_3)_2Cl_3$, and its K-analogue

Vadim M. Kovrugin · Oleg I. Siidra · Marie Colmont · Olivier Mentré · Sergey V. Krivovichev

Received: 11 November 2014 / Accepted: 6 February 2015 / Published online: 19 February 2015

Abstract The K- and Na-synthetic analogues of the fumarolic mineral ilinskite have been synthesized by the chemical vapor transport (CVT) reactions method. The A-$[Cu_5O_2](SeO_3)_2Cl_3$ ($A^+ = K^+$, Na^+) compounds crystallize in the orthorhombic space group *Pnma*: a = 18.1691(6) Å, b = 6.4483(2) Å, c = 10.5684(4) Å, V = 1238.19(7) Å^3, R_1 = 0.018 for 1957 unique reflections with $F > 4\sigma_F$ for $K[Cu_5O_2](SeO_3)_2Cl_3$ (**KI**), and a = 17.7489(18) Å, b = 6.4412(6) Å, c = 10.4880(12) Å, V = 1199.0(2) Å^3, R_1 = 0.049 for 1300 unique reflections with $F > 4\sigma_F$ for $Na[Cu_5O_2](SeO_3)_2Cl_3$ (**NaI**). The crystal structures of **KI** and **NaI** are based upon the $[O_2Cu_5]^{6+}$ sheets consisting of corner-sharing $(OCu_4)^{6+}$ tetrahedra. The Na-for-K substitution results in the significant expansion of the interlayer space and changes in local coordination of some of the Cu^{2+} cations. The A^+ cation coordination changes from fivefold (for Na^+) to ninefold (for K^+). The CVT reactions method provides a unique opportunity to model physicochemical conditions existing in fumarolic environments and may be used not only to model exhalative processes, but also to predict possible mineral phases that may form in fumaroles. In particular, the K analogue of ilinskite is not known in nature, whereas it may well form from volcanic gases in a K-rich local geochemical environment.

Editorial handling: A. Beran

V. M. Kovrugin · M. Colmont · O. Mentré
UCCS, ENSCL, Université Lille 1, CNRS, UMR 8181,
59652 Villeneuve d'Ascq, France

V. M. Kovrugin · O. I. Siidra · S. V. Krivovichev (✉)
Department of Crystallography, Institute of Earth Sciences,
St. Petersburg State University, University emb. 7/9, 199034
St. Petersburg, Russia
e-mail: s.krivovichev@spbu.ru

Introduction

Exhalative geochemistry and mineralogy have attracted considerable attention recently, owing to the discovery of a wide range of minerals that form during condensation of volcanic gases in fumaroles (Demartin et al. 2013, 2014; Garavelli et al. 2013; Mitolo et al. 2013; Krivovichev et al. 2013a; Shuvalov et al. 2013; Pinto et al. 2014; Pekov et al 2013a, b, c, d, 2014a, b, c; Murashko et al. 2013; Vergasova et al. 2014). Of particular interest are copper oxoselenite chlorides, which, in addition to their mineralogical interest, possess rich and unique structural chemistry and special magnetic properties (Burns and Hawthorne 1995; Bastide et al. 2000; Millet et al. 2001; Burns et al. 2002; Krivovichev et al. 2006; Zhang et al. 2010; Berdonosov et al. 2013).

Most of naturally occurring copper selenite oxyhalide minerals contain "additional" oxygen atoms that are coordinated solely by Cu^{2+} cations, resulting in the formation of oxocentered $(OCu_4)^{6+}$ tetrahedra: allochalcoselite, $Cu^+[PbCu^{2+}{}_5O_2](SeO_3)_2Cl_5$ (Krivovichev et al. 2006), burnsite, $KCd[Cu_7O_2](SeO_3)_2Cl_9$ (Burns et al. 2002), chloromenite $[Cu_9O_2](SeO_3)_4Cl_6$ (Krivovichev et al. 1998), francisite, $[Cu_3BiO_2](SeO_3)_2Cl$ (Pring et al. 1990), georgbokiite, α–$[Cu_5O_2](SeO_3)_2Cl_2$ (Krivovichev et al. 1999a), nicksobolevite, $[Cu_7O_2](SeO_3)_2Cl_6$ (Vergasova et al. 2014), parageorgbokiite β–$[Cu_5O_2](SeO_3)_2Cl_2$ (Krivovichev et al. 2007), prewittite $KPb_{0.5}Cu[PbCu_5O_2]Zn(SeO_3)_2Cl_{10}$ (Shuvalov et al. 2013). It is the unique feature of Cu^{2+} to form anion-centered units of different dimensionalities reviewed recently by Krivovichev et al. (2013b). These minerals form as a result of volcanic exhalative processes that can be modeled using gas transport reactions as was originally suggested by Filatov et al. (1992) and confirmed by a number of successful syntheses of mineral analogues under laboratory conditions by chemical vapor transport (CVT)

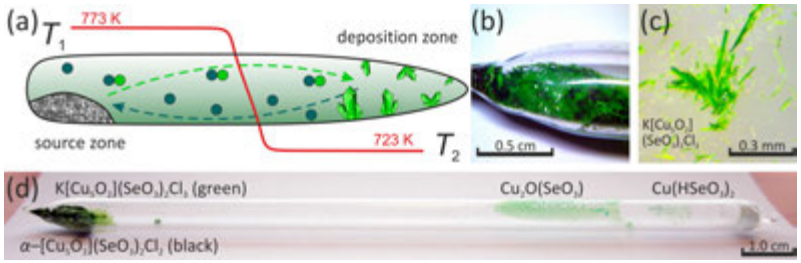

Fig. 1 General scheme of the CVT method (**a**), the source zone of the tube (**b**), the crystals of $K[Cu_5O_2](SeO_3)_2Cl_3$ picked out from the source zone (**c**), and a common view of the sealed silica tube after the CVT synthesis (**d**)

reactions method (Millet et al. 2001; Krivovichev et al. 2004; Berdonosov et al. 2009; Zhang et al. 2010; Kovrugin et al. 2015).

In this paper, we report on the synthesis and crystal structures of K- and Na-synthetic analogues of ilinskite (Vergasova et al. 1997; Krivovichev et al. 2013c), a rare mineral from volcanic fumaroles of the Tolbachik volcano (Kamchatka peninsula, Russia).

Experimental

Single crystals of $K[Cu_5O_2](SeO_3)_2Cl_3$ (**KI**) and $Na[Cu_5O_2](SeO_3)_2Cl_3$ (**NaI**) were prepared by the chemical vapor transport (CVT) reactions method (Binnewies et al. 2013). In the course of the CVT reactions a precursor is partially transported by a gaseous agent from a source zone to a deposition zone under the action of a temperature gradient.

Table 1 Crystallographic data and refinement parameters for **KI** and **NaI**

	$K[Cu_5O_2](SeO_3)_2Cl_3$	$Na[Cu_5O_2](SeO_3)_2Cl_3$
Crystal data:		
Temperature	293 K	293 K
Radiation	MoK_α, 0.71073 Å	MoK_α, 0.71073 Å
Crystal system	orthorhombic	orthorhombic
Space group	*Pnma*	*Pnma*
a (Å)	18.1691(6)	17.7489(18)
b (Å)	6.4483(2)	6.4412(6)
c (Å)	10.5684(4)	10.4880(12)
Volume ($Å^3$)	1238.19(7)	1199.0(2)
Z	4	4
D_{calc} (g/cm^3)	4.018	4.060
μ (mm^{-1})	15.333	15.523
Crystal size (mm^3)	0.25 × 0.10 × 0.08	0.21 × 0.11 × 0.08
Data collection:		
θ range	2.23 – 31.54°	2.27 – 31.02°
h, *k*, *l* ranges	−26 → 26, −8 → 9, −14 → 15	−17 → 25, −9 → 6, −15 → 15
Total reflections collected	9584	7946
Unique reflections (R_{int})	2233 (0.0265)	2042 (0.0984)
Unique reflections $F > 4\sigma_F$	1957	1300
Structure refinement:		
Refinement method	Full-matrix least-squares on F^2	
Weighting scheme	$w = 1/[\sigma^2(F_o^2) + (0.023P)^2]$, where $P = (F_o^2 + 2F_c^2)/3$	
Extinction coefficient	0.00079(8)	none
$R_1[F > 4\sigma_F]$, $wR_2[F > 4\sigma_F]$	0.018, 0.040	0.049, 0.065
R_1 all, wR_2 all	0.023, 0.041	0.099, 0.077
Goodness-of-fit	1.035	0.991
Largest diff. peak and hole, e $Å^{-3}$	0.735, −0.765	1.617, −1.668

The general scheme of the CVT method is shown in Fig. 1a. A mixture of CuO (0.318 g, 4 mmol), $CuCl_2$ (0.134 g, 1 mmol), SeO_2 (0.222 g, 2 mmol) and KCl (0.075 g, 1 mmol) for **KI** (NaCl (0.058 g, 1 mmol) for **NaI**) were grounded and loaded into a silica tube (*ca.* 15 cm), which was further evacuated to 10^{-2} mbar and sealed. The tubes were placed horizontally into a tubular two-zone furnace, heated to 773 K for 3 days and subsequently slowly cooled to room temperature. The temperature gradient between the source (hot) and deposition (cold) zones of the tube in the furnace was about 50 K. Green needle-like single crystals of **KI** (Fig. 1c) and **NaI** were observed in the source zones of the tubes (Fig. 1b) in association with black block-shaped crystals of synthetic georgbokiite, α–$[Cu_5O_2](SeO_3)_2Cl_2$ (Krivovichev et al. 1999a). Green platy crystals of $Cu_2O(SeO_3)$ (Effenberger and Pertlik 1986) were found in the middle part, while transparent elongated crystals of $Cu(HSeO_3)_2$ (Effenberger 1985) occurred in the deposition zone of the tubes (Fig. 1d).

The crystals of **KI** and **NaI** selected for the X-ray diffraction data collection were mounted on a Bruker APEX II X-ray diffractometer equipped with a microfocus MoK_α (λ = 0.71073 Å) X-ray tube operated at 50 kV and 40 mA. The unit-cell dimensions (Table 1) for both compounds were refined by the least-squares techniques. The data were integrated and corrected for absorption and background effects using the Bruker program packages. The solution and refinement of the crystal structures of **KI** and **NaI** were performed using the SHELXL program package (Sheldrick 2008). Both

Table 2 Atomic coordinates and equivalent isotropic displacement parameters of atoms in the structures of $A[Cu_5O_2](SeO_3)_2Cl_3$ ($A^+ = K^+$, Na^+) and ilinskite (Krivovichev et al. 2013c). $U_{eq} = (1/3)\Sigma_i\Sigma_j U_{ij} a_i a_j \mathbf{a_i}\cdot\mathbf{a_j}$

Atom		A = K	A = Na	ilinskite	Atom		A = K	A = Na	ilinskite
	x	0.40349(4)	0.4076(3)	0.40541(13)	Cl2	x	0.54316(5)	0.53659(16)	0.53666(9)
	y	1/4	1/4	1/4		y	1/4	1/4	1/4
	z	0.74241(7)	0.7359(5)	0.7360(3)		z	−0.12462(11)	−0.1356(3)	−0.13445(17)
	U_{eq}/Å^2	0.02347(15)	0.0502(15)	0.0370(7)		U_{eq}/Å^2	0.0431(3)	0.0375(8)	0.0361(4)
Cu1	x	0.59855(2)	0.59928(6)	0.59925(3)	Cl3	x	0.74081(5)	0.75484(16)	0.75419(9)
	y	1/4	1/4	1/4		y	1/4	1/4	1/4
	z	0.49282(3)	0.49980(11)	0.49944(6)		z	0.76767(9)	0.7729(3)	0.77233(15)
	U_{eq}/Å^2	0.01207(8)	0.0123(3)	0.0123(1)		U_{eq}/Å^2	0.0347(2)	0.0330(7)	0.0339(3)
Cu2	x	0.64034(2)	0.63266(7)	0.63306(3)	O1	x	0.76868(10)	0.7730(3)	0.77281(17)
	y	1/4	1/4	1/4		y	−1/4	−1/4	−1/4
	z	−0.00210(4)	−0.00159(11)	−0.00162(6)		z	0.59776(18)	0.5958(5)	0.5962(3)
	U_{eq}/Å^2	0.01364(8)	0.0135(3)	0.0134(1)		U_{eq}/Å^2	0.0099(4)	0.0088(13)	0.0095(5)
Cu3	x	0.71965(2)	0.71861(7)	0.71866(3)	O2	x	0.70183(10)	0.7041(3)	0.70363(17)
	y	1/4	1/4	1/4		y	1/4	1/4	1/4
	z	0.27638(3)	0.27544(11)	0.27592(6)		z	0.45476(18)	0.4551(6)	0.4560(3)
	U_{eq}/Å^2	0.01261(8)	0.0131(3)	0.0132(1)		U_{eq}/Å^2	0.0094(3)	0.0089(13)	0.0104(5)
Cu4	x	0.73299(2)	0.73701(5)	0.73671(2)	O3	x	0.65743(7)	0.6516(2)	0.65176(13)
	y	0.00432(4)	0.00171(13)	0.00221(6)		y	−0.0537(2)	−0.0522(6)	−0.0515(4)
	z	0.53549(2)	0.53098(8)	0.53143(4)		z	0.01066(14)	0.0075(4)	0.0081(2)
	U_{eq}/Å^2	0.01281(6)	0.01442(19)	0.01384(9)		U_{eq}/Å^2	0.0136(3)	0.0124(10)	0.0147(4)
s	x	0.43000(2)	0.43047(6)	0.43037(2)	O4	x	0.49551(10)	0.4939(3)	0.49404(18)
	y	1/4	1/4	1/4		y	1/4	1/4	1/4
	z	0.41824(3)	0.42166(9)	0.42118(5)		z	0.53153(19)	0.5421(6)	0.5412(3)
	U_{eq}/Å^2	0.01051(6)	0.0106(2)	0.01026(9)		U_{eq}/Å^2	0.0158(4)	0.0149(15)	0.0161(7)
Se2	x	0.62105(2)	0.61514(5)	0.61556(2)	O5	x	0.67294(11)	0.6697(4)	0.67054(19)
	y	−1/4	−1/4	−1/4		y	−1/4	−1/4	−1/4
	z	−0.08073(3)	−0.08525(9)	−0.08483(4)		z	−0.21020(19)	−0.2131(6)	−0.2130(3)
	U_{eq}/Å^2	0.01014(6)	0.0101(2)	0.01012(9)		U_{eq}/Å^2	0.0166(4)	0.0168(15)	0.0169(7)
Cl1	x	0.59034(4)	0.58643(15)	0.58668(7)	O6	x	0.37690(7)	0.3753(2)	0.37550(13)
	y	1/4	1/4	1/4		y	0.0512(2)	0.0508(6)	0.0504(4)
	z	0.24841(7)	0.2508(3)	0.25060(13)		z	0.47371(15)	0.4727(5)	0.4733(3)
	U_{eq}/Å^2	0.01870(15)	0.0261(6)	0.0246(3)		U_{eq}/Å^2	0.0168(3)	0.0187(11)	0.0189(5)

structures were solved by direct methods in the orthorhombic *Pnma* space group and refined to the R_1 values of 0.018 for **KI** and 0.049 for **NaI**. The crystal quality of **NaI** was relatively poor that most probably results from a local intergrowth of twinned domains. Atom coordinates and displacement parameters are given in Table 2 and selected distances are in Table 3. The results of the bond-valence sum (BVS) analysis for **KI**, **NaI** and ilinskite are given in Table 4. All empirical bond-valence parameters required for the BVS calculations were taken from (Brese and O'Keeffe 1991). The BVS values obtained for Cl(3) are rather low (0.42 and 0.46 valence units (v.u.) for **KI** and **NaI**, respectively). This phenomenon is rather typical for copper oxoselenite chlorides (Krivovichev et al. 2013c; Kovrugin et al. 2015). Additional structural information is provided in the Supporting Information as Crystallographic information files (CIFs).

Results

$K[Cu_5O_2](SeO_3)_2Cl_3$ (**KI**) and $Na[Cu_5O_2](SeO_3)_2Cl_3$ (**NaI**) are isotypic and crystallize in the *Pnma* space group. The structural data for **NaI** are in full agreement with the data reported for natural ilinskite by (Krivovichev et al. 2013c). The differences between the structures of synthetic K- and Na-ilinskites are discussed below.

The crystal structures of **KI** and **NaI** contain four symmetrically independent Cu sites with different mixed-ligand coordination environments (Fig. 2). The Cu(1) site is coordinated by five ligands to form [(4O)+Cl] square pyramids. The similar coordination geometries have previously been reported in the crystal structures of nabokoite, $K_2Cu_7(TeO_4)(SO_4)_5Cl$ (Pertlik and Zemann 1988), and bobkingite, $Cu_5Cl_2(OH)_8(H_2O)_2$ (Hawthorne et al. 2002). The average <Cu(1)–O> distances are 1.971 and 1.965 Å for **KI** and **NaI**, respectively, whereas the Cu(1)–Cl(1) bond lengths are 2.587 and 2.621 Å for **KI** in **NaI**, respectively. The Cu(3) site has a distorted square coordination by three oxygen and one chlorine atom. This type of coordination geometry, [3O+Cl], has been observed recently in the crystal structure of $Na_2[Cu_7O_2](SeO_3)_4Cl_4$ (Kovrugin et al. 2015). The Cu(3)–O bond lengths are in the ranges of 1.900–1.957 Å in **KI** and of 1.890–1.985 Å in **NaI**. The Cu(3)–Cl1 bonds are 2.368 Å and 2.360 Å in **KI** and **NaI**, respectively.

The coordinations of the Cu(2) and Cu(4) sites in **KI** and **NaI** are different due to the shift of the Cl(3) site induced by the greater size of the K^+ cations compared to Na^+. The Cu(2) site has a distorted square pyramidal [(3O+Cl)+Cl] coordination in **NaI**, similar to the one observed in $Cu_3(MoO_4)(TeO_3)Cl_2(H_2O)_{0.5}$ (Takagi et al. 2006). In the crystal structure of **KI**, the Cu–Cl distance to the sixth nearest neighboring site Cl(3) (3.042 Å (0.06 v.u.)) is shorter than that in **NaI** (3.209 Å (0.04 v.u.)). Thus Cl(3) anion can be considered as a sixth ligand of a Jahn-Teller-distorted [(3O+Cl)+2Cl] octahedral environment of the Cu2 atom in the structure of **KI**, but not in the structure of **NaI**. The same coordinations were observed in the crystal structures of belloite, Cu(OH)Cl (Effenberger 1984), avdoninite, $K_2Cu_5Cl_8(OH)_4(H_2O)_2$ (Kahlenberg 2004; Chukanov et al. 2007), $SrCu_2(SeO_3)_2Cl_2$ (Berdonosov et al. 2009), and nicksobolevite, $Cu_7(SeO_3)_2O_2Cl_6$ (Vergasova et al. 2014). The opposite apical Cl(1) atom of the Cu(2) octahedron is located at the distance of 2.780 Å and 2.772 Å in **KI** and **NaI**, respectively. In the square plane of the polyhedron, the average <Cu(2)–O> bond length is equal to 1.979 Å in **KI** and

Table 3 Selected interatomic distances (Å) in the structures of $A[Cu_5O_2](SeO_3)_2Cl_3$ ($A^+ = K^+$, Na^+) and ilinskite (Krivovichev et al. 2013c). The italicized values are not considered as bonds owing to their bond-valences smaller than 0.05 v.u

	$K[Cu_5O_2](SeO_3)_2Cl_3$	$Na[Cu_5O_2](SeO_3)_2Cl_3$	ilinskite
*A*1–O4	2.786(2)	2.545(8)	2.585(4)
*A*1–Cl2	2.9009(11)	2.657(6)	2.688(3)
*A*1–Cl3	2.9575(11)	2.713(6)	2.702(3)
*A*1–Cl1	3.2276(1) 2x	3.2253(4) 2x	3.230(1) 2x
	3.1529(18) 2x	*3.098(7) 2x*	*3.095(5) 2x*
	3.1043(16) 2x	*3.157(7) 2x*	*3.150(4) 2x*
Cu1–O2	1.9163(19)	1.919(6)	1.910(3)
Cu1–O4	1.9191(18)	1.922(6)	1.921(3)
Cu1–O6	2.0238(15) 2x	2.010(4) 2x	2.009(2) 2x
Cu1–Cl1	2.5874(8)	2.621(3)	2.628(2)
Cu2–O1	1.9611(18)	1.961(6)	1.964(3)
Cu2–O3	1.9876(15) 2x	1.977(4) 2x	1.975(2) 2x
Cu2–Cl2	2.1896(9)	2.210(3)	2.211(2)
Cu2–Cl1	2.7989(8)	2.772(3)	2.779(2)
Cu2–Cl3	3.0419(9)	3.209(3)	3.208(2)
Cu3–O1	1.8996(19)	1.890(6)	1.897(3)
Cu3–O2	1.9128(19)	1.902(6)	1.914(3)
Cu3–O5	1.957(2)	1.985(7)	1.972(3)
Cu3–Cl1	2.3680(7)	2.360(3)	2.360(2)
Cu3–Cl3	*3.3045(2) 2x*	*3.2550(5) 2x*	*3.260(3) 2x*
Cu4–O1	1.8823(9)	1.871(3)	1.876(2)
Cu4–O2	1.8863(10)	1.879(3)	1.878(2)
Cu4–O3	2.0333(13)	2.019(4)	2.022(2)
Cu4–O6	2.0307(14)	2.022(4)	2.023(2)
Cu4–Cl3	2.9242(9)	3.016(3)	3.012(2)
Cu4–Cl3	3.3057(9)	3.159(3)	3.179(2)
Se1–O4	1.688(2)	1.692(6)	1.695(3)
Se1–O6	1.7083(14) 2x	1.701(4) 2x	1.705(2) 2x
<Se1–O>	1.702	1.698	1.702
Se2–O5	1.662(2)	1.655(6)	1.665(4)
Se2–O3	1.7238(14) 2x	1.729(4) 2x	1.734(2) 2x
<Se2–O>	1.703	1.704	1.711

1.972 Å in **NaI**; the Cu(2)–Cl(2) is 2.190 Å and 2.210 Å in **KI** and **NaI**, respectively.

In the crystal structure of **NaI**, the Cu(4) atom possesses an octahedral environment with four short equatorial Cu–O and two longer axial Cu–Cl bonds. The [(4O)+(2Cl)] type of an octahedral environment of Cu^{2+} cations is commonly observed in Pb-Cu oxyhalides, and has been described *e.g.*, in the crystal structures of leningradite, $PbCu_3(VO_4)_2Cl_2$ (Siidra et al. 2007), and chloroxiphite, $Pb_3CuO_2(OH)_2Cl_2$ (Siidra et al. 2008). The shift of the Cl(3) atoms is influenced by the larger size of K^+ cations in the structure of **KI** and results in the change of the two symmetrically inequivalent

Table 4 Bond-valence analysis (in valence units = v.u.) for the crystal structures of $A[Cu_5O_2](SeO_3)_2Cl_3$ ($A^+ = K^+$, Na^+) and ilinskite (Krivovichev et al. 2013c). The italicized values in brackets are given for interatomic distances that are not considered as bonds, and do not sum up in total

Compound	Site	O1	O2	O3	O4	O5	O6	Cl1	Cl2	Cl3	Σ
KI	*A*1			$0.07^{2x\rightarrow}$	0.17		$0.06^{2x\rightarrow}$	$0.13^{\times2\rightarrow\downarrow}$	0.23	0.20	1.12
NaI				(*0.03*$^{2x\rightarrow}$)	0.14		(*0.03*$^{2x\rightarrow}$)	$0.07^{\times2\rightarrow\downarrow}$	0.31	0.26	0.85
ilinskite				(*0.03*$^{2x\rightarrow}$)	0.12		(*0.03*$^{2x\rightarrow}$)	$0.07^{\times2\rightarrow\downarrow}$	0.28	0.27	0.81
KI	Cu1		0.53		0.52		$0.39^{2x\rightarrow}$	0.20			2.03
NaI			0.52		0.52		$0.41^{2x\rightarrow}$	0.19			2.05
ilinskite			0.54		0.52		$0.41^{2x\rightarrow}$	0.18			2.06
KI	Cu2	0.47		$0.43^{2x\rightarrow}$				0.12	0.60	0.06	2.11
NaI		0.47		$0.45^{2x\rightarrow}$				0.12	0.57	(*0.04*)	2.06
ilinskite		0.46		$0.45^{2x\rightarrow}$				0.12	0.57	(*0.04*)	2.05
KI	Cu3	0.55	0.53			0.47		0.37		(*0.03*$^{2x\rightarrow\downarrow}$)	1.92
NaI		0.57	0.55			0.44		0.38		(*0.03*$^{2x\rightarrow\downarrow}$)	1.94
ilinskite		0.55	0.53			0.45		0.38		(*0.03*$^{2x\rightarrow\downarrow}$)	1.91
KI	Cu4	$0.58^{2x\downarrow}$	$0.57^{2x\downarrow}$	0.38			0.39			$0.08^{2x\downarrow}$, (*0.03*$^{2x\downarrow}$)	2.00
NaI		$0.60^{2x\downarrow}$	$0.58^{2x\downarrow}$	0.40			0.40			$0.06^{2x\downarrow}$, $0.04^{2x\downarrow}$	2.08
ilinskite		$0.59^{2x\downarrow}$	$0.58^{2x\downarrow}$	0.39			0.40			$0.06^{2x\downarrow}$, $0.04^{2x\downarrow}$	2.06
KI	Se1				1.39		$1.32^{2x\rightarrow}$				4.03
NaI					1.38		$1.35^{2x\rightarrow}$				4.08
ilinskite					1.37		$1.33^{2x\rightarrow}$				4.03
KI	Se2			$1.27^{2x\rightarrow}$		1.50					4.04
NaI				$1.25^{2x\rightarrow}$		1.52					4.02
ilinskite				$1.23^{2x\rightarrow}$		1.48					3.94
KI	Σ	2.18	2.20	2.15	2.09	1.97	2.16	0.95	0.83	0.42	
NaI		2.24	2.23	2.10	2.04	1.96	2.16	0.83	0.88	0.46	
ilinskite		2.19	2.23	2.07	2.01	1.93	2.14	0.82	0.85	0.47	

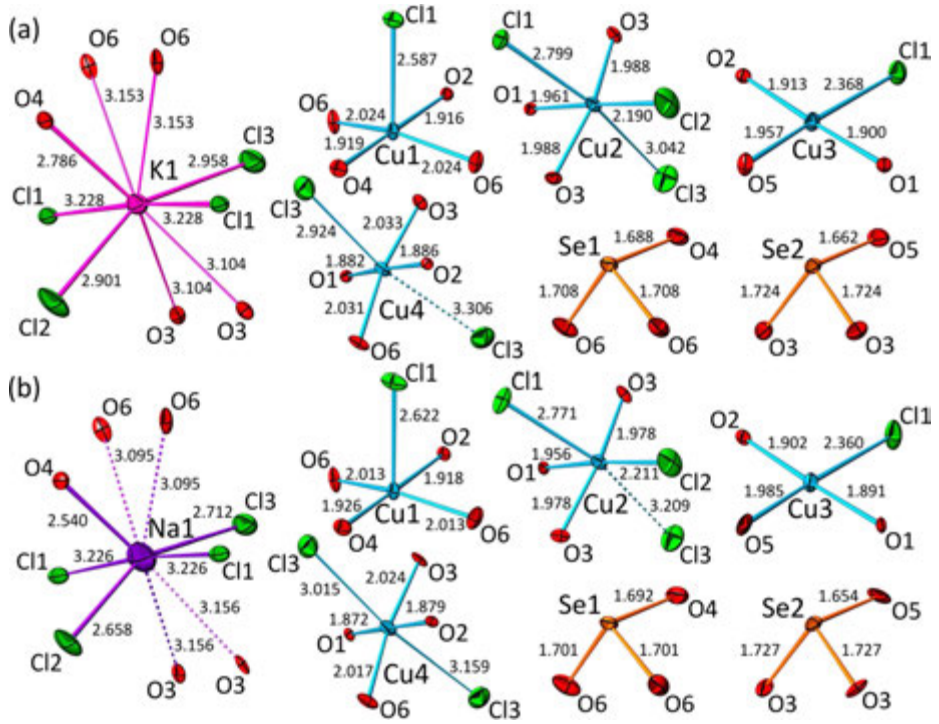

Fig. 2 Coordination of cations in the crystal structures of $K[Cu_5O_2](SeO_3)_2Cl_3$ (**a**) and $Na[Cu_5O_2](SeO_3)_2Cl_3$ (**b**). Legend: K^+ = *pink*; Na^+ = *violet*; Cu^{2+} = *cyan*; Se^{4+} = *orange*; O^{2-} = *red*; Cl^- = *green*. Displacement ellipsoids are drawn at the 50 % probability level

axial Cu(4)–Cl(3) bonds within the Cu(4) polyhedron: 2.924 Å (0.08 v.u.) and 3.306 Å (0.03 v.u.) in **KI** in contrast to 3.016 Å (0.06 v.u.) and 3.159 Å (0.04 v.u.) in **NaI**. Thus, the coordination of the Cu(4) site in **KI** can be regarded as a five-fold square [(4O)+(Cl)] pyramid with one axial Cu(4)–Cl(3) bond, analogous to the environment of the Cu(1) sites in both structures. The average <Cu(4)–O> bond lengths within the square plane of the Cu(4) polyhedron are equal to 1.958 Å and 1.948 Å in **KI** and **NaI**, respectively.

There are two symmetrically independent selenium sites in the crystal structures of **KI** and **NaI**. The Se^{4+} cations have typical oxygen coordination of triangular pyramid with a stereochemically active lone pair of electrons as a complementary ligand. The average <Se–O> distances are equal 1.702 Å and 1.703 Å for Se1 and Se2 sites, respectively in **KI**, and 1.698 Å and 1.704 Å for Se1 and Se2 sites, respectively in **NaI**.

According to the calculated BVSs (Table 4), the arrangement of alkali cations in the crystal structures of **KI** and **NaI** is different. The arrangement of coordinating ligands of Na^+ in **NaI** consists of one oxygen and four chlorines, forming a distorted [(O+2Cl)+2Cl] trigonal bipyramid (Fig. 2b). K^+ cations in **KI** are surrounded by five oxygen and four chlorine atoms each (Figs. 2a and 3).

The crystal structures of **KI** and **NaI** contain "additional" oxygen atoms, which are coordinated solely by Cu^{2+} cations,

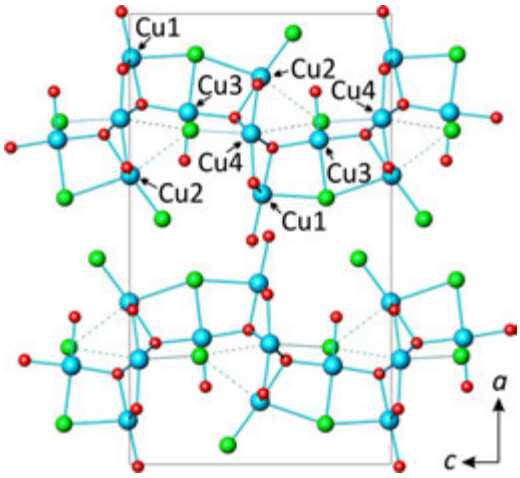

Fig. 3 Mode of linkage of the Cu coordination polyhedra in the crystal structures of $A[Cu_5O_2](SeO_3)_2Cl_3$ (A^+ = K^+, Na^+). Legend: Cu^{2+} = *cyan*; O^{2-} = *red*; Cl^- = *green*

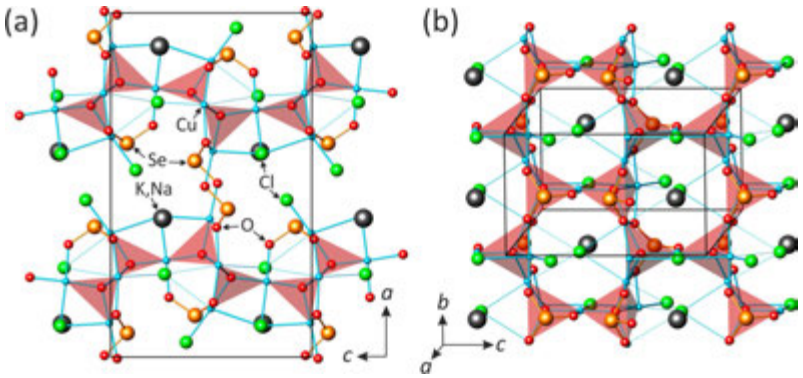

Fig. 4 The crystal structures of $A[Cu_5O_2](SeO_3)_2Cl_3$ ($A^+ = K^+$, Na^+) in two different projections featuring side and top view of the $[O_2Cu_5]^{6+}$ layer of oxocentered $(OCu_4)^{6+}$ tetrahedra. Legend: A^+ = *black*; Cu^{2+} = *cyan*; Se^{4+} = *orange*; O^{2-} = *red*; Cl^- = *green*; the $(OCu_4)^{6+}$ tetrahedra are highlighted by red. The *A*–O and *A*–Cl bonds are omitted for clarity

resulting in the formation of oxocentered $(OCu_4)^{6+}$ tetrahedra. The $(OCu_4)^{6+}$ tetrahedra share common corners to form the $[Cu_5O_2]^{6+}$ sheets parallel to (100) (Fig. 4a). These two-dimensional (2*D*) structural units resemble the $[Si_2O_5]^{2-}$ groups in phyllosilicates, where the cations and anions are inverted. Similar copper-oxide sheets with large pseudohexagonal pores were observed in the crystal structure of averievite, $[Cu_5O_2](VO_4)_2{\cdot}MCl$ ($M = Cu^+$, Rb^+, Cs^+) (Starova et al. 1997), and synthetic $[Pb_2Cu_3O_2](SeO_3)_2(NO_3)_2$ (Effenberger 1986). An important topological distinction between these 2*D* units is that the non-bonded apices of the $(OCu_4)^{6+}$ tetrahedra in 6-membered rings have different "up" and "down" orientations relative to the plane of the sheet. The sheet in the crystal structures of ilinskite-type compounds, $A[Cu_5O_2](SeO_3)_2Cl_3$ ($A^+ = K^+$, Na^+), is based upon **UUDUUD** rings (Fig. 4b), whereas the structure of averievite and synthetic $[Pb_2Cu_3O_2](SeO_3)_2(NO_3)_2$ consist of the sheets with **UDUDUD** topology (the **U** and **D** symbols identify the "up" and "down" orientations of the $O–Cu_{terminal}$ bond relative to the plane of the sheet).

The $[Cu_5O_2]^{6+}$ sheets in the crystal structures of **KI** and **NaI** are surrounded by selenite triangular pyramids and chlorine anions to produce a microporous framework. The pores are filled with alkali metal cations and lone pairs of electrons of selenite groups. It is noteworthy that two crystallographically independent selenite groups play different roles in the structural architecture. The O–O–O triangular planes of the $(Se(2)O_3)$ pyramids are parallel and attached to the Cu–Cu–Cu face of the $(O(2)Cu_4)^{6+}$ tetrahedra according to the 'face-to-face' principle (Krivovichev and Filatov 1999; Krivovichev et al. 1999b). The $(Se(1)O_3)$ groups are oriented perpendicular to the copper-oxide $[Cu_5O_2]^{6+}$ sheets and link them into a three-dimensional (3*D*) framework through strong Se–O–Cu bonds (Fig. 4a).

Discussion

The size of alkali cations in the crystal structures of **KI** and **NaI** has a significant influence upon their organization. The

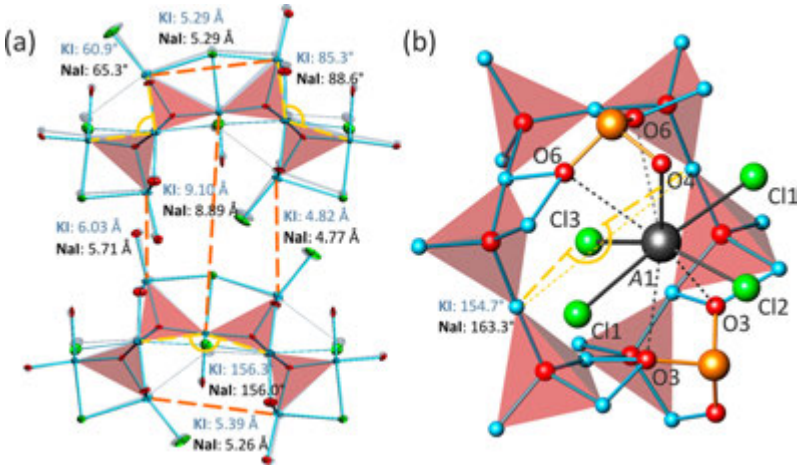

Fig. 5 Comparison of the superimposed crystal structures of $Na[Cu_5O_2](SeO_3)_2Cl_3$ (on top in color) and $K[Cu_5O_2](SeO_3)_2Cl_3$ (below in greyscale) (a: Na^+ and K^+ are omitted for clarity) and the coordination environments of the *A*1 atoms (**b**). Legend is the same as in Fig. 4. Displacement ellipsoids in (**a**) are drawn at the 50 % probability level

substitution of smaller Na^+ cations (R_{ion} = 1.02 Å, Shannon (1976)) by larger K^+ cations (R_{ion} = 1.38 Å) leads to the expansion of alkali metal coordination polyhedra and, as a result, in the enlarged unit-cell parameters of $K[Cu_5O_2](SeO_3)_2Cl_3$ compared to its Na analogue.

The *a* parameter value is most seriously influenced by the increased size of an alkali metal atom: it enlarges by 0.420 Å from 17.749 Å in **NaI** to 18.169 Å in **KI**, whereas the *b* and *c* unit-cell parameters do not undergo significant changes (Δ = + 0.071 Å and Δ = +0.080 Å for the *b* and *c* parameters, respectively). It can be explained by the fact that the major size-effect occurs in separating further the complex copper oxide-selenite sheets parallel to (100). One of the shortest distance between the two closest copper cations from the adjacent sheets changes from 5.705 Å in **NaI** to 6.034 Å in **KI** (Δ = +0.329 Å). The longest Cu–Cu distance increases from 8.891 Å in **NaI** to 9.102 Å in **KI** (Δ = +0.211 Å) as shown in Fig. 5a. Geometry of the linkage of the corner-sharing $(OCu_4)^{6+}$ tetrahedra varies in both structures due to the difference in the interlayer distance. The dihedral angles between triangular Cu–Cu–Cu faces of the adjacent $(OCu_4)^{6+}$ tetrahedra with alternating orientations of the 'pendant' vertices relative to the sheet plane differ significantly (60.87 ° in **KI** and 65.30 ° in **NaI**), whereas the adjacent faces of the tetrahedra oriented in the same direction are inclined to each other at approximately the same angle in both structures (156.27 ° in **KI**, and 155.97 ° in **NaI**).

The shift of the Cl(3) site (Fig. 5b) relative to its coordination environment is influenced by the cation size and deserves a special remark. The *A*(1)–Cl(3) bond length increases from 2.713 Å in **NaI** to 2.956 Å in **KI** (Δ = +0.243 Å). The Cu(3)–Cl(3)–Cu(3) angle between the chlorine anion and the plane of the $[O_2Cu_5]^{6+}$ sheet is smaller in **KI**: 154.68° versus 163.33° in **NaI**.

The $[O_2Cu_5]_n^{6n+}$ sheets in the crystal structures of **KI** and **NaI** are slightly bent due to the Na→K substitution. The planes formed by the oxygen atoms of the parallel adjacent $(OCu_4)^{6+}$ tetrahedra are inclined one to each other at 16.17° and 12.31° in **KI** and **NaI**, respectively.

The present work further demonstrates that CVT reactions method provides a unique opportunity to model physicochemical conditions existing in fumarolic environments and may be used not only to model exhalative processes, but also to predict possible mineral phases that may form in fumaroles. In particular, the K analogue of ilinskite is not known in nature, whereas it may well be formed from volcanic gases. The similar case of the Na→K substitution is present in many fumarolic minerals, *e.g.* euchlorine ($NaKCu_3O(SO_4)_3$) – fedotovite ($K_2Cu_3O(SO_4)_3$) (Scordari and Stasi 1990; Vergasova et al. 1988; Starova et al. 1991), wulffite ($K_3NaCu_4O_2(SO_4)_2$) – parawulffite ($K_5Na_3Cu_8O_4(SO_4)_4$) (Pekov et al. 2013c, d; Karpov et al. 2013). It is therefore well-probable that the K analogue of ilinskite, $K[Cu_5O_2](SeO_3)_2Cl_3$, may form in nature in a K-rich fumarolic environment.

Acknowledgements We are grateful to two anonymous referees and Associate Editor Anton Beran for helpful comments on the manuscript. This work was carried out under the framework of the Multi-InMaDe project supported by the ANR (Grant ANR 2011-JS-08 00301). VMK, OIS and SVK have been supported in this work by the Russian Science Foundation (grant 14-17-00071). The Fonds Européen de Développement Régional (FEDER), CNRS, Région Nord Pas-de-Calais, and Ministère de l'Education Nationale de l'Enseignement Supérieur et de la Recherche are acknowledged for funding the X-ray diffractometers.

References

Bastide B, Millet P, Johnsson M, Galy J (2000) Synthesis of copper(II) and selenium(IV) oxochlorides by chemical transport reaction: crystal structure of $Cu_9O_2(SeO_3)_4Cl_6$. Mater Res Bull 35:847–855

Berdonosov PS, Janson O, Olenev AV, Krivovichev SV, Rosner H, Dolgikh VA, Tsirlin AA (2013) Crystal structures and variable magnetism of $PbCu_2(XO_3)_2Cl_2$ with *X* = Se, Te. Dalton Trans 42:9547–9554

Berdonosov PS, Olenev AV, Dolgikh VA (2009) Strontium–copper selenite–chlorides: synthesis and structural investigation. J Solid State Chem 182:2368–2373

Binnewies M, Glaum R, Schmidt M, Schmidt P (2013) Chemical vapor transport reactions—a historical review. Z Anorg Allg Chem 639: 219–229

Brese NE, O'Keeffe M (1991) Bond-valence parameters for solids. Acta Crystallogr B47:192–197

Burns PC, Hawthorne FC (1995) Coordination-geometry structural pathways in Cu^{2+} oxysalt minerals. Can Mineral 33:889–905

Burns PC, Krivovichev SV, Filatov SK (2002) New Cu^{2+} coordination polyhedra in the crystal structure of burnsite, $KCdCu_7O_2(SeO_3)_2Cl_9$. Can Mineral 40:1587–1595

Chukanov NV, Murashko MN, Zadov AE, Bushmakin AF (2007) Avdoninite, $K_2Cu_5Cl_8(OH)_4 \cdot H_2O$, a new mineral species from volcanic exhalations and the technogenic zone at volcanic-hosted massive sulfide deposits. Geol Ore Depos 49:505–508

Demartin F, Castellano C, Campostrini I (2013) Aluminopyracmonite, $(NH_4)_3Al(SO_4)_3$, a new ammonium aluminium sulfate from La Fossa Crater, Vulcano, Aeolian Islands, Italy. Mineral Mag 77: 443–451

Demartin F, Castellano C, Campostrini I (2014) Therasiaite, $(NH_4)_3KNa_2Fe^{2+}Fe^{3+}(SO_4)_3Cl_5$, a new sulfate chloride from La Fossa Crater, Vulcano, Aeolian islands, Italy. Mineral Mag 78: 203–213

Effenberger H (1984) Verfeinerung der Kristallstruktur von Kupfer(II)-hydroxichlorid, Cu(OH)Cl. Monatsh Chem 115:725–730

Effenberger H (1985) $Cu(SeO_2OH)_2$: synthesis and crystal structure. Z Kristallogr 173:167–272

Effenberger H (1986) $PbCu_3(OH)(NO_3)(SeO_3)_3 \cdot 1/2H_2O$ und $Pb_2Cu_3O_2(NO_3)_2(SeO_3)_2$: synthese und Kristallstrukturuntersuchung. Monatsh Chem 117:1099–1106

Effenberger H, Pertlik F (1986) Die Kristallstrukturen der Kupfer(II)-oxo-selenite $Cu_2O(SeO_3)$ (kubisch und monoklin) und $Cu_4O(SeO_3)_3$ (monoklin und triklin). Monatsh Chem 117:887–896

Filatov SK, Semenova TF, Vergasova LP (1992) Types of polymerization of $[OCu_4]^{6+}$ in inorganic compounds with "additional" oxygen atoms. Dokl Akad Nauk SSSR (in russian) 322:539–539

Garavelli A, Mitolo D, Pinto D, Vurro F (2013) Lucabindiite, $(K, NH_4)As_4O_6(Cl,Br)$, a new fumarole mineral from the "La Fossa" crater at Vulcano, Aeolian Islands, Italy. Am Mineral 98:470–477

Hawthorne FC, Cooper MA, Grice JD, Roberts AC, Hubbard N (2002) Description and crystal structure of bobkingite, $Cu^{2+}{}_5Cl_2(OH)_8(H_2O)_2$, a new mineral from New Cliffe Hill

Quarry, Stanton-under-Bardon, Leicestershire, UK. Mineral Mag 66:301–311

Kahlenberg V (2004) On the crystal structure of $K_2Cu_5Cl_8(OH)_4{\cdot}2H_2O$. Z Anorg Allg Chem 630:900–903

Karpov GA, Krivovichev SV, Vergasova LP, Chernyat'eva AP, Anikin LP, Moskaleva SV, Filatov SK (2013) Oxysulfates of copper, sodium, and potassium in the lava flows of the 2012–2013 Tolbachik Fissure Eruption. J Volcanol Seismol 7:362–370

Kovrugin VM, Colmont M, Mentré O, Siidra OI, Krivovichev SV (2015) Dimers of oxocentered $[OCu_4]^{6+}$ tetrahedra in two novel copper selenite chlorides, $K[Cu_3O](SeO_3)_2Cl$ and $Na_2[Cu_7O_2](SeO_3)_4Cl_4$, and related minerals and inorganic compounds. Mineral Mag: submitted

Krivovichev SV, Filatov SK (1999) Structural principles for minerals and inorganic compounds containing anion-centered tetrahedra. Am Mineral 84:1099–1106

Krivovichev SV, Filatov SK, Semenova TF, Rozhdestvenskaya IV (1998) Crystal chemistry of inorganic compounds based on chains of oxocenterd tetrahdera. I. Crystal structure of chloromenite, $Cu_9O_2(SeO_3)_4Cl_6$. Z Krist 213:645–649

Krivovichev SV, Shuvalov RR, Semenova TF, Filatov SK (1999a) Crystal chemistry of inorganic compounds based on chains of oxocentered tetrahedra. III. Crystal structure of georgbokiite, $Cu_5O_2(SeO_3)_2Cl_2$. Z Krist 214:135–138

Krivovichev SV, Starova GL, Filatov SK (1999b) "Face-to-face" relationships between oxocentred tetrahedra and cation-centred tetrahedral oxyanions in crystal structures of minerals and inorganic compounds. Mineral Mag 63:263–266

Krivovichev SV, Filatov SK, Armbruster T, Pankratova OY (2004) Crystal structure of $Cu^{(I)}Cu^{(II)}{}_4O(SeO_3)Cl_5$, a new heterovalent copper compound. Dokl Chem 399:226–228

Krivovichev SV, Filatov SK, Burns PC, Vergasova LP (2006) The crystal structure of allochalcoselite, $Cu^+Cu^{2+}{}_5PbO_2(SeO_3)_2Cl_5$, a mineral with well-defined Cu^+ and Cu^{2+} positions. Can Mineral 44:507–514

Krivovichev SV, Filatov SK, Burns PC, Vergasova LP (2007) The crystal structure of parageorgbokiite, β–$Cu_5O_2(SeO_3)_2Cl_2$. Can Mineral 45: 929–934

Krivovichev SV, Vergasova LP, Filatov SK, Rybin DS, Britvin SN, Ananiev VV (2013a) Hatertite, $Na_2(Ca, Na)(Fe^{3+}, Cu)_2(AsO_4)_3$, a new alluaudite-group mineral from Tolbachik fumaroles, Kamchatka peninsula, Russia. Eur J Mineral 25:683–691

Krivovichev SV, Mentré O, Siidra OI, Colmont M, Filatov SK (2013b) Anion-centered tetrahedra in inorganic compounds. Chem Rev 113: 6459–6535

Krivovichev SV, Filatov SK, Vergasova LP (2013c) The crystal structure of ilinskite, $NaCu_5O_2(SeO_3)_2Cl_3$, and review of mixed-ligand CuO_mCl_n coordination geometries in minerals and inorganic compounds. Mineral Petrol 107:235–242

Millet P, Bastide B, Pashchenko V, Gnatchenko S, Ksari Y, Stepanov A (2001) Syntheses, crystal structures and magnetic properties of francisite compounds $Cu_3Bi(SeO_3)_2O_2X$ (X = Cl, Br and I). J Mater Chem 11:1152–1157

Mitolo D, Demartin F, Garavelli A, Campostrini I, Pinto D, Gramaccioli CM, Acquafredda P, Kolitsch U (2013) Adranosite-(Fe), $(NH_4)_4NaFe_2(SO_4)_4Cl(OH)_2$, a new ammonium sulfate chloride from La Fossa Crater, Vulcano, Aeolian Islands, Italy. Can Mineral 51:57–66

Murashko MN, Pekov IV, Krivovichev SV, Chernyatyeva AP, Yapaskurt VO, Zadov AE, Zelensky ME (2013) Steklite, $KAl(SO_4)_2$: a finding at the Tolbachik Volcano, Kamchatka, Russia, validating its status as a mineral species and crystal structure. Geol Ore Depos 55:594–600

Pekov IV, Zelenski ME, Yapaskurt VO, Polekhovsky YS, Murashko MN (2013a) Starovaite, KCu5O(VO4)3, a new mineral from fumarole sublimates of the Tolbachik volcano, Kamchatka, Russia. Eur J Mineral 25:91–96

Pekov IV, Zubkova NV, Yapaskurt VO, Belakovskiy DI, Chukanov NV, Lykova IS, Sidorov EG, Pushcharovsky DY (2013b) Wulffite. IMA 2013-035. CNMNC Newsletter No. 17. Mineral Mag 77:2998

Pekov IV, Zubkova NV, Yapaskurt VO, Belakovskiy DI, Chukanov NV, Lykova IS, Sidorov EG, Pushcharovsky DY (2013c) Parawulffite, IMA 2013–036. CNMNC Newsletter No. 17. Mineral Mag 77:2998

Pekov IV, Zubkova NV, Zelenski ME, Yapaskurt VO, Polekhovsky YS, Fadeeva OA, Pushcharovsky DY (2013d) Yaroshevskite, $Cu_9O_2(VO_4)_4Cl_2$, a new mineral from the Tolbachik volcano, Kamchatka, Russia. Mineral Mag 77:107–116

Pekov IV, Siidra OI, Chukanov NV, Yapaskurt VO, Belakovskiy DI, Murashko MN, Sidorov EG (2014a) Kaliochalcite, $KCu_2(SO_4)_2[(OH)(H_2O)]$, a new tsumcorite-group mineral from the Tolbachik volcano, Kamchatka, Russia. Eur J Mineral 26:597–604

Pekov IV, Zubkova NV, Yapaskurt VO, Belakovskiy DI, Lykova IS, Vigasina MF, Sidorov EG, Pushcharovsky DYu (2014b) New arsenate minerals from the Arsenatnaya fumarole, Tolbachik volcano, Kamchatka, Russia. I. Yurmarinite, $Na_7(Fe^{3+},Mg,Cu)_4(AsO_4)_6$. Mineral Mag 78:905–917

Pekov IV, Zubkova NV, Yapaskurt VO, Kartashov PM, Polekhovsky YS, Murashko MN, Pushcharovsky DY (2014c) Koksharovite, $CaMg_2Fe^{3+}{}_4(VO_4)_6$, and grigorievite, $Cu_3Fe^{3+}{}_2Al_2(VO_4)_6$, two new howardevansite-group minerals from volcanic exhalations. Eur J Mineral 26:667–677

Pertlik F, Zemann J (1988) The crystal structure of nabokoite, $Cu_7TeO_4(SO_4)_5 \cdot KCl$: the first example of a $Te^{(IV)}O_4$ pyramid with exactly tetragonal symmetry. Mineral Petrol 38:291–298

Pinto D, Garavelli A, Mitolo D (2014) Balićžunićite, $Bi_2O(SO_4)_2$, a new fumarole mineral from La Fossa crater, Vulcano, Aeolian Islands, Italy. Mineral Mag 78:1043–1055

Pring A, Gatehouse BM, Birch WD (1990) Francisite, $Cu_3Bi(SeO_3)_2O_2Cl$, a new mineral from Iron Monarch, South Australia: description and crystal structure. Am Mineral 75:1421–1425

Scordari F, Stasi F (1990) The crystal structure of euchlorine, $NaKCu_3O(SO_4)_3$. N Jb Mineral Abh 161:241–253

Shannon RD (1976) Revised effective ionic radii and systematic studies of interatomic distances in halides and chalcogenides. Acta Crystallogr A32:751–767

Sheldrick GM (2008) A short history of SHELX. Acta Crystallogr A64: 112–122

Shuvalov RR, Vergasova LP, Semenova TF, Filatov SK, Krivovichev SV, Siidra OI, Rudashevsky NS (2013) Prewittite, $KPb_{1.5}Cu_6Zn(SeO_3)_2O_2Cl_{10}$, a new mineral from Tolbachik fumaroles, Kamchatka peninsula, Russia: description and crystal structure. Am Mineral 98:463–469

Siidra OI, Krivovichev SV, Armbruster T, Pekov IV (2007) The crystal structure of leningradite, $PbCu_3(VO_4)_2Cl_2$. Can Mineral 45:445–449

Siidra OI, Krivovichev SV, Turner RW, Rumsey MS (2008) Chloroxiphite $Pb_3CuO_2(OH)_2Cl_2$: structure refinement and description in terms of oxocentred OPb_4 tetrahedra. Mineral Mag 72:793–798

Starova GL, Filatov SK, Vergasova LP (1991) The crystal structure of fedotovite, $K_2Cu_3O(SO_4)_3$. Mineral Mag 55:613–616

Starova GL, Krivovichev SV, Fundamensky VS, Filatov SK (1997) The crystal structure of averievite, $Cu_5O_2(VO_4)_2{\cdot}nMX$; comparison with related compounds. Mineral Mag 61:441–446

Takagi R, Duc F, Johnsson M (2006) $MoCu_3TeO_7Cl_2{\cdot}0.5H_2O$. Acta Crystallogr C62:i16–i18

Vergasova LP, Filatov SK, Serafimova YK, Varaksina TV (1988) Kamchatkite $KCu_3OCl(SO_4)_2$—a new mineral from volcanic sublimates. Zap VMO 117:459–461

Vergasova LP, Semenova TF, Shuvalov RR, Filatov SK, Ananiev VV (1997) Ilinskite $NaCu_5O_2(SeO_3)_2Cl_3$—a new mineral of volcanic exhalations. Dokl Akad Nauk (in russian) 353:641–644

Vergasova LP, Semenova TF, Krivovichev SV, Filatov SK, Zolotarev Jr AA, Ananiev VV (2014) Nicksobolevite, $Cu_7(SeO_3)_2O_2Cl_6$, a new complex copper oxoselenite chloride from Tolbachik fumaroles, Kamchatka peninsula, Russia. Eur J Mineral 26:439–449

Zhang D, Berger H, Kremer RK, Wulfering D, Lemmens P, Johnsson M (2010) Synthesis, crystal structure, and magnetic properties of the copper selenite chloride $Cu_5(SeO_3)_4Cl_2$. Inorg Chem 49:9683–9688

A-VIII
$[NaCl][Cu(HSeO_3)_2]$, NaCl-intercalated $Cu(HSeO_3)_2$: synthesis, crystal structure and comparison with related compounds

Vadim M. Kovrugin, Sergey V. Krivovichev, Olivier Mentré, and Marie Colmont

Published in: *Zeitschrift für Kristallographie - Crystalline Materials*, in press, first-pub-online: 7 August 2015.

DOI: 10.1515/zkri-2015-1849

Vadim M. Kovrugin, Sergey V. Krivovichev*, Olivier Mentré and Marie Colmont

$[NaCl][Cu(HSeO_3)_2]$, NaCl-intercalated $Cu(HSeO_3)_2$: synthesis, crystal structure and comparison with related compounds

DOI 10.1515/zkri-2015-1849
Received March 2, 2015; accepted May 29, 2015

Abstract: Single crystals of $[NaCl][Cu(HSeO_3)_2]$ have been prepared by the chemical vapor transport reactions. Its crystal structure (monoclinic, *C*2/*c*, *a* = 13.9874(7), *b* = 7.2594(4), *c* = 9.0421(5) Å, β = 127.046(2)°, *V* = 732.81(7) Å^3) is based upon electroneutral $[Cu(HSeO_3)_2]$ sheets formed by corner sharing between the $[CuO_4]$ squares and $(HSeO_3)$ groups that are parallel to the (100) plane. Each $(SeO_2OH)^-$ group forms the $O_h1\cdots O2$ hydrogen bond to an adjacent hydroselenite group to constitute a $[(SeO_2OH)_2]^{2-}$ dimer that provides additional stabilization of the copper diselenite sheet. The $[Cu(HSeO_3)_2]$ sheets alternate with the sheets consisting of zigzag–Na–Cl–Na–Cl–chains formed by Cl atoms and disordered Na sites. The chains are parallel to the *c* axis. The linkage between the alternating electroneutral $[Cu(HSeO_3)_2]$ and [NaCl] sheets is provided by the Cu–Cl and Na–O bonds. The coordination of Na is fivefold and consists of three O and two Cl atoms. $[NaCl][Cu(HSeO_3)_2]$ is a new member of the group of compounds based upon the $M(HSeO_3)_2$ layers (M^{2+} = Cu, Co, Cd). The prototype structure for this group is $[Cu(HSeO_3)_2]$ that does not have any chemical species separating the copper hydroselenite layers. In other compounds, the interlayer space between the $[Cu(HSeO_3)_2]^0$ layers is occupied by structural units of different complexity. $[NaCl][Cu(HSeO_3)_2]$ can be considered as $[Cu(HSeO_3)_2]$ intercalated with the NaCl layers consisting of one-dimensional–Na–Cl–Na–Cl–chains.

***Corresponding author: Sergey V. Krivovichev,** Department of Crystallography, St. Petersburg State University, Universitetskaya nab. 7/9, 199034 St. Petersburg, Russia; and Institute of Silicate Chemistry, Russian Academy of Sciences, Makarova Emb. 6, 199034 St. Petersburg, Russia, E-mail: skrivovi@mail.ru
Vadim M. Kovrugin: Department of Crystallography, St. Petersburg State University, Universitetskaya nab. 7/9, 199034 St. Petersburg, Russia; and UCCS, ENSCL, Université Lille 1, CNRS, UMR 8181, 59652 Villeneuve d'Ascq, France
Olivier Mentré and Marie Colmont: UCCS, ENSCL, Université Lille 1, CNRS, UMR 8181, 59652 Villeneuve d'Ascq, France

Keywords: copper; crystal structure; intercalated structures; layered compounds; selenite.

Introduction

Transition metal selenites have been the focus of a number of recent studies due to their interesting physical properties, arising in part due to the interplay between the stereochemical activity of lone pairs of electrons on the Se^{4+} cations and electronic properties of transition metal cations [1–9]. The interest has also been stimulated by the attempts to understand purely fundamental reasons for structural diversity in selenites and its underlying crystal chemical mechanisms [10–12]. In this regard, copper selenite chlorides are of particular importance, due to their natural occurrences as minerals [13–17] and the structures featuring 'scissor'-type disruption of a bonding network induced by the well-localized stereochemically active but chemicall inactive lone electron pairs [18–22].

In this paper, we report on the synthesis and crystal structure of $[NaCl][Cu(HSeO_3)_2]$, a novel compound prepared by the chemical vapor techniques (CVT) and a new member of the family of inorganic and organic-inorganic compounds based upon the electroneutral $M(HSeO_3)_2$ layers (M^{2+} = Cu, Co, Cd) [23–29].

Experimental

Synthesis

Single crystals of $[NaCl][Cu(HSeO_3)_2]$ have been prepared by the CVT method. Mixture of CuO, $CuCl_2$, SeO_2, and NaCl taken in the 4:1:2:3 molar ratio were loaded into a fused silica tube (*ca.* 15 cm), which was evacuated to 10^{-2} mbar before sealing. The tubes were placed horizontally into a tubular two-zone furnace, and heated to 500°. The temperature difference between the source and deposition zones of the tube was about 50 °C. After 3 days, the tubes were cooled down to room temperature over 24 h. The products of the synthesis consisted of green crystals of $Na_2[Cu_7O_2](SeO_3)_4Cl_4$ [30] and few

pale blue translucent block-shaped crystals of [NaCl][Cu(HSeO$_3$)$_2$] (Figure 1).

X-ray experiment

Single crystals of [NaCl][Cu(HSeO$_3$)$_2$] selected for data collection were examined under an optical microscope and mounted on a glass fiber with epoxy for single crystal X-rays diffraction analysis. More than a hemisphere of the X-ray diffraction data were collected with the frame width of 0.5° in ω, and 45 s spent counting for each frame using a Bruker APEX DUO diffractometer equipped with a micro-focus X-ray tube operated with MoK_α radiation at 50 kV and 40 mA. The data were integrated and corrected for absorption using a multi-scan type model using the Bruker programs *APEX* and *SADABS*. The crystal structure was solved by direct methods and refined to the crystallographic agreement factor $R_1 = 0.021$ by means of the *SHELX* program package [31]. Relevant crystallographic information is listed in Table 1. The final atomic coordinates, site-occupation factors (SOFs) and anisotropic displacement parameters are given in Table 2. Selected interatomic distances are in Table 3. Hydrogen atom positions have been determined from difference Fourier map.

Further details of the crystal structure investigation are available from the Fachinformationszentrum Karlsruhe, D-76344 Eggenstein-Leopoldshafen, Germany, on quoting the depository number CSD-429287, the names of the authors and the citation of the paper.

Tab. 1: Crystallographic data and refinement parameters for [NaCl][Cu(HSeO$_3$)$_2$].

Crystal data	
Crystal system	monoclinic
Space group	*C*2/*c*
a (Å)	13.9874(7)
b (Å)	7.2594(4)
c (Å)	9.0421(5)
β (°)	127.046(2)
Unit-cell volume (Å^3)	732.81(7)
Z	2
Calculated density (g/cm^3)	3.425
Absorption coefficient (mm^{-1})	13.313
Crystal size (mm)	0.17 × 0.12 × 0.09
Data collection	
Temperature	293 K
Radiation, wavelength (Å)	MoK_α, 0.71073
F(000)	700
θ range (°)	3.35–30.97
h, *k*, *l* ranges	−20 → 11, -9 → 10, −12 → 13
Total reflections collected	3926
Unique reflections (R_{int})	1170 (0.026)
Unique reflections $F>4\sigma_F$	989
Structure refinement	
Refinement method	Full-matrix least-squares on F^2
Weighting coefficients *a*, *b* *	0.0232, 1.3732
Data/restraints/parameters	1170/0/62
$R_1[F > 4\sigma_F]$, $wR_2[F > 4\sigma_F]$	0.021, 0.051
R_1 all, wR_2 all	0.030, 0.053
Goodness-of-fit on F^2	1.081
Largest diff. peak and hole	0.702, −0.645 *e*Å^{-3}

Results

The crystal structure of the title compound contains one symmetrically independent Cu site octahedrally coordinated by four O and two Cl atoms. The coordination is typical for the mixed-metal CuO_nCl_m configurations occurring in inorganic copper oxysalts [14]. The Cu site forms four short Cu–O bonds (1.967–1.968 Å) that define a [CuO_4] square complemented by two long Cu–Cl bonds. This type of coordination (four short equatorial and two long apical bonds) is a consequence of the Jahn–Teller distortion of octahedral geometry. The similar [CuO_4Cl_2] octahedra have been observed, e.g. in atacamite, $Cu_2(OH)_3Cl$ [32], and leningradite, $PbCu_3(VO_4)_2Cl_2$ [33]. There is one Se site coordinated by three O atoms to form a trigonal (SeO_3) pyramid characteristic for selenites. One of the three Se–O bonds is elongated (Se–O_h1 = 1.751 Å) compared to two other bonds (1.671 and 1.680 Å), owing to the protonation of the O_h1 site. The [CuO_4] squares and ($HSeO_3$) groups share O atoms to form electroneutral [Cu(HSeO$_3$)$_2$] sheets parallel to the (100) plane (Figure 2a). The $(SeO_2OH)^-$ group form the O_h1···O2 hydrogen bond to an adjacent hydroselenite group to form a $[(SeO_2OH)_2]^{2-}$ dimer that provides additional stabilization of the copper diselenite sheet.

In the crystal structure, the [Cu(HSeO$_3$)$_2$] sheets alternate with the sheets consisting of zigzag–Na–Cl–Na–Cl–chains formed by Cl atoms and disordered Na sites (Figure 2b). The chains are parallel to the *c* axis. The Na–Cl distances are 2.917 and 2.881 Å, which is comparable to the distance 2.82 Å observed in halite, NaCl. The Na–Cl–Na angle is equal to 97.1–110.5°, which can be compared to the ideal angle of 90° observed in halite.

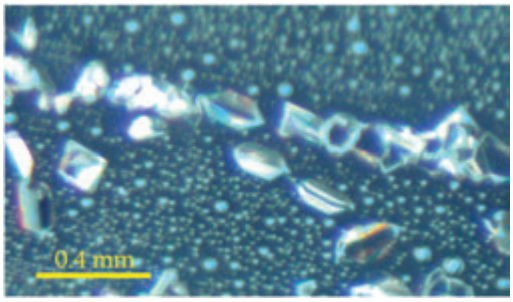

Fig. 1: Crystals of [NaCl][Cu(HSeO$_3$)$_2$] under optical microscope.

Tab. 2: Atomic coordinates, site-occupation factors (SOFs) and displacement parameters (Å^2) of atoms in the crystal structure [NaCl][Cu(HSeO$_3$)$_2$].

Atom	*x*	*y*	*z*	U_{eq}	U_{11}	U_{22}	U_{33}	U_{23}	U_{13}	U_{12}
Se	0.16713(2)	0.41354(4)	0.11467(3)	0.01585(8)	0.0205(1)	0.0116(1)	0.0198(1)	0.00158(9)	0.0145(1)	0.00050(9)
Cu	3/4	1/4	0	0.0180(1)	0.0319(3)	0.0103(2)	0.0187(2)	−0.0005(2)	0.0189(2)	−0.0028(2)
Cl	0	0.2461(2)	1/4	0.0271(2)	0.0217(4)	0.0334(6)	0.0243(4)	0.000	0.0129(4)	0.000
O_h1	0.3996(2)	0.2790(3)	0.0302(3)	0.0278(5)	0.029(1)	0.024(1)	0.035(1)	−0.0110(9)	0.022(1)	−0.0101(9)
O2	0.7484(2)	−0.0146(3)	0.0451(3)	0.0226(4)	0.034(1)	0.0122(9)	0.037(1)	0.0044(8)	0.029(1)	0.0005(8)
O3	0.2755(2)	0.3130(3)	0.3144(3)	0.0230(4)	0.030(1)	0.026(1)	0.0189(9)	0.0072(8)	0.0174(8)	0.0089(9)
Na*	0.5242(4)	0.4802(9)	0.0326(10)	0.0437(13)	0.047(3)	0.029(3)	0.079(5)	−0.017(2)	0.051(4)	−0.017(2)
H	0.350(5)	0.333(8)	0.034(7)	0.069(16)						

*Site-occupation factor = 0.5.

Tab. 3: Selected bond lengths (Å) and angles (deg) in the crystal structure [NaCl][Cu(HSeO$_3$)$_2$].

Se–O3	1.671(2)	Na–O_h1	2.265(7)
Se–O2	1.680(2)	Na–O_h1	2.290(7)
Se–O_h1	1.751(2)	Na–O3	2.562(4)
<Se–O>	1.701	Na–Cl	2.881(8)
		Na–Cl	2.918(8)
Cu–O2	1.967(2) 2×		
Cu–O3	1.968(2) 2×	O_h1–H	0.81(5)
Cu–Cl	2.7954(2) 2×	H···O2	1.85(5)

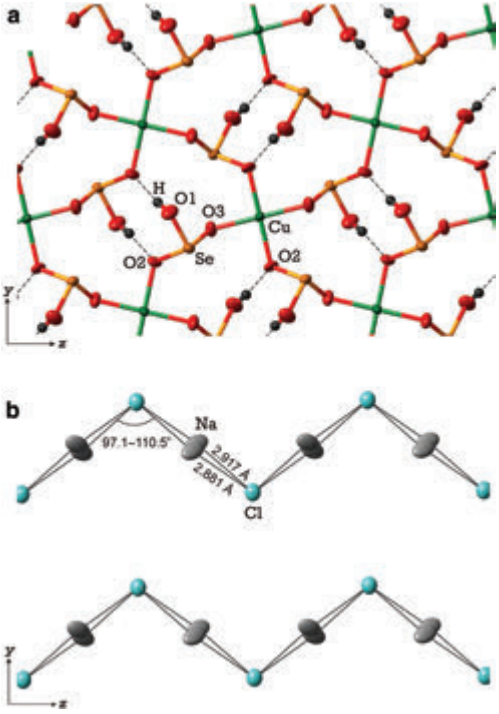

Fig. 2: Projections of the [Cu(HSeO$_3$)$_2$]^0 layer (a) and the layer of the …–Na–Cl–Na–Cl–… chains (b) onto the (100) plane.

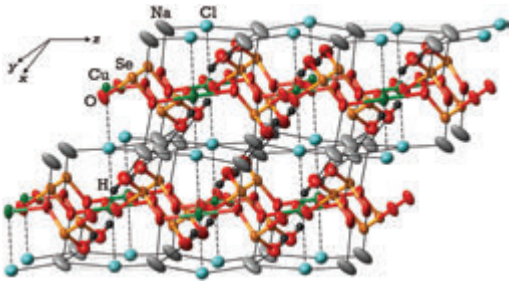

Fig. 3: Crystal structure of [NaCl][Cu(HSeO$_3$)$_2$] featuring two-dimensional [Cu(HSeO$_3$)$_2$]^0 layers with intercalated …–Na–Cl–… chains.

The linkage between the alternating electroneutral [Cu(HSeO$_3$)$_2$] and [NaCl] sheets is provided by the Cu–Cl and Na–O bonds (Figure 3). The coordination of Na is five-fold and consists of three O and two Cl atoms.

Discussion

According to the results of this study, the title compound can be considered as a member of the group of compounds based upon the M(HSeO$_3$)$_2$ layers (M^{2+} = Cu, Co, Cd) [23–29]. Crystallographic data and geometrical parameters of the layers are given in Table 4. The prototype structure for this group is [Cu(HSeO$_3$)$_2$] [23] that does not have any chemical species separating the copper hydroselenite layers. In other compounds, the interlayer space between the [Cu(HSeO$_3$)$_2$]^0 layers is occupied by structural units of different complexity. In all Cu compounds, the [Cu(HSeO$_3$)$_2$]^0 layers have approximately the same linear parameters, except for [Cu(HSeO$_3$)$_2$](H$_2$O)$_2$, where the layers are strongly corrugated.

In general, the compound [NaCl][Cu(HSeO$_3$)$_2$] reported herein can be considered as [Cu(HSeO$_3$)$_2$] intercalated

Tab. 4: Crystallographic data for inorganic compounds containing electroneutral [M(HSeO$_3$)] layers (M = Cu, Co).

Chemical formula	Space group	*a*, Å	*b*, Å/β, °	*c*, Å	Layer orientation: parameters	References
[Cu(HSeO$_3$)$_2$]	$P2_1/n$	5.766	7.352/93.28	6.447	(101): 8.892 × 7.352 Å^2	[23]
[Cu(HSeO$_3$)$_2$](H$_2$O)$_2$	$P2_1/c$	6.279	6.258/90.97	9.091	(100): 9.091 × 6.258 Å^2	[25]
[(NH$_4$)(NO$_3$)]$_3$[Cu(HSeO$_3$)$_2$]	*Pnma*	8.881	24.010/90	7.220	(010): 8.881 × 7.220 Å^2	[25]
[Mn(H$_2$O)$_4$Cl$_2$][Cu(HSeO$_3$)$_2$]	*Pnma*	9.125	18.179/90	7.188	(010): 9.125 × 7.188 Å^2	[26]
[(NH$_4$)Cl][Cu(HSeO$_3$)$_2$]	*Pnma*	8.975	12.118/90	7.265	(010): 8.975 × 7.265 Å^2	[27]
[Cu(H$_2$O)$_4$Cl$_2$][Cu(HSeO$_3$)$_2$]	*Pnma*	9.149	17.835/90	7.229	(010): 9.149 × 7.229 Å^2	[28]
[Co(H$_2$O)$_4$Cl$_2$][Co(HSeO$_3$)$_2$]	*Pnma*	9.338	17.345/90	7.320	(010): 9.338 × 7.320 Å^2	[29]
[NaCl][Cu(HSeO$_3$)$_2$]	*C*2/*c*	13.987	7.259/127.05	9.042	(100): 9.042 × 7.259 Å^2	this work

with the NaCl layers consisting of one-dimensional –Na–Cl–Na–Cl–chains.

Acknowledgments: VMK and SVK have been supported in this work by the Russian Science Foundation (grant 14-17-00071). This work was carried out under the framework of the Multi-InMaDe project supported by the ANR (Grant ANR 2011-JS-0800301). The Fonds Européen de Développement Régional (FEDER), CNRS, Région Nord Pas-de-Calais, and Ministére de l'Education Nationale de l'Enseignement Supérieur et de la Recherche are acknowledged for funding the X-ray diffractometers. VMK also thanks l'Ambassade de France en Russie and l'Agence Campus France (Contract Nos. 768231K, 779116K, 794852B, 808399A, and 808400J) for the partial support of this work.

References

[1] S. Hu, M. Johnsson, Synthesis and crystal structure of two synthetic oxofluoride framework compounds – $Co_2TeO_3F_2$ and $Co_2SeO_3F_2$. *Dalton Trans*. **2012**, *41*, 12786.

[2] P. S. Berdonosov, O. Janson, A. V. Olenev, S. V. Krivovichev, H. Rosner, V. A. Dolgikh, A. A. Tsirlin, Crystal structures and variable magnetism of $PbCu_2(XO_3)_2Cl_2$ with X = Se, Te. *Dalton Trans*. **2013**, *42*, 9547.

[3] Y. H. Kim, D. W. Lee, K. M. Ok, α-$ScVSe_2O_8$, β-$ScVSe_2O_8$, and $ScVTe_2O_8$: new quaternary mixed metal oxides composed of only second-order Jahn-Teller distortive cations. *Inorg. Chem*. **2013**, *52*, 11450.

[4] Y. Shin, D. W. Lee, K. Y. Choi, H.-J. Koo, K. M. Ok, $VSb(SeO_3)_4$, first selenite containing V^{3+} cation: synthesis, structure, characterization, magnetic properties, and calculations. *Inorg. Chem*. **2013**, *52*, 14224.

[5] Y. H. Kim, D. W. Lee, K. M. Ok, Noncentrosymmetric $YVSe_2O_8$ and centrosymmetric $YVTe_2O_8$: macroscopic centricities influenced by the size of lone pair cation linkers. *Inorg. Chem*. **2014**, *53*, 1250.

[6] T. Eaton, J. Lin, J. N. Cross, J. T. Stritzinger, T. E. Albrecht-Schmitt, $Th(VO_3)_2(SeO_3)$ and $Ln(VO_3)_2(IO_3)$ (Ln = Ce, Pr, Nd, Sm, and Eu): unusual cases of aliovalent substitution. *Chem. Comm*. **2014**, *50*, 3668.

[7] S. Hu, M. Johnsson, J. M. Law, J. L. Bettis, M.-H. Whangbo, R. K. Kremer, Crystal structure and magnetic properties of $FeSeO_3F$ – alternating antiferromagnetic $S = 5/2$ chains. *Inorg. Chem*. **2014**, *53*, 4250.

[8] X.-L. Cao, F. Kong, C.-L. Hu, X. Xu, J.-G. Mao, $Pb_4V_6O_{16}(SeO_3)_3(H_2O)$, $Pb_2VO_2(SeO_3)_2Cl$, and $PbVO_2(SeO_3)F$: new lead(II)-vanadium(V) mixed-metal selenites featuring novel anionic skeletons. *Inorg. Chem*. **2014**, *53*, 8816.

[9] K. L. Kilminster, F. J. Lincoln, B. W. Skelton, A. H. White, A barium vanadium(V) selenite hydrate, $Ba(VO_2)_2(SeO_3)_2{\cdot}H_2O$: a novel 3D polymer of cross-linked sheets with embedded …V-O-V… 2_1 helices. *Austr. J. Chem*. **2014**, *67*, 1878.

[10] J. H. Koffer, J. H. Olshansky, M. D. Smith, K. J. Hernandez, M. Zeller, G. M. Ferrence, J. Schrier, A. J. Norquist, Formation principles for templated vanadium selenite oxalates. *Cryst. Growth Des*. **2013**, *13*, 4504.

[11] A. Aliev, V. M. Kovrugin, M. Colmont, C. Terryn, M. Huve, O. I. Siidra, S. V. Krivovichev, O. Mentre, Revised bismuth chloroselenite system: evidence of a noncentrosymmmetric structure with a giant unit cell. *Cryst. Growth Des*. **2014**, *14*, 3026.

[12] J. H. Olshansky, K. J. Wiener, M. D. Smith, A. Nourmahnad, M. J. Charles, M. Zeller, J. Schrier, A. J. Norquist, Formation principles for vanadium selenites: the role of pH on product composition. *Inorg. Chem*. **2014**, *53*, 12027.

[13] M. Gemmi, I. Campostrini, F. Demartin, T. E. Gorelik, C. M. Gramaccioli, Structure of the new mineral sarrabusite, $Pb_5CuCl_4(SeO_3)_4$, solved by manual electron-diffraction tomography. *Acta Crystallogr*. **2012**, *B68*, 15.

[14] S. V. Krivovichev, S. K. Filatov, L. P. Vergasova, The crystal structure of ilinskite, $NaCu_5O_2(SeO_3)_2Cl_3$, and review of mixed-ligand CuO_mCl_n coordination geometries in minerals and inorganic compounds. *Mineral. Petrol*. **2013**, *107*, 235.

[15] R. R. Shuvalov, L. P. Vergasova, T. F. Semenova, S. K. Filatov, S. V. Krivovichev, O. I. Siidra, N. S. Rudashevsky, Prewittite, $KPb_{1.5}Cu_6Zn(SeO_3)_2O_2Cl_{10}$, a new mineral from Tolbachik Fumaroles, Kamchatka Peninsula, Russia: description and crystal structure. *Amer. Mineral*. **2013**, *98*, 463.

[16] S. J. Mills, A. R. Kampf, A. G. Christy, R. M. Housley, B. Thorne, Y.-S. Chen, I. M. Steele, Favreauite, a new selenite mineral from the El Dragon mine, Bolivia. *Eur. J. Mineral*. **2014**, *26*, 771.

[17] L. P. Vergasova, T. F. Semenova, S. V. Krivovichev, S. K. Filatov, A. A. Zolotarev, Jr., V. V. Ananiev, Nicksobolevite, $Cu_7(SeO_3)_2O_2Cl_6$, a new complex copper oxoselenite chloride from Tolbachik fumaroles, Kamchatka peninsula, Russia. *Eur. J. Mineral*. **2014**, *26*, 439.

[18] Z. Mayerová, M. Johnsson, S. Lidin, Lone-pair interfaces that divide inorganic materials into ionic and covalent parts. *Angew. Chem. Int. Ed*. **2006**, *45*, 5602.

[19] V. Jo, M. K. Kim, D. W. Lee, I. W. Shim, K. M. Ok, Lone pairs as chemical scissors in new antimony oxychlorides, $Sb_2ZnO_3Cl_2$ and $Sb_{16}Cd_8O_{25}Cl_{14}$. *Inorg. Chem*. **2010**, *49*, 2990.

[20] S. Hu, M. Johnsson, Synthesis and crystal structure of $Fe_6Ca_2(SeO_3)_9Cl_4$ – a porous oxohalide. *Dalton Trans.* **2013**, *42*, 7859.

[21] I. Zimmermann, M. Johnsson, A synthetic route toward layered materials: introducing stereochemically active lone-pairs into transition metal oxohalides. *Cryst. Growth Des.* **2014**, *14*, 5252.

[22] I. Zimmermann, A. Corgnet, M. Johnsson, S. Lidin, Synthesis and crystal structure of a series of incommensurately modulated composite oxohalide compounds. *Dalton Trans*. **2014**, *43*, 15812.

[23] H. Effenberger, $Cu(SeO_2OH)_2$: synthesis and crystal structure. *Z. Kristallogr*. **1985**, *173*, 267.

[24] L. Hiltunen, M. Leskela, L. Niinisto, M. Tammenmaa, Crystal structure of copper hydrogenselenite monohydrate. *Acta Chem. Scand*. **1985**, *A39*, 809.

[25] A. M. Lafront, J. C. Trombe, 'Layered hydrogenselenites'. I. Synthesis, structure redetermination of $Cu(HSeO_3)_2(H_2O)_2$ and determination of $(Cu(HSeO_3)_2(NO_3)_2)^{2-}.2(NH_4)^+$, NH_4NO_3. Structural relationships of these complexes with $(Cu(HSeO_3)_2)$. *Inorg. Chim. Acta* **1995**, *234*, 19.

[26] A. M. Lafront, J. C. Trombe, J. Bonvoisin, 'Layered hydrogenselenites'. II. Synthesis, structure studies and magnetic properties of a novel series of bimetallic hydrogenselenites: $Cu(HSeO_3)_2MCl_2(H_2O)_4$, M(II) = Mn, Co, Ni, Cu, Zn. *Inorg. Chim. Acta* **1995**, *238*, 15.

[27] J. C. Trombe, A. M. Lafront, J. Bonvoisin, Synthesis, structure and magnetic measurement of a new layered copper hydrogenselenite: $(Cu(HSeO_3)_2)\cdot((NH_4)Cl)$. *Inorg. Chim. Acta* **1997**, *262*, 47.

[28] W. T. A. Harrison, M. G. Johnston, Syntheses and structures of two selenite chloride hydrates: $Co(HSeO_3)Cl\cdot3(H_2O)$ and $Cu(HSeO_3)Cl\cdot2(H_2O)$. *Z. Anorg. Allg. Chem*. **2000**, *626*, 2487.

[29] M. G. Johnston, W. T. A. Harrison, Cobalt hydrogen selenite chloride dihydrate, $Co(HSeO_3)Cl\cdot2(H_2O)$. *Acta Crystallogr*. **2003**, *E59*, i62.

[30] V. M. Kovrugin, M. Colmont, O. Mentré, O. I. Siidra, S. V. Krivovichev, Dimers of oxocentered $[OCu_4]^{6+}$ tetrahedra in two novel copper selenite chlorides, $K[Cu_3O](SeO_3)_2Cl$ and $Na_2[Cu_7O_2](SeO_3)_4Cl_4$, and related minerals and inorganic compounds. *Mineral. Mag*. **2015**, in press.

[31] G. M. Sheldrick, A short history of SHELX. *Acta Crystallogr.* **2008,** *A64*, 112.

[32] J. B. Parise, B. G. Hyde, The structure of atacamite and its relationships to spinel. *Acta Crystallogr*. **1986**, *B42*, 1277.

[33] O. I. Siidra, S. V. Krivoivchev, T. Armbruster, S. K. Filatov, I. V. Pekov, The crystal structure of leningradite, $PbCu_3(VO_4)_2Cl_2$. *Can. Mineral*. **2007**, *45*, 445.

Ковругин Вадим Михайлович

Кристаллохимия новых кислородных соединений четырех- и шестивалентного селена (Russian translation)

Диссертационная работа
на соискание ученой степени Ph.D. СПбГУ в области наук о Земле

АННОТАЦИЯ

Настоящая работа посвящена изучению кристаллохимии новых кислородных соединений, содержащих селен в степенях окисления +4 и +6. Тридцать три известных к настоящему времени оксоселенитных минерала обладают удивительным структурным многообразием, которое открывает широкий простор для дальнейших исследований, поиска и обнаружения их возможных инновационных физических свойств. Данное диссертационное исследование ставит своей целью синтезировать и изучить с точки зрения кристаллохимии новые оксидные соединения селена, применяя различные лабораторные методы, моделирующие процессы природного кристаллообразования.

Для кристаллохимического описания структур новых кристаллических фаз применяется как традиционная описательная процедура, в основе которой лежит рассмотрение кристаллической структуры с позиции координации катионов, так и современная теория анионоцентрированных полиэдров, разработанная Санкт-Петербургской кристаллографической школой и в дальнейшем успешно применяемая в Лаборатории катализа и химии твердого тела университета Лилля-1. Эта теория незаменима в случаях, когда традиционная структурная интерпретация не отражает основных принципов структурной архитектуры.

В работе представлены результаты изучения нескольких металл-оксидных систем с $Se^{4+/6+}$ и различными химическими элементами ($Cu^{+/2+}$, Ni^{2+}, Co^{2+}, $V^{4+/5+}$, Mn^{2+}, Fe^{3+}, Pb^{2+}, Bi^{3+}, U^{6+}). Диссертация содержит кристаллохимическое описание 39 новых металл-селенитов, селенатов и селенит-селенатов. Также проведена аналогия между селенитными и фосфитными оксоанионами. Полученные результаты в работе сопровождаются ссылками на их более детальное представление в публикациях автора в приложении к настоящей работе.

Ключевые слова: селенит, селенат, уранил, ванадат, фосфит, медь, никель, кобальт, марганец, свинец, висмут, железо, синтез, кристаллическая структура, рентгеноструктурный анализ, оксоцентрированные тетраэдры

1 ВВЕДЕНИЕ

В последнее время наблюдается смещение исследовательского интереса от создания новых, инновационных соединений с уникальными структурными архитектурами в сторону детального изучения, модифицирования и корректирования свойств уже известных неорганических материалов, использующихся в различных технологических отраслях. Данное обстоятельство служит причиной сложившейся негативной ситуации в материаловедении – нехватки новых соединений, обладающих принципиально новыми структурными архитектурами, обусловливающими физико-химические характеристики материалов, необходимые для их применения в индустрии. Таким образом, в настоящее время ощущается серьезная потребность в получении новых материалов в различных химических системах.

Природа еще не до конца раскрыла свои секреты, касающиеся происхождения и физических условий кристаллического роста многих минеральных видов на Земле. Структурные архитектуры, обнаруженные в известных кристаллических соединениях, созданных природой, крайне разнообразны: от основанных на нульмерных островных комплексах до сложных трехмерных каркасных построек. Такое многообразие форм дает широкий простор для дальнейших исследований с точки зрения поиска и обнаружения возможных инновационных физических свойств. При этом способы природного образования множества минеральных видов все еще остаются неизвестными. В то же время исследователи в своих работах стараются применять новейшие синтетические методы, регулярно появляющиеся в ходе развития науки, с целью познать искусное мастерство природы и воссоздать ее технику в лаборатории. Так, метод химических газотранспортных реакций дает уникальную возможность смоделировать физические и химические условия, существующие на фумарольных полях. Он может быть использован не только для моделирования эксгаляционных процессов, но также и для предсказания возможных минеральных фаз, которые могут образовываться на фумаролах. В частности,

синтезированный в рамках настоящей исследовательской работы калиевый аналог ильинскита – редкого минерального сублимата, обнаруженного на фумаролах вулкана Толбачик на Камчатке, – неизвестен в природе, тогда как весьма вероятно, что такая калиевая форма может образовываться из вулканических газов в богатых калием локальных геохимических обстановках. Это лишь один пример из множества возможных других.

Исследовательская работа, положенная в основу настоящей диссертации, находится на пересечении химии твердого тела, кристаллографии и минералогии. Она является одной из первых работ, в которой синтез различных серий новых металл-оксидных соединений осуществляется с применением инновационного подхода, основанного на использовании минералогической информации: о составе, структуре, свойствах и способе формирования объектов природного мира. В рамках данного подхода моделировались природные процессы кристаллического роста в лабораторных условиях с целью получения комплексных функциональных материалов, обладающих потенциалом с точки зрения дальнейшего изучения физических свойств.

В течение двух последних десятилетий химия селенсодержащих соединений интенсивно развивалась. Многие исследователи получили большое количество экспериментальных данных по химии селена в различных фундаментальных и прикладных областях: в медицине [Rayman 2000], биохимии [Tapiero et al. 2003], органической химии [Pyrzynska 1996], физической химии [Qu and Peng 2002; Hsu et al. 2008], ядерных технологий [Puranen et al. 2010], наук о Земле [Mandarino 1994; Séby et al. 2001] и структурной химии [Choudhury et al. 2002; Krivovichev et al. 2005a].

Селен является «полиморфным» химическим элементом с точки зрения кристаллохимии. В зависимости от условий роста селен может оказываться в разных степенях окисления. В настоящей работе изучены новые кислородные соединения селена в степенях окисления +4 (селениты) и +6 (селенаты), обладающие широким структурным разнообразием. Селениды (Se^{2-}), существенно не растворимые в воде, остались за пределами настоящего исследования. Однако следует заметить, что последние обладают более широким распространением в природе по сравнению с кислородсодержащими минералами селена. К настоящему времени Международная минералогическая ассоциация (далее – ММА) официально подтверждает существование 85 различных селенидных минеральных видов.

В природных геохимических обстановках селениты и селенаты относительно редки. К концу XX столетия было известно только 16 кислородных минералов селена. За последние 20 лет произошел значительный прогресс в химии природных селенсодержащих фаз, что привело к открытию еще 17 новых минералов. В результате, по данным ММА, сегодня официально известно 33 оксидных минерала селена. В природе

селенитные формы заметно превосходят по общему количеству селенаты, что может быть объяснено возможным результатом легко протекающих в водной среде процессов восстановления Se^{6+} до Se^{4+} и даже до элементарного селена Se^{0}.

Изучение селенитов и селенатов занимает ученых уже более полутора столетий. Первое селеновое соединение, так называемый керстенит (дискредитирован ММА в 2006 году и отнесен к молибдениту или олзахериту), был кратко описан *К. Керстеном* [Kersten 1839]. Тем не менее, несмотря на большое количество накопившейся информации о соединениях селена, лишь несколько обзорных работ было опубликовано к настоящему времени. В 1994 году *Дж. Мандарино* посвятил свой обзор геохимическим характеристикам природных и синтетических селенитов [Mandarino 1994]. А пять лет спустя *В. Верма* представил большую работу, посвященную синтезу, ИК и рамановской спектроскопии, термическому и рентгеноструктурному анализам селенитов металлов [Verma 1999]. Отсутствие актуальных обзорных материалов, посвященных селенитам и селенатам, также послужило дополнительной мотивацией для выполнения настоящей исследовательской работы, в которой была предпринята попытка рационализировать характерные для селена структурные особенности и принципы кристаллического роста с целью будущего осуществления целенаправленного создания кислородных материалов с заданными свойствами.

Атом селена обладает электронной конфигурацией [Ar] $3d^{10}$ $4s^2$ $4p^4$ и, таким образом, шестью валентными электронами на внешней электронной оболочке. В кристаллической структуре селенатов катионы Se^{6+} тетраэдрически координированы четырьмя анионами O^{2-}, формируя в результате анионные группы $(Se^{6+}O_4)^{2-}$, обычно описываемые как содержащие две одиночные Se–O и две двойные Se=O связи. В селенитах же Se^{4+} катион находится в апикальных вершинах тригонально-пирамидальных групп $(Se^{4+}O_3)^{2-}$, образуя две одиночные Se–O и одну двойную Se=O связь. Неподеленная пара $4s^2$ оказывается стереохимически активной и выступает в качестве дополнительного внешнего лиганда, формируя $(ESe^{4+}O_3)^{2-}$ тетраэдры (E – неподеленная электронная пара). Достойны упоминания любопытные случаи, в которых неподеленная электронная пара атомов мышьяка фактически напрямую связывается с металлами, что можно обнаружить, например, в соединении $BaCoAs_2O_5$ [David et al. 2014]. Наличие в структуре неподеленных пар в комбинации с электронными свойствами других металлов (переходных, тяжелых и актинидных) приводит к увлекательной неорганической химии таких соединений. Кроме того, интерес к оксидным соединениям селена в настоящей работе также был простимулирован попытками понять основные фундаментальные причины их большого структурного разнообразия и лежащих в его основе кристаллохимических механизмов.

Неорганические медные селениты привлекают к себе заметный интерес не только ввиду их удивительных структурных и физических свойств, но и за их минералогическую

и геохимическую распространенность. Особый интерес представляют смешанновалентные Cu^{+}–Cu^{2+} системы с кристаллографически независимыми моно- и двухвалентными позициями меди, обладающими заметно отличающимися координациями в одной кристаллической структуре. Важной особенностью многих медных оксоселенитов является наличие в их структурах оксоцентрированных (μ_4–O)Cu_4 тетраэдрических групп, которые полимеризуются с образованием протяженных структурных комплексов [Krivovichev et al. 2013b]. Далее в главе 2.2 представлено структурное описание восьми новых медных оксоселенитов, синтезированных лабораторным способом, моделирующим такие необычные геологические условия, как вулканические фумаролы.

До настоящего времени в литературе не нашлось сведений об исследованиях тройных оксоселенитных систем со свинцом и с никелем/кобальтом в роли переходных металлов. В главе 2.3 представлено подробное исследование кристаллического роста в PbO–NiO–SeO_2 системе в гидротермальных условиях. Исследование, проведенное в рамках данной диссертационной работы, позволило получить четыре новых свинцовых никель/кобальтовых селенита.

Кристаллохимия селенсодержащих ванадатов весьма разнообразна ввиду специфических структурных особенностей, присущих VO_4, VO_5 и VO_6 группам. Богатству всевозможных координаций атомов ванадия способствует в том числе возможность его нахождения в различных валентных состояниях в кристаллических структурах [Evans and Hughes 1990; Schindler et al. 2000; Boudin et al. 2000]. Добавление несимметричных селенитных групп и тяжелых катионов, таких как Pb^{2+} со стереохимически активными неподеленными электронными парами, в структуры ванадатов приводит к формированию структурных полостей и соответственно материалов с открытыми архитектурами, имеющими важное прикладное значение и применяющимися, например, в катализе. В главе 2.4 описаны возможные пути синтеза свинцовых ванадат селенитов, дано описание кристаллических структур трех новых фаз, а также на примере полученных соединений продемонстрировано явление полиморфизма, широко проявляющееся в ванадатах.

В главе 2.5 представлено структурное описание семи новых соединений: одного марганцевого селената, трех хлор-селенитов висмута и трех марганцевых селенитов с висмутом. Последние три фазы являются первыми примерами кислородных соединений, содержащих как висмутовые, так и марганцевые катионы.

В шестнадцати новых уранил-селенатах и смешанных селенит-селенатах, охарактеризованных в главе 2.6, проявилось исключительное структурное многообразие, которое дополнительно изучалось с помощью теории графов. Разнообразие полиэдрических комплексов, обнаруживающееся в уранил-селенатах и селенит-

селенатах, сформированных полимеризацией координационных полиэдров U и Se, поистине уникально: начиная от изолированных островных и кластерных группировок до нанотубуленов [Krivovichev et al. 2005b; Krivovichev et al. 2005a; Alekseev et al. 2008]. Топология и геометрия этих групп контролируются множеством различных факторов, управляющих взаимодействиями между органическими и неорганическими подструктурами: гидрофильными-гидрофобными взаимодействиями, зарядовой плотностью, слабым водородным связыванием. Корреляция состав – структура в уранил-селенатах проведена с применением принципа размерностного понижения, впервые предложенного *Дж. Лонгом* с соавторами [Long et al. 1996; Tulsky and Long 2001; Alekseev et al. 2007; Krivovichev 2009].

В главе 2.7, проведена аналогия между неподеленными электронными парами селенитных групп и H–P связями в фосфитных анионах на примере соединений $Fe_2(SeO_3)_3$ и $Fe_2(HPO_3)_3$. Демонстрируется, что в кристаллических соединениях, содержащих $(HPO_3)^{2-}$ анионы, атом водорода оказывается заряженным отрицательно, по аналогии с неподеленной электронной парой в $(ESeO_3)^{2-}$, и обладает частично гидридным характером в фосфитах.

Настоящая работа выполнена в рамках международного проекта написания диссертации с совместным российско-французским руководством: Санкт-Петербургский государственный университет (Россия) и Университет наук и технологий Лилля-1 (Франция). В работе представлены результаты синтезов и кристаллохимического описания 39 новых кислородных соединений четырех- и шестивалентного селена.

Описание результатов приводится в части 2 настоящей диссертационной работы. Она состоит из 7 разделов:

1. Объекты и методы.
2. Кристаллохимическое исследование новых селенитов меди.
3. Кристаллохимическое исследование новых селенитов никеля и кобальта.
4. Кристаллохимическое исследование новых ванадат-селенитов.
5. Кристаллохимическое исследование новых соединений селена с марганцем и висмутом.
6. Кристаллохимическое исследование новых уранил-селенатов и селенит-селенатов.
7. Аналогия между селенитными и фосфитными оксоанионами.

Детальное описание теоретических и экспериментальных результатов может быть найдено в 8 публикациях в разделе Included Articles.

2 КРАТКОЕ ОПИСАНИЕ РЕЗУЛЬТАТОВ

Настоящая работа содержит результаты синтезов и кристаллохимического описания нескольких серий новых кислородных кристаллических соединений, содержащих селен в степенях окисления +4 и +6. Эти два состояния характеризуются образованием различных оксоанионов: $(SeO_3)^{2-}$ и $(SeO_4)^{2-}$. В рамках исследовательской работы был применен инновационный подход, предполагающий моделирование природных кристаллогенетических процессов. Для кристаллохимического изучения использовалась как традиционная описательная процедура, в основе которой лежит рассмотрение кристаллической структуры с позиции координации катионов, так и современная теория анионоцентрированных полиэдров [Krivovichev et al. 2013b], разработанная Санкт-Петербургской кристаллографической школой и в дальнейшем успешно применяемая в Лаборатории катализа и химии твердого тела университета Лилля-1. Эта теория незаменима в случаях, когда традиционная структурная интерпретация не отражает основных принципов структурной архитектуры. Экспериментальные результаты приведены в соответствующих главах данного раздела диссертации.

2.1 Объекты и методы

Кристаллические образцы, изученные в настоящей работе, были синтезированы и изучены на кафедре кристаллографии Санкт-Петербургского государственного университета (Россия) и в лаборатории катализа и химии твердого тела Университета Лилля-1 (Франция). В работе использовалось несколько разных методов для синтеза кристаллических образцов, которые были выбраны по аналогии с известными

кристаллогенетическими процессами, протекающими в природных геохимических обстановках.

Метод химических газотранспортных реакций (далее – ХГТ реакции) [Binnewies et al. 2013] был применен для синтеза серий медных оксоселенитов, висмутовых селенит-оксохлоридов и одного ванадат-селенита. Этот метод может рассматриваться как модель кристаллогенетических природных условий, в которых, к примеру, медные оксоселениты формируются под действием конденсации вулканических газов, выделившихся из охлаждающихся магматических камер, располагающихся в течение длительного времени после эруптивной активности под земной поверхностью. Согласно идее, первоначально предложенной *С. К. Филатовым* с соавторами [Filatov et al. 1992], в ходе таких вулканических ХГТ реакций селениты и галогениды металлов играют роль транспортных агентов.

Кристаллические образцы свинцовых никель/кобальтовых селенитов, свинцовых ванадат-селенитов и одного марганцевого висмут-селенита были приготовлены с помощью *гидротермальных методов*. Гидротермальные реакции проводились в 23 миллилитровых стальных автоклавах с тефлоновыми вставками, которые нагревались в печах с механической конвекцией. Автоклавы выдерживались при постоянной температуре в течение нескольких дней, а затем медленно охлаждались до комнатной температуры. Описанный лабораторный метод рассматривается как аналог процессов, проходящих в зонах окисления минеральных месторождений на малых глубинах или в приповерхностных зонах, где было обнаружено большинство из известных ныне природных селеновых оксосолей.

Для синтеза большой серии уранил-селенатов и селенит-селенатов применялся *метод изотермического испарения* из водных растворов при комнатных условиях. Аналогичный процесс окисления отходов отработанного ядерного топлива в зонах расположения геологических могильников, сопровождающийся распадом нестабильных изотопов урана, приводит к образованию и попаданию в окружающую среду различных водорастворимых кристаллических соединений уранила. Хотя ^{79}Se изотоп содержится в отходах отработанного ядерного топлива в малых количествах (<0.05% [Choppin 2001]), его длительный период полураспада, составляющий $3.27 \cdot 10^5$ years [Jörg et al. 2010], вкупе с его высокой химической подвижностью приводит к большому геохимическому и минералогическому распространению селенсодержащих уранильных соединений в зонах окисления урановых месторождений и в областях расположения геологических могильников для отработанного ядерного топлива.

Монокристальные рентгеновские дифракционные исследования проведены с использованием следующего оборудования: Stoe IPDS II Image-Plate X-ray дифрактометр (СПбГУ, Россия), Bruker DUO APEX II CCD четырехкружный дифрактометр,

оборудованный микрофокусной Mo-IμS трубкой (СПбГУ, Россия; Университет Лилля-1, Франция) и Bruker X8 APEX II CCD дифрактометр (Университет Лилля-1, Франция). Более полусферы *3D* данных было собрано для каждого изученного кристалла с использованием монохроматического источника рентгеновского MoK_α излучения, λ = 0.71073 Å.

Кристаллические структуры были решены прямыми методами и уточнены в программном комплексе SHELX [Sheldrick 2008]. Симметрия структурных моделей была проверена в программе PLATON [Spek 2009]. В некоторых случаях для удобства использовались кристаллографическая система JANA 2006 [Petříček et al. 2014] и метод переворота заряда, встроенный в программу SUPERFLIP [Palatinus and Chapuis 2007]. Окончательные уточненные структурные модели всех изученных соединений включают атомные позиционные параметры и параметры анизотропного смещения.

Порошковые дифракционные анализы выполнены при комнатной температуре с использованием D8 Advance Bruker AXS дифрактометра с CuK_α рентгеновским излучением, λ = 1.5418 Å (Университет Лилля-1, Франция).

ИК абсорбционные спектры измерены в диапазоне 4000 – 400 см$^{-1}$ на спектрометре Perkin–Elmer Spectrum Two, оборудованном универсальной приставкой НПВО с алмазным кристаллом и контролем степени прижима (Университет Лилля-1, Франция).

Сканирующая электронная микроскопия и энергодисперсионные рентгеновские анализы были выполнены на микроскопе HITACHI S4700 microscope при 20 кВ и 15 μA на различных увеличениях (Университет Лилля-1, Франция). Атомарные соотношения были определены с использованием метода полуколичественной деконволюции.

Магнитные свойства образцов анализировали совместно с доктором Сильвиу Коли из Страсбургского института физики и химии материалов (Франция) с использованием магнитометра MPMS SQUID-VSM (Quantum Design) при температуре 1.8–300 K и поле 0–7 T. Зависимость магнитной восприимчивости от температуры была измерена в поле 0.02 T после того, как образец был предварительно охлажден. В некоторых случаях порошковые образцы были предварительно магнитно «выровнены» при 7 T в полимерном геле, замораживающем ориентацию частиц при температуре ниже ~303 K.

Микроскопия генерации второй гармоники была выполнена совместно с доктором Кристин Террин из Реймского университета (Франция). Для измерений применялся лазерный сканирующий микроскоп LSM 710 NLO Zeiss. Для генерации гармоники на монокристаллах использовалась фемто-секундная лазерная установка CHAMELEON Titanium-Sapphire laser на 860 нм. Для детектирования сигнала применялся полосовой фильтр (420 до 440 нм).

2.2 Кристаллохимическое исследование новых селенитов меди

Основные кристаллографические сведения и параметры уточнения кристаллических структур восьми новых соединений, приведенных ниже, представлены в табл. 2.1.

c2.1 – $K[Cu_5O_2](SeO_3)_2Cl_3$
c2.2 – $Na[Cu_5O_2](SeO_3)_2Cl_3$
c2.3 – $K[Cu_3O](SeO_3)_2Cl$
c2.4 – $Na_2[Cu_7O_2](SeO_3)_4Cl_4$
c2.5 – $[NaCl][Cu(SeO_2OH)_2]$
c2.6 – $[Cu^{+}Cl_2][Pb_2Cu^{2+}{}_9O_4](SeO_3)_4Cl_5$
c2.7 – $[Cu^{+}Cl_2][PbCu^{2+}{}_5O_2](SeO_3)_2Cl_3$
c2.8 – $K_{(1-x)}[Cu^{+}Cl_2][Pb_xCu^{2+}{}_{(6-x)}O_2](SeO_3)_2Cl_{(4-x)}$, $x = 0.20$

ТАБЛИЦА 2.1 Кристаллографические сведения и параметры уточнения структур соединений **c2.1**, **c2.2**, **c2.3**, **c2.4**, **c2.5**, **c2.6**, **c2.7** и **c2.8**

	c2.1	**c2.2**	**c2.3**	**c2.4**	**c2.5**	**c2.6**	**c2.7**	**c2.8**
M_r (г моль$^{-1}$)	749.07	732.96	535.09	1172.40	755.83	1869.77	2103.20	1992.64
пр. гр.	*Pnma*	*Pnma*	*P*–1	*P*–1	*C*2/*c*	*C*2/*m*	*C*2/*m*	*C*2/*m*
a (Å)	18.1691(6)	17.749(2)	7.6821(5)	7.4362(6)	13.9874(7)	18.605(17)	18.4956(4)	15.116(1)
b (Å)	6.4483(2)	6.4412(6)	8.1179(5)	8.3361(7)	7.2594(4)	6.204(6)	6.1454(1)	6.1853(4)
c (Å)	10.5684(4)	10.488(1)	8.7836(6)	9.134(1)	9.0421(5)	12.673(11)	15.2985(4)	9.2672(9)
α (°)	90	90	113.19(1)	110.28(1)	90	90	90	90
β (°)	90	90	108.73(1)	106.21(1)	127.04(1)	109.87(2)	119.31(1)	95.965(5)
γ (°)	90	90	98.245(4)	105.16(1)	90	90	90	90
V (Å^3)	1238.19(7)	1199.0(2)	453.32(5)	467.94(8)	732.81(7)	1376(2)	1516.3(1)	861.7(1)
Z	4	4	2	1	2	2	2	1
ρ (г/см^3)	4.018	4.060	3.920	4.160	3.425	4.514	4.607	3.840
μ (мм$^{-1}$)	15.333	15.523	15.757	16.263	13.313	25.78	25.02	15.52
λ (MoK_α) (Å)	0.71073	0.71073	0.71073	0.71073	0.71073	0.71073	0.71073	0.71073
всего рефл.	9584	7946	5607	11190	3926	12055	8423	5430
независ. рефл.	2233	2042	1749	2842	1170	3370	2841	1479
R_{int}	0.027	0.098	0.050	0.047	0.026	0.093	0.025	0.030
R_1 [$I > 2\sigma(I)$]	0.018	0.049	0.048	0.027	0.021	0.035	0.028	0.045
wR_2 [$I > 2\sigma(I)$]	0.040	0.065	0.117	0.060	0.051	0.040	0.077	0.116
R_1 [all data]	0.023	0.099	0.080	0.032	0.030	0.095	0.029	0.061
wR_2 [all data]	0.041	0.077	0.133	0.062	0.053	0.048	0.078	0.125
GOF	1.035	0.991	1.014	1.070	1.081	0.716	1.126	1.070
$\Delta\rho_{max}$, $\Delta\rho_{min}$,	0.74,	1.62,	1.62,	0.85,	0.70,	1.75,	4.19,	4.25,
(e Å^{-3})	−0.77	−1.67	−1.62	−0.95	−0.65	−1.86	−3.39	−1.99

2.2.1 Экспериментальные процедуры

Монокристаллы всех новых медных селенитов были синтезированы методом химических газотранспортных реакций. В ходе ХГТ реакции начальное вещество частично переносится газовым транспортным агентом из зоны-источника в зону осаждения под действием температурного градиента. Общая схема метода ХГТ реакции изображена на рис. 2.1а.

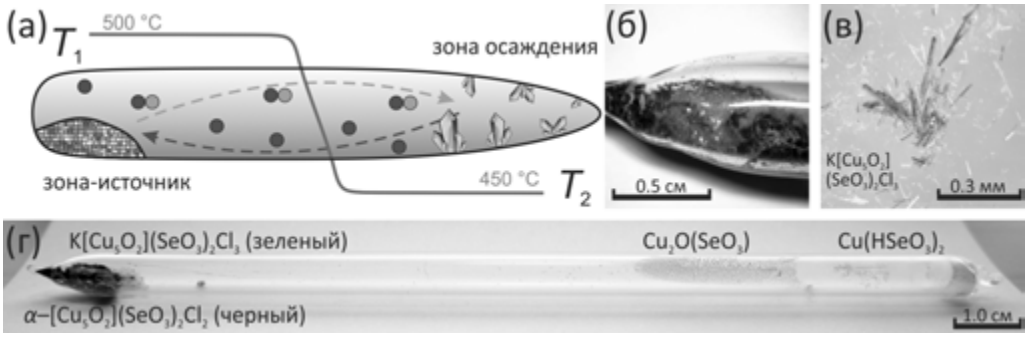

РИСУНОК 2.1 Общая схема метода ХГТ реакции – (а), зона-источник в ампуле – (б), кристаллы $K[Cu_5O_2](SeO_3)_2Cl_3$ (**c2.1**), отобранные из зоны-источника – (в), общий вид запаянной стеклянной ампулы после ХГТ реакции – (г)

Смеси начальных реагентов в различных молярных соотношениях (табл. 2.2) были тщательно перемешаны и загружены в стеклянные ампулы длиной около 15 см, давление в которых было понижено до 10^{-2} мбар, после чего они были запаяны. Ампулы располагались горизонтально в трубчатой печи, нагревались до 500–550 °C в течение 3-4 дней, а затем медленно охлаждались до комнатной температуры. Температурный градиент между зоной-источником (горячей) и зоной осаждения (холодной) ампул в печи был около 50 °C. Кристаллы новых фаз были обнаружены в различных частях ампул в ассоциации с уже известными соединениями (рис. 2.1г).

ТАБЛИЦА 2.2 Экспериментальные условия синтезов новых селенитов меди методом химических газотранспортных реакций

Молярные соотношения:	**c2.1**	**c2.2**	**c2.3**	**c2.4**	**c2.5**	**c2.6**	**c2.7**	**c2.8**
SeO_2	2	2	2	2	2	1	1	1
CuO	4	4	4	4	4	0	2	2
$CuCl_2$	1	1	1	1	1	2.25	1.50	1.50
CuCl	0	0	0	0	0	1.25	0	0
KCl	1	0	3	0	0	0	0	1
NaCl	0	1	0	3	3	0.50	1	0
PbO	0	0	0	0	0	0.75	0.50	0.50
Условия синтеза:	**c2.1**	**c2.2**	**c2.3**	**c2.4**	**c2.5**	**c2.6**	**c2.7**	**c2.8**
температура (°C)	500	500	500	500	500	500	550	550
время синтеза (ч)	72	72	72	72	72	96	72	72
охлаждение (ч)	24	24	24	24	24	12	6	6

2.2.2 Структурное описание восьми новых фаз

$A[Cu_5O_2](SeO_3)_2Cl_3$ ($A = K^+, Na^+$)

$K[Cu_5O_2](SeO_3)_2Cl_3$ (**c2.1**) и $Na[Cu_5O_2](SeO_3)_2Cl_3$ (**c2.2**) принадлежат к одному структурному типу и являются синтетическими аналогами минерала Na-ильинскита [Vergasova et al. 1997; Krivovichev et al. 2013a]. Кристаллические структуры **c2.1** (K) и **c2.2** (Na) содержат по четыре симметрично независимые медные позиции с различным смешанно-лигандным окружением. Атомы в позиции Cu(1) координированы 5 анионами, которые формируют квадратные пирамиды {Cu[(4O)+Cl]}. Медные катионы в позиции Cu(3) обладают искаженной квадратной координацией [3O+Cl]. Окружения катионов в позициях Cu(2) и Cu(4) в структурах **c2.1** (K) и **c2.2** (Na) оказываются разными по причине смещения позиции Cl(3) под влиянием большего радиуса катионов K^+ по сравнению с Na^+. В результате катионы в позиции Cu(2) обладают искаженным квадратно пирамидальным окружением [(3O+Cl)+Cl] в **c2.2** (Na) и искаженным октаэдрическим окружением [(3O+Cl)+2Cl] в кристаллической структуре **c2.1** (K). Атомы Cu(4) обладают октаэдрической координацией [(4O)+2Cl] в **c2.2** (Na), тогда как смещение Cl(3) анионов, вызванное большим размером K^+ катионов в **c2.1** (K), приводит к изменению координационного полиэдра Cu(4) до квадратной пирамиды {Cu[(4O+Cl)]} с одной аксиальной Cu(4)–Cl(3) связью аналогично окружению Cu(1) в обеих структурах. В кристаллических структурах **c2.1** (K) и **c2.2** (Na) находятся две симметрично независимые Se^{4+} позиции, которые имеют кислородную координацию тригональной пирамиды со стереохимически активной неподеленной электронной парой в качестве дополнительного лиганда. Катионы Na^+ в **c2.2** (Na) окружены одним атомом кислорода и четырьмя атомами хлора, формируя искаженную тригональную бипирамиду {Na[(O+2Cl)+2Cl]}. В **c2.1** (K) катионы K^+ обладают искаженной координацией и окружены пятью O^{2-}- и четырьмя Cl^- анионами.

Интересной особенностью кристаллических структур **c2.1** (K) и **c2.2** (Na) является наличие «дополнительных» кислородных атомов, которые окружены четырьмя катионами Cu^{2+}, так что в результате образуют оксоцентрированные тетраэдры $(OCu_4)^{6+}$ (рис. 2.2). Тетраэдрические комплексы объединяются через общие медные вершины, формируя слои $[Cu_5O_2]^{6+}$ параллельно плоскости (100). В кристаллических структурах **c2.1** (K) и **c2.2** (Na) слои $[Cu_5O_2]^{6+}$ окружены тригональными селенитными пирамидами и анионами хлора с образованием микропористого каркаса. Пустоты заполняются катионами щелочных металлов и неподеленными электронными парами селенитных групп. Детальное описание кристаллических структур соединений **c2.1** (K) и **c2.2** (Na) приведено в статье **A-VII** (см. Included Articles).

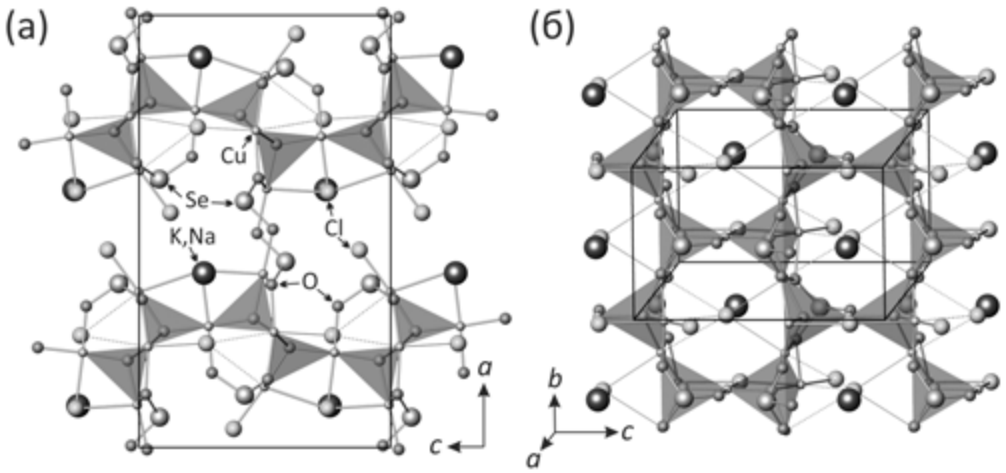

РИСУНОК 2.2 Кристаллические структуры $A[Cu_5O_2](SeO_3)_2Cl_3$ ($A^+ = K^+$ (**c2.1**), Na^+ (**c2.2**)) в двух проекциях, демонстрирующих слой $[O_2Cu_5]^{6+}$, образованный оксоцентрированными тетраэдрами $(OCu_4)^{6+}$ (выделен красным цветом)

K[Cu₃O](SeO₃)₂Cl и Na₂[Cu₇O₂](SeO₃)₄Cl₄

Структура $K[Cu_3O](SeO_3)_2Cl$ (**c2.3**) содержит три симметрично независимые позиции Cu^{2+}. Позиция Cu(1) окружена четырьмя атомами O и одним атомом Cl с образованием необычной искаженной тригональной бипирамиды {Cu[(2O+Cl)+2O]}. Атомы Cu(2) имеют типичное для катионов Cu^{2+} квадратное окружение [(4O)]. Координационный полиэдр Cu(3) может быть описан как искаженный октаэдр {Cu[(4O)+(O+Cl)]}. Все эти разнообразные координационные полиэдры меди объединяются в слои, параллельные плоскости (001). Структура **c2.3** содержит два симметрично независимых катиона Se, которые образуют тригональные пирамиды $(SeO_3)^{2-}$, характерные для состояния окисления +4. Катионы K^+ обладают искаженной координацией и окружены семью O^{2-}- и двумя Cl^- анионами.

В кристаллической структуре $Na_2[Cu_7O_2](SeO_3)_4Cl_4$ (**c2.4**) находятся четыре симметрично независимых медных катиона. Атомы в позиции Cu(1) образуют квадратные комплексы {Cu[(4O)]} по аналогии с позицией Cu(2) в структуре **c2.3**. Позиции Cu(2) и Cu(4) окружены тремя O и одним Cl с образованием искаженных квадратных группировок {Cu[(3O+Cl)]}. Точно такая же координация [(3O+Cl)] была обнаружена в кристаллических структурах **c2.1** и **c2.2**. Позиция Cu(3) в кристаллической структуре **c2.4** обладает тригонально бипирамидальной координацией [(2O+Cl)+2O]. Два симметрично неэквивалентных атома селена формируют типичные тригональные пирамиды $(SeO_3)^{2-}$. Катионы Na^+ окружены шестью O^{2-}- и одним Cl^- анионом с образованием искаженного тригонально-призматического кислородного окружения.

В кристаллической структуре **c2.3** два тетраэдра $(OCu_4)^{6+}$ объединяются через общее ребро Cu···Cu с образованием димера $[O_2Cu_6]^{8+}$. В структуре **c2.4** также можно выделить димерные комплексы, но другого состава – $[O_2Cu_7]^{10+}$, сформированные объединением двух тетраэдров $(OCu_4)^{6+}$ через общий атом Cu. Селенитные группы и атомы Cl окружают эти димеры, образуя структурные комплексы $\{[O_2Cu_6](SeO_3)_4Cl_2]\}^{2-}$ и $\{[O_2Cu_7](SeO_3)_4Cl_4]\}^{2-}$ в **c2.3** и **c2.4** соответственно, которые затем связываются между собой в слои (рис. 2.3). Межслоевое пространство в структурах занято щелочными катионами. Сравнение способов связывания групп $(SeO_3)^{2-}$ с оксоцентрированными димерами в известных медных оксосолях приведено в главе 2.2.3.

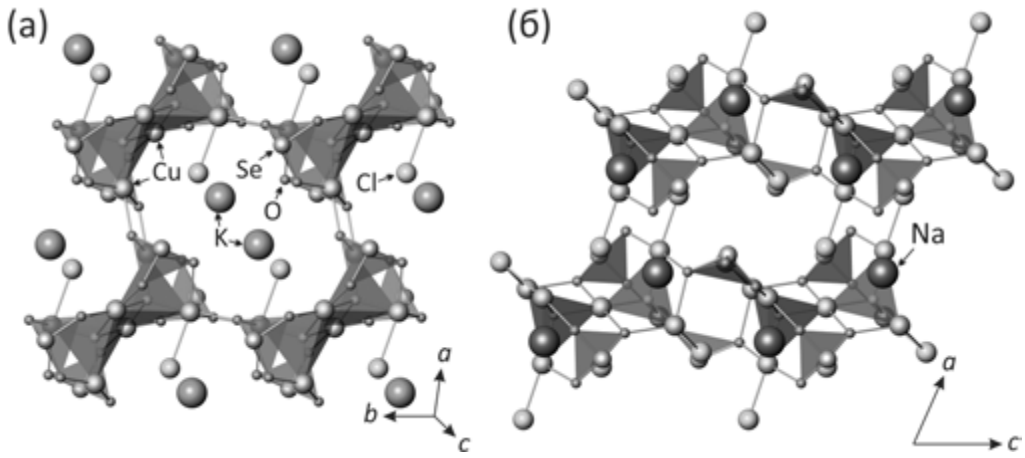

РИСУНОК 2.3 Кристаллические структуры $K[Cu_3O](SeO_3)_2Cl$ (**c2.3**) – (а) и $Na_2[Cu_7O_2](SeO_3)_4Cl_4$ (**c2.4**) – (б). Тетраэдры $(OCu_4)^{6+}$ показаны серым

[NaCl][Cu(SeO$_2$OH)$_2$]

Кристаллическая структура $[NaCl][Cu(SeO_2OH)_2]$ (**c2.5**) содержит один симметрично независимый атом Cu, октаэдрически координированный четырьмя O- и двумя Cl атомами. Катионы меди образуют правильные квадратные группы (CuO_4), которые дополняются двумя длинными связями Cu–Cl, что приводит в результате к координации [(4O)+(2Cl)] аналогичной октаэдрической позиции Cu(4) в структуре **c2.2**. В структуре соединения **c2.5** единственная кристаллографически независимая позиция Se окружена тремя атомами кислорода, образуя характерную для селенитов тригональную пирамиду (SeO_3). Одна из трех связей Se–O оказывается заметно длиннее (1.751 Å) двух других (1.671 Å и 1.680 Å), что может быть объяснено протонированием кислородной позиции $O_h(1)$. Квадратные (CuO_4) и тригонально пирамидальные (SeO_2OH) группы объединяются через общие кислородные вершины с образованием электронейтральных слоев

$[Cu(SeO_2OH)_2]^0$, параллельных плоскости (100) (рис. 2.4). Между двумя протонированными селенитными группами $(SeO_2OH)^-$ водородная связь $O_h(1)\cdots O(2)$ образует димер $[(SeO_2OH)_2]^{2-}$, который дополнительно стабилизирует медный диселенитный слой.

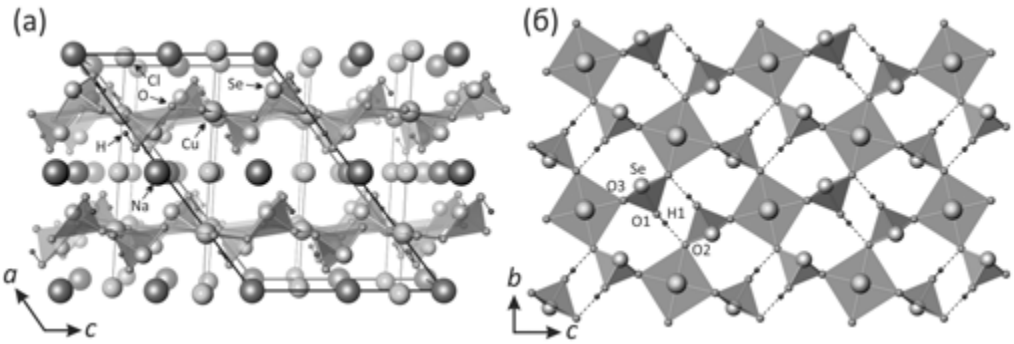

РИСУНОК 2.4 Проекция кристаллической структуры $[NaCl][Cu(HSeO_3)_2]$ (**c2.5**) – (а) и ее электронейтрального слоя $[Cu(HSeO_3)_2]$ – (б)

В кристаллической структуре **c2.5** слои $[Cu(HSeO_3)_2]^0$ чередуются со слоями, содержащими зигзагообразные цепочки –Na–Cl–Na–Cl–, образованные атомами хлора и разупорядоченными позициями натрия. Цепочки параллельны кристаллографической оси *c*. Связывание между чередующимися электронейтральными слоями $[Cu(HSeO_3)_2]^0$ и $[NaCl]^0$ достигается за счет взаимодействий Cu–Cl и Na–O. Катионы натрия обладают искаженной координацией и окружены тремя O- и двумя Cl атомами.

Соединение **c2.5** может считаться членом серии соединений, основанных на слоях $M(SeO_2OH)_2$ (M = Cu^{2+}, Co^{2+}, Cd^{2+}). Структурным прототипом для данной группы соединений является $[Cu(SeO_2OH)_2]$ [Effenberger 1985], которое не содержит никаких дополнительных ионов, разделяющих медные гидроселенитные слои. В структурах других соединений из этой группы пространство между слоями $[Cu(SeO_2OH)_2]^0$ занято химическими компонентами различной размерности. Во всех соединениях слои $[Cu(SeO_2OH)_2]^0$ обладают приблизительно одинаковыми плоскостными размерами (измеренные как расстояния между парами атомов, связанных операциями симметрии). Исключением является фаза $[Cu(SeO_2OH)_2](H_2O)_2$ [Lafront and Trombe 1995], в структуре которой слои сильно изогнуты. Детальное описание кристаллической структуры соединения **c2.5** приведено в статье **A-VIII** (см. Included Articles).

$[Cu^{+}Cl_2][Pb_2Cu^{2+}{}_9O_4](SeO_3)_4Cl_5$, $[Cu^{+}Cl_2][PbCu^{2+}{}_5O_2](SeO_3)_2Cl_3$ и $K_{(1-x)}[Cu^{+}Cl_2][Pb_xCu_{(6-x)}O_2](SeO_3)_2Cl_{(4-x)}$, $x = 0.20$

Весьма необычной структурной особенностью этих трех соединений является присутствие линейных группировок $(Cu^{+}Cl_2)^{-}$ в пустотах ячеистых псевдогексагональных слоистых комплексов, образованных оксоцентрированными тетраэдрами $(O(Cu/Pb)_4)^{6+}$ и группами $(SeO_3)^{2-}$, объединенными через общие вершины.

В структурах $[Cu^{+}Cl_2][Pb_2Cu_9O_4](SeO_3)_4Cl_5$ (**c2.6**), $[Cu^{+}Cl_2][PbCu_5O_2](SeO_3)_2Cl_3$ (**c2.7**) и $K_{(1-x)}[Cu^{+}Cl_2][Pb_xCu^{2+}{}_{(6-x)}O_2](SeO_3)_2Cl_{(4-x)}$, x = 0.20 (**c2.8**), однозарядные катионы Cu^{+} образуют две относительно короткие связи Cu^{+}–Cl, что приводит к формированию прочно связанных анионных группировок $(Cu^{+}Cl_2)^{-}$. Катионы же Cu^{2+} обладают смешанным оксохлоридным окружением, имеющим склонность к деформационному эффекту Яна – Теллера. Двухвалентные атомы меди в позициях Cu(1) и Cu(2) в **c2.6**, Cu(4) в **c2.7** и Cu(3) в **c2.8** образуют такие же искаженные октаэдры {Cu[(4O)+(2Cl)]}, как и в позициях Cu(4) и Cu(1) в структурах **c2.2** и **c2.5** соответственно. Позиции Cu(3) в **c2.6**, Cu(2), Cu(3) в **c2.7** и Cu(1) в **c2.8** обладают октаэдрической координацией [(3O+Cl)+2Cl]. Та же координация была обнаружена и в позиции Cu(2) в структуре соединения **c2.1**. Катионы в позиции Cu(4) в **c2.6** формируют тригональные бипирамиды {Cu[(3O)+(O+Cl)]}, тогда как Cu(1) в **c2.7** и Cu(4) в **c2.8** обладают похожей координацией [(2O+Cl)+(O+Cl)]. Атомы Pb имеют несимметричное окружение, состоящее из трех сильных связей Pb–O, расположенных в одной координационной сфере, и четырех коротких связей Pb–Cl – в другой. Подобная координация катионов Pb^{2+} согласуется с присутствием стереоактивных неподеленных электронных пар. Катионы Se^{4+} образуют типичные тригонально-пирамидальные оксоанионы $(SeO_3)^{2-}$. Кристаллическая структура **c2.8** содержит одну симметрично независимую позицию K с фактором заселенности позиции (s.o.f.), равным 0.8. Калиевый координационный полиэдр может быть описан как искаженная гексагональная бипирамида.

В кристаллической структуре **c2.6** также присутствуют два «дополнительных» атома O, которые образуют тетраэдры $(OCu^{2+}{}_3Pb)$ и $(OCu^{2+}{}_4)$. Эти оксоцентрированные тетраэдрические группы объединяются через общие вершины с образованием двойных цепочек $[O_4Pb_2Cu^{2+}{}_9]^{14+}$. В структуре этого соединения цепочки оказываются вытянуты вдоль кристаллографической оси *b*. Приблизительно одинаковое значение параметра *b* элементарных ячеек ($b \approx 6.2$ Å) во всех трех структурах дополнительно подчеркивает схожее расположение оксоцентрированных комплексов.

Двойная анионоцентрированная цепочка, обнаруженная в структуре **c2.6**, в неорганических соединениях встречена впервые. Селенитные группы SeO_3 прикрепляются к треугольным основаниям оксоцентрированных тетраэдров, что

приводит в результате к образованию *1D* комплексов $\{[O_4Pb_2Cu^{2+}_9](SeO_3)_4\}^{6+}$, связанных между собой через связи Pb–O в *2D* метал-оксидные двойные слои (рис. 2.5а).

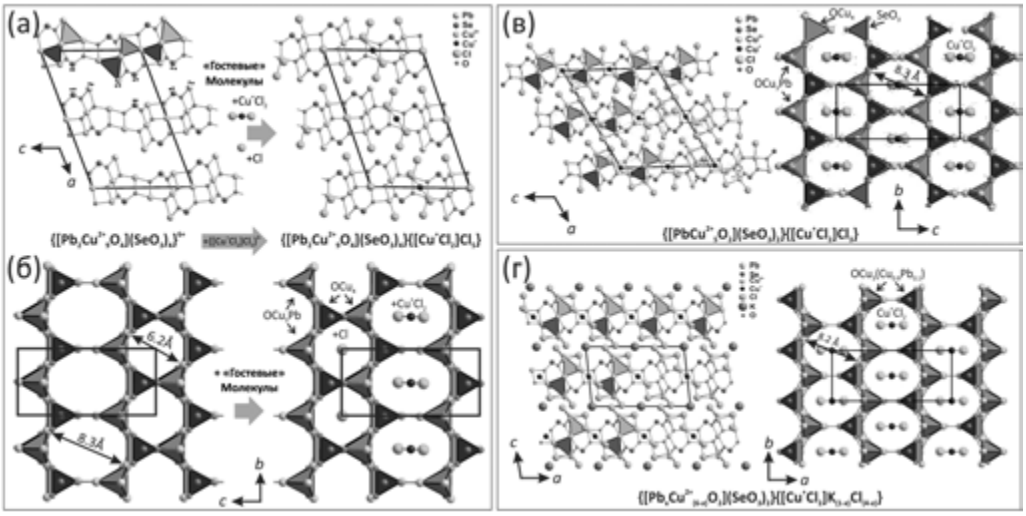

РИСУНОК 2.5 Проекции структур $[Cu^+Cl_2][Pb_2Cu_9O_4](SeO_3)_4Cl_5$ (**c2.6**) – (а) и (б), $[Cu^+Cl_2][PbCu_5O_2](SeO_3)_2Cl_3$ (**c2.7**) – (в) и $K_{(1-x)}[Cu^+Cl_2][Pb_xCu^{2+}_{(6-x)}O_2](SeO_3)_2Cl_{(4-x)}$, $x = 0.20$ (**c2.8**) – (г)

В проекции на плоскость (*b*, *c*) эти слои выглядят как гексагональные ячеистые комплексы, составленные из тетраэдров (рис. 2.5б). В межслоевом пространстве ячеистых комплексов анионы Cl^- располагаются таким образом, что линейные группировки $[Cu^+Cl_2]^-$ и одиночные ионы Cl^- оказываются в центральных частях соответственно больших и малых гексагональных ячеек. Принимая во внимание относительную силу связи Cu^+–Cl и слабые взаимодействия между этими группировками и другими частями структуры, они могут рассматриваться в качестве «гостевых» анионов, вошедших в комплекс оксохлоридной матрицы, основанной на оксоцентрированных тетраэдрах.

Похожий принцип «гость – хозяин» работает также и в структурах соединений **c2.7** и **c2.8**. Здесь тетраэдры (OCu^{2+}_3Pb) и (OCu^{2+}_4) объединяются через общие вершины с образованием простых цепочек составов $[O_2PbCu_5]^{8+}$ и $[O_2Pb_xCu^{2+}_{(6-x)}]^{8+}$, вытянутых вдоль кристаллографических осей *b* в обеих структурах. Обнаруженное в процессе уточнения кристаллической структуры **c2.8** частичное замещение катионов Pb^{2+} на Cu^{2+} оказывается допустимым и не влияет существенным образом на топологию оксоцентрированного комплекса. Вместе с группами SeO_3 эти цепочки образуют *1D* металл-оксидные остовы $\{[O_2M_6](SeO_3)_2\}^{4+}$ (M = Cu^{2+}, Pb^{2+}), которые располагаются в структурах в виде ячеистых псевдослоев (рис. 2.5 г, д). В центральных частях ячеек слоев располагаются только «гостевые» анионы $(Cu^+Cl_2)^-$. Структура **c2.8** также содержит катионы K^+, находящиеся в

пространстве между оксохлоридными медноселенитными слоями. Во всех трех структурах неподеленные электронные пары катионов Pb^{2+} и Se^{4+} ориентированы в межслоевое пространство, подчиняясь принципу «химических ножниц» для структур с катионами, обладающих химически стереоактивными неподеленными электронными парами. Детальное описание кристаллических структур соединений **c2.6**, **c2.7** и **c2.8** приведено в статье **A-V** (см. Included Articles).

2.2.3 Связывание селенитных групп с димерами $[OCu_4]^{6+}$

Соединения **c2.3** и **c2.4** являются представителями структурной группы минералов и синтетических соединений (табл. 2.3), отличительной особенностью которых является наличие димеров $[O_2(Cu/Pb)_6]^{8+}$ или $[O_2Cu_7]^{10+}$, образованных объединением тетраэдров $(O(Cu/Pb)_4)^{6+}$ по общему ребру или тетраэдров $(OCu_4)^{6+}$ через общую вершину соответственно. На рис. 2.6 показаны способы связывания селенитных групп с такими димерами в кристаллических структурах известных медных минералов и неорганических соединений. Существование и частое появление таких оксоцентрированных группировок в различных структурах служит косвенным свидетельством роли подобных комплексов в качестве зародышевых строительных блоков, существующих в газовых средах, таких как вулканические фумаролы или вакуумированные стеклянные ампулы, используемые в методе ХГТ реакций.

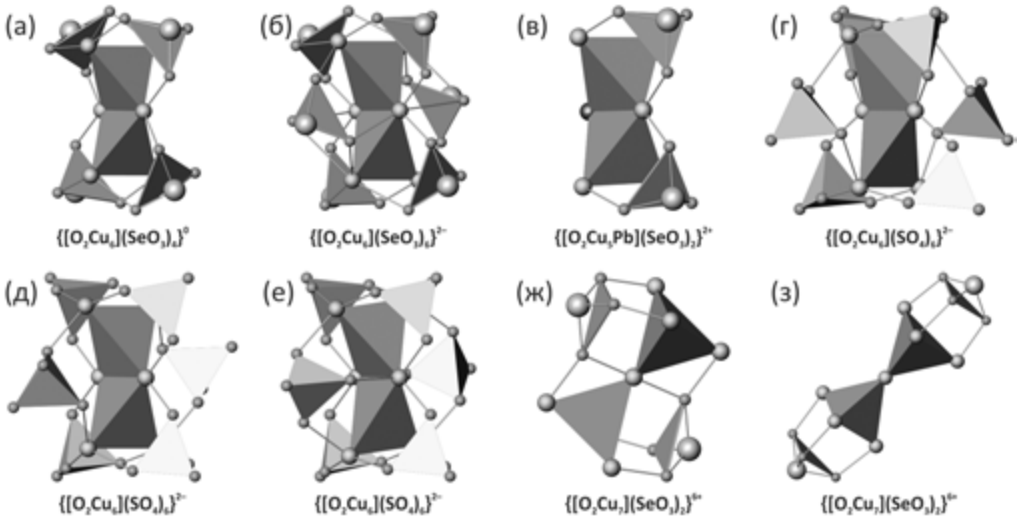

РИСУНОК 2.6 Координационное окружение димеров оксоцентрированных тетраэдров в кристаллических структурах минералов и синтетических соединений, приведенных в табл. 2.3.

ТАБЛИЦА 2.3 Кристаллографические сведения о минералах и синтетических медных соединениях, структуры которых основаны на димерах оксоцентрированных тетраэдров

Cu:O	Рис.	Химическая формула	Минерал	Простр. группа	*a* (Å); *α* (°)	*b* (Å); *β* (°)	*c* (Å); *γ* (°)	*V* (Å^3)	Ссылка
6:2	2.6а	$K[Cu_3O](SeO_3)_2Cl$		*P*–1	7.682; 113.2	8.118; 108.7	8.784; 98.2	453	**c2.3**
6:2	2.6а	$Cu[Cu_3O](SeO_3)_3$–I		$P2_1/a$	15.990	13.518; 90.5	17.745	3836	[1]
6:2	2.6б	$Cu[Cu_3O](SeO_3)_3$–II		*P*–1	7.992; 77.3	8.141; 66.6	8.391; 81.4	484	[1]
6:2	2.6в	$KPb_{0.5}Cu[PbCu_5O_2]Zn(SeO_3)_2Cl_{10}$	превиттит	*Pnnm*	9.132	19.415	13.213	2343	[2]
6:2	2.6г	$NaK[Cu_3O](SO_4)_3$	эвхлорин	*C*2/*c*	18.41	9.43; 113.7	14.21	2259	[3]
6:2	2.6г	$K_2[Cu_3O](SO_4)_3$	федотовит	*C*2/*c*	19.037	9.479; 111.0	14.231	2397	[4]
6:2	2.6д	$(NMe_2H_2)_4[Cu_6O_2](SO_4)_6(DMF)_4$		$P2_1/n$	13.105	10.514; 103.2	18.753	2516	[5]
6:2	2.6е	$(NMe_2H_2)_4[Cu_6O_2](SO_4)_6(DMF)_2$		*P*–1	8.588; 106.5	10.684; 104.6	12.817; 105.9	1012	[5]
7:2	2.6з	$KCd[Cu_7O_2](SeO_3)_2Cl_9$	бернсит	$P6_3/mmc$	8.781	8.781	15.521	1036	[6]
7:2	2.6ж	$Na_2[Cu_7O_2](SeO_3)_4Cl_4$		*P*–1	7.436; 110.3	8.336; 106.2	9.134; 105.2	468	**c2.4**

Ссылки: 1 – [Effenberger and Pertlik 1986]; 2 – [Shuvalov et al. 2013]; 3 – [Scordari and Stasi 1990]; 4 – [Starova et al. 1991]; 5 – [Burrows et al. 2012]; 6 – [Krivovichev et al. 2002; Burns et al. 2002].

2.3 Кристаллохимическое исследование новых селенитов никеля и кобальта

В этом разделе продолжается рассмотрение селенитов с двухвалентными переходными металлами, для которых характерен деформационный эффект Яна – Теллера. Одной из поставленных задач было изучение структурных топологий селенитных соединений, в которых катионы переходных металлов обладают октаэдрическим окружением. Основные кристаллографические сведения и параметры уточнения кристаллических структур четырех новых соединений, описанных в этой главе, представлены в табл. 3.1. Детальное описание полученных фаз в изученной системе и анализ обнаруженных магнитных свойств приведены в статье **A-IV** (см. Included Articles).

ТАБЛИЦА 3.1 Кристаллографические сведения и параметры уточнения структур соединений α–$PbNi(SeO_3)_2$ (**c3.1**), β–$PbNi(SeO_3)_2$ (**c3.2**), $PbNi_2(SeO_2OH)_2(SeO_3)_2$ (**c3.3**) и α–$PbCo(SeO_3)_2$ (**c3.4**)

	c3.1	**c3.2**	**c3.3**	**c3.4**
M_r (г моль$^{-1}$)	519.82	519.82	834.47	520.04
простр. группа	*Pnma*	*Cmc*2$_1$	*P*2/*c*	*Pnma*
a (Å)	12.7476(4)	5.4715(4)	13.6824(10)	12.8208(4)
b (Å)	5.4562(2)	9.1963(6)	5.2692(5)	5.4902(2)
c (Å)	7.8332(2)	11.4436(9)	19.3476(13)	7.9085(2)
β (°)	90	90	129.524(4)	90
V (Å^3)	544.83(3)	575.81(7)	1075.94(16)	556.67(3)
Z	4	4	4	4
ρ (г/см^3)	6.337	5.996	5.151	6.205
μ (мм$^{-1}$)	47.637	45.074	32.668	46.221
λ (MoK_α) (Å)	0.71073	0.71073	0.71073	0.71073
всего рефл.	10212	2345	5454	3226
независ. рефл.	823	686	2083	742
R_{int}	0.0336	0.0260	0.0459	0.0260
R_1 [$I > 2\sigma(I)$]	0.0139	0.0141	0.0496	0.0186
wR_2 [$I > 2\sigma(I)$]	0.0360	0.0346	0.0992	0.0429
R_1 [all data]	0.0165	0.0142	0.0783	0.0203
wR_2 [all data]	0.0387	0.0346	0.1104	0.0439
GOF	1.090	1.109	1.187	1.142
$\Delta\rho_{max}$,$\Delta\rho_{min}$ (*e* Å^{-3})	1.573, –1.110	1.310, –1.073	2.916, –2.912	0.971, –1.887
ICSD	428905	428906	428907	428904

2.3.1 Рост кристаллов в системе $PbO–NiO–SeO_2–H_2O$

В данной главе представлены результаты систематического изучения кристаллизации в системе $PbO–NiO–SeO_2–H_2O$ гидротермальным методом, относящимся к группе сольвотермальных кристаллогенетических техник, при котором образование большинства кристаллических фаз происходит незакономерно.

Экспериментальные процедуры

Для исследования кристаллического роста в системе PbO–NiO–SeO$_2$–H$_2$O возникла необходимость в изучении 36 возможных комбинаций молярных соотношений начальных реагентов, нанесенных на треугольник Гиббса (рис. 3.1).

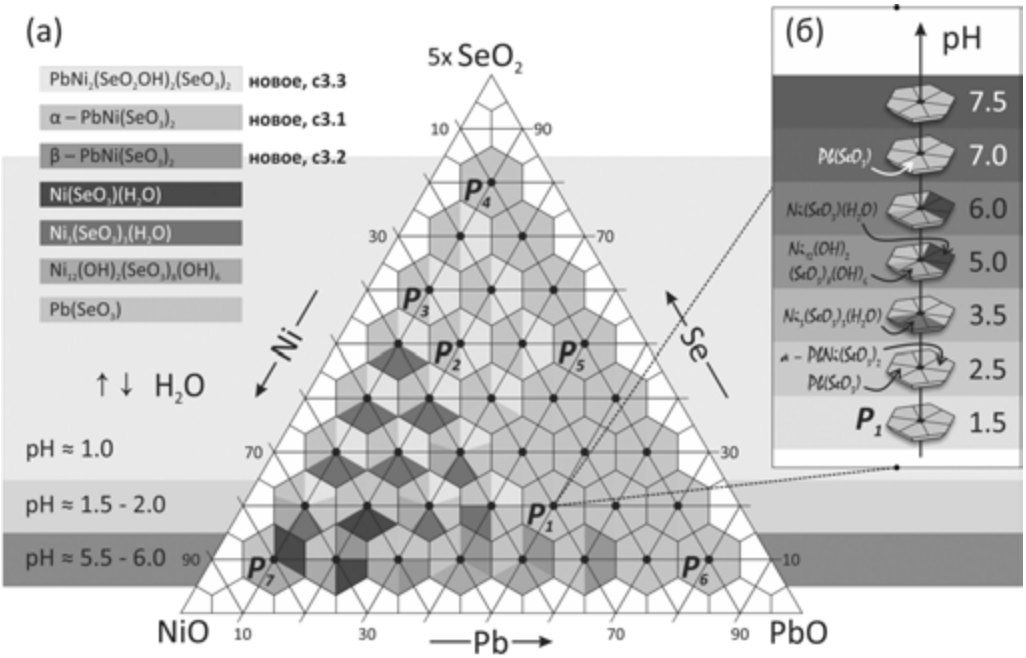

РИСУНОК 3.1 Экспериментальная кристаллизационная фазовая диаграмма системы PbO–NiO–SeO$_2$–H$_2$O при 200 °C – (а). Области с различными значениями pH показаны в фоне оттенками серого. Серия экспериментов с молярным соотношением PbO : NiO : SeO$_2$, равным 5 : 3 : 10, соответствующим точке ***P*$_1$**, но с разными значениями pH – (б)

Во всех синтезах молярные суммы mPbO + nNiO + (k/5)SeO$_2$ (m, n, k = 1, 2,… 8) были равны 10 ммоль, а смеси реагентов растворялись в 6 мл дистиллированной воды. В ходе пробных экспериментов было установлено, что существенно кислая среда благоприятствует появлению кристаллического многообразия и росту монокристальных фаз. Поэтому в экспериментах всегда использовался избыток SeO$_2$, для чего количество диоксида селена в молярных расчетах умножалось на пять. Измеренные значения pH увеличиваются от ~1 до ~5.5–6.0, обратно пропорционально содержанию SeO$_2$ в изучаемой системе. Все синтезированные поликристаллические фазы были систематически проанализированы методом порошковой рентгеновской дифракции, а представительные монокристаллы каждой из обнаруженных фаз были изучены методом монокристального дифракционного анализа. По полученным результатам была

составлена кристаллизационная фазовая диаграмма (рис. 3.1а), на которой кристаллизационные области, соответствующие различным фазам, обозначены разным цветом.

Гидротермальные реакции протекали в течение 36 часов в 23 мл стальных автоклавах с тефлоновыми вставками, нагретыми в печи до 200 °C. В конце эксперимента автоклавы медленно охлаждались в течение 48 часов. Продукты синтезов отфильтровывались через фильтровальную бумагу. Монокристаллы трех новых свинцовых никелевых селенитов – α–$PbNi(SeO_3)_2$ (**c3.1**), β–$PbNi(SeO_3)_2$ (**c3.2**) и $PbNi_2(SeO_2OH)_2(SeO_3)_2$ (**c3.3**) – были обнаружены в смеси с уже известными соединениями: $Ni(SeO_3)(H_2O)$ [Engelen et al. 1996], $Ni_3(SeO_3)_3(H_2O)$ [Wildner 1991; Mcmanus et al. 1991], $Ni_{12}(OH)_6(SeO_3)_8(OH)_2$ [Amorós et al. 1996] и $Pb(SeO_3)$ [Popovkin et al. 1963; Fischer 1972; Koskenlinna and Valkonen 1977]. Монокристаллы кобальтового селенита α–$PbCo(SeO_3)_2$ (**c3.4**) были получены в результате реакции, аналогичной той, которая использовалась для синтеза соединения **c3.1**. Попытки синтезировать Co-аналоги соединений **c3.2** и **c3.3**, используя аналогичную технику, оказались безуспешными. Кристаллы новых свинцовых селенитов представляли собой желтые иголки (**c3.1**), желтые призматические кристаллы (**c3.2**), салатовые пластинки (**c3.3**) и фиолетовые иголки (**c3.4**) размером до 300 μм.

Краткий анализ синтезированных фаз в системе

Анализ всех полученных кристаллических фаз в системе дает возможность провести грубую рационализацию, основанную на начальной стехиометрии и значениях pH. Соединение $Pb(SeO_3)$ оказалось наиболее часто встречаемым в системе и было обнаружено с различной степенью кристалличности в каждом гидротермальном эксперименте. Это может свидетельствовать в пользу предпочитаемой комплексации катионов Pb^{2+} анионами $(SeO_3)^{2-}$ вне зависимости от pH среды. Также следует обратить внимание на формирование богатых свинцом соединений в правом углу кристаллизационной диаграммы и свободных от свинца никелевых селенитов на левой стороне на треугольнике Гиббса. Этот результат, несмотря на свою ожидаемость, демонстрирует работу механизмов кристаллического роста, контролируемых концентрацией в растворе каждого из участвующих в реакции компонентов. Наконец, опуская систематическое появление соединения $Pb(SeO_3)$, можно заключить, что низкие значения pH благоприятствуют реакционной способности протонированных групп $(SeO_2OH)^-$ (например, в **c3.3**), тогда как селенитные группы $(SeO_3)^{2-}$ доминируют в водной среде при высоких значениях pH (например, в полиморфах **c3.1** и **c3.2**).

Роль pH

Для получения большей информации о реакционных процессах в системе PbO–NiO–SeO_2–H_2O было проведено более глубокое исследование отдельной стехиометрической смеси, соответствующей точке ***P*** *1* на диаграмме (PbO : NiO : SeO_2 = 5 : 3 : 10), при разных значениях pH вплоть до 7.5 (при более высоких значениях в растворе происходит восстановление SeO_2 до металлического γ – Se [Pourbaix 1974; Takeno 2005]). Перемешанные реагенты растворялись в 1.75 M водном растворе NaOH для достижения необходимых значений pH. Затем применялась классическая гидротермальная техника. Серия полученных продуктов синтеза в зависимости от значений pH показана на рис. 3.1б. Эти результаты наглядно демонстрируют существенное влияние pH среды на степень конденсации ионов в гидротермальном растворе. Соединение $Pb(SeO_3)$ вновь оказалось самым стабильным при любых значениях pH. В отношении всех других синтезированных фаз можно сделать следующий вывод: молекулы воды и затем гидроксид-анионы прогрессивно входят в структуры соединений с ростом pH. В частности, при pH 1.5–2.5 образуются только конденсированные соединения, такие как α–$PbNi(SeO_3)_2$ (**c3.1**) и $Pb(SeO_3)$. Реакция, протекающая при pH 3.5, приводит к образованию соединения $Ni_3(SeO_3)_3(H_2O)$, в котором одна треть катионов Ni^{2+} координируется молекулами воды. Рост pH до 5.0–6.0 заметно увеличивает вхождение водных молекул и/или гидроксильных групп в структуры соединений и делает возможным синтез $Ni_{12}(OH)_6(SeO_3)_8(OH)_2$ и $Ni(SeO_3)(H_2O)$. Кристаллическая структура последнего соединения собрана только из полиэдров $NiO_5(H_2O)$, тогда как в тубулярной структуре $Ni_{12}(OH)_2(SeO_3)_8(OH)_6$ половина позиций никеля образует протонированные октаэдры $NiO_5(OH)$. При значении pH больше 7.0 образуется только очень стабильная в системе фаза $Pb(SeO_3)$.

2.3.2 Структурное описание четырех новых соединений

α–$PbM(SeO_3)_2$ ($M = Ni^{2+}$, Co^{2+})

Изоструктурные соединения **c3.1** и **c3.4** основаны на *3D* каркасах, построенных из анионных комплексов $(SeO_3)^{2-}$ и $(MO_6)^{10-}$ (M = Ni^{2+}, Co^{2+}), объединенных через общие кислородные вершины (рис. 3.2). В структуре находится одна симметрично независимая позиция M^{2+}, формирующая правильный октаэдр $(MO_6)^{10-}$. Также в структуре на формульную единицу приходится два атома Se, которые образуют типичные тригональные пирамиды $(SeO_3)^{2-}$. Кристаллографически единственная позиция Pb^{2+} окружена атомами O, принадлежащими группам $(SeO_3)^{2-}$ и $(MO_6)^{10-}$. Катионы Pb^{2+} обладают несимметричной координацией со стереохимически активной неподеленной электронной парой, направленной внутрь полостей в структуре. На рис. 3.2б

3D металлический катионный каркас кристаллических структур соединений **c3.1** и **c3.4** представлен в виде черно-белого графа, в котором черные и белые вершины символизируют координационные полиэдры катионов M^{2+} и Se^{4+} соответственно. На приведенном графе хорошо видно, как полиэдры SeO_3 и MO_6 топологически связываются в сложный *3D* каркас, в котором обнаруживаются прямоугольные каналы, вытянутые вдоль направления [010] и занятые катионами свинца и неподеленными электронными парами четырехвалентных катионов селена. В проекции на плоскость (010) каналы располагаются взаимно перпендикулярно, ориентируясь поочередно вдоль [201] и [20-1] в соответствии с пространственной группой симметрии *Pnma*. Каналы ограничены шестью MO_6 и шестью SeO_3 полиэдрами (рис. 3.2а). Двухвалентные катионы свинца располагаются в структурных полостях и уравновешивают отрицательный заряд каркасов соединений **c3.1** и **c3.4**. Детальное описание кристаллической структуры соединений **c3.1** и **c3.4** приведено в статье **A-IV** (см. Included Articles).

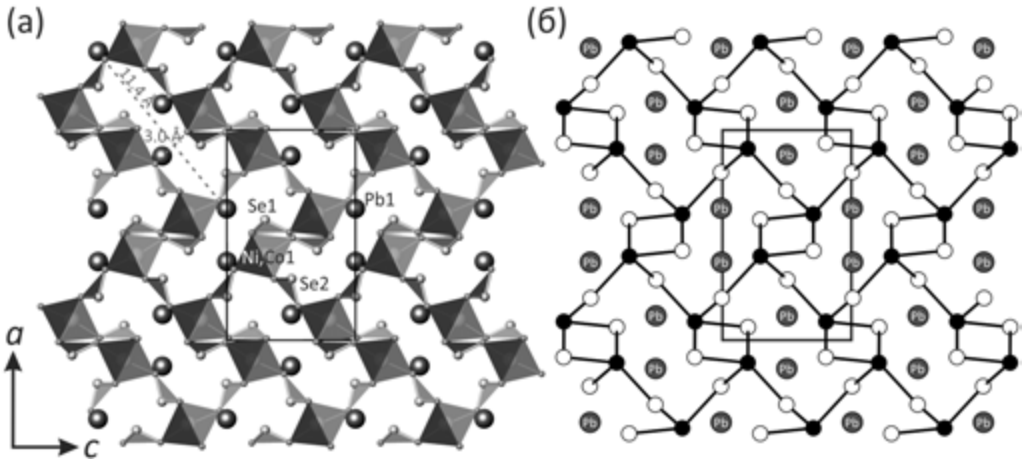

РИСУНОК 3.2 Общая проекция кристаллических структур соединений α–Pb$M$$(SeO_3)_2$ (M = Ni^{2+} (**c3.1**), Co^{2+} (**c3.4**)) вдоль кристаллографической оси *b* – (а) и соответствующий черно-белый граф – (б); катионы M^{2+} и Se^{4+} изображены черными и белыми кружками соответственно

β–PbNi(SeO₃)₂

Кристаллическая структура соединения **c3.2** содержит один симметрично независимый катион Ni^{2+}, который формирует слегка искаженный октаэдр NiO_6. Две кристаллографически неэквивалентные позиции Se^{4+} имеют тригонально пирамидальную координацию. В структуре **c3.2** координационный полиэдр единственного иона Pb^{2+} является несимметричным и явно указывает на положение стереохимически активной неподеленной электронной пары $6s^2$. По аналогии со структурой α–формы (**c3.1**), β–форма

построена из изолированных октаэдров NiO_6, связанных между собой группами SeO_3 через общие кислородные вершины. Однако способ связывания полиэдров в обеих структурах отличается. Кристаллическая структура соединения **c3.2** (рис. 3.3) оказывается существенно слоистой, основанной на слоях $[Ni(SeO_3)_2]^{2-}$, лежащих параллельно плоскости (001). Неподеленные электронные пары катионов Se^{4+} направлены в межслоевое пространство вдоль направления [001]. Пустоты в структуре заполняются катионами Pb^{2+}, которые уравновешивают заряд и связывают слои между собой. Кратчайшее межслоевое расстояние O···O составляет около 3.36 Å, что заметно превосходит сумму Ван-дер-Ваальсовых радиусов и указывает на явный *2D* характер структуры.

Черно-белый граф, соответствующий слоистому никель-селенитному комплексу, показан на рис. 3.3в. Такая топология слоя является одной из самых распространенных в известных *2D* неорганических оксосолях [Krivovichev 2004; Krivovichev 2009]. Нецентросимметричный характер структуры соединения **c3.2** хорошо виден на рис. 3.3а, где все вершины пирамид SeO_3 в структуре ориентированы «вверх». Детальное описание кристаллической структуры соединения **c3.2** приведено в статье **A-IV** (см. Included Articles).

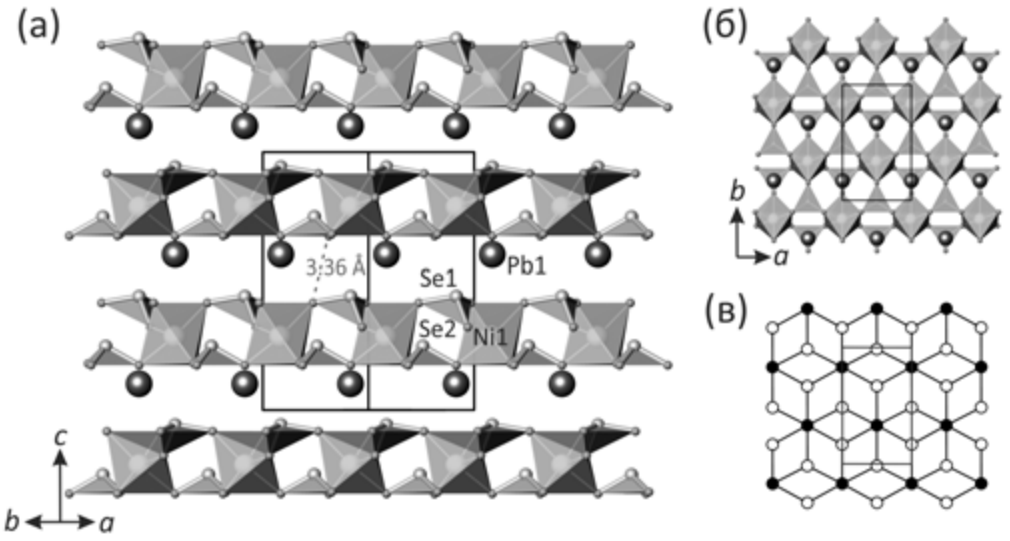

РИСУНОК 3.3 Кристаллическая структура β–$PbNi(SeO_3)_2$ (**c3.2**) в двух разных проекциях – (а) и (б); черно-белый граф, соответствующий Ni–Se слою в структуре – (в)

$PbNi_2(SeO_2OH)_2(SeO_3)_2$

В кристаллической структуре **c3.3** присутствуют две симметрично независимые позиции, занятые катионами Ni^{2+}, которые обладают достаточно правильным октаэдрическим окружением. Четыре кристаллографически неэквивалентных катиона Se^{4+} окружены тремя атомами кислорода, образуя тригональные пирамиды. При этом две из них оказываются протонированными, формируя искаженные группы $(Se(3)O_2OH)^-$ и $(Se(4)O_2OH)^-$ с одной удлиненной и двумя короткими связями Se–O. Два симметрично независимых катиона Pb^{2+} координированы восемью атомами, образуя искаженные квадратные антипризмы с неподеленными электронными парами, ориентированными в сторону удлиненных кислородных контактов.

В структуре **c3.3** октаэдры NiO_6 объединяются через общие кислородные вершины с группами SeO_3, формируя *3D* каркас с каналами вдоль направления [010] (рис. 3.4а). Четыре кристаллографически независимых канала заняты поочередно двухвалентными катионами свинца и неподеленными электронными парами четырехвалентных катионов селена.

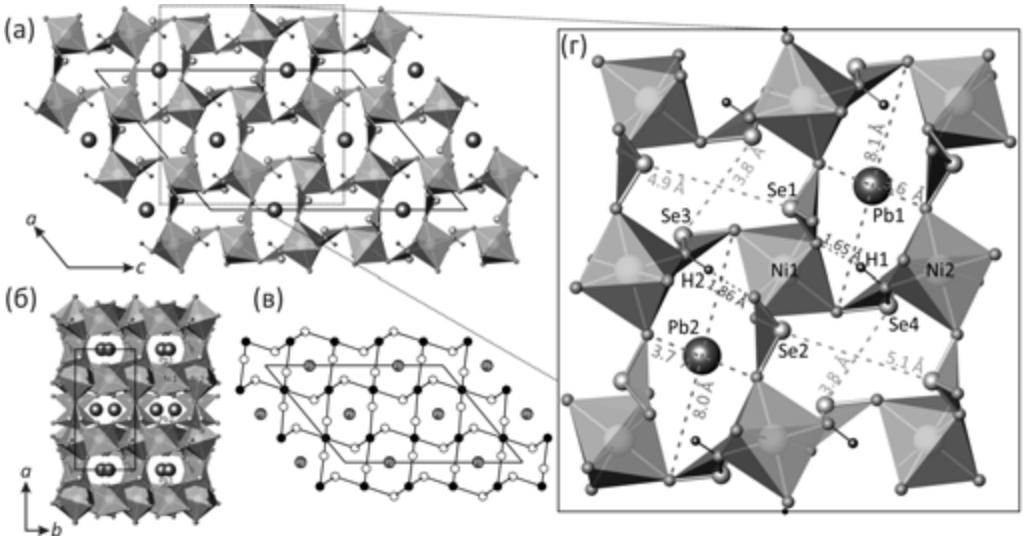

РИСУНОК 3.4 Общие проекции кристаллической структуры соединения $PbNi_2(SeO_2OH)_2(SeO_3)_2$ (**c3.3**) вдоль кристаллографических осей *b* и *c* – (а) и (б); черно-белый граф – (в); увеличенный фрагмент структуры – (г)

При взгляде на проекцию структуры на плоскость (*a*, *c*) может сложиться впечатление, что позиции Pb(1) и Pb(2) эквивалентны, а элементарная ячейка структуры должна иметь в два раза меньший объем. Доказательством правильности выбора ячейки и кристаллографического различия между катионами свинца может служить проекция

структуры на плоскость (*a*, *b*), показывающая каналы, идущие вдоль кристаллографической оси *c*, и расположенные в них неэквивалентные позиции Pb(1) и Pb(2) (рис. 3.4б).

Рисунок 3.4в содержит черно-белый граф, соответствующий *3D* металлическому катионному каркасу соединения **c3.3**. Его топология близко связана со структурой соединения $PbFe_2(SeO_3)_4$ [Johnston and Harrison 2004] и представляет собой интересную вариацию примитивной кубической сетки (**pcu**) [Krivovichev 2014]. Детальное описание кристаллической структуры соединения **c3.3** приведено в статье **A-IV** (см. Included Articles).

2.4 Кристаллохимическое исследование ванадат-селенитов

Основные кристаллографические сведения и параметры уточнения кристаллических структур трех новых соединений: β–$(V_2O_3)(SeO_3)_2$ (**c4.1**), $Pb_2(VO)(SeO_3)_3$ (**c4.2**) и β-$Pb_4(V_3O_8)_2(SeO_3)_3(H_2O)$ (**c4.3**), описанных в этой главе, представлены в табл. 4.1.

ТАБЛИЦА 4.1 Кристаллографические сведения и параметры уточнения структур соединений β-$(V_2O_3)(SeO_3)_2$ (**c4.1**), $Pb_2(VO)(SeO_3)_3$ (**c4.2**) и β–$Pb_4(V_3O_8)_2(SeO_3)_3(H_2O)$ (**c4.3**)

	c4.1	**c4.2**	**c4.3**
M_r (г моль$^{-1}$)	403.80	862.20	1789.30
пространственная группа	$P2_1/c$	$P2_1/n$	P–1
a (Å)	7.1812(3)	5.1938(3)	7.1425(2)
b (Å)	7.0753(2)	16.1141(9)	7.1933(2)
c (Å)	14.0486(5)	11.2533(6)	21.5261(7)
α (°)	90	90	90.0190(10)
β (°)	101.5462(15)	90.527(2)	98.1800(10)
γ (°)	90	90	94.5980(10)
V (Å^3)	699.35(4)	941.79(9)	1091.12(6)
Z	4	4	2
ρ (г/см^3)	3.835	6.081	5.446
μ (мм$^{-1}$)	13.105	48.272	38.305
λ (MoK_α) (Å)	0.71073	0.71073	0.71073
всего рефл.	7488	9381	21653
независ. рефл.	2126	3062	6579
R_{int}	0.0252	0.0305	0.0272
R_1 [$I > 2\sigma(I)$]	0.0232	0.0236	0.0260
wR_2 [$I > 2\sigma(I)$]	0.0503	0.0411	0.0535
R_1 [all data]	0.0298	0.0322	0.0302
wR_2 [all data]	0.0527	0.0429	0.0549
GOF	1.065	1.059	1.042
$\Delta\rho_{max}$,$\Delta\rho_{min}$ (e Å^{-3})	1.03, –0.49	1.40, –1.34	5.06, –2.96

2.4.1 Способы синтеза свинцовых ванадат-селенитов

Тройную систему PbO–VO_x–SeO_2 исследователи начали изучать совсем недавно, и к настоящему времени в ней было обнаружено только шесть смешаннометальных кристаллических фаз: $Pb_2(V^{5+}{}_2O_5)(SeO_3)_2$ [Li et al. 2010], $Pb_2(V^{4+}O)_3(SeO_3)_5$ [Li et al. 2010], $Pb_4(V^{5+}O_2)_2(SeO_3)_4(Se_2O_5)$ [Yeon et al. 2012], α–$Pb_4(V^{5+}{}_3O_8)_2(SeO_3)_3(H_2O)$ [Cao et al. 2014], $Pb_2(V^{5+}O_2)(SeO_3)_2Cl$ [Cao et al. 2014] и $Pb(V^{5+}O_2)(SeO_3)F$ [Cao et al. 2014]. Дальнейшее развитие этого направления послужило мотивацией для выполнения данной части настоящего диссертационного исследования. Большинство из упомянутых соединений были синтезированы гидротермальным методом при температурах 200–230 °C, что вполне ожидаемо ввиду высокой растворимости и подвижности анионов $(Se^{4+}O_3)^{2-}$ в растворе,

а также того факта, что оксосоли Pb^{2+} предрасположены к фазообразованию именно в водных условиях, что было продемонстрировано предыдущими результатами. Два соединения – $Pb_4(V^{5+}O_2)_2(SeO_3)_4(Se_2O_5)$ [Yeon et al. 2012] и $Pb_2(V^{5+}O_2)(SeO_3)_2Cl$ [Cao et al. 2014] – были синтезированы методом ХГТ реакций. Стоит отметить, что последнее соединение было также получено и гидротермальным методом [Cao et al. 2014].

Синтезированные в рамках настоящей работы монокристаллы нового соединения β–$(V^{5+}{}_2O_3)(SeO_3)_2$ (**c4.1**) были выращены методом ХГТ реакций, описанным в разделе 2.1, а новые свинецсодержащие фазы – $Pb_2(V^{4+}O)(SeO_3)_3$ (**c4.2**) и β–$Pb_4(V^{5+}{}_3O_8)_2(SeO_3)_3(H_2O)$ (**c4.3**) – были получены путем использования гидротермального метода в процессе изучения фазовых диаграмм тройных систем. Из-за ограничения времени, «гидротермальные» кристаллизационные диаграммы систем с PbO и с $PbCl_2$ не были изучены так подробно и систематически, как это было сделано для никелевой системы, описанной в главе 2.3.1. Настоящее исследование, как и прежде, состояло в экспериментальном изучении комбинаций молярных соотношений начальных компонентов системы, нанесенных на треугольник Гиббса (рис. 4.1).

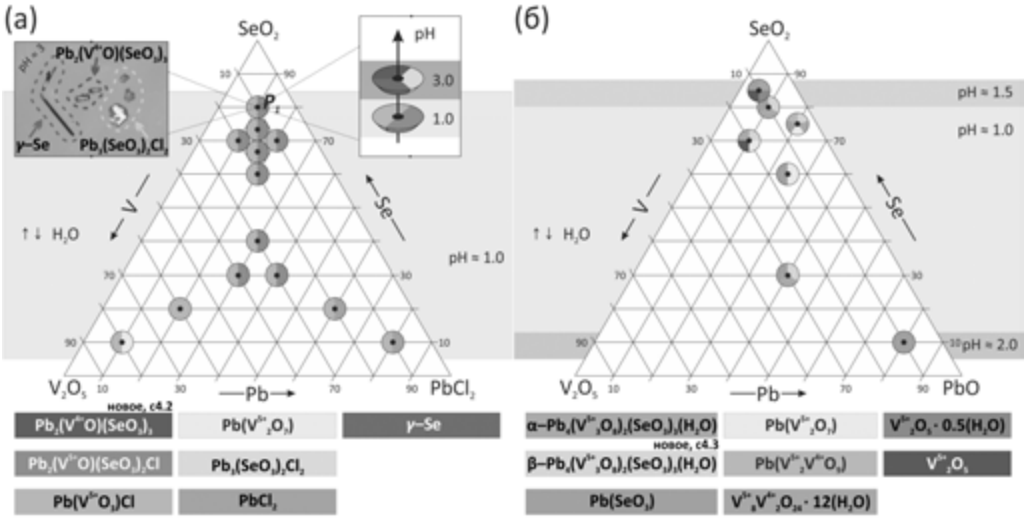

РИСУНОК 4.1 Экспериментальные кристаллизационные диаграммы систем $PbCl_2$–V_2O_5–SeO_2–H_2O (а) и PbO–V_2O_5–SeO_2–H_2O (б) при 200 °C. Области с различными значениями pH показаны в фоне оттенками серого

Кристаллические продукты синтезов были проанализированы при помощи монокристальной (для обеих систем) и порошковой (для системы PbO–V_2O_5–SeO_2–H_2O) рентгеновской дифрактометрии. Было установлено, что, как и в случае с системой с Ni, процессы самоокисления проходили за счет реакции SeO_2 с водой согласно следующим химическим реакциям:

$$SeO_2 + H_2O \leftrightarrow H_2SeO_3 \quad (1)$$

$$H_2SeO_3 \leftrightarrow H^+ + (HSeO_3)^- \ (pK_a = 2.62) \quad (2)$$

$$(HSeO_3)^- \leftrightarrow H^+ + (SeO_3)^{2-} \ (pK_a = 8.32) \quad (3)$$

В системе $PbCl_2$–V_2O_5–SeO_2–H_2O доминирующими фазами оказались $Pb_2(VO_2)(SeO_3)_2Cl$ [Cao et al. 2014] и $Pb(VO_3)Cl$ [Jo et al. 2009], тогда как простые соединения $PbCl_2$ или $Pb(V_2O_7)$ кристаллизовались соответственно в богатых $PbCl_2$ или V_2O_5 областях диаграммы. Использование PbO в качестве начального компонента системы вместо хлорида свинца привело к более разнообразному фазообразованию в системе. В результате в каждой из систем было получено по одному новому соединению: $Pb_2(V^{4+}O)(SeO_3)_3$ (**c4.2**) и β–$Pb_4(V^{5+}{}_3O_8)_2(SeO_3)_3(H_2O)$ (**c4.3**), описанных в следующей главе данного раздела.

2.4.2 Структурное описание трех новых фаз

β–$(V_2O_3)(SeO_3)_2$

Кристаллическая структура новой полиморфной β–модификации $(V_2O_3)(SeO_3)_2$ (**c4.1**) содержит два независимых катиона V^{5+} и два катиона Se^{4+}. Атомы в позиции V(1) координированы шестью атомами кислорода с образованием неправильного октаэдра $[1_s+4+1_t]$, характерного для V^{5+} с одной короткой (V(1)–O(4) = 1.586 Å) и одной удлиненной (V(1)–O(3) = 2.385 Å) связью. Катионы позиции V(2) образуют квадратные пирамиды $[1_s+4]$ с одной короткой связью V(2)–O(9) = 1.570 Å. Подобная координация была обнаружена, к примеру, в структурах соединений $A_4Cd(VO)(V_2O_7)_2Cl$ (A = Rb, Tl) [Mertens and Müller-Buschbaum 1997]. Катионы Se^{4+} образуют характерные тригональные пирамиды $(SeO_3)^{2-}$ со стереоактивными неподеленными электронными парами, выступающими в роли дополнительных лигандов.

В структуре **c4.1** пара ванадатных октаэдров, сочлененных по ребру, объединяется через общие кислородные вершины с двумя соседними квадратными пирамидами, образуя тетрамер $(V_4O_{18})^{16-}$ (рис. 4.2a).

Селенитные анионы играют разные структурные роли. Тригональные пирамиды $Se(2)O_3$ присоединяются к тетрамеру таким образом, что селенитные треугольные основания O–O–O оказываются параллельными плоскости тетрамера, образованной четырьмя атомами ванадия. Группы $Se(1)O_3$ располагаются между ванадатными тетрамерами и связывают их между собой в металл-оксидные слои путем образования мостиковых связей. Слоистые ванадат-селенитные комплексы с межслоевым расстоянием около 3.3 Å ориентированы параллельно плоскости (–201). Структурной

особенностью этого типа слоев, в дополнение к его электронейтральности является также наличие вытянутых каналов вдоль направления [100] размерами около 3 × 10 Å^2.

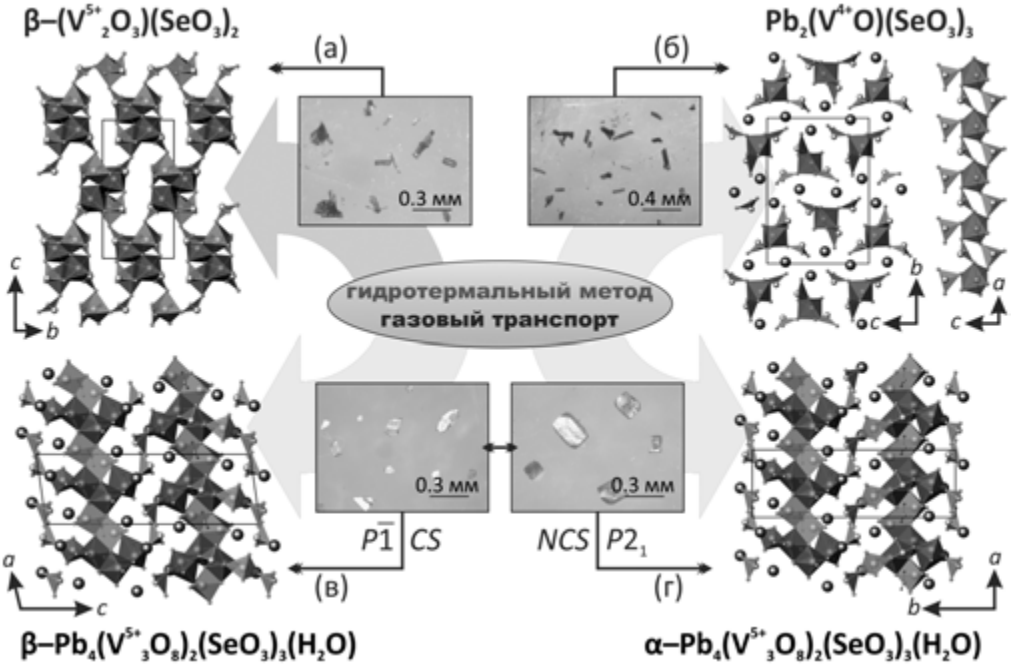

РИСУНОК 4.2 Проекции кристаллических структур и фотографии кристаллов соединений **c4.1**, **c4.2**, **c4.3** и α–$Pb_4(V_3O_8)_2(SeO_3)_3(H_2O)$. Октаэдры VO_6, квадратные пирамиды VO_5, тригональные пирамиды SeO_3 и катионы Pb^{2+} показаны соответственно синим, зеленым, оранжевым и серым

Полиморфизм $(V_2O_3)(SeO_3)_2$

Кристаллические структуры двух полиморфных модификаций – α–$(V_2O_3)(SeO_3)_2$ [Lee and Kwon 1996] и β–$(V_2O_3)(SeO_3)_2$ (**c4.1**) – содержат ванадатные тетрамерные структурные комплексы разной геометрии. Структура α–модификации основана на цепочках, вытянутых вдоль кристаллографической оси *a* и состоящих из пирамид $(SeO_3)^{2-}$ и квадратных тетрамеров $(V_4O_{18})^{16-}$, изображенных на рис. 4.3а. Эти тетрамеры построены из двух пар реберносочлененных октаэдров V^{5+}, связанных через общие кислородные вершины. V^{5+} центры имеют достаточно правильную плоскую квадратную геометрию с взаимно перпендикулярными расстояниями V(1)···V(2), равными 3.41 Å и 3.53 Å, а также углами V–V–V в диапазоне между 88.7° и 91.3°. В структуре же β–формы (**c4.1**) тетрамер имеет крестообразную форму (рис. 4.3б). Два взаимно перпендикулярных расстояния V(1)···V(1)' и V(2)···V(2)' составляют 3.20 Å и 6.28 Å соответственно.

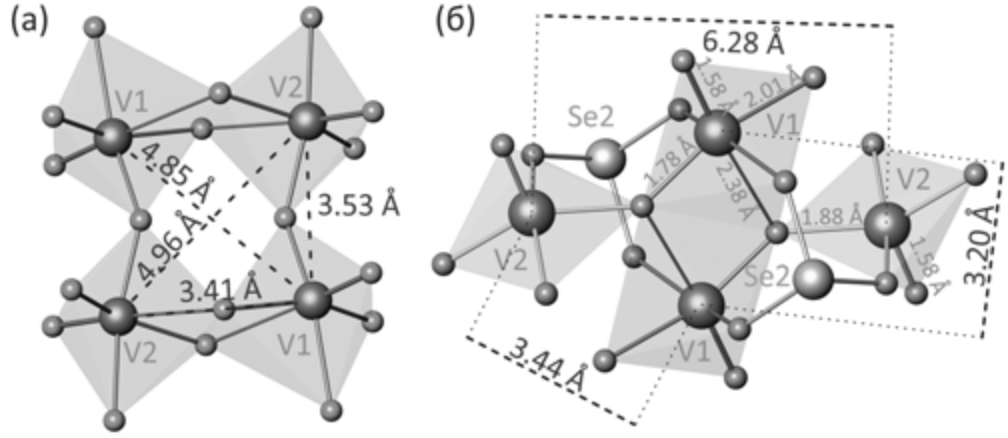

РИСУНОК 4.3 Ванадатные тетрамерные комплексы в структурах соединений α– $(V_2O_3)(SeO_3)_2$ и β–$(V_2O_3)(SeO_3)_2$ (**c4.1**) – (а) и (б) соответственно

Следует отметить, что кристаллические структуры обеих полиморфных модификаций находятся в тесной связи с группой соединений, сходных с ними по химическому составу, но отличающихся по структуре: $(V_2O_3)(TeO_3)_2$ [Darriet and Galy 1973; Millet et al. 1999] и $(V_2O_3)(XO_4)_2$ (X = S, Se) [Tudo et al. 1969; Richter and Mattes 1992; Tyutyunnik et al. 2010]. Такое многообразие структурных форм, наблюдающееся у химически похожих фаз, может быть обусловлено присутствием разных по своей прочности коротких, экваториальных и длинных связей в полиэдрах VO_n, что в результате и приводит к проявлению полиморфизма. Несимметричные селенитные или теллуритные оксоанионы со стереохимически активными неподеленными электронными парами также вносят свой вклад в разнообразие структурных архитектур подобных соединений.

$Pb_2(V^{4+}O)(SeO_3)_3$

Эта фаза существенным образом отличается от других полученных ванадат селенитов тем, что содержит так называемые *ванадил*-ионы $(V{=}O)^{2+}$. В кристаллической структуре соединения $Pb_2(V^{4+}O)(SeO_3)_3$ (**c4.2**) находится одна кристаллографически неэквивалентная позиция V^{4+}, координированная шестью атомами кислорода и образующая изолированный октаэдр $(VO_6)^{8-}$. Он содержит одну короткую ванадильную связь (V(1)–O(7) = 1.615 Å), четыре связи со средней длиной 2.035 Å в экваториальной плоскости октаэдра и одну укороченную *транс*-связь (V(1)–O(5) = 2.096 Å). Появление такой укороченной шестой связи нетипично для соединений с октаэдрическими позициями четырехвалентного ванадия [Schindler et al. 2000], для которых характерна длина *транс*-связи около 2.2 Å. Тем не менее такая особенность уже была встречена в структурах некоторых соединений, например, $A_2(VO)_3(P_2O_7)_2$ (A = Rb, K) [Leclaire et al.

1988; Lii et al. 1990]. В обоих случаях шестая «дальняя» кислородная вершина октаэдра связывается с оксоанионами SeO_3 или P_2O_7, тогда как ванадильный атом кислорода остается терминальным, образуя единственную короткую двойную связь V=O. Три независимых атома селена в структуре находятся в степени окисления +4 и образуют типичные тригональные пирамиды $(SeO_3)^{2-}$. Структура соединения **c4.2** также содержит две симметрично независимые позиции Pb^{2+}. Оба свинцовых катиона окружены десятью атомами кислорода, являющимися общими для ванадатных и селенитных групп. Оба катиона Pb^{2+} обладают короткими прочными связями Pb–O в одной координационной сфере и длинными – в другой.

Структура соединения **c4.2** может рассматриваться как основанная на ванадат-селенитных цепочках, между которыми располагаются катионы двухвалентного свинца, связывающие *1D* комплексы в *3D* каркас (рис. 4.2б). Изолированные ванадатные октаэдры объединяются пятью кислородными вершинами с соседними селенитными группами, формируя цепочки $[(VO_2)(SeO_3)_3]^{4-}$, протянутые вдоль кристаллографической оси *a*. Две бидентатные тригональные пирамиды $Se(2)O_3$ и $Se(3)O_3$ связывают между собой соседние октаэдры $V(1)O_6$. Селенитная группа $Se(1)O_3$ является монодентатной и связывается только через одну кислородную вершину с октаэдром ванадия. Структуру соединения можно также рассматривать как сложенную из *2D* комплексов, собранных их ванадат-селенитных цепочек, лежащих параллельно плоскости (010). С такой точки зрения за связь между слоями отвечают катионы двухвалентного свинца (рис. 4.2б).

β–$Pb_4(V_3O_8)_2(SeO_3)_3(H_2O)$

Новая полиморфная β–модификация соединения $Pb_4(V_3O_8)_2(SeO_3)_3(H_2O)$ (**c4.3**) содержит шесть V^{5+}, три Se^{4+} и четыре Pb^{2+} катиона в одной элементарной ячейке. Катионы пятивалентного ванадия обладают шестерной и пятерной координациями. Атомы в позициях V(1), V(2) и V(4) октаэдрически координированы $[1_s+4+1_t]$ шестью атомами O с одной короткой металл-кислородной связью. Позиции V(3), V(5) и V(6) имеют окружение, описываемое искаженной квадратной пирамидой $[1_s+(1_s+3)]$ с двумя короткими связями (среднее расстояние $<V–O_s>$ составляет 1.643 Å, 1.651 Å и 1.652 Å для V(3), V(5) и V(6) соответственно) и тремя экваториальными связями средней длины около 1.9 Å. В структуре соединения **c4.3** также присутствуют три симметрично независимых катиона Se^{4+}, имеющих типичную кислородную координацию тригональной пирамиды. Координационные полиэдры четырех неэквивалентных катионов Pb^{2+} сильно искажены ввиду стереохимической активности их неподеленных электронных пар $6s^2$. Атомы в позициях Pb(1) и Pb(2) окружены восемью O атомами соответственно с шестью и семью относительно короткими прочными связями Pb–O. Атом кислорода в позиции O(26),

расположенный на расстоянии 2.616 Å от позиции Pb(1), принадлежит молекуле воды. Он связывается водородными связями с терминальной кислородной вершиной селенитной группы Se(3)O (O(26)···O(20) = 2.644 Å) и образует удлиненный контакт (O(26)···O(17) = 3.269 Å) с мостиковым кислородным атомом между группами Se(3)O и $V(3)O_5$. Позиции Pb(3) и Pb(4) окружены девятью атомами кислорода. Шесть из них находятся на относительно коротких расстояниях от атомов свинца.

Кристаллическая структура соединения β–$Pb_4(V_3O_8)_2(SeO_3)_3(H_2O)$ (**c4.3**) построена из *1D* ванадат-селенитных структурных комплексов (рис. 4.4), связанных двухвалентными катионами в *3D* каркас (рис. 4.5). В следующем параграфе будет описано тонкое кристаллографическое различие между α– и β–полиморфными модификациями.

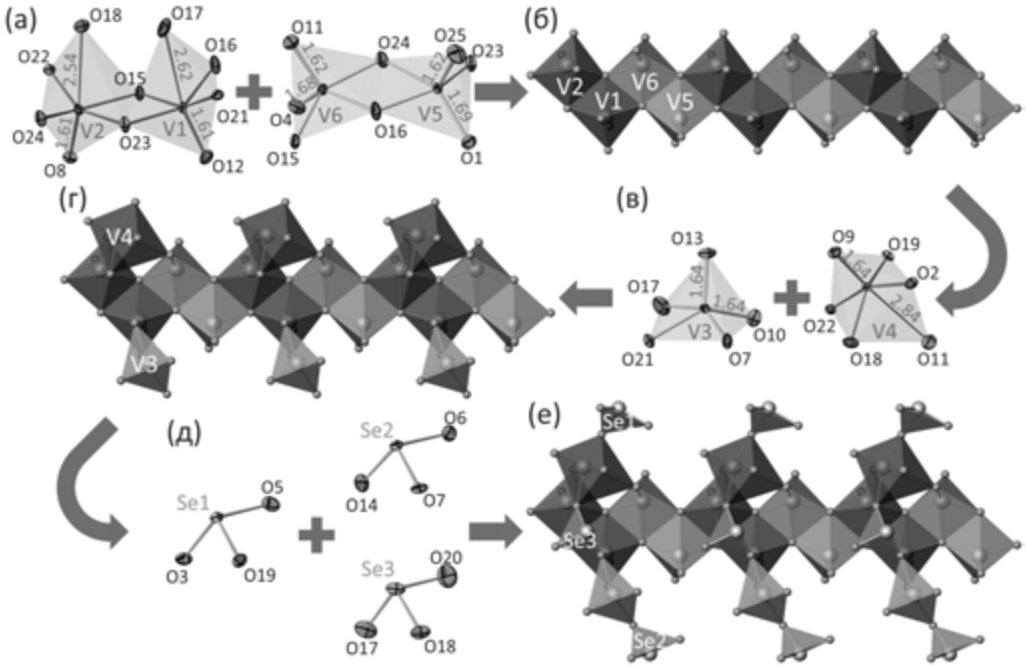

РИСУНОК 4.4 Структурные комплексы в кристаллической структуре соединения β-$Pb_4(V^{5+}{}_3O_8)_2(SeO_3)_3(H_2O)$ (**c4.3**)

Интересной особенностью кристаллической структуры соединения **c4.3** является сосуществование двух хиральных ванадат-селенитных аркообразных лент, связанных между собой центром инверсии (рис. 4.2в). Расположенные рядом ленты связываются между собой через прочные металл-оксидные связи, формируя *2D* структурные комплексы, параллельные плоскости (010) (рис. 4.5б). Катионы Pb(1) и Pb(2) обеспечивают дальнейшее связывание слоистых комплексов в *3D* каркас. Молекулы воды заполняют оставшееся свободное пространство в структуре, при этом водородные связи

практически не принимают участия в связывании сложных ванадат-селенитных структурных комплексов.

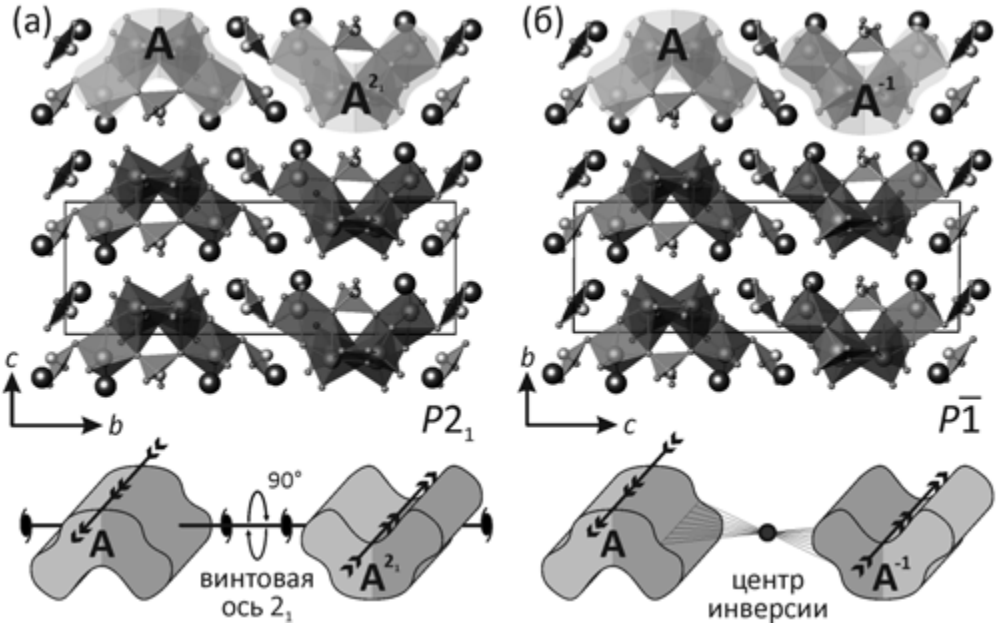

РИСУНОК 4.5 Способ укладки ванадат-селенитных лент в кристаллических структурах соединений α–$Pb_4(V_3O_8)_2(SeO_3)_3(H_2O)$ – (а) и β–$Pb_4(V_3O_8)_2(SeO_3)_3(H_2O)$ (**c4.3**) – (б)

Полиморфизм $Pb_4(V_3O_8)_2(SeO_3)_3(H_2O)$

В рамках настоящего диссертационного исследования были синтезированы обе α– и β-модификации соединения $Pb_4(V_3O_8)_2(SeO_3)_3(H_2O)$. Описание α–полиморфа было совсем недавно опубликовано в работе [Cao et al. 2014]. Эта фаза кристаллизуется в моноклинной нецентросимметричной пространственной группе $P2_1$, в то время как β–форма (**c4.3**) имеет триклинную симметрию (пространственная группа $P\bar{1}$). Кристаллические структуры обоих полиморфов, содержащих одинаковые *1D* ванадат-селенитные комплексы, очень похожи и обладают близкими параметрами элементарных ячеек с практически одинаковым объемом (рис. 4.2в, г).

Главное различие между ними состоит в том, что структура соединения α-$Pb_4(V_3O_8)_2(SeO_3)_3(H_2O)$ содержит две ванадат-селенитные ленты (обозначенные **A** и $\mathbf{A}^{21}$), повернутые в результате операции вращения вокруг винтовой оси 2_1, тогда как структура β–модификации (**c4.3**) содержит две хиральные инвертированные ванадат-селенитные ленты (обозначенные **A** и $\mathbf{A}^{-1}$), связанные между собой центром инверсии (рис. 4.5). Способ укладки таких ванадат-селенитных комплексов вдоль

кристаллографических осей соответственно *b* и *c* для двух форм остается одинаковым в обеих полиморфных модификациях, что достигается за счет идентичного расположения групп SeO_3 и катионов свинца в обеих структурах. Последнее является очень редким и специфичным структурным явлением в неорганических кислородных соединениях. В структуре α–полиморфа ленты **A** и связанные с ней соседние повернутые ленты $\mathbf{A^{21}}$ образуют слои с чередованием лент в последовательности …**A** – $\mathbf{A^{21}}$ – **A** – $\mathbf{A^{21}}$ – **A**… (рис. 4.5а). В структуре β–фазы (**c4.3**) ванадат селенитные ленты уложены в соответствии с последовательностью …**A** – $\mathbf{A^{-1}}$ – **A** – $\mathbf{A^{-1}}$ – **A**… (рис. 4.5б). В обеих структурах выше- и нижележащие соседние слои располагаются строго друг под другом.

2.5 Кристаллохимическое исследование новых соединений селена с марганцем и висмутом

Как известно, ионы Bi^{3+} имеют сильную предрасположенность к образованию оксоцентрированных топологий в структурах оксидных материалов [Huvé et al. 2006; Colmont et al. 2008; Aliev et al. 2012; Kozin et al. 2013; Colmont et al. 2013; Aliev et al. 2013; Lü et al. 2014], и поэтому их комбинирование с несимметричными группами SeO_3 обещает привести к образованию очень необычных фаз с точки зрения кристаллохимии. Недавние работы, посвященные изучению замещения тяжелых катионов Bi^{3+} ионами Mn^{2+} в некоторых оксоцентрированных фазах [Abraham et al. 2002; Aliev et al. 2014], также вдохновили на продолжение работы в этом направлении.

Несмотря на то, что эксперименты привели к синтезу только одной оксоцентрированной фазы (**c5.2**), помимо нее было получены еще шесть новых соединений, которые несомненно также заслуживают самого детального рассмотрения. Основные кристаллографические сведения и параметры уточнения кристаллических структур всех семи новых соединений, приведенных ниже, представлены в табл. 5.1.

c5.1 – $Mn(SeO_4)(H_2O)_2$
c5.2 – $Mn_2[Bi_2O](SeO_3)_4$
c5.3 – $MnBi(SeO_3)_2Cl$
c5.4 – $Mn_4(Mn_5,Bi)(SeO_3)_8Cl_5$
c5.5 – $Bi_6(SeO_3)_4Cl_{10}$
c5.6 – β–$Bi(SeO_3)Cl$
c5.7 – $PbBi_{10}(SeO_3)_{12}Cl_8$

ТАБЛИЦА 5.1 Кристаллографические сведения и параметры уточнения структур соединений **c5.1**, **c5.2**, **c5.3**, **c5.4**, **c5.5**, **c5.6** и **c5.7**

	c5.1	**c5.2**	**c5.3**	**c5.4**	**c5.5**	**c5.6**	**c5.7**
M_r (г моль$^{-1}$)	233.93	1051.68	553.29	1896.37	2116.22	371.4	4104.1
пр. группа	*Pbca*	*Pccn*	*P*–1	*Pbcm*	$P2_1/c$	*Cc*	*Ccca*
a (Å)	10.4353(5)	10.8771(3)	7.0926(8)	10.7914(2)	21.460(2)	22.7052(3)	15.819(6)
b (Å)	9.2420(5)	19.9770(5)	7.2695(6)	15.9782(3)	8.4012(9)	76.785(4)	17.871(7)
c (Å)	10.5349(6)	5.5058(1)	8.0160(8)	17.5682(3)	15.3370(18)	16.0550(3)	15.857(6)
α (°)	90	90	88.226(4)	90	90	90	90
β (°)	90	90	72.005(3)	90	110.639(5)	135.000(2)	90
γ (°)	90	90	64.560(4)	90	90	90	90
V (Å^3)	1016.02(9)	1196.37(5)	352.47(6)	3029.23(10)	2587.7(5)	19792.4(12)	4483(3)
Z	8	4	2	4	4	192	4
ρ (г/см^3)	3.059	5.839	5.213	4.158	5.432	5.981	6.079
μ (мм$^{-1}$)	9.71	43.63	37.40	19.55	47.37	52.08	53.17
λ (Mo$K_α$) (Å)	0.71073	0.71073	0.71073	0.71073	0.71073	0.71073	0.71073
всего рефл.	6089	8112	7238	32242	25390	242854	10469
независ. рефл.	1808	1895	2194	4767	4534	35097	2253
R_{int}	0.0295	0.0247	0.0198	0.0310	0.0421	0.0962	0.0496
R_1 [$I > 2σ(I)$]	0.0227	0.0285	0.0208	0.0220	0.0291	0.0612	0.0667
wR_2 [$I > 2σ(I)$]	0.0467	0.0620	0.0436	0.0529	0.0711	0.0645	0.0639

ТАБЛИЦА 5.1 *Продолжение*

	c5.1	**c5.2**	**c5.3**	**c5.4**	**c5.5**	**c5.6**	**c5.7**
R_1 [all data]	0.0302	0.0325	0.0219	0.0317	0.0333	0.1124	0.1057
wR_2 [all data]	0.0489	0.0637	0.0441	0.0565	0.0767	0.0694	0.0859
GOF	1.030	1.143	1.056	1.021	1.088	1.32	0.92
$\Delta\rho_{max},\Delta\rho_{min}$ (e Å^{-3})	0.70, −0.93	2.54, −1.47	1.90, −1.67	0.73, −1.16	3.42, −2.95	5.39, −4.51	5.38, −7.01

2.5.1 Экспериментальные процедуры

Новые соединения, описанные в этом разделе, были получены различными экспериментальными методами.

Метод выпаривания из водного раствора четырехводного хлорида двухвалентного марганца (2.4 ммоль), 40% селеновой кислоты H_2SeO_4 (4.7 ммоль) и дистиллированной воды (10 мл) был использован для синтеза соединения $Mn(SeO_4)(H_2O)_2$ (**c5.1**). Раствор выпаривался при 80 °C и постоянно перемешивался при помощи магнитной мешалки до полной гомогенизации в течение 3 часов. Затем вязкая жидкость молочно-розового цвета была вылита на часовое стекло и оставлена в вытяжном шкафу при комнатной температуре. Здесь уместно добавить, что при нагревании выше 160 °C селеновая кислота $H_2Se^{6+}O_4$ легко разлагается с образованием селенистой кислоты $H_2Se^{4+}O_3$ и выделением кислорода [De 2003]. Розоватые прозрачные кристаллы соединения **c5.1**, подходящие для монокристального рентгеноструктурного эксперимента, выросли на часовом стекле через два дня.

Монокристаллы соединения $Mn_2[Bi_2O](SeO_3)_4$ (**c5.2**) были получены при помощи гидротермальной реакции SeO_2 (2.5 ммоль), MnO_2 (2.0 ммоль), Mn_2O_3 (0.25 ммоль) и BiOCl (3.0 ммоль) в 6 мл дистиллированной воды. Реакция проходила в 23 мл автоклавах с тефлоновыми вставками при 200 °C в течение двух дней. Затем автоклавы медленно охлаждались до комнатной температуры со скоростью 3.7 °C в час.

Все остальные соединения были получены при помощи метода ХГТ реакций. Соединения $MnBi(SeO_3)_2Cl$ (**c5.3**) и $Bi_6(SeO_3)_4Cl_{10}$ (**c5.5**) выросли в одной стеклянной ампуле в результате одной и той же химической газотранспортной реакции SeO_2 (4 ммоль), Mn_2O_3 (1.0 ммоль), Bi_2O_3 (1.0 ммоль) и $BiCl_3$ (2.0 ммоль), протекавшей с температурным градиентом 400–350 °C в течение 100 часов. Фаза $Mn_4(Mn_5,Bi)(SeO_3)_8Cl_5$ (**c5.4**) была синтезирована газотранспортной реакцией смеси с такой же стехиометрией, что использовалась для получения предыдущих двух соединений, но с температурным градиентом 450–400 °C в течение 240 часов.

Параллельно с этими экспериментами в Лилльской лаборатории катализа и химии твердого тела еще два родственных соединения – β–$Bi(SeO_3)Cl$ (**c5.6**) и $PbBi_{10}(SeO_3)_{12}Cl_8$ (**c5.7**) – были синтезированы доктором Алмазом Алиевым. Кристаллы

c5.6 были получены методом ХГТ реакций из смеси SeO_2 (1.0 ммоль), MnO_2 (1.0 ммоль), BiOCl (1.0 ммоль) и капли концентрированной соляной кислоты HCl, тогда как газотранспортная реакция смеси SeO_2 (1.0 ммоль), PbO (1.0 ммоль), BiOCl (1.0 ммоль) и капли концентрированного раствора HCl привела к образованию нового соединения **c5.7**. В этих экспериментах пары соляной кислоты рассматриваются в качестве дополнительного транспортного газового агента, участвующего в ходе процессов переноса начального вещества из зоны-источника в зону осаждения в вакуумированной запаянной стеклянной ампуле под действием температурного градиента.

2.5.2 Структурное описание семи новых фаз

$Mn(SeO_4)(H_2O)_2$

Кристаллическая структура соединения $Mn(Se^{6+}O_4)(H_2O)_2$ (**c5.1**) содержит одну симметрично независимую октаэдрическую позицию, занятую катионами Mn^{2+}. Четверо из шести его кислородных лигандов взаимодействуют с соседними катионами Se^{6+}, а другие два принадлежат молекулам воды, расположенным в *cis*-ориентации относительно друг друга. Единственная кристаллографически неэквивалентная позиция Se^{6+} имеет правильное тетраэдрическое окружение, связываясь всеми своими четырьмя кислородными вершинами с соседними октаэдрами $MnO_4(H_2O)_2$ в *3D* архитектуру (рис. 5.1а).

Каркас кристаллической структуры соединения **c5.1** можно рассматривать как состоящий из взаимосвязанных гетерополиэдрических слоев (рис. 5.1б). Структурная топология аналогичного каркаса была описана *С. В. Кривовичевым* на примере соединения $Zn(SeO_4)(H_2O)_2$ с применением графического подхода [Krivovichev 2007]. Представление слоя в качестве черно-белого графа показано на рис. 5.1в. Граф основан на гексагональных неплоских кольцах. Ориентация черных (Mn^{2+}) и белых (Se^{6+}) вершин относительно плоскости графа обозначена символами U (вверх) and D (вниз). Эти символы также обозначают направления, в котором один слой связывается с соседним, формируя *3D* каркас кристаллической структуры.

Структура соединения **c5.1** принадлежит к варисцитовому структурному типу $M(TO_4)(H_2O)_2$, где M = Fe^{3+}, Al^{3+}, Ga^{3+}, In^{3+} или Zn^{2+}, а T = P^{5+}, As^{5+} или Se^{6+}. К этому типу относятся такие минералы, как мансфильдит $Al(AsO_4)(H_2O)_2$, скородит $Fe(AsO_4)(H_2O)_2$, яномамит $In(AsO_4)(H_2O)_2$, штренгит $Fe(PO_4)(H_2O)_2$ и сам варисцит $Al(PO_4)(H_2O)_2$. Следует заметить, что новая фаза $Mn(SeO_4)(H_2O)_2$ – это лишь второй пример варисцитоподобного соединения, содержащего металлические катионы в степени окисления +2.

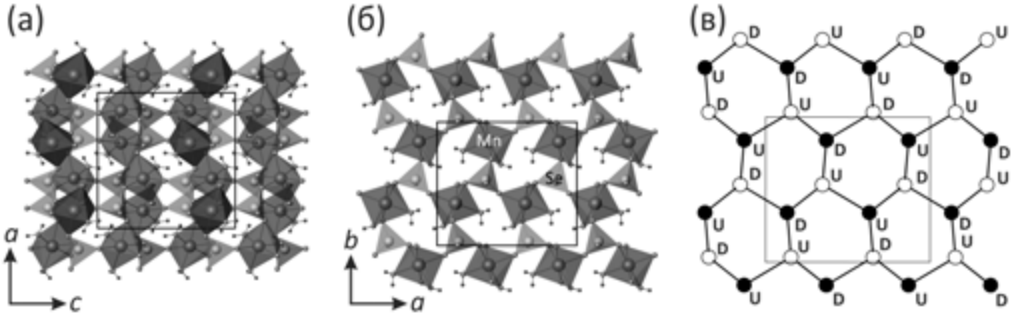

РИСУНОК 5.1 Вид кристаллической структуры соединения $Mn(SeO_4)(H_2O)_2$ (**c5.1**) вдоль кристаллографической оси *a* – (а); гетерополиэдрический слой параллельный плоскости (001) – (б) и его черно-белый граф – (в)

$Mn_2[Bi_2O](SeO_3)_4$

Структура соединения $Mn_2[Bi_2O](SeO_3)_4$ (**c5.2**) содержит единственную кристаллографическую позицию Bi^{3+}, координированную восемью атомами кислорода. Координационный полиэдр Bi^{3+} может быть описан как искаженная квадратная антипризма. Единственный симметрично независимый катион Mn^{2+} обладает искаженной октаэдрической координацией. Каждый октаэдр MnO_6 объединяется по двум ребрам с двумя соседними октаэдрами, тем самым формируя загзагообразную цепочку $[MnO_4]^{6-}$ вдоль кристаллографической оси *c* (рис. 5.2а).

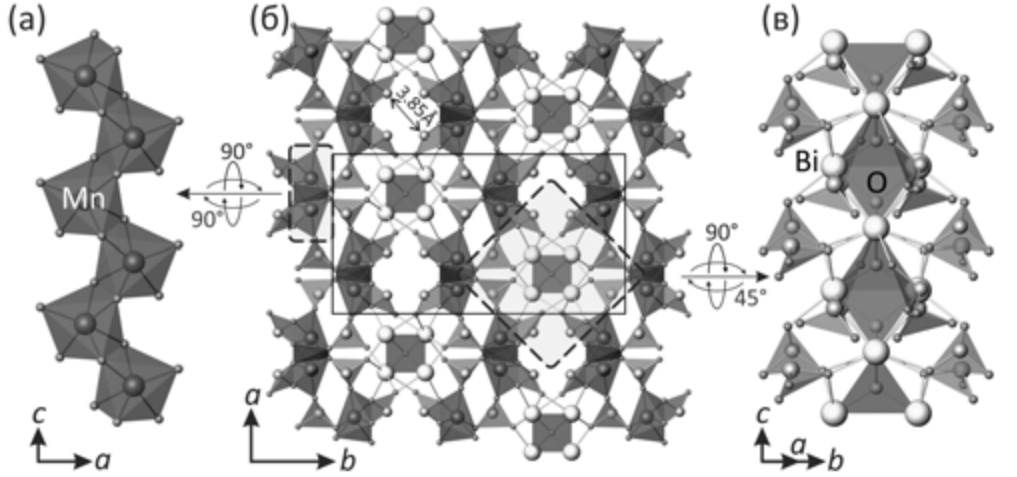

РИСУНОК 5.2 Проекция кристаллической структуры соединения $Mn_2[Bi_2O](SeO_3)_4$ (**c5.2**) (б), состоящей из цепочек $[MnO_4]^{6-}$ (а) и $[Bi_2O]^{4+}$ (в)

Две кристаллографические независимые позиции Se^{4+} образуют типичные тригональные пирамиды. Кристаллическая структура **c5.2** также содержит один «дополнительный» атом кислорода, который координируется четырьмя катионами Bi^{3+} с образованием оксоцентрированных тетраэдров $(OBi_4)^{10+}$. Они объединяются между собой по общим ребрам, лежащим друг напротив друга, составляя бесконечные цепочки $[Bi_2O]^{4+}$ идущих вдоль кристаллографической оси *c* (рис. 5.2в). Такие цепочки довольно распространены в оксоцентрированных структурах висмутовых фаз, и встречены, например, в структуре соединения $[Bi_2O]AuO_4$ [Krivovichev et al. 2013b]. Далее эти оксоцентрированные висмутовые цепочки связываются с группами SeO_3 и цепочками $[MnO_4]^{6-}$ в *3D* каркас с псевдотетрагональными каналами, заполненными неподеленными электронными парами катионов Se^{4+} (рис. 5.2б).

Архитектура соединения **c5.2** тесно связана со структурами, обнаруженными в $Tb_2O[SeO_3]_2$ [Wontcheu and Schleid 2002] и $M_3O_2Cl[SeO_3]_2$ (M^{3+} = Tb [Wontcheu and Schleid 2005] и Y [Zitzer et al. 2011]). В структурах этих фаз неподеленные электронные пары катионов Se^{4+} образуют похожие каналы вокруг катионных цепочек $[Tb_2O]^{4+}$ в $Tb_2O[SeO_3]_2$ и двойных цепочек $[M_3O_2]^{5+}$ в $M_3O_2Cl[SeO_3]_2$ (M^{3+} = Tb и Y).

$MnBi(SeO_3)_2Cl$

В кристаллической структуре соединения $MnBi(SeO_3)_2Cl$ (**c5.3**) находится одна симметрично независимая позиция, занятая атомами марганца. Катионы Mn^{2+} образуют октаэдры $(MnO_4Cl_2)^{8-}$, которые связываются между собой через общие ребра Cl–Cl и O–O в бесконечные загзагообразные цепочки, протянувшиеся вдоль кристаллографической оси *a* (рис. 5.3). Цепочки затем связываются характерными для четырехвалентного селена тригональными пирамидами в слои, лежащие параллельно плоскости (001).

В процессе решения и уточнения кристаллической структуры были определены две возможные конформации одного из двух селенитных оксоанионов в структуре ввиду обнаруженного разупорядочения двух кислородных позиций. Уточнение заселенностей разупорядоченных позиций дало отношения: 0.50/0.50 и 0.67/0.33 для O(5)a/O(5)b и O(6)a/O(6)b соответственно. Уточнение анизотропных тепловых параметров позиции O(3), расположенной в третьей вершине треугольного кислородного основания селенитной пирамиды $Se(2)O_3$, показало нормальные тепловые значения, тогда как уточнение самой позиции Se(2) дало значения выше нормы. Две возможные конформации группы $Se(2)O_3$ показаны на рис. 5.3в. В структуре соединения **c5.3** единственный независимый катион Bi^{3+} находится в искаженной девятикратной координации с восемью атомами кислорода и одним атомом хлора (рис. 5.3в). Катионы

Bi^{3+} разделяют слои, собранные из селенитных и марганцевых полиэдров, и уравновешивают заряд в структуре.

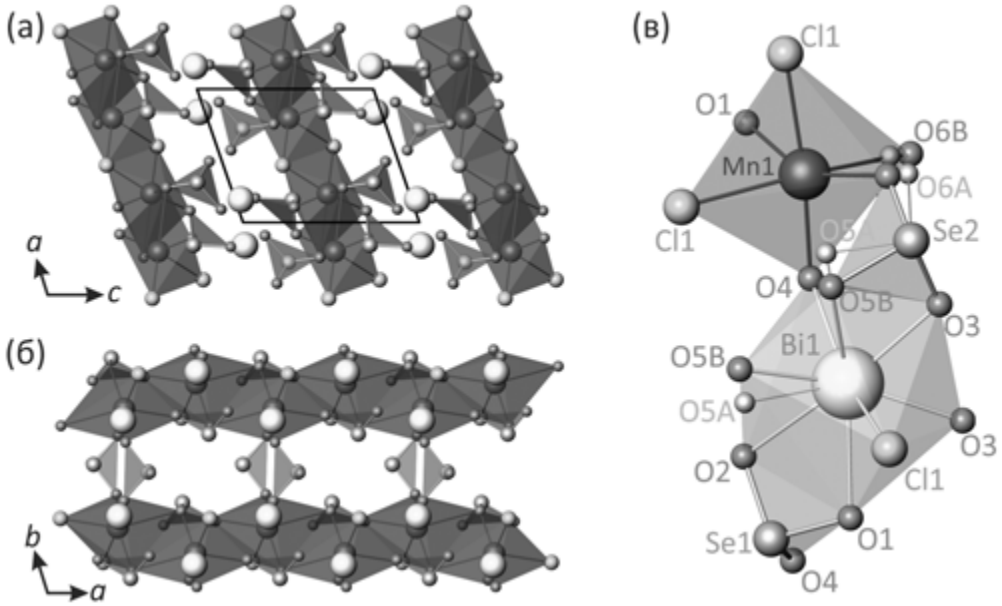

РИСУНОК 5.3 Общие проекции кристаллической структуры $MnBi(SeO_3)_2Cl$ (**c5.3**) вдоль [010] – (а) и вдоль [001] – (б) (разупорядоченные позиции O опущены для визуальной ясности); анионное окружение металлических катионов в структуре – (в)

В процессе решения и уточнения кристаллической структуры были определены две возможные конформации одного из двух селенитных оксоанионов в структуре ввиду обнаруженного разупорядочения двух кислородных позиций. Уточнение заселенностей разупорядоченных позиций дало отношения: 0.50/0.50 и 0.67/0.33 для O(5)a/O(5)b и O(6)a/O(6)b соответственно. Уточнение анизотропных тепловых параметров позиции O(3), расположенной в третьей вершине треугольного кислородного основания селенитной пирамиды $Se(2)O_3$, показало нормальные тепловые значения, тогда как уточнение самой позиции Se(2) дало значения выше нормы. Две возможные конформации группы $Se(2)O_3$ показаны на рис. 5.3в. В структуре соединения **c5.3** единственный независимый катион Bi^{3+} находится в искаженной девятикратной координации с восемью атомами кислорода и одним атомом хлора (рис. 5.3в). Катионы Bi^{3+} разделяют слои, собранные из селенитных и марганцевых полиэдров, и уравновешивают заряд в структуре.

К структурному типу новой фазы **c5.3** можно также отнести ранее изученные соединения $MnSm(SeO_3)_2Cl$, $CoSm(SeO_3)_2Cl$ и $CuGd(SeO_3)_2Cl$ [Wickleder and Hamida 2003].

$Mn^{2+}_4(Mn^{2+}_5,Bi^{3+})(SeO_3)_8Cl_5$

Соединение $Mn_4(Mn_5,Bi)(SeO_3)_8Cl_5$ (**c5.4**) является примером интересной фазы с частичным разупорядочением Bi/Mn в структуре, при котором некоторые структурные комплексы обладают статистическим катионным распределением в нескольких смешанных позициях. Кристаллическая структура соединения **c5.4** основана на *2D* структурных комплексах, образованных из искаженных квадратных антипризм четырех кристаллографически неэквивалентных смешанных позиций, занятых катионами Mn^{2+} и Bi^{3+}, распределенных по ним статистически. В слое реберно-сочлененные квадратные антипризмы располагаются в шахматном порядке (рис. 5.4а). Уточнение смешанных позиций с учетом сохранения нейтральности общей химической формулы соединения дало следующее распределение катионов: $0.97Mn^{2+}/0.03Bi^{3+}$, $0.92Mn^{2+}/0.08Bi^{3+}$, $0.87Mn^{2+}/0.13Bi^{3+}$ и $0.37Mn^{2+}/0.63Bi^{3+}$ для позиций Mn(3), Mn(4), Mn(5) и Bi(6) соответственно.

В структуре соединения **c5.4** также находятся две полностью заселенные позиции Mn^{2+}, каждая из которых октаэдрически окружена тремя атомами кислорода и тремя атомами хлора. Пара этих октаэдров объединяется через общую треугольную плоскость Cl–Cl–Cl в димер, который в свою очередь связывается через одну из вершин занятых анионами хлора с соседним димером, образуя квадратный тетрамерный комплекс. Четыре симметрично независимых тригональных пирамиды катионов Se^{4+} присоединяются к кислородным вершинам тетрамера (рис. 5.4г).

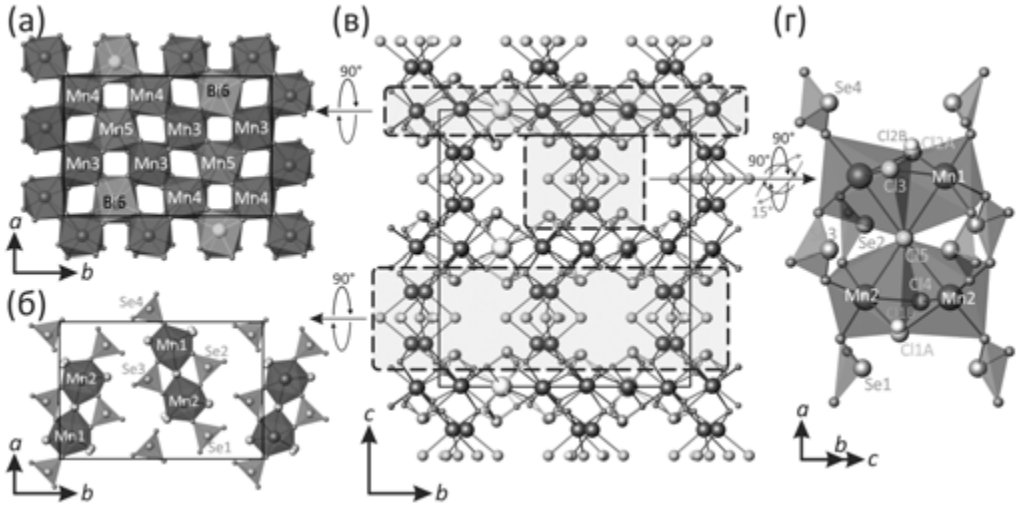

РИСУНОК 5.4 Проекция кристаллической структуры соединения $Mn_4(Mn_5,Bi)(SeO_3)_8Cl_5$ (**c5.4**) вдоль [100] – (в), слой квадратных антипризм – (а), тетрамерный комплекс – (г) и способ его расположения в структуре – (б)

Изучение распределения электронной плотности на карте Фурье позволило выявить разупорядочение двух из пяти присутствующих в структуре кристаллографически неэквивалентных позиций анионов хлора. Уточнение их заселенностей дало отношение 0.58/0.42 для обеих позиций Cl(1)a/Cl(1)b и Cl(2)a/Cl(2)b. Расположение тетрамерных комплексов в структуре соединения **c5.4** показано на рис. 5.4б. Тетрамеры соединяются со слоями из квадратных антипризм через общие ребра O-O полиэдров катионов металлов, образуя в результате сложную каркасную архитектуру с большими псевдотетрагональными каналами, идущими вдоль кристаллографической оси *a* и заполненными неподеленными электронными парами катионов Se^{4+} (рис. 5.4в).

$Bi_6(SeO_3)_4Cl_{10}$

Кристаллическая структура соединения $Bi_6(SeO_3)_4Cl_{10}$ (**c5.5**) сформирована шестью искаженными оксохлоридными полиэдрами висмута – $Bi(1)O_3Cl_4$, $Bi(2)O_5Cl_4$, $Bi(3)O_3Cl_5$, $Bi(4)O_5Cl_4$, $Bi(5)O_5Cl_4$ и $Bi(6)O_5Cl_4$, – связанными через атомы кислорода с четырьмя кристаллографически независимыми катионами Se^{4+} в *3D* каркас. Стереохимическая активность неподеленных электронных пар катионов висмута подтверждается их несимметричным координационным окружением. Полиэдры Bi^{3+} объединяются через общие ребра и вершины, образуя блоки $Bi_6(SeO_3)_4Cl_{10}$, которые связываются между собой с образованием открытой архитектуры: со структурными полостями, ограниченными главным образом анионами Cl^- и простирающимися вдоль кристаллографической оси *b* (рис. 5.5). В структуре соединения **c5.5** полости имеют размеры около 9.7 Å в длину и 3.8 Å в ширину.

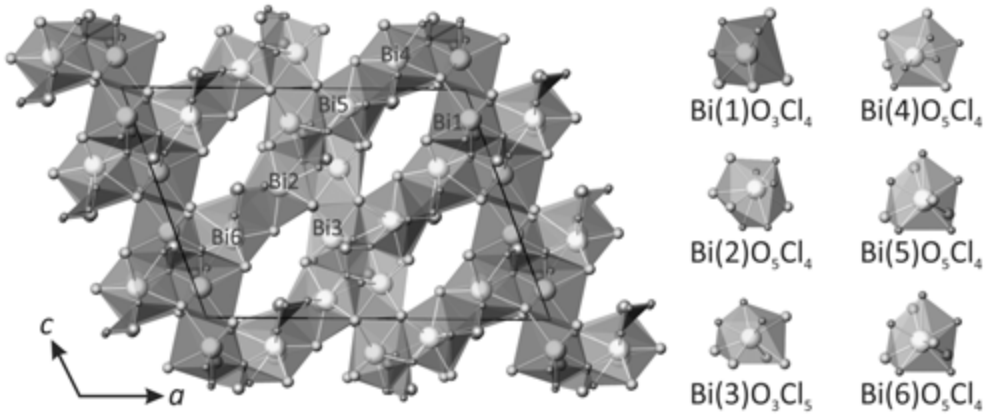

РИСУНОК 5.5 Проекция кристаллической структуры соединения $Bi_6(SeO_3)_4Cl_{10}$ (**c5.5**) на плоскость (010), показывающая объединенные через общие вершины и ребра полиэдры BiO_xCl_y (желтые) и группы SeO_3 (оранжевые)

На карте распределения электронной плотности на расстоянии 0.86 Å от позиции Se(3) был обнаружен сильный остаточный пик (8.71 *e*/Å^3), указывающий на возможное разупорядочение этой позиции. Уточнение заселенности позиций Se(3)/Se(3)' дало отношение 0.95/0.05. Измеренные длины связей Se–O для позиции Se(3)' оказались неправдоподобно большими (2.09–2.41 Å) по сравнению с ожидаемыми расстояниями, рассчитанными для Se(3) (1.71–1.74 Å), находящимися в рамках нормы. Это позволило предположить, что данная позиция частично занята также катионами Bi^{3+}. Окончательное уточнение заселенности позиций Bi(3)a/Bi(3)b и Se(3)a/Se(3)b привело к отношению 0.96/0.04. Детальное описание кристаллической структуры соединения **c5.5** приведено в статье **A-III** (см. Included Articles).

β–Bi(SeO$_3$)Cl с гигантской элементарной ячейкой

Кристаллическая структура соединения β–Bi(SeO_3)Cl (**c5.6**) весьма необычна и сложна. Достоин отдельного внимания не только ее нецентросимметричный характер, но и поразительный объем элементарной ячейки (19 792 Å^3). Всего в структуре было локализовано по 48 кристаллографически неэквивалентных ионов висмута, селена и хлора. Структура соединения **c5.6** может быть описана как построенная из двух блоков $[Bi_8Cl_{16}]^{8+}$ (рис. 5.6г) и $[Bi_{12}Cl_{32}]^{4+}$ (рис. 5.6в), закономерно расположенных между слоями $[Bi_{14}(SeO_3)_{24}]^{6-}$ (рис. 5.6б). На рис. 5.6а полиэдры BiO_x показаны желтым цветом, тогда как слои $[Bi_8Cl_{16}]^{8+}$ и $[Bi_{12}Cl_{32}]^{4+}$ для визуальной ясности представлены в виде шариков Bi (желтый) и Cl (зеленый).

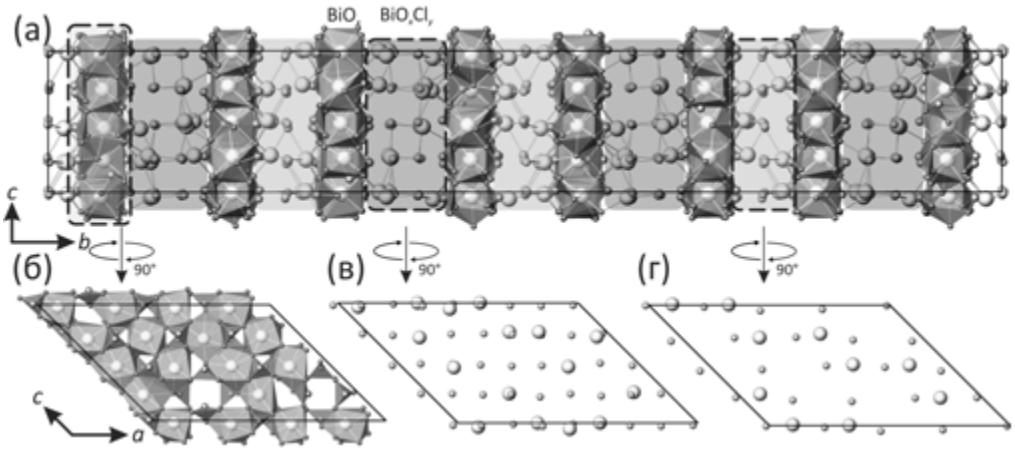

РИСУНОК 5.6 Проекция кристаллической структуры соединения β–Bi(SeO_3)Cl (**c5.6**) вдоль [100] – (а). Чередование трех разных параллельных слоев: $[Bi_{14}(SeO_3)_{24}]^{6-}$ – (б), $[Bi_{12}Cl_{32}]^{4+}$ – (в) и $[Bi_8Cl_{16}]^{8+}$ – (г)

Следует заметить, что похожие галогенидные слои состава $[Bi_8Cl_{16}]^{8+}$ были также обнаружены и в структуре нового соединения $PbBi_{10}(SeO_3)_{12}Cl_8$ (**c5.7**), которое будет описано ниже. Структурные комплексы $[Bi_{14}(SeO_3)_{24}]^{6-}$ образованы группировкой катионов Bi^{3+} и тригональных пирамид SeO_3. В полиэдрах BiO_x значение x находится между 8 и 10. Все найденные в структуре позиции висмута имеют искаженную координацию, что указывает на стереохимическую активность неподеленной электронной пары катионов тяжелых металлов.

Большая величина параметра b (~76 Å) элементарной ячейки может быть объяснена встреченным разнообразием различных структурных блоков, слагающих сложную структуру соединения **c5.6** вдоль направления [010]. Иными словами, закономерное упорядочение катионных блоков $[Bi_8Cl_{16}]^{8+}$ и $[Bi_{12}Cl_{32}]^{4+}$, заключенных между анионными слоистыми комплексами $[Bi_{14}(SeO_3)_{24}]^{6-}$, является ключевым фактором для формирования такой гигантской элементарной ячейки и ответственно за фактическое удваивание параметра b. Детальное описание кристаллической структуры соединения **c5.6** и анализ фазовых переходов α→β→γ полиморфных модификаций $Bi(SeO_3)Cl$, сопровождающийся резким изменением структурной сложности соединений, приведены в статье **A-III** (см. Included Articles).

$PbBi_{10}(SeO_3)_{12}Cl_8$

Кристаллическая структура соединения $PbBi_{10}(SeO_3)_{12}Cl_8$ (**c5.7**) содержит пять симметрично независимых позиций, занятых тяжелыми катионами. Одна из них – Bi(1) – полностью заселена катионами Bi^{3+}, тогда как уточнение четырех других выявило одинаковую для всех смешанную заселенность Bi^{3+}/Pb^{2+}, равную отношению 0.9/0.1. Принимая во внимание только длины связей Bi/Pb–O и Bi–Cl меньше 3.10 Å, были определены следующие координационные полиэдры тяжелых катионов: $Bi(1)O_8$, $Bi(2)O_{10}$, $Bi(3)O_{10}$, $Bi(4)O_{10}$ и $Bi(5)O_4Cl_4$ (рис. 5.7).

Три кристаллографически неэквивалентные тригонально пирамидальные селенитные группы присоединяются к *2D* слоистым комплексам, состоящим из полиэдров $Bi(1)O_8$, $Bi(2)O_{10}$, $Bi(3)O_{10}$ и $Bi(4)O_{10}$, через общие ребра O–O.

Структуру соединения **c5.7** можно описать как сложенную из *2D* слоев $[(Pb,Bi)_{14}(SeO_3)_{24}]^{n-}$ (рис. 5.7а), заключенных между слоистыми комплексами $[(Pb,Bi)_8Cl_{16}]^{n+}$ (рис. 5.7в), лежащих параллельно плоскости (010). Структурная архитектура навой фазы **c5.7** находится в тесной связи с кристаллической структурой соединения $CaNd_{10}(SeO_3)_{12}Cl_{18}$ [Berdonosov et al. 2007]. Детальное описание кристаллической структуры соединения **c5.7** приведено в статье **A-III** (см. Included Articles).

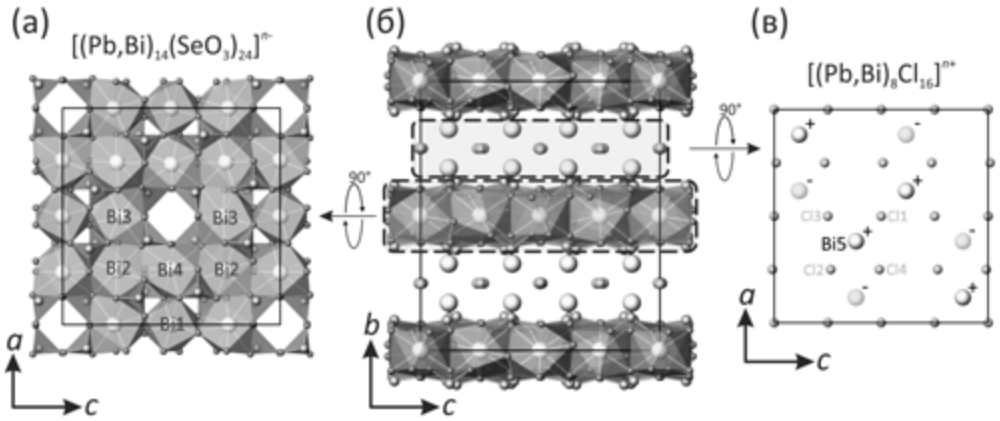

РИСУНОК 5.7 Проекция кристаллической структуры соединения $PbBi_{10}(SeO_3)_{12}Cl_8$ (**c5.7**) вдоль кристаллографической оси *a* – (б). Два параллельных катионных и анионных слоя: $[(Pb,Bi)_{14}(SeO_3)_{24}]^{n-}$ – (а) и $[(Pb,Bi_8)Cl_{16}]^{n+}$ – (в)

2.6 Кристаллохимическое исследование новых уранил-селенатов и селенит-селенатов

Основные кристаллографические сведения и параметры уточнения кристаллических структур 16 новых соединений, приведенных ниже, представлены в табл. 6.1 и 6.2.

c6.1 –	$[CH_6N]_2$ $[(UO_2)(SeO_4)_2(H_2O)](H_2O)$	**c6.9** –	$[C_2H_8N]_2$ $[(UO_2)(SeO_4)_2(H_2O)]$
c6.2 –	$[CH_6N]_2$ $[(UO_2)(SeO_4)_2(H_2O)]$	**c6.10** –	$[C_2H_8N]_2$ $[(UO_2)_2(SeO_4)_3(H_2O)]$
c6.3 –	$[CH_6N]_2$ $[(UO_2)_2(SeO_4)_3]$	**c6.11** –	$[C_4H_{15}N_3][H_3O]_{0.5}[(UO_2)_2$ $(SeO_4)_{2.93}(SeO_3)_{0.07}(H_2O)](NO_3)_{0.5}$
c6.4 –	$[CH_6N](H_3O)$ $[(UO_2)_2(SeO_4)_3(H_2O)](H_2O)$	**c6.12** –	$[C_2H_8N]_3[H_5O_2]$ $[(UO_2)_2(SeO_4)_3(H_2O)_2]_2(H_2O)_5$
c6.5 –	$[CH_6N]_4$ $[(UO_2)_3(SeO_4)_5](H_2O)_4$	**c6.13** –	$[C_2H_8N]_2[H_3O][(UO_2)_3$ $(SeO_4)_4(HSeO_3)(H_2O)](H_2SeO_3)_{0.2}$
c6.6 –	$[CH_6N](H_5O_2)(H_3O)_2$ $[(UO_2)_3(SeO_4)_5](H_2O)_4$	**c6.14** –	$[C_4H_{12}N]_3[H_3O]$ $[(UO_2)_3(SeO_4)_5(H_2O)]$
c6.7 –	$[CH_6N]_4(H_3O)_2$ $[(UO_2)_5(SeO_4)_8(H_2O)](H_2O)_4$	**c6.15** –	$[C_2H_8N]_3(C_2H_7N)$ $[(UO_2)_3(SeO_4)_4(HSeO_3)(H_2O)]$
c6.8 –	$[CH_6N]_{1.5}(H_5O_2)_{1.5}(H_3O)_3[(UO_2)_5$ $(SeO_4)_8(H_2O)](H_2SeO_4)_{2.6}(H_2O)_3$	**c6.16** –	$[C_2H_8N][(H_5O_2)(H_2O)]$ $[(UO_2)_2(SeO_4)_3(H_2SeO_3)](H_2O)$

ТАБЛИЦА 6.1 Кристаллографические сведения и параметры уточнения структур соединений **c6.1**, **c6.2**, **c6.3**, **c6.4**, **c6.5**, **c6.6**, **c6.7** и **c6.8**

	c6.1	**c6.2**	**c6.3**	**c6.4**	**c6.5**	**c6.6**	**c6.7**	**c6.8**
M_r (г моль$^{-1}$)	639.99	623.99	1020.98	1042.96	1692.97	1678.91	2709.91	2946.25
пр. гр.	*Pnma*	$P2_1/c$	$P2_1$	$P2_1/c$	*Pnna*	*Ibca*	$Pca2_1$	*Pnma*
a (Å)	7.5496(7)	8.2366(10)	8.583(1)	8.4842(10)	16.422(1)	20.956(2)	31.505(2)	30.973(2)
b (Å)	12.014(1)	7.5888(6)	10.073(1)	10.2368(8)	18.4773(9)	34.767(8)	10.369(1)	37.022(2)
c (Å)	15.836(1)	22.260(2)	10.095(1)	24.228(2)	10.3602(5)	18.663(2)	16.242(1)	10.417(1)
β (°)	90	104.566(9)	95.98(1)	102.803(9)	90	90	90	90
V (Å^3)	1436.3(2)	1346.7(2)	867.7(2)	2051.9(3)	3143.7(3)	13597(4)	5305.9(6)	11945(1)
Z	4	4	2	4	4	16	4	8
ρ (г/см^3)	2.960	3.078	3.908	3.376	3.577	3.280	3.392	3.277
μ (мм$^{-1}$)	16.423	17.507	25.012	21.166	21.319	19.720	20.814	20.086
λ (MoK_α) (Å)	0.71073	0.71073	0.71073	0.71073	0.71073	0.71073	0.71073	0.71073
всего рефл.	10099	12119	5477	12326	18468	32094	27846	61466
независ. рефл.	1605	3656	2931	3602	2774	4913	8463	10116
R_{int}	0.0875	0.0828	0.1271	0.1698	0.1191	0.3280	0.2070	0.2139
R_1 [$I > 2\sigma(I)$]	0.0467	0.0466	0.1072	0.0674	0.0541	0.1040	0.0852	0.0858
wR_2 [$I > 2\sigma(I)$]	0.0860	0.0637	0.2712	0.1551	0.1119	0.1867	0.1901	0.1736
R_1 [all data]	0.0566	0.0785	0.1126	0.0957	0.0790	0.2138	0.1305	0.1556
wR_2 [all data]	0.0882	0.0688	0.2766	0.1693	0.1216	0.2287	0.2150	0.2083
GOF	1.334	0.996	1.083	1.049	1.104	0.968	0.997	1.055
$\Delta\rho_{max}$, $\Delta\rho_{min}$ (e Å^{-3})	1.44, −3.13	1.59, −2.21	8.61, −3.16	2.84 −1.99	2.23, −1.82	2.58, −1.43	2.44, −1.84	2.90, −1.49
CCDC #	866552	866549	866547	866553	866546	866551	866548	866550

ТАБЛИЦА 6.2 Кристаллографические сведения и параметры уточнения структур соединений **c6.9**, **c6.10**, **c6.11**, **c6.12**, **c6.13**, **c6.14**, **c6.15** и **c6.16**

	c6.9	**c6.10**	**c6.11**	**c6.12**	**c6.13**	**c6.14**	**c6.15**	**c6.16**
M_r (г моль$^{-1}$)	666.15	1079.14	2256.03	2267.28	1685.05	1770.70	1685.07	1217.08
пр. гр.	$P2_12_12_1$	$P2_12_12_1$	$P2_1/c$	$P2_1/c$	$P2_1/m$	$P2_1/m$	$Pnma$	$P2_1/n$
a (Å)	7.5363(7)	11.2154(5)	11.1679(4)	12.451(5)	8.3116(4)	8.941(2)	11.659(1)	14.7979(8)
b (Å)	12.202(1)	11.2263(5)	10.9040(4)	31.126(5)	18.6363(8)	19.300(4)	14.956(2)	10.0238(6)
c (Å)	16.760(2)	16.9138(8)	17.9913(6)	14.197(4)	11.5623(5)	11.377(3)	22.194(2)	16.4176(9)
β (°)	90.00	90.00	98.019(1)	120.39(2)	97.582(1)	97.510(4)	90.00	111.628(1)
V (Å^3)	1541.2(2)	2129.6(2)	2169.6(2)	4746(2)	1775.3(1)	1946.5(7)	3870.0(7)	2263.8(2)
Z	4	4	2	4	2	2	4	4
ρ (г/см^3)	2.871	3.366	3.457	3.173	3.152	3.021	2.892	3.571
μ (мм$^{-1}$)	15.306	20.394	20.036	18.323	19.286	17.217	17.310	20.822
λ (MoK_α) (Å)	0.71073	0.71073	0.71073	0.71073	0.71073	0.71073	0.71073	0.71073
всего рефл.	13644	17184	23671	34682	23753	18435	10911	25431
независ. рефл.	4492	6112	4988	10896	5323	4597	1680	5476
R_{int}	0.056	0.065	0.072	0.096	0.076	0.120	0.112	0.073
R_1 [$I > 2\sigma(I)$]	0.031	0.029	0.033	0.048	0.036	0.040	0.060	0.027
wR_2 [$I > 2\sigma(I)$]	0.063	0.048	0.074	0.106	0.097	0.058	0.096	0.052
R_1 [all data]	0.035	0.038	0.049	0.104	0.055	0.099	0.095	0.041
wR_2 [all data]	0.064	0.050	0.077	0.122	0.102	0.066	0.105	0.054
GOF	0.940	0.934	0.964	0.875	0.979	0.737	1.127	0.928
$\Delta\rho_{max}$, $\Delta\rho_{min}$ (e Å^{-3})	2.34, −1.45	1.10, −1.20	2.82, −2.00	4.61, −4.34	2.79, −2.23	1.65, −1.38	1.05, −1.21	2.39, −1.81
CCDC #	901940	901941	901942	901943	901944	901945	901946	824406

2.6.1 Экспериментальные процедуры

Монокристаллы всех новых уранил-селенатов и селенит-селенатов были приготовлены методом изотермического испарения при комнатных условиях из водных растворов шестиводного уранил-нитрата, 40%-ного раствора селеновой кислоты, соответствующего амина и дистиллированной воды. Желто-зеленая гомогенная жидкость выливалась на часовые стекла, которые помещались в вытяжной шкаф на несколько дней при комнатной температуре, после чего часовые стекла накрывались стеклянными крышками и оставлялись в таком полузаконсервированном виде. Экспериментальные подробности условия синтеза 16 новых соединений приведены в табл. 6.3.

ТАБЛИЦА 6.3 Экспериментальные детали синтезов новых уранил-селенатов и селенит-селенатов, выполненных методом изотермического испарения (во всех случаях температура: 23 °C; время роста кристаллов: 72 часа).

Молярные соотношения:	**c6.1**	**c6.2**	**c6.3**	**c6.4**	**c6.5**	**c6.6**	**c6.7**	**c6.8**
SeO_2	0.5	0.4	0.7	0.4	0.8	0.7	0.4	0.7
$UO_2(NO_3)_2{\cdot}6H_2O$ [1]	0.1	0.1	0.1	0.1	0.1	0.2	0.1	0.2
CH_5N [2]	0.4	0.5	0.2	0.5	0.1	0.1	0.5	0.1
H_2O (ml)	2	2	2	2	2	2	2	2

ТАБЛИЦА 6.3 *Продолжение*

Молярные соотношения:	**c6.9**	**c6.10**	**c6.11**	**c6.12**	**c6.13**	**c6.14**	**c6.15**	**c6.16**
SeO_2	4.1	4.1	0.7	0.7	0.7	4.7	0.5	0.8
$UO_2(NO_3)_2{\cdot}6H_2O$ [1]	0.4	0.4	0.2	0.1	0.1	0.1	0.1	0.1
C_2H_7N [3]				0.2	0.2		0.4	0.1
$C_4H_{11}N$ [4]						0.1		
$C_4H_{13}N_3$ [5]			0.1					
C_3H_7NO [6]	1.3	1.3						
H_2O (ml)	2	2	2	2	2	2	2	2

[1]Все урановые материалы в экспериментах были деплетированными; [2]метиламин (MA); [3]диметиламин (DMA); [4]диэтиламин (DEA); [5]диэтилентриамин (DETA); [6]*N*,*N*-диметилформамид (DMF)

2.6.2 Структурное описание шестнадцати новых фаз

Все новые фазы органически темплатированных уранил-селенатов и селенит-селенатов, представленные в настоящей работе, можно разделить на несколько групп в соответствии с разным соотношением U^{6+}: $Se^{6+/4+}$ в структурных комплексах соединений: 1 : 2 – **c6.1**, **c6.2**, **c6.9**, **c6.16**; 2 : 3 – **c6.3**, **c6.4**, **c6.10** – **c6.12**; 3 : 5 – **c6.5**, **c6.6**, **c6.13** – **c6.15**; и 5 : 8 – **c6.7**, **c6.8**. Кристаллические структуры всех фаз содержат уранильные пентагональные бипирамиды $(UO_7)^{8-}$, тетраэдры $(Se^{6+}O_4)^{2-}$ и/или тригональные пирамиды $(Se^{4+}O_3)^{2-}$ со стереохимически активными неподеленными электронными парами, выступающими в роли дополнительных лигандов. Катионные полиэдры связываются в неорганические структурные комплексы с открытыми архитектурами (т.е. с такими, в которых связывание через общие вершины происходит значительно чаще, чем связывание по ребрам). В кристаллических структурах катионы U^{6+} формируют приблизительно линейные уранил-ионы $[UO_2]^{2+}$ со средней длиной связи <U=O>, равной 1.756 Å, посчитанной для всех структур, описываемых в данном разделе. Эти элементарные уранильные группы координируются в экваториальной плоскости пятью атомами кислорода (или четырьмя O и одной молекулой H_2O), образуя пентагональные бипирамиды UO_7 (или $UO_6(H_2O)$) со средней длиной связи <U–O_{eq}>, равной 2.390 Å. В целом, связи U–$O_{eq}H_2$ оказываются длиннее и лежат в диапазоне 2.42–2.54 Å. Среднее расстояние <Se–O> в селенитных и селенатных группах составляет 1.628 Å. Во всех синтезированных структурах неорганические *1D* и *2D* структурные комплексы разделены между собой и темплатированы органическими и/или водными молекулами. Подробное описание кристаллических структур всех новых фаз приведено в статьях **A-I** (**c6.16**), **A-II** (**c6.1** – **c6.8**) и **A-VI** (**c6.9** – **c6.15**) (см. Included Articles). В настоящей диссертации ниже будут описаны только топологические и геометрические особенности уранил-селенатных и селенит-селенатных структурных комплексов.

Топология неорганических комплексов в рассматриваемых структурах может быть описана при помощи вспомогательного графического представления. Согласно этому подходу [Krivovichev 2004; Krivovichev 2009; Krivovichev 2010] координационные полиэдры катионов U^{6+} и $Se^{6+/4+}$ обозначаются соответственно черными и белыми узлами. Эти узлы могут быть соединены ребром в случае, если два соответствующих полиэдра объединены через общую вершину. Получающийся в результате такого построения граф применяется для изучения топологических взаимоотношений между похожими структурами. Рис. 6.1 показывает все топологическое многообразие неорганических структурных комплексов, обнаруженных в кристаллических структурах новых синтезированных соединений **c6.1** – **c6.16**.

Соединения с U : Se = 1 : 2

Кристаллические структуры соединений $[CH_6N]_2[(UO_2)(SeO_4)_2(H_2O)](H_2O)$ (**c6.1**), $[CH_6N]_2[(UO_2)(SeO_4)_2(H_2O)]$ (**c6.2**) и $[C_2H_8N]_2[(UO_2)(SeO_4)_2(H_2O)]$ (**c6.9**) построены на структурных комплексах состава $[(UO_2)(SeO_4)_2(H_2O)]^{2-}$. В структурах соединений **c6.1** и **c6.9** пентагональные бипирамиды $(UO_6(H_2O))^{6-}$ объединяются через общие вершины с двумя соседними тетраэдрами $(SeO_4)^{2-}$, формируя цепочки $[(UO_2)(SeO_4)_2(H_2O)]^{2-}$, укладывающиеся в параллельные псевдослои (рис. 6.1а, б), тогда как структура **c6.2** основана уже на полноценных слоях того же химического состава (рис. 6.1в, г).

Такие цепочки были впервые описаны в структуре соединения $Mn[(UO_2)(SO_4)_2(H_2O)](H_2O)_5$ [Tabachenko et al. 1975], а позднее во множестве других уранильных оксосолей, темплатированных различными с аминами. Слоистая топология фазы **c6.2** также является достаточно распространенной и встречается во множестве соединений состава $[A_nO_2(SO_4)_2(H_2O)]$ [Krivovichev 2009].

Кристаллическая структура соединения $[C_2H_8N][(H_5O_2)(H_2O)][(UO_2)_2(SeO_4)_3(H_2SeO_3)](H_2O)$ (**c6.16**) основана на слоях $[(UO_2)_2(SeO_4)_3(H_2SeO_3)]^{2-}$, образованных в результате полимеризации координационных комплексов $(UO_7)^{8-}$, $(Se^{6+}O_4)^{2-}$ и $(Se^{4+}O(OH)_2)^0$ через общие атомы кислорода. В топологической структуре слоя (рис. 6.1д, е) каждая селенатная группа связывает сразу три уранил-иона, а дважды протонированные селенитные комплексы присоединяются только одной кислородной вершиной к одному уранильному полиэдру. Эта топология ранее не встречалась в структурах неорганических оксосолей.

Соединения с U : Se = 2 : 3

В кристаллических структурах соединений с отношением U : Se, равным 2 : 3, – $[CH_6N]_2[(UO_2)_2(SeO_4)_3]$ (**c6.3**), $[CH_6N](H_3O)[(UO_2)_2(SeO_4)_3(H_2O)](H_2O)$ (**c6.4**),

$[C_2H_8N]_2[(UO_2)_2(SeO_4)_3(H_2O)]$ (**c6.10**), $[C_4H_{15}N_3][H_3O]_{0.5}[(UO_2)_2(SeO_4)_{2.93}(SeO_3)_{0.07}(H_2O)](NO_3)_{0.5}$ (**c6.11**) и $[C_2H_8N]_3[H_5O_2][(UO_2)_2(SeO_4)_3(H_2O)_2]_2(H_2O)_5$ (**c6.12**) – координационные полиэдры U^{6+} and $Se^{6+/4+}$ объединяются через общие лиганды с образованием *2D* комплексов с химическими составом $[(UO_2)_2(SeO_4)_{3-x}(SeO_3)_x(H_2O)_n]^{2-}$ (n = 0, 1, 2; x = 0, 0.07).

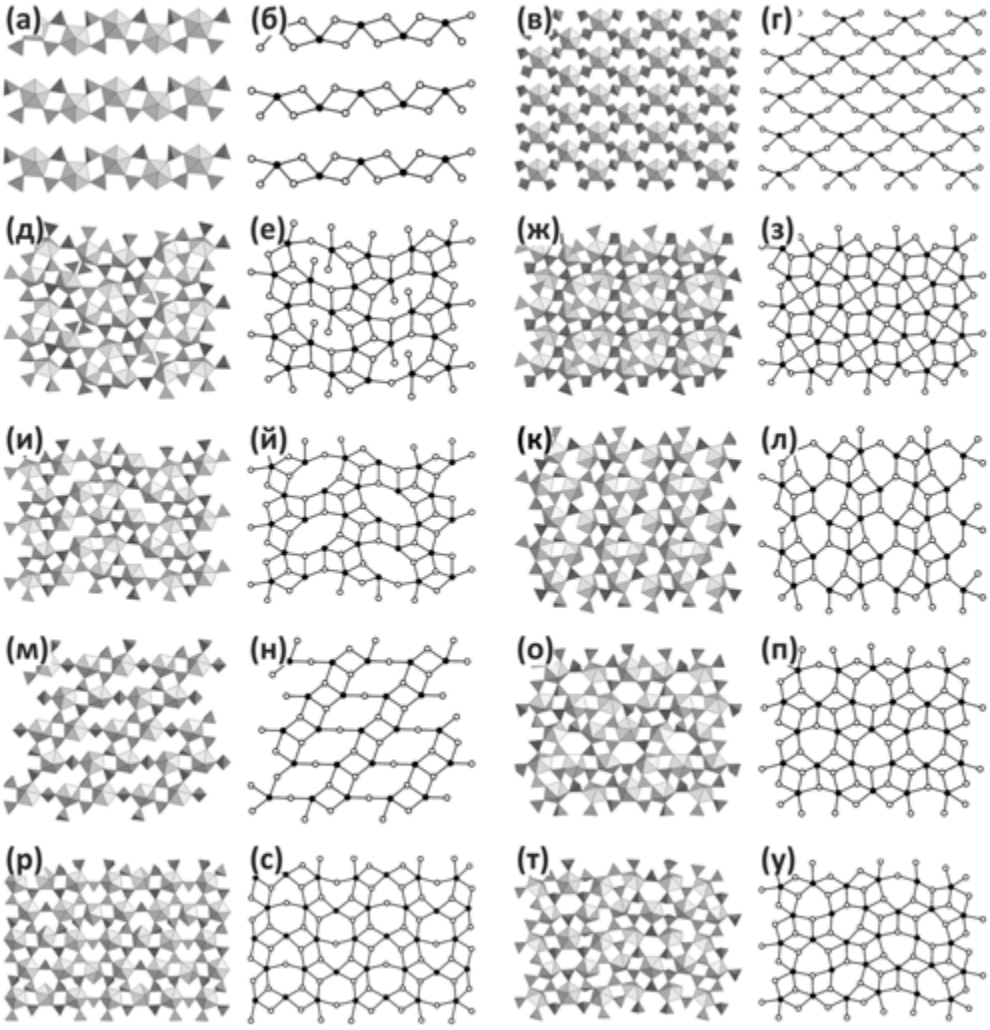

РИСУНОК 6.1 Топологическое разнообразие неорганических структурных комплексов в кристаллических структурах новых соединений. Уранильные пентагональные бипирамиды и селенатные/селенитные группы показаны желтым и оранжевым цветом в полиэдрическом представлении и черными и белыми вершинами на графах

Топология слоя при n = 0, обнаруженная в соединении **c6.3**, основана только на четырехчленных кольцах, составленных из чередующихся уранильных и селенатных полиэдров (рис. 6.1ж, з). Ранее уже встречалась, например, в соединении $[CH_6N_3]_2[(UO_2)_2(SeO_4)_3]$ [Krivovichev et al. 2009].

Кристаллические структуры соединений **c6.4**, **c6.10** и **c6.11** при n = 1 основаны на структурных комплексах с одинаковым химическим составом $[(UO_2)_2(SeO_4)_3(H_2O)]^{2-}$, но имеют разный способ топологической связи полиэдров U и Se. Структура соединения **c6.4** содержит слои (рис. 6.1и, й), похожие на слоистые неорганические комплексы, встреченные в структуре **c6.16**. Главная разница между этими двумя топологиями заключается в присутствии дополнительных селенитных полиэдров, координирующих уранильные группы и расположенных в больших пустых восьмичленных кольцах слоев в структуре соединения **c6.16**. Топология слоя **c6.4** является редкой. Она была обнаружена ранее только в одном уранил-селенате $K(H_3O)[(UO_2)_2(SeO_4)_3(H_2O)](H_2O)_6$ [Ling et al. 2010].

В слоях соединений **c6.10** и **c6.11** (рис. 6.1к, л) незаполненные шестичленные кольца объединяются по общему ребру с образованием цепочек, параллельных друг другу, разделенных между собой более сложными по топологии цепочечными комплексами плотных четырехчленных колец. Такой тип топологии структурных комплексов был встречен в полудюжине органически темплатированных оксосолей уранила [Krivovichev 2009].

Анализ топологии слоев **c6.10** и **c6.11** показал, что несвязанные вершины селенатных групп могут иметь различную ориентацию относительно плоскости слоя: вверх, вниз или разупорядоченную (вверх и вниз). Эта неоднозначность обусловливает возможность выявления геометрических изомеров с разной ориентацией полиэдров селена в слое. С целью идентификации и классификации подобных изомеров *С. В. Кривовичев* и *П. Бернс* предложили подход, основанный на составлении ориентационных матриц для изомеров [Krivovichev and Burns 2003]. В соответствии с этим подходом каждому белому узлу графа присваиваются символы **u** (вверх), **d** (вниз), **m** (ориентация вверх – вниз топологически эквивалентна) или □ (вершина в графе отсутствует). Любопытно, что составленные таким образом ориентационные матрицы слоев в кристаллических структурах **c6.10** и **c6.11** оказались эквивалентными. Полученная матрица может быть записана как (**u□dd**)(**uu□d**). Таким образом, уранил-селенатные слои в этих структурах отвечают одному и тому же геометрическому изомеру.

Слой $[(UO_2)_2(SeO_4)_3(H_2O)_n]^{2-}$ при n = 2 в структуре соединения **c6.12** составлен из колонок реберно-сочлененных больших полых восьмичленных и плотных четырехчленных колец (рис. 6.1м, н). Такая топология слоя ранее не встречалась в уранил-селенатах.

Соединения с U : Se = 3 : 5

Кристаллические структуры соединений $[CH_6N]_4[(UO_2)_3(SeO_4)_5](H_2O)_4$ (**c6.5**) и $[CH_6N](H_5O_2)(H_3O)_2[(UO_2)_3(SeO_4)_5](H_2O)_4$ (**c6.6**) основаны на топологически одинаковых неорганических слоях состава $[(UO_2)_3(SeO_4)_5]^{4-}$ (рис. 6.1о, п). Слои построены из четырех- и шестичленных колец. Эта топология ранее была встречена в некоторых уранил-селенатах и хроматах [Krivovichev 2009].

Используя геометрический подход, основанный на определении ориентации несвязанных вершин селенатных тетраэдров, ориентационные последовательности селенатных групп в слоях соединений **c6.5** и **c6.6** могут быть записаны как (□**uu**□**dd**)(**mddmuu**) и (□**ud**□**ud**)(**duuddd**)(□**du**□**du**)(**ddddud**) соответственно. Таким образом, селенатные и селенит-селенатные слои, обнаруженные в кристаллических структурах этих соединений, отвечают разным геометрическим изомерам.

Кристаллические структуры соединений $[C_2H_8N]_2[H_3O][(UO_2)_3(SeO_4)_4(HSeO_3)(H_2O)](H_2SeO_3)_{0.2}$ (**c6.13**), $[C_4H_{12}N]_3[H_3O][(UO_2)_3(SeO_4)_5(H_2O)]$ (**c6.14**) и $[C_2H_8N]_3(C_2H_7N)[(UO_2)_3(SeO_4)_4(HSeO_3)(H_2O)]$ (**c6.15**) обладают одинаковой топологией неорганических слоев (рис. 6.1р, с), построенной из четырех- и шестичленных колец. Эта топология является весьма характерной для немногих известных к настоящему моменту уранил-селенит-селенатов. Она была обнаружена, например, в кристаллической структуре соединения $[C_5H_{14}N]_4[(UO_2)_3(SeO_4)_4(HSeO_3)(H_2O)](H_2SeO_3)(HSeO_4)$ [Krivovichev et al. 2006]. Ориентационные матрицы для слоев в **c6.13**, **c6.14** и **c6.15** имеют размеры 6 × 2. Последовательности символов, записанных в ряд, – (**duuudd**)(**ud**□**du**□), (**dumudm**)(**ud**□**du**□) и (**udududd**)(**ud**□**du**□) – дополнительно характеризуют топологическую структуру неорганических слоистых комплексов, относя их к разным геометрическим изомерам.

Соединения с U : Se = 5 : 8

Кристаллические структуры $[CH_6N]_4(H_3O)_2[(UO_2)_5(SeO_4)_8(H_2O)](H_2O)_4$ (**c6.7**) и $[CH_6N]_{1.5}(H_5O_2)_{1.5}(H_3O)_3[(UO_2)_5(SeO_4)_8(H_2O)](H_2SeO_4)_{2.6}(H_2O)_3$ (**c6.8**) основаны на слоях с химическим составом $[(UO_2)_5(SeO_4)_8(H_2O)]^{6-}$ (рис. 6.1т, у). Они составлены таким образом, что пары шестичленных колец, объединенных через общую вершину, разделяются между собой цепочками реберно-сочлененных четырехчленных колец. При этом пары располагаются поочередно вдоль взаимно перпендикулярных направлений. Соединения **c6.7** и **c6.8** являются первыми уранил-селенатами с такой топологией слоев.

Используя геометрический подход, основанный на составлении матрицы ориентации оказавшихся несвязанными вершин селенатных тетраэдров, ориентационные последовательности для слоев в **c6.7** и **c6.8** можно записать как

(**uu□uu**)(**ddud□**) и (**dd□dd**)(**duuu□**) соответственно. Таким образом, уранил-селенатные слои, обнаруженные в кристаллических структурах этих соединений, отвечают разным геометрическим изомерам.

2.6.3 Понижение размерности

Для проведения корреляции состав – структура в уранил-селенатах был применен принцип размерностного понижения [Long et al. 1996; Tulsky and Long 2001]. В рамках настоящего диссертационного исследования была проанализирована большая группа соединений с общей формулой $A_n(UO_2)_p(TO_4)_q(H_2O)_r$ (A^+ = однозарядный катион, T^{6+} = Se, S, Cr, Mo). Было предположено, что базовой высокополимеризованной *3D* структурой является $(UO_2)(TO_4)$, тогда как в роли агентов, понижающих размерность, выступают $A_2(TO_4)$ и H_2O. В соответствии с этим предположением соотношение между разными составами и структурами было решено графически отобразить на композиционной диаграмме UO_2TO_4 – A_2TO_4 – H_2O (рис. 6.2). Список всех нанесенных на нее соединений и размерностных характеристик их структур может быть найден в статье **A-II** (см. Included Articles).

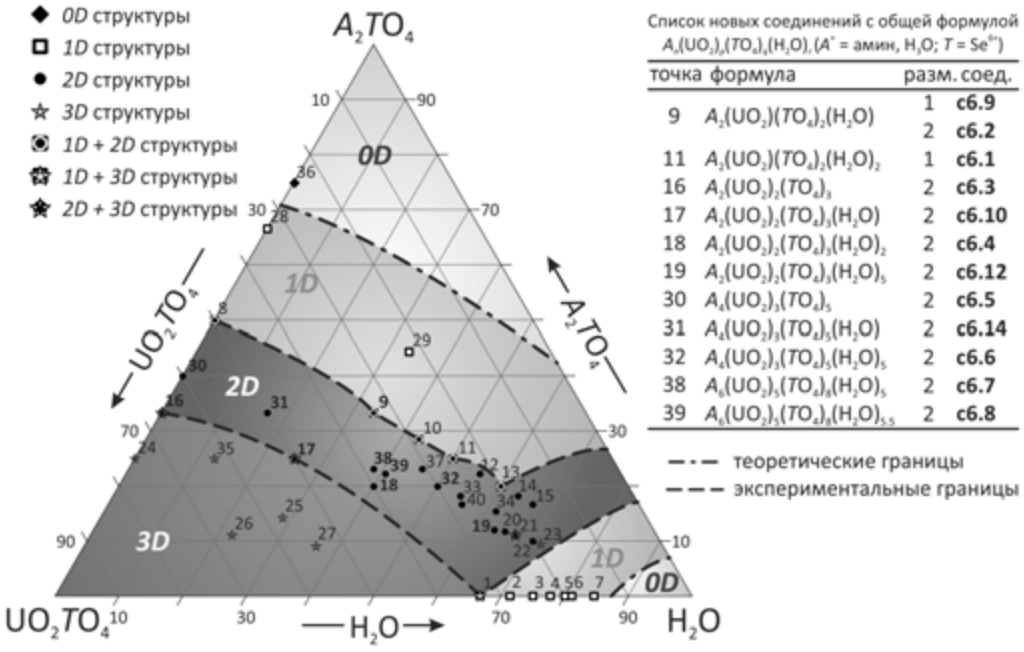

РИСУНОК 6.2 Поля разной размерности на композиционной диаграмме системы UO_2TO_4 – A_2TO_4 – H_2O (A = однозарядный катион, T = S, Se, Cr, Mo)

Диаграмма может быть разделена на поля, в которых структуры имеют одинаковое значение размерности (0 = конечные кластеры, 1 = цепочки, 2 = слои, 3 = каркасы). Определение границ между полями не является однозначным и имеет ориентировочный характер. Так, например, по причине наличия всего одной точки (**36**), соответствующей *0D* фазам, границы между полями *0D* и *1D* проведены гипотетически. Можно предположить, что эти границы должны быть более-менее параллельными границам между полями *1D*-и-*2D* и *2D*-и-*3D* и не противоречить принципу размерностного понижения для неорганических оксосолей.

Тем не менее были обнаружены некоторые расхождения с ожиданиями. В частности, точки **21** и **23** расположены в *2D* поле, но соответствуют *3D* каркасам структур с составами $A_6(UO_2)_2(TO_4)_3(H_2O)_6$ и $A_6(UO_2)_2(TO_4)_3(H_2O)_{7.5}$ соответственно. Эти отклонения можно связать с двоякой ролью H_2O: в большинстве случаев молекулы воды выступают в качестве агентов, понижающих размерность, тогда как в случаях соединений **21** и **23** они просто заполняют пустоты в уранильном каркасе.

Для наглядной демонстрации принципа размерностного понижения в системе можно рассмотреть линию, выходящую из левого угла диаграммы и заканчивающуюся в ее вершине. Линия соответствует серии соединений с химическим составом $A_n(UO_2)_p(TO_4)_q$. Точки **24**, **30**, **28** и **36** отвечают структурам с размерностью, равной соответственно 3, 2, 1 и 0. Точки **16** и **8** лежат на границах между полями *2D*-и-*3D* и *1D*-и-*2D* соответственно. Таким образом, размерность структурных комплексов уменьшается от точки **24** к точке **36**, что полностью согласуется с принципом размерностного понижения.

2.7 Аналогия между селенитными и фосфитными оксоанионами

В этом разделе представлены чрезвычайно интересные результаты, полученные в самом конце работы над диссертацией, явно указывающие на отрицательный заряд водорода в фосфитах. Анионы $(HPO_3)^{2-}$, образованные депротонированием ортофосфористой кислоты $HPO(OH)_2$, обычно встречаются в виде тридентатных тетраэдрических комплексов в кристаллических соединениях. Образование связи H–P в группе $(HPO_3)^{2-}$ обычно рассматривается как результат протонирования неподеленной электронной пары атома фосфора. И хотя в растворах фосфитам было уделено достаточно внимания со стороны спектроскопических исследований [Loub 1991], в кристаллических фазах связь H–P в фосфитных анионах до сих пор не была должным образом охарактеризована.

В рамках настоящей работы были синтезированы два изоструктурных соединения $Fe_2(SeO_3)_3$ и $Fe_2(HPO_3)_3$. Туннельные кристаллические структуры обеих фаз демонстрируют аналогию между неподеленными электронными парами селенитных пирамид и связями H–P в фосфитных тетраэдрах (рис. 7.1). Напрашивается предположение, что в кристаллических материалах, содержащих анионы $(HPO_3)^{2-}$ и $(ESeO_3)^{2-}$, связь H–P играет ту же роль в фосфитах, что и неподеленная электронная пара *E* в селенитах, считая, что атом H заряжен отрицательно, а связь H–P обладает существенно гидридным характером в анионах $(HPO_3)^{2-}$.

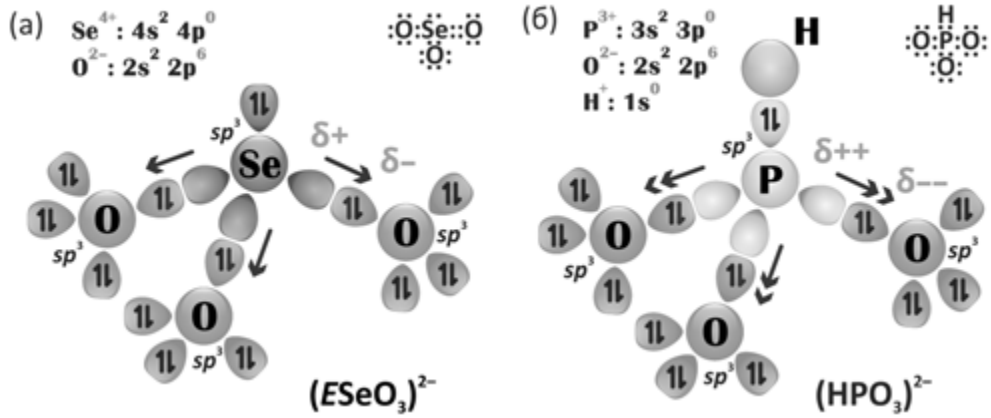

РИСУНОК 7.1 Структуры Льюиса и упрощенное художественное представление орбитальных моделей анионов $(ESeO_3)^{2-}$ (а) и $(HPO_3)^{2-}$ (б), которое подчеркивает схожую геометрическую роль H_{HPO3} и E_{SeO3}

2.7.1 Синтез и структурное описание селенита и фосфита железа

Монокристаллы соединений $Fe_2(SeO_3)_3$ (**c7.1**) и $Fe_2(HPO_3)_3$ (**c7.2**) были получены гидротермальным методом. Реагенты $FeCl_3{\cdot}6H_2O$, Li_2CO_3 и SeO_2/H_3PO_3 были перемешаны в молярном соотношении 1 : 1.5 : 2.5 и растворены в 6 мл дистиллированной воды. Гидротермальные реакции протекали в 23 мл стальных автоклавах с тефлоновыми вставками, которые нагревались в печи до 160 °C. При такой температуре автоклавы выдерживались в течение двух суток, а затем медленно охлаждались до комнатной температуры в течение еще 48 часов. Следует заметить, что ранее в работе [Sghyar et al. 1991] был описан другой способ синтеза фазы $Fe_2(HPO_3)_3$, при котором кристаллические соединения росли методом медленного выпаривания при 90 °C водного раствора, содержащего 20% Fe_2O_3, 30% H_3PO_3 и 50% воды.

Основные кристаллографические сведения и параметры уточнения кристаллических структур двух соединений представлены в табл. 7.1.

ТАБЛИЦА 7.1 Кристаллографические сведения и параметры уточнения структур соединений $Fe_2(SeO_3)_3$ (**c7.1**) и $Fe_2(HPO_3)_3$ (**c7.2**)

	c7.1	**c7.2**
M_r (г моль$^{-1}$)	492.58	351.63
пространственная группа	$P6_3/m$	$P6_3/m$
a (Å)	7.8720(9)	8.0195(2)
c (Å)	7.3258(10)	7.3700(2)
V (Å^3)	393.15(10)	410.48(2)
Z	2	2
ρ (г/см^3)	4.161	2.845
μ (мм$^{-1}$)	17.603	4.144
λ (MoK_α) (Å)	0.71073	0.71073
всего рефл.	3894	8590
независ. рефл.	472	475
R_{int}	0.0303	0.0325
R_1 [$I > 2\sigma(I)$]	0.0141	0.0133
R_1 [$I > 2\sigma(I)$]	0.0141	0.0133
R_1 [all data]	0.0157	0.0154
wR_2 [all data]	0.0311	0.0433
GOF	1.098	1.249
$\Delta\rho_{max}$,$\Delta\rho_{min}$ (e Å^{-3})	0.451, –0.426	0.423, –0.309

Кристаллические структуры соединений $Fe_2(SeO_3)_3$ (**c7.1**) и $Fe_2(HPO_3)_3$ (**c7.2**) содержат димеры $[Fe_2O_9]^{12-}$, собранные из октаэдров $Fe^{3+}O_6$, объединенных через общую треугольную грань. Средние длины связей Fe–O в обеих фазах приблизительно равны, так же как и расстояния Fe···Fe (2.987 Å и 2.980 Å соответственно в **c7.1** и **c7.2**). Димеры $[Fe_2O_9]^{12-}$ соединяются всеми своими шестью вершинами с тетраэдрами $(ESeO_3)^{2-}$ или $(HPO_3)^{2-}$, образуя гексагональные каналы вдоль кристаллографической оси c (рис. 7.2). Связи H–P направлены внутрь каналов по аналогии с неподеленными электронными

парами *E* селенитных групп $(ESeO_3)^{2-}$. Связи Se–O (1.676–1.722 Å) оказываются ожидаемо длиннее связей P–O (1.513–1.540 Å). Тем не менее диаметр центрального канала в структуре $Fe_2(HPO_3)_3$ больше, чем в соединении $Fe_2(SeO_3)_3$. Длина связи H–P составляет 1.310 Å, тогда как геометрический центр неподеленных электронных пар селенитных анионов расположен на расстоянии ≈0.260 Å от атома Se, что было рассчитано с использованием программы HYBRIDE, написанной на основе теории неподеленных пар, разработанной *А. Вербером* с соавторами [Verbaere et al. 1978].

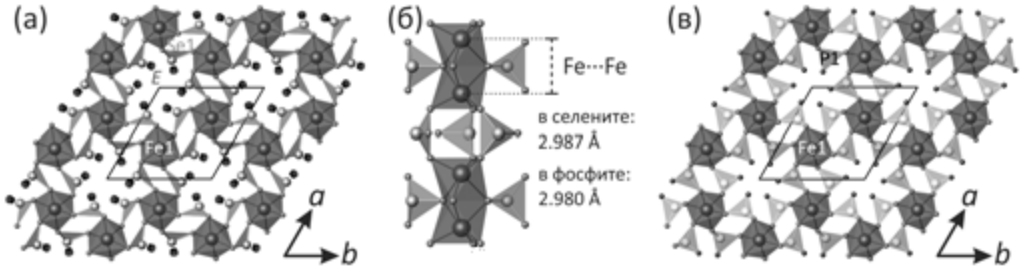

РИСУНОК 7.2 Вид кристаллических структур соединений $Fe_2(SeO_3)_3$ (**c7.1**) и $Fe_2(HPO_3)_3$ (**c7.2**) вдоль кристаллографической оси *c* – (а) и (в) соответственно; способ связывания полиэдров железа (коричневый) и селена (оранжевый) в структуре **c7.1** – (б)

2.7.2 Расчет частичных зарядов

Для большого числа известных фосфитных фаз с разнообразными кристаллическими структурами различной размерности с целью выяснения остаточных частичных отрицательных зарядов водорода были рассчитаны частичные заряды ионов фосфитных групп (табл. 7.2), используя метод *М. Анри* [Henry 2002; Henry 2008]. Расчеты показали слабый, но определенно гидридный характер связи H–P: например, слабо отрицательный заряд, составляющий –0.024 электронных единиц (*э. е.*), был получен для атомов H в соединении $Fe_2(HPO_3)_3$, а заряды –0.108 *э. е.* и –0.099 *э. е.* были рассчитаны для двух кристаллографически неэквивалентных водородных позиций в структуре соединения $Sr(H_2O)_2[(UO_2)(HPO_3)_2]$ [Villa et al. 2013].

В соединении $Fe_2(HPO_3)_3$ рассчитанные частичные заряды для ионов O и P составляют $\delta_O \approx -0.34$ *э. е.* и $\delta_P \approx +0.17$ *э. е.* соответственно. Переходя к большим лигандам, например, анионам хлора в соединении PCl_3, поляризованность связи P^{3+}–Cl^- смещена в сторону более положительного частичного заряда иона фосфора ($\delta_{Cl} = -0.11$ и $\delta_P = +0.34$), что не подходит для образования связи H–P. Похожий эффект наблюдается в арсенитах с пониженной электроотрицательностью мышьяка по сравнению с фосфором ($\chi_P > \chi_{As}$), что способствует стереохимической активности «свободной» неподеленной электронной

пары группы AsO_3. Более электроотрицательный катион селена ($\chi_{Se} >> \chi_P$) образует менее поляризованные связи Se–O, такие как в $Fe_2(SeO_3)_3$, что дает значение $\delta_{Se} \approx +0.056$ *э. е.*, и что также не позволяет формироваться связям H–Se, но хорошо подходит для образования оксоанионов $(ESeO_3)^{2-}$ в кристаллических соединениях.

ТАБЛИЦА 7.2 Рассчитанные частичные заряды некоторых соединений

	частичные заряды, $\pm q$			
	H	P / Se / As	O / Cl	ссылка
$Fe_2(HPO_3)_3$	–0.024	+0.170	–0.382 (×2), –0.293	[1], **c7.2**
$Sc_2(HPO_3)_3$	–0.068	+0.304	–0.602 (×2), –0.695	[2]
$Al_2(HPO_3)_3$	–0.042	+0.454	–0.504 (×2), –0.573	[3]
$Ga_2(HPO_3)_3$	–0.032	+0.479	–0.437 (×2), –0.483	[3]
$Fe_2(HPO_3)F_2$	–0.048	+0.401	–0.453 (×2), –0.452	[4]
$Sr(H_2O)_2[(UO_2)(HPO_3)_2]$	–0.108	+0.170	–0.539, –0.707, –0.695	[5]
	–0.099	+0.199	–0.666, –0.585, –0.676	
$Ni_{11}(HPO_3)_2(OH)_6$	–0.045	+0.478	–0.420 (×3)	[6]
	–0.048	+0.459	–0.432 (×3)	
PCl_3		+0.340	–0.114 (×2), –0.113	[7]
$Fe_2(SeO_3)_3$		+0.056	–0.353 (×2), –0.280	**c7.1**
$Sc_2(SeO_3)_3$		+0.088	–0.558 (×2), –0.661	[8]
$Zn_3(AsO_3)_2$		+0.231	–0.468 (×2), –0.467	[9]
		+0.206	–0.469 (×2), –0.470	

[1] – [Sghyar et al. 1991]; [2] – [Ewald et al. 2003]; [3] – [Morris et al. 1994]; [4] – [Liu et al. 2009]; [5] – [Villa et al. 2013]; [6] – [Marcos et al. 1993]; [7] – [Enjalbert et al. 1980]; [8] – [Wontcheu and Schleid 2003]; [9] – [Ghose et al. 1977]

Дополнительно выполненные *ab-initio* молекулярные расчеты в сотрудничестве с профессором Майком Вангбо также подтвердили наличие отрицательного заряда у атома водорода. Кроме того, при помощи магнитных исследований было получено свидетельство, что из-за своей геометрии и заряда группы HPO_3 являются очень слабыми магнитными соединительными узлами в структурах кристаллических материалов. Работа, описанная в этом разделе, еще не завершена и обещает привести к новым интересным результатам.

3 ЗАКЛЮЧЕНИЕ И ПЕРСПЕКТИВЫ

В диссертационной работе представлены результаты изучения нескольких металл-оксидных химических систем, содержащих различные химические элементы ($Cu^{+/2+}$, Ni^{2+}, Co^{2+}, $V^{4+/5+}$, $Mn^{2+/3+}$, Fe^{3+}, Pb^{2+}, Bi^{3+}, U^{6+}). Кристаллохимия большой группы новых кислородных соединений четырех- и шестивалентного селена была изучена главным образом методом монокристального рентгеноструктурного анализа. Результаты дальнейших экспериментальных работ в тексте не описаны, но могут быть найдены в опубликованных статьях, приложенных в конце диссертации. С кристаллографической точки зрения большинство синтезированных соединений представляют собой монокристаллы хорошего качества с высокоупорядоченными архитектурами, состоящими из разнообразных структурных комплексов. Только соединения на основе оксоцентрированных комплексов $O(Bi/Mn)_4$ демонстрируют тенденцию к разупорядочению. Это ситуация характерна для катионов Bi^{3+} в случаях, когда валентное усилие связи O–Bi дает вклад больше 0.5 *в. е.*, что приводит к искажению и разупорядочению позиций Bi. Как раз это и наблюдается в некоторых новых соединениях, описанных в данной работе.

Настоящая диссертация является одной из первых, в которой синтез различных серий новых металл-оксидных соединений осуществляется с применением инновационного подхода, основанного на использовании минералогической информации, т. е. информации о составе, структуре, свойствах и способе формирования объектов природного мира. В рамках данного подхода была предпринята попытка смоделировать природные процессы кристаллического роста в лабораторных условиях с целью получения комплексных фаз, обладающих потенциалом с точки зрения дальнейшего изучения их физических свойств. Большое разнообразие синтезированных соединений явно указывает на пригодность и применимость этого подхода для разработки и получения новых функциональных материалов. Замечательные результаты,

полученные с применением различных лабораторных методов, подтвердили, что селенитные и селенатные оксоанионные группировки могут играть роль темплатирующих агентов при кристаллическом росте минералов в различных геохимических обстановках.

В рамках настоящей работы было получено восемь новых медных оксоселенитов методом ХГТ реакций. Этот результат доказывает эффективность газотранспортного метода для синтеза необычных смешанно-валентных Cu^{+}–Cu^{2+} кислородных соединений. Соединения, описанные в диссертации, основаны на оксоцентрированных тетраэдрах $(\mu_4\text{–O})Cu_4$, которые полимеризуются с образованием структурных комплексов разной размерности.

Тройная водная система PbO–NiO–SeO_2 была скрупулезно исследована в гидротермальных условиях. Три новых свинцовых селенита никеля и один новый свинцовый селенит кобальта были синтезированы и структурно охарактеризованы. Экспериментальные результаты показали, что значения pH раствора играют существенную роль в процессах гидролиза и конденсации в гидротермальных реакциях в изученной системе и определяют структурные архитектуры образующихся кристаллических продуктов синтеза.

Три новых соединения были синтезированы в результате исследования тройных водных систем со свинцом, с ванадием и селеном. Две фазы оказались новыми полиморфными модификациями уже известных соединений. Изучение полиморфизма указало на большое разнообразие возможных структурных форм ванадат-селенитов, которое может быть вызвано отчасти присутствием химически различных связей в полиэдрах $V^{5+}O_n$. Вклад в это многообразие вносят также несимметричные селенитные группировки со стереохимически активными неподеленными электронными парами, которые приводят к формированию открытых структурных архитектур.

Семь новых соединений селена, содержащих марганец и/или висмут, были синтезированы разными лабораторными методами: выпаривание из водного раствора, гидротермальные реакции, химические газотранспортные реакции. Три полученные фазы являются первыми примерами оксоселенитов, содержащих одновременно и марганцевые, и висмутовые катионы.

Кроме того, было синтезировано и изучено 16 новых селенсодержащих оксосолей уранила, темплатированных органическими аминами. Обнаруженные топологии структурных комплексов новых соединений были проанализированы при помощи теории графов и специального подхода (основанного на составлении ориентационнной матрицы), применяемого для выявления разных геометрических изомеров уранил-селенатов и селенит-селенатов, обладающих одной той же структурной топологией. Анализ известных соединений $A_n(UO_2)_p(TO_4)_q(H_2O)_r$ (A^{+} = однозарядный катион и T^{6+} = Se,

S, Cr, Mo) с использованием принципа размерностного понижения в комбинации с составлением композиционной корреляционной диаграммы состав – структура позволил выделить на ней поля, соответствующие формированию уранильных структур различной размерности.

Проведенная аналогия между неподеленными электронными парами селенитных групп и связями H–P в фосфит-анионах на примере синтезированных изоструктурных фаз с димерами трехвалентного железа, подкрепленная расчетом частичных зарядов, указывает на вероятную отрицательность заряда атома водорода и гидридный характер связи H–P в группе $(HPO_3)^{2-}$. Это открывает потенциальную возможность для синтеза кристаллических соединений с открытыми архитектурами, обладающими поляризованными группировками P–H или Se–*E*, которые могут найти применение в качестве, например, интеркаляционных материалов, молекулярных сит, в катализе и пр.

Общие результаты, представленные в настоящей исследовательской работе, вносят вклад в фундаментальное представление о кристаллохимии синтетических и природных кислородных соединений четырех- и шестивалентного селена. Использованный в работе подход, основанный на минералогической информации, для синтеза новых металл-оксидных соединений является инновационным и может быть применен в рамках программы по обновлению современной неорганической химии и целенаправленного создания новых комплексных функциональных материалов, имеющих потенциал в области изучения их возможных физических свойств. Большое разнообразие новых синтетических селеновых кислородных соединений позволяет предсказать существование возможных аналогичных минеральных фаз, которые могут формироваться в различных геохимических обстановках. Обнаруженные открытые структурные постройки большинства новых соединений дают возможность для использования их структурных полостей для интеркаляции/экстракции мобильными органическими ионами, что может быть востребовано в перспективе в катализе и ионнообменной химии. Дальнейшее же изучение конденсированных селенсодержащих структур обещает привести к обнаружению интересных магнитных свойств. В этом аспекте единственным ограничением может оказаться только высокая летучесть оксосолей селена в процессах синтеза.